Mechanisms of cell death induced by betulinic acid and dihydroartemisinin polymer-drug conjugates on pancreatic cancer cells

Karabo Sekopi Mosiane

(1473512)

Submitted to the Faculty of Health Sciences, University of the Witwatersrand,

in fulfilment of the requirements for the degree of

Master of Science

Johannesburg, South Africa, 2023

DECLARATION

I, Karabo Sekopi Mosiane (1473512), declare this dissertation is my own, unaided work. It is being submitted for the Degree of Master of Science in Medicine by Research at the University of the Witwatersrand, Johannesburg. It has not been submitted before for any degree or examination at any other University.

(Signature of candidate)

___17th___ day of _____July_____ 2023 ____ at _____Itsoseng_____

DEDICATION

For my best friend, Dineo Poopedi, for consistently reminding me of the importance of obtaining this master's degree and achieving another first in my family. For my mother, Rosinah Mapule Mosiane, a courageous woman who sacrificed a lot for me.

Of utmost importance, in memory of my grandmother, who never knew how to read or write but continuously motivated us to get educated.

Franscinah Mosiane

1932 – 2015

PRESENTATIONS FROM THIS RESEARCH

The data obtained in this study was presented at the following conferences:

1. **Karabo Sekopi Mosiane**, Emmanuel Nweke, Mohammed Balogun and Pascaline Fru. The effect of betulinic acid polymer-drug conjugation on pancreatic cancer cells. GradFlash Presentation. Molecular Biosciences Research Thrust (MBRT) Symposium. December 2021.
2. **Karabo Sekopi Mosiane**, Emmanuel Nweke, Mohammed Balogun and Pascaline Fru. The effect of betulinic acid polymer-drug conjugation on pancreatic cancer cells. Poster presentation. 13th Annual Cross-Faculty Symposium. July 2022.
3. **Karabo Sekopi Mosiane**, Emmanuel Nweke, Mohammed Balogun and Pascaline Fru. The effect of betulinic acid polymer-drug conjugation on pancreatic cancer cells. Oral presentation. Faculty of Health Sciences Research Day. September 2022.
4. **Karabo Sekopi Mosiane**, Emmanuel Nweke, Mohammed Balogun and Pascaline Fru. The effect of betulinic acid polymer-drug conjugation on pancreatic cancer cells. Oral presentation. Hepato-Pancreato-Biliary Association of Southern Africa (HPBASA) Congress. November 2022.
5. **Karabo Sekopi Mosiane**, Emmanuel Nweke, Mohammed Balogun and Pascaline Fru. The effect of betulinic acid polymer-drug conjugation on pancreatic cancer cells. Oral presentation. Bert Myburgh Forum. November 2022.
6. **Karabo Sekopi Mosiane**, Emmanuel Nweke, Mohammed Balogun and Pascaline Fru. The effect of betulinic acid polymer-drug conjugation on pancreatic cancer cells. Poster presentation. Molecular Biosciences Research Thrust (MBRT) Symposium. December 2022.

PUBLICATIONS FROM THIS RESEARCH

PDF Copies of the following publications are provided at the end of this dissertation (Appendix I).

1. Mthimkhulu, N.; **Mosiane, K.S**.; Nweke, E.E.; Balogun, M.; Fru, P.N. (2021). Prospects of delivering natural compounds by polymer-drug conjugates in cancer therapeutics. *Anticancer Agents in Medicinal Chemistry*. **22**, 1699–1713. https://doi.org/10.2174/1871520621666210419094623
2. **Mosiane, K.S**.; Nweke, E.E.; Balogun, M.; Fru, P.N. (2023). Polyethyleneglycol-Betulinic Acid (PEG-BA) Polymer-Drug Conjugate Induces Apoptosis and Antioxidation in a Biological Model of Pancreatic Cancer. *Polymers*. **15**, 448. https://doi.org/10.3390/polym15020448

ABSTRACT

Introduction: Pancreatic cancer (PC) is a lethal malignancy characterised by a poor response to standard chemotherapy. Like other cancers, PC employs apoptosis evasion mechanisms to ensure tumour survival. This makes apoptosis evasion an important cancer hallmark that can be targeted for effective treatment. Betulinic acid (BA) and Dihydroartemisinin (DHA) have shown promising anticancer properties via induction of apoptosis; however, limitations such as poor aqueous solubility and high molecular weights limit their overall therapeutic effect. Polymer drug conjugation is a promising solution. This project aimed to confirm the cytotoxic potential and determine the mechanism of cell death induced by BA and DHA polymer-drug conjugates on pancreatic cancer cells.

Methodology: The cytotoxic effect of the free drugs, BA and DHA, and the complimentary conjugates on Vero (non-cancerous cells) and MIA PaCa-2 pancreatic cancer cells was confirmed using tetrazolium salt assays. The antioxidant potential and effect of reactive oxygen species (ROS) activity were conducted using the 2,2-Diphenyl-1-picrylhydrazyl (DPPH) and N, N-Dimethyl-p-phenylenediamine (DEPPD) assays. The mode of cell death and the effect of the drugs on the cycling characteristics of the cells were determined using flow cytometric assays. Their effect on the expression of proapoptotic genes was assessed using real-time polymerase chain reaction (PCR). The apoptosis evasion mechanism of the pancreatic cancer cells was determined using the human nuclear factor kappa-B p65 subunit (NF-κB/p65) enzyme-linked immunosorbent assay (ELISA) kit.

Results: The conjugates PEG-BA and PEG-DHA demonstrated lower IC_{50} values compared to the free compounds BA and DHA with a selectivity index of 3.00 and 1.61 for the conjugates, and 1.12 and 1.71 for BA and DHA, respectively. Antioxidant analysis showed that the free drugs, BA and DHA, had a weak antioxidant potential with IC_{50} values of more than 100 µM while the conjugates resulted in lower IC_{50}. PEG-BA (4 µM) induced higher apoptosis than free BA (53.07% vs 7.68%) on the MIA PaCa-2 cells. Furthermore, PEG-DHA resulted in 50.99% of the MIA PaCa-2 cells undergoing apoptosis compared to free DHA (12.90%). Both conjugates induced low levels of necrosis (< 1%). After treatment with PEG-BA, the MIA PaCa-2 cells underwent a dose-dependent Sub-G_1 arrest, which further indicated apoptosis. Similarly, PEG-DHA also induced a Sub-G_1 arrest in addition to G_2/M arrest on the MIA PaCa-2 cells. Compared to the free BA, PEG-BA treatment resulted in the highest overexpression of the following proapoptotic genes: *TNF*, *BAX*, *CASPASE 3*,

CASPASE 2 and *CASPASE 8*. Both BA and PEG-BA induced a moderate increase in the concentration of NF-κB compared to the untreated MIA PaCa-2 cells.

Conclusion: This study confirmed that conjugation of the polymer PEG to natural compounds with anticancer properties, such as BA, further improves the apoptosis-inducing ability against pancreatic cancer cells with the overexpression of proapoptotic genes, necessitating further exploration.

ACKNOWLEDGEMENTS

Completing my MSc would have never been possible if it was not for the grace of God, the support from my family and friends and, most importantly, guidance from my supervisors. I want to thank Professor Pascaline Fru and Dr Emmanuel Nweke for their invaluable support throughout this project. I am grateful for the motivation I always received from them, constantly reminding me of my potential as a future researcher. I would also like to thank Dr Mohammed Balogun and Dr Sindisiwe Mvango for synthesising, characterising, and providing the polymer-drug conjugates that played a crucial role in this project.

I would also like to thank the following departments that made it easier for me to perform the techniques mentioned in this dissertation. Dr Philemon Ubenako from the Pharmacy department for providing their spectrophotometer for ROS analysis. Mrs Ali and Professor Tanya Augustine from the Anatomical Sciences department for allowing me to use the thermocycler for real-time PCR. I also acknowledge the Unit for Somatic Cell Genetics for their plate centrifuge that played an essential role in the cytotoxicity studies. Lastly, I would like to thank Dr Marietha Nel for patiently teaching me cell culture and other laboratory techniques that made it possible for me to work on my own.

I also express my heartfelt gratitude to the National Research Foundation (NRF) of South Africa for financial support. I would also like to thank the Department of Surgery for its facilities, colleagues, friends, and family.

TABLE OF CONTENTS

LIST OF FIGURES

Chapter 1

Chapter 2

Chapter 3

Chapter 4

Chapter 5

LIST OF TABLES

Chapter 1

Chapter 2

Chapter 3

Chapter 4

NOMENCLATURE

APAF-1	Apoptotic protease activating factor 1
BA	Betulinic acid
BSA	Bovine serum albumin
CP	Chronic pancreatitis
CPT	Camptothecin
DEPPD	N, N-Dimethyl-p-phenylenediamine
DHA	Dihydroartemisinin
DM	Diabetes mellitus
DMEM	Dulbecco's Modified Eagle's Medium
DMSO	Dimethylsulfoxide
DPPH	2,2- diphenyl-1-picrylhydrazyl
FITC	Fluorescein isothiocyanate
ELISA	Enzyme-linked immunosorbent assay
EPR	Enhanced Permeability and Retention
FADD	Fas-associated death domain protein
FBS	Foetal bovine serum
FCS	Flow cytometry standard
HA	Hyaluronic acid
HPMA	N-(2-hydroxypropyl) methacrylamide
IC_{50}	50% inhibitory concentration
IPMN	Intraductal papillary mucinous neoplasms
MCN	Mucinous cystic neoplasm
MTT	3-(4,5-dimethylthiazol-2-yl)-2,5-diphenyl-2H-tetrazolium bromide
NF-κB	Nuclear Factor kappa B
PanIN	Pancreatic intraepithelial neoplasia
PBS	Phosphate buffered saline
PDAC	Pancreatic ductal adenocarcinoma
PEG	Polyethylene glycol
PI	Propidium iodide
PS	Phosphatidylserine
SI	Selectivity index
TNF	Tumour necrosis factor
TRAIL	Tumour necrosis factor-related apoptosis-inducing ligand
VEGF	Vascular endothelial growth factor
XTT	2,3-Bis-(2-methoxy-4-nitro5-sulfophenyl)-2H-tetrazolium-5-carboxanilide salt

CHAPTER 1

BACKGROUND AND LITERATURE REVIEW

1.1. Background

1.1.1. Epidemiology and biology of pancreatic cancer

Pancreatic ductal adenocarcinoma (PDAC) is the most prevalent malignancy and accounts for more than 90% of all neoplastic diseases of the pancreas (Orth et al., 2019). In developed countries, such as the United States of America, the European Union, and Australia, it is currently ranked the 4th leading cause of cancer-related mortality behind lung, colon, and breast cancer (Sellam et al., 2015; Loveday et al., 2019; Maisonneuve, 2019). This disease was estimated to account for 62 210 cases of incidence and 49 830 deaths in 2022 worldwide (Siegel et al., 2021). The lethality of this disease is visible mainly in the fact that the incidence rate parallels the mortality rate with a mortality-incidence ratio of 0.80 (Loveday et al., 2019; Siegel et al., 2021). Worldwide statistics show it is ranked the 7th leading cause of cancer deaths (Rawla et al., 2019; Hu et al., 2021). According to Hu and colleagues, it is estimated that Africa will account for the world's highest growth rate in incidence and mortality of pancreatic cancer by 2040 (Hu et al., 2021).

Several cancer types are caused by exposure to single agents, such as cervical cancer, mainly caused by chronic infection with human papillomavirus subtypes 16 and 18 (Chan et al., 2019; Boon et al., 2022). However, pancreatic cancer has an unknown aetiology associated with numerous risk factors (Khan et al., 2019; Maisonneuve, 2019). Smoking is associated with a 6-fold increase in pancreatic cancer risk due to numerous carcinogens in cigarette smoke (Zhang et al., 2016). Other risk factors have been reported to have a positive association with the risk of pancreatic cancer. Advanced age, greater than seven decades, is associated with greater incidence (median age of 71 years) and mortality (median age of 73 years) (Stark & Eibl, 2015; Zhang et al., 2016). African American ethnicity, non-O blood groups, genetic predisposition (10% of reported cases), and elevated body mass index (BMI) are all risk factors for the disease (Vincent et al., 2011; Stark & Eibl, 2015; Sellam et al., 2015; Ilic & Ilic, 2016; Zhang et al., 2016; McGuigan et al., 2018; Maisonneuve, 2019).

Chronic type 2 diabetes mellitus (DM) is a well-known risk factor for PC (Duan et al., 2021). In addition, PC can also cause an abrupt onset of DM, with the cancer being diagnosed within

a few months after the appearance of the DM (Khan et al., 2019). Therefore, DM and PC have a bidirectional relationship (Hu et al., 2021). There is a strong correlation between heavy alcohol consumption and chronic pancreatitis (CP). Studies found that CP accounts for a 20-fold greater risk of pancreatic cancer than in individuals who do not have CP. Briefly, this results from the long-term inflammation that occurs in the pancreas due to the various inflammatory mediators released from the pancreas, promoting genomic damage, which are coding errors leading to deleterious mutations and cellular proliferation, resulting in pancreatic malignancy (Lowenfels & Maisonneuve, 2005; Zhang et al., 2016; Maisonneuve, 2019).

Pancreatic precursor lesions can lead to pancreatic cancer

Several studies have shown that PDAC is a malignant disease originating in the ductal epithelium. The ductal epithelium contains the cells responsible for producing inactive enzymes delivered to the duodenum for digestion (Grapin-Botton, 2005; Puri & Saif, 2014; Ansari et al., 2015). To date, five precursor lesions of PDAC have been identified (Kim and Hong, 2018); however, only three will be discussed in this section. These are pre-malignant, non-invasive lesions which show heterogeneous glandular-like structures that infiltrate the pancreatic parenchyma with a distinct desmoplastic stroma (Demir, 2012; Neureiter, 2014). The lesions include pancreatic intraepithelial neoplasia (PanIN), intraductal papillary mucinous neoplasms (IPMNs), and the least frequent mucinous cystic neoplasm (MCN) (Distler et al., 2014). These lesions (especially PanINs) can progress to invasive cancer, forming tumours at the head in most cases but sometimes in the body and tail of the pancreas (Hruban et al., 2007; Hidalgo, 2010; Vincent et al., 2011; Sellam et al., 2015; Ilic & Ilic, 2016; McGuigan et al., 2018). This occurs because of the successive accumulation of gene mutations in the cells within the lesions, resulting in the evolution to PDAC (Vincent et al., 2011; Ansari et al., 2015; Stark & Eibl, 2015).

Genetic mutations prevalent in pancreatic cancer

The oncogene most frequently mutated in PC, accounting for over 95% of reported cases, is the Kirsten rat sarcoma viral oncogene homolog 2 (*KRAS2*) (Bryant et al., 2019). The oncogene results in the production of an abnormal Ras protein fixed in an activated state that leads to further activation of survival signalling pathways such as the phosphatidylinositol 3-kinase (PI3K)- protein kinase B (AKT)- mammalian target of rapamycin (mTOR) and the mitogen-activated protein kinase (MAPK)-rapidly accelerated fibrosarcoma (RAF)/MAP

kinase (MEK)/extracellular signal-related kinase (ERK) pathways (Beganovic, 2010; Puri & Saif, 2014; Nan et al., 2015; Cook et al., 2021). In the PI3K-AKT-mTOR pathway, the highly activated Ras protein activates PI3K, catalysing the conversion of phosphatidylinositol 4,5-bisphosphate (PIP_2) to phosphatidylinositol 3,4,5-trisphosphate (PIP_3), which leads to the phosphorylation of AKT. This phosphorylation step activates protein kinase B, inhibiting apoptosis and regulating cell proliferation, favouring survival. Furthermore, AKT can also activate mTOR, proteins which play a crucial role in cell proliferation, exacerbating the promotion of survival. Again, AKT also targets anti-apoptotic proteins and activates them, inhibiting apoptosis (Huang et al., 2021). In the RAF/MEK/ERK pathway, the GTP-bound Ras leads to the recruitment, translocation, heterodimerisation and eventual phosphorylation of members of the RAF family (Hymowitz and Malek., 2018). This is followed by an activation/phosphorylation cascade of MEK1/2 then ERK1/2 (Takacs et al., 2020; Zhu et al., 2021). The activated ERK eventually leads to phosphorylation of nuclear transcription factors and cytoplasmic targets that regulate expression of genes and proteins involved in cell survival, cell cycle progression, and cell migration (Huang et al., 2021; Zhu et al., 2021; Vendramini et al., 2022). The KRAS2 has been reported to modulate the activity of the pro-inflammatory cytokine, interleukin- (IL-6) and the sonic hedgehog signalling pathway, which plays a significant role in chemoresistance and tumour aggression (Fan et al., 2018).

In addition, specific genes undergo downregulation or silencing, resulting in lower levels of essential proteins that regulate cellular homeostasis (Hruban et al., 2007). These include cyclin-dependent kinase inhibitor 2A (*CDKN2A*), tumour protein p53 (*TP53*) and Mothers against decapentaplegic homolog 4 (*SMAD 4*) (Neureiter, 2014). Downregulation of *CDKN2A* results in the loss of the p16 protein, a negative regulator of the cell cycle (Foulkes et al., 1997; Iwatate et al., 2020). This enables PDAC cells to bypass the G_1 cell cycle checkpoint, permitting entry of the cells into the S phase and eventually the M phase. These phases promote DNA synthesis and increase cellular proliferation, factors necessary for tumour progression and metastasis (Foulkes et al., 1997; Straume et al., 2000; Ansari et al., 2015; Iwatate et al., 2020). The *CDKN2A* mutation is reported in at least 50-95% of PDAC cases (Hidalgo, 2010; Iwatate et al., 2020). *TP53* mutations are reported in 50-75% of PDAC cases (Ansari et al., 2015). This gene encodes mutant p53 protein that permits cells to bypass DNA checkpoints, leading to the replication of damaged DNA and genetic instability (Hidalgo, 2010). Furthermore, the activation of pro-apoptotic proteins, such as p53, an upregulated modulator of apoptosis (Puma), is inhibited, leading to apoptosis evasion

(Petitjean et al., 2007; Ansari et al., 2015). Studies have shown that the *KRAS2* mutation promotes the formation of the p53-SNAIL suppressive complex, a necessary inhibitory mechanism for the functioning of the Ras protein in cancer cells (Lee et al., 2009; Hidalgo, 2010; Lim et al., 2010; Lee & Park, 2011; Ansari et al., 2015). *SMAD 4* tumour suppressor gene is mutated in 55% of PDAC cases (occurs in other cancers but has higher sensitivity and specificity in PDAC) (Ansari et al., 2015). *SMAD 4* plays a crucial role in transforming growth factor (TGF) β signalling leading to the inhibition of cell proliferation and migration (Schwarte-Waldhoff et al., 2000; Lin et al., 2019; Wang et al., 2019). Mutations in *SMAD 4* lead to a loss of function, favouring tumour formation and survival (Schwarte-Waldhoff et al., 2000; Ahmed et al., 2017). Furthermore, this late-stage mutation is associated with poor prognosis and potential metastasis (Ansari et al., 2015; Ahmed et al., 2017; Wang et al., 2019). Most PC cases have been reported to carry one of the mentioned mutations, the most common being point mutations (Puri & Saif, 2014).

1.1.2. Treatment of pancreatic cancer

Currently, the best curative option for PC is surgery, with only 15% of patients presenting with resectable disease (Ansari et al., 2015; Khan et al., 2019). The primary goal of resection is the complete removal of the tumour because it is associated with higher survival rates (Beger et al., 2003; Ansari et al., 2015; Kleeff et al., 2016). However, as with any other surgery, postoperative complications can occur, including anastomotic leaks in the pancreas and delayed gastric emptying (Vincent et al., 2011; Stark & Eibl, 2015). Therefore, additional treatment strategies are combined before, with or after the operation to increase the chances of survival (Beger et al., 2003; Sellam et al., 2015). Adjuvant therapy is recommended for patients who underwent curative resection one to two months after the surgery or when the patient recovers (Vincent et al., 2011; Sellam et al., 2015). Another form of treatment is neoadjuvant (preoperative) chemotherapy which can shrink the primary tumour, potentially downstaging patients with borderline resectable disease, eliminating micro-metastases and reducing the percentage of positive lymph nodes (Ansari et al., 2015; Kleeff et al., 2016). However, the disadvantages of neoadjuvant treatment include preoperative complications, transition from resectable to unresectable tumours as a result of fibrosis in the pancreas and the tumour becoming unresponsive to the chemotherapy (Hidalgo, 2010; Ansari et al., 2015).

Most patients (80-90%) present with an advanced stage of pancreatic cancer and an irresectable tumour (Stark & Eibl, 2015; Asombang et al., 2016; da Costa et al., 2020). Hence, in the last two decades, patients have been given monotherapy with gemcitabine, the first line of treatment for advanced disease (Puri & Saif, 2014). Gemcitabine is a pyrimidine nucleoside analogue that has successfully treated many solid tumours, such as pancreatic cancer (Linskens, 2000; Dasanu, 2008; El-Sheikh et al., 2021). The drug functions by inhibiting progression through the cell cycle, specifically through the G_1/S checkpoint and kills cells synthesising DNA (S-phase), thereby inducing apoptosis (Tavil et al., 2007; Dasanu, 2008). However, most patients do not respond to the treatment because of chemoresistance (Ansari et al., 2015; Doi et al., 2017). There are several cellular pathways that gemcitabine uses to aid activation and transportation. The drug is activated via a series of phosphorylation steps by deoxycytidine deaminase (dCK). Studies have found that low levels of dCK are associated with reduced cytotoxic effects against cancer cells (Moysan et al., 2013). Gemcitabine is rapidly inactivated via deamination by cytidine deaminase, resulting in a low plasma half-life (Moysan et al., 2013; El-Sheikh et al., 2021). Furthermore, a reduced expression of transporter proteins such as human equilibrative nucleoside transporter 1 (hENT1) is associated with decreased drug uptake, affecting the overall and progression-free survival of the patient (Ansari et al., 2015; Vincenzi et al., 2017). All these factors affect the therapeutic index of gemcitabine, which forces clinicians to increase the drug dose to obtain the theoretical potency (Moysan et al., 2013; El-Sheikh et al., 2021). Although this improves treatment efficacy, the high doses (1000mg/m^2) are associated with adverse side effects such as vascular-related diseases (Dasanu, 2008), severe neurotoxicity (Larsen & Hansen, 2004), nausea and vomiting (Linskens, 2000; Moysan et al., 2013), diarrhoea (Tavil et al., 2007) and myelosuppression (Linskens, 2000; Tavil et al., 2007), among others.

Studies have shown the benefit of combination therapies compared to monotherapy (Labrie et al., 1988; O'Shaughnessy et al., 2002; Clyburn et al., 2010; Motomura et al., 2011; Saputra et al., 2018). These regimens can potentially reduce drug resistance and promote other anti-cancer mechanisms (Greco & Vicent, 2009; Mokhtari et al., 2017). Therefore, combination treatment enables the multi-targeting of cancer cells via diverse strategies (Greco & Vicent, 2009; Mokhtari et al., 2017). Furthermore, since combination affects several pathways, the development of evasion mechanisms, such as with the monotherapy of doxorubicin, where the cancer cells eventually overexpress transporters that export the drugs, may be impeded (Greco & Vicent, 2009; Khdair et al., 2010; Mokhtari et al., 2017). Gemcitabine has been

combined with several other drugs resulting in better survival rates in patients with metastatic disease and good health status (Ansari et al., 2015; Stark & Eibl, 2015).

The combination of gemcitabine and nanoparticle albumin-bound paclitaxel (nab-paclitaxel), marketed under the name of Abraxane®, has shown a combined effect of inhibition of DNA synthesis (gemcitabine mechanism) coupled with an ability to break the tumour stroma (Abraxane®) allowing accumulation and retention of gemcitabine and paclitaxel (Iglesias, 2009; Ansari et al., 2015). However, despite the improvement, the toxicity of this combination therapy is not any different from gemcitabine monotherapy as it increases the rate of peripheral neuropathy and myelosuppression (Ansari et al., 2015; Ruess et al., 2017). Another combination therapy of gemcitabine and erlotinib (CONKO-005 clinical trial), an epidermal growth factor receptor (EGFR)-tyrosine kinase inhibitor, has shown modest improvement in overall patient survival compared to gemcitabine monotherapy (Yang et al., 2013; Zhang et al., 2016; Khorana et al., 2017; Hoyer et al., 2021). However, the function of erlotinib can be limited by the *KRAS2* mutation, which predominates in most of the reported pancreatic cancer cases (Beganovic, 2010; Puri & Saif, 2014). The fluorouracil (5-FU) prodrug, capecitabine, has also been used in combination with gemcitabine for adjuvant therapy (post-surgical chemotherapy) and improved overall survival in patients with resectable disease (Walko & Lindley, 2005; Zhang et al., 2016; Khorana et al., 2017).

Besides gemcitabine, fluorouracil (5-FU)-based therapies have been considered the mainstay of pancreatic cancer treatment, especially the FOLFIRINOX (5-FU, leucovorin, irinotecan, and oxaliplatin) multi-drug regimen (Kleeff et al., 2016; Pereira & Corrêa, 2018). The 5-FU inhibits thymidine synthesis by blocking its enzyme, thymidylate synthase. Leucovorin is a folinic acid metabolite that reduces the subsequent side effects of 5-FU. Irinotecan is a topoisomerase I inhibitor that results in dsDNA breaks and cell death. Oxaliplatin produces reactive species that cross-link with DNA on guanine-cytosine (G-C) rich areas and inhibits DNA synthesis and transcription of messenger RNA (Pereira & Corrêa, 2018). FOLFIRINOX has shown significantly improved overall survival compared to treatment only with gemcitabine (11.1 months vs 6.8 months); however, it has side effects such as neutropenia, thrombocytopenia, diarrhoea, sensory neuropathy, and alopecia (Ruess et al., 2017). Furthermore, this treatment option is only suitable for a limited number of patients, i.e. younger patients with good performance status (Ansari et al., 2015; Kleeff et al., 2016). Fluorouracil-based second-line therapy after first-line therapy with gemcitabine in

combination with nab-paclitaxel (reciprocal therapy) is advised, including the oxaliplatin, 5-FU and folinic acid (OFF) regimen that has improved median overall survival from 7.9 months to 9.1 months. Other second-line therapies such as the FF regimen (5-FU combined with folinic acid) or 5-FU plus liposomal irinotecan improved progression-free survival from 2.0 months to 2.8 months (Ruess et al., 2017).

According to the World Health Organisation (2002), palliative care improves the quality of life of patients through early identification and assessment and treatment of pain and other problems that are either physical, psychosocial, or spiritual (Abu-Odah et al., 2020). In PC, patients experience numerous complications, including tumour-associated pain, gastric outlet, and biliary obstruction; hence palliation is necessary (Stark & Eibl, 2015). This treatment is given to relieve symptoms associated with cancer progression (Abu-Odah et al., 2020).

1.2. Literature Review

1.2.1. The use of phytochemicals for cancer treatment

Given the adverse side effects observed when using standard chemotherapeutic drugs, natural products possessing anticancer activity are a more suitable alternative for cancer therapy. According to the literature, natural products can target crucial cell signalling pathways altered in most cancer types (Chamberlin et al., 2019; Majolo et al., 2019; Noel et al., 2020; Hashem et al., 2022). These products can be derived from any living system, such as plants, animals, marine life, fungi, and microorganisms (Yogeeswari & Sriram, 2005; Huang et al., 2021). Plant-based compounds serve as a suitable alternative to conventional chemotherapy because of their ability to target multiple cancer signalling pathways and because they exhibit reduced toxicity to non-malignant cells or tissues (Singh et al., 2016, 2019). The two plant-derived compounds known as betulinic acid and dihydroartemisinin, which are the subject of this dissertation, will be discussed in more detail.

Betulinic acid (3β-hydroxy-lup-20(29)-en-28-oic acid) occurs naturally and is a widely distributed pentacyclic lupine-type triterpene in the plant kingdom (Yogeeswari & Sriram, 2005; Ali-Seyed et al., 2016; Liu et al., 2017). Small amounts of betulinic acid (BA) can be sourced from the outer bark of various tree species, for example, the *Betula alba* (White birch bark). This is because many white-barked birch trees consist of a closely related compound called betulin that makes up at least a quarter of the tree's outer bark weight (Csuk, 2014).

Betulin is easily converted into BA by oxidation reactions, which is why BA is referred to as the carboxylic acid derivative of betulin, as it contains a –COOH group instead of the native CH_2OH on carbon 28 (Figure 1.1) (Cichewicz & Kouzi, 2004; Yogeeswari & Sriram, 2005; Şoica et al., 2012; Csuk, 2014; Ali-Seyed et al., 2016).

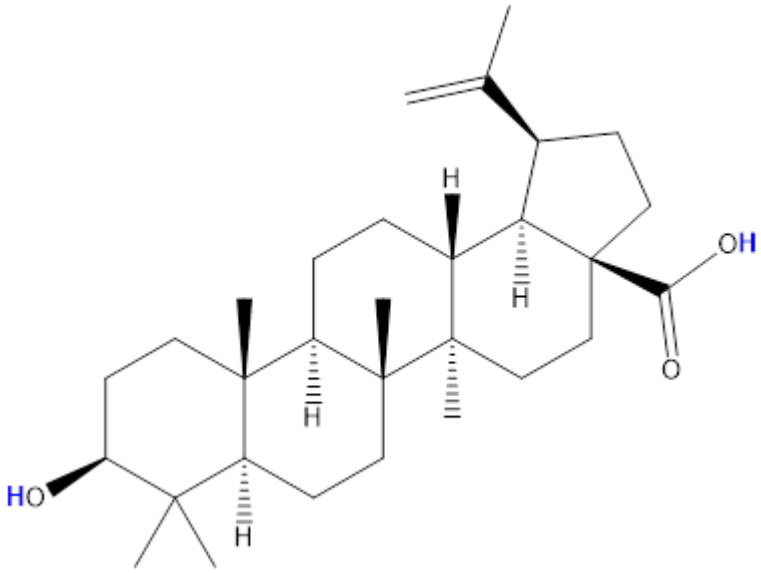

Figure 1.1: Chemical structure of betulinic acid (BA) with the acidic hydrogens highlighted in blue (drawn using the ChemDraw Ultra software)

BA possesses numerous pharmacological properties such as anti-HIV-1 (Cichewicz & Kouzi, 2004; Aiken & Chen, 2005), anti-inflammatory (Oliveira-Costa et al., 2022), anti-diabetic (Ríos & Máñez, 2018), anti-bacterial (Fontanay et al., 2008; Haque et al., 2014), and anti-malarial (de Sá et al., 2009) activities. The compound has also shown antiangiogenic activity by inhibition of aminopeptidase N overexpressed in cancer cells and by activating degradation of the specificity proteins (Sp1, 3 and 4) responsible for the regulation of vascular endothelial growth factor (VEGF) expression (Chintharlapalli et al., 2007; Fulda, 2008; Chintharlapalli et al., 2011). Angiogenesis is very crucial in cancer as it aids survival (provision of nutrition and oxygen as the tumour grows) and enables invasion and metastasis to distant sites (Chen et al., 2004; Saman et al., 2020). Knowledge of this irregularity has given clinical relevance to angiogenesis-targeting remedies for cancer inhibition (Wang et al., 2015).

BA has shown cytotoxic, anti-tumour activity against several cancer types, such as cervical cancer (IC_{50}: 30.42 ± 2.39 µM), melanoma, carcinomas, leukaemia, and blastoma (IC_{50} range

of 2.41-37.22 µM) by inducing apoptosis (Fulda, 2008; Ali-Seyed et al., 2016). Most standard chemotherapeutic drugs are prone to exportation via the ATP-binding cassette (ABC) proteins that result in multi-drug resistance (MDR) (Saeed et al., 2018; Mthimkhulu et al., 2021). In a study by Saeed et al. (2018), it was shown that BA is not a substrate of these ABC proteins when tested against several drug-resistant human embryonic kidney (HEK293), breast cancer, glioblastoma and leukaemic cell lines and their sensitive counterparts (Saeed et al., 2018). This finding showed that BA's broad anticancer activity is coupled with an ability to evade drug resistance, a problem of most tested anticancer drugs. Furthermore, the advantage of BA is that, in most studies reported in the literature, it has shown selective cytotoxicity against cancer cells with minimal effects on normal cell lines, primary cells and *in vivo* (Zuco et al., 2002).

Of importance to this study, BA is well-documented as an inducer of apoptosis. In bladder cancer cells, BA inhibits cell proliferation and induced a partial G_2/M cell cycle phase arrest through reduction of cyclin proteins (A and B1), cyclin dependent kinase 2 and cell division cycle proteins (2 and 25c). This is associated with an induction of apoptosis via disruption of the mitochondrial membrane potential, upregulation of B-cell lymphoma 2 (Bcl-2) associated X protein (Bax) and poly-ADP ribose polymerase (PARP) and inhibition of Bcl-2 (Kim et al., 2021). Park and colleagues assessed the anticancer efficacy of BA in human leukaemia cells (U937). Similarly, BA induced a G_2/M phase arrest, however it was only associated with a reduction in cyclins A and B1. Furthermore, BA treatment led to a sub-G_1 arrest, change in mitochondrial membrane potential and an increase in the activity of caspase 9 and caspase 3 (Park et al., 2021). A tabulated summary of some of the studies performed in different biological models using betulinic acid is shown in Table 1.1 below.

Table 1.1: The anticancer effect of betulinic acid on nine different cancer biological models

Biological Model	**Anticancer mechanism or findings**	**References**
MDA-MB-231 and BT549 breast cancer cell lines	Inhibited growth, epithelial to mesenchymal transition, and aerobic glycolysis. Apoptosis induction. Blocked expression of metalloproteinases	Zheng et al., 2019
Female Balb/c nude mice	Inhibited breast cancer colony formation in the lungs.	

H460 lung cancer cell line	Inhibition of cell proliferation. Induced apoptosis via the mitochondrial pathway (activation of Bax and inhibition of Bcl-2). G_2/M phase arrest.	Zhan et al., 2018
HCT116 and SW480 colorectal cancer cell lines	Inhibition of cell proliferation. Induced apoptosis via the mitochondrial pathway (caspases 3 and 9 and Bax activation coupled with Bcl-2 inactivation). Inhibition of heat shock protein A (HSPA).	Yurasakpong et al., 2021
A172 and U87MG glioblastoma cell lines	Growth inhibition. Induced apoptosis via mitochondrial pathway (activation of caspase 3 and 9, suppression of IAPs). Inhibition of NF-κB-p65.	Yaozu et al., 2021
786-O and ACHN renal cancer cell lines Mice model	Suppressed cell growth. Induced apoptosis via mitochondrial pathway (caspase 3 activation, Bax elevation, Bcl-2 decreased expression and change in mitochondrial membrane potential). Inhibition of tumour.	Yang et al., 2018
Hela cervical cancer cell line	Growth inhibition. Induced apoptosis via the mitochondrial pathway (Bax upregulation and Bcl-2 downregulation) and ER stress response (upregulation of HSPA5). Downregulation of members of the pentose phosphate pathway.	Xu et al., 2014
U266 and RPMI 8226 multiple myeloma cancer cell lines Multiple myeloma xenograft	Cell growth inhibition. Induced apoptosis via the mitochondrial pathway (Bax upregulation and Bcl-2 downregulation, activation of caspases 3, 8 and 9, change in mitochondrial outer membrane permeabilization (MOMP)). S-phase arrest. Inhibition of xenograft tumour growth.	Shen et al., 2019
LNCaP prostate cancer cell line	Growth inhibition. Induced apoptosis via the mitochondrial pathway (inhibition of IAPs (survivin) and PARP activation).	Chintharlapalli et al., 2007
PANC-1 and SW1990 pancreatic cancer cell lines Xenograft model	Cell proliferation inhibition. Induced apoptosis (upregulation of caspase 3, 8 and Bax and downregulation of Bcl-2). Growth inhibition of tumour.	Guo et al., 2020

Artemisinin (Qinghaosu) is a sesquiterpene lactone isolated from the plant *Artemisia annua* (sweet wormwood) and is used for treating malaria and fever (Singh & Lai, 2001; Chen et al., 2004; Dai et al., 2014; Lu et al., 2020). The artemisinin molecule contains an endoperoxide bridge that allows it to react with a ferrous iron atom. Since cancer cells have over-expression of transferrin receptors on their cell surfaces, this causes the cells to be more susceptible to the cytotoxic effects of artemisinin (Singh & Lai, 2001; Lu et al., 2020). A derivative of artemisinin called dihydroartemisinin (DHA) which contains an -OH group instead of the native double-bonded oxygen at carbon 10 (Figure 1.2), has shown antiangiogenic properties. This is via inhibiting vascular endothelial growth factor (VEGF) and other angiogenesis-associated genes, which are important targets in cancer treatment as they are often dysregulated, favouring tumour progression (Huang et al., 2007).

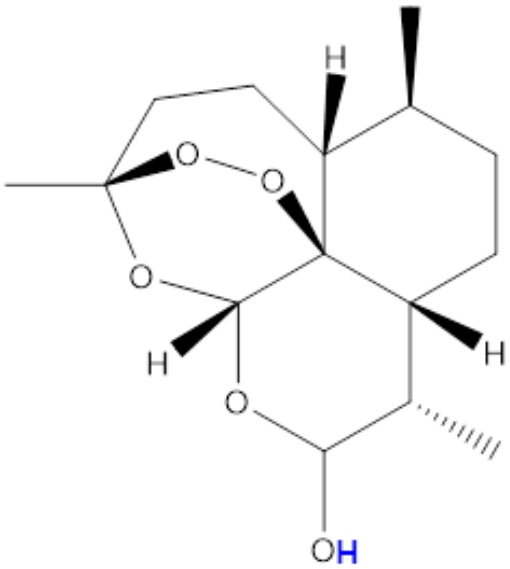

Figure 1.2: Chemical structure of dihydroartemisinin (DHA) with the acidic hydrogen atom shown in blue (drawn using the ChemDraw Ultra software).

DHA also presents with anti-tumour activity *in vitro* and *in vivo* (Chen et al., 2004; Dai et al., 2014). This drug has been tested against several cancers and has shown promising therapeutic indices. A study by Wang and colleagues in 2011 tested the effect of DHA on BxPC3 and PANC-1 pancreatic cancer cells at varying concentrations (12.5-100 µM). They reported IC_{50} values of 40.6 ± 6.8 µM and 48.9 ± 6.1 µM on BxPC3 and PANC-1, respectively (Wang et al., 2011). In 2008, Mu and colleagues tested DHA (5-320 µM) against lung cancer cells (PC-14) for 48 hours, and post-treatment analysis showed an IC_{50} value of 17.8 ± 1.2 µM (Mu et

al., 2008). Several mechanisms have been reported in the literature on the antitumour potential of DHA in different cancer cell lines.

One important aspect of the effects of DHA is its ability to induce apoptosis. In ovarian cancer cells, DHA inhibits growth and cell cycle progression and induces apoptosis via disruption of the mitochondrial membrane potential and release of cytochrome c (Jiao et al., 2007; T. Chen et al., 2009). The apoptosis-inducing effect of DHA was assessed by Lu and colleagues (2010) and Chen and colleagues (2013) on lung adenocarcinoma cancer cells (ASTC-a-1 and A549). They found that the compound results in apoptosis by activating initiators 8 and 9, effector 3 caspase proteins and up- and downregulation of B-cell lymphoma 2 (Bcl-2) associated X protein (Bax) and Bcl-extra large (Bcl-x_L), respectively (Lu et al., 2009; Chen et al., 2013). The anticancer effect of DHA and associated studies are summarised in Table 1.2 below.

Table 1.2: The anticancer effect of dihydroartemisinin on six different cancer models

Biological Model	**Anticancer Mechanism or Findings**	**References**
Primary glioma cells U251 and U373 glioma cell lines Xenograft model	Growth inhibition. Activation of ROS (lipid peroxidation and ferroptosis) and ER stress (cell death). Suppressed tumour growth	Chen et al., 2019
ASTC-a-1 lung cancer cell line	Growth inhibition. ROS activation. G_2/M phase cell cycle arrest associated with accumulation of cells in Sub-G_1 Induced apoptosis via mitochondrial pathway (change in MOMP, Bax translocation and activation, the release of cytochrome c, activation of caspases 9 and 3, caspase 8 and cleavage of Bid)	Lu et al., 2010
HCT116 colorectal cancer cell line	Growth inhibition. Induced apoptosis induction (through c-MYC depletion). G_1/G_0 phase arrest.	Lu et al., 2010
OVCA-420 ovarian cancer cell line	Growth inhibition. Induced apoptosis via mitochondrial pathway (sub-G_1 accumulation, DNA fragmentation, Bax and Bad upregulation and Bcl-2 and Bcl-x_L downregulation).	Jiao et al., 2007

	G_2/M phase arrest.	
BxPC-3 and AsPC-1 pancreatic cancer cell lines Male nude BALB/c mice	Inhibition of cell proliferation (downregulation of cyclin D1). Induced apoptosis via mitochondrial pathway (Bax and caspase 9 upregulation and Bcl-2 downregulation). Tumour growth inhibition *In situ* cell proliferation inhibition (reduction of Ki-67^+ cells) and apoptosis activation (Bax and caspase 9 upregulation and Bcl-2 downregulation).	Chen et al., 2009
Jurkat T-lymphoma cell lines	Induced apoptosis via mitochondrial pathway (sub-G_1 accumulation, upregulation of caspases 3 and 9, PARP. activation, caspase 8, Bcl-2 and Bcl-x_L downregulation) ROS elevation	Handrick et al., 2010

1.2.2. The use of BA and DHA formulations for cancer treatment

Regardless of the anticancer potential that BA and DHA possess, these natural compounds are associated with several limitations. These include high molecular weights that inhibit passage through the lipid bilayer of cells and poor aqueous solubility that reduces bioavailability due to poor absorption and rapid metabolism, coupled with subsequent reduction in overall therapeutic indices (Bonifácio et al., 2013). Sousa and colleagues (2019) provided an extensive review of manipulations to the chemical structure of BA, forming at least 140 derivatives that could potentially improve the therapeutic index of the native BA against cancer cells (Sousa et al., 2021). This suggests that modifying an anti-cancer agent, such as adding a carrier molecule or manipulating the chemical structure, could improve the anticancer potential through cell and tissue targeting (Bonifácio et al., 2013; Parveen et al., 2019; Sousa et al., 2021). Nanoparticles, nanomaterials possessing dimensions below 100 nm, have the potential to provide an efficient and selective drug delivery system that targets tumour cells (Blakney et al., 2014; Zhang et al., 2014; Wan et al., 2018). One advantage of a selective drug delivery system is the ability to increase drug efficacy through improved solubility, biodistribution and targeting of tumour cells while sparing non-cancerous cells (Mthimkhulu et al., 2021). An example of this type of drug delivery system is polymer-drug

conjugation which comprises the potential chemotherapeutic drug covalently linked to a polymeric carrier (Figure 1.3).

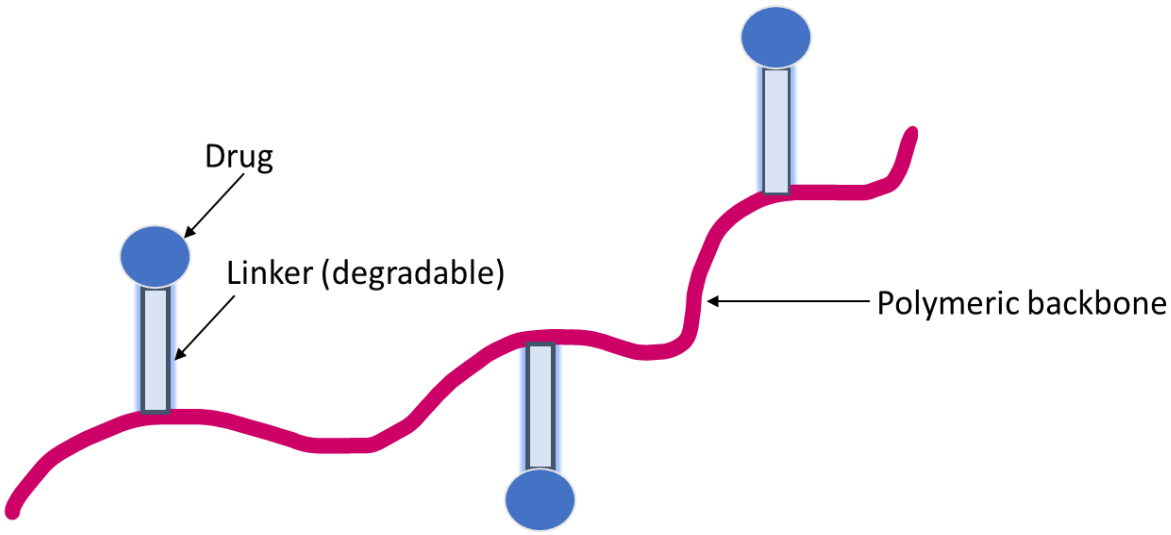

Figure 1.3: Schematic diagram of polymer-drug conjugate (drawn using Microsoft PowerPoint)

Polymer drug conjugates are used to maximise efficacy, reduce adverse side effects, prolong blood circulation, enable passive delivery of drugs to tumours via the enhanced permeability and retention (EPR) effect and overcome tumour resistance (Kost & Langer, 2012; Camacho et al., 2016; Wan et al., 2018). Some review papers have provided extensive information regarding the benefit of polymer-drug conjugation in cancer treatment compared to current standard chemotherapeutic drugs, suggesting the need for studies such as the current one (Alven et al., 2020; Mthimkhulu et al., 2021). In this section, several BA and DHA formulations and their potential benefit in cancer treatment will be discussed in more detail.

Several studies have shown that adding a polymer to betulinic acid improves aqueous solubility (Zhang et al., 2021), reduces haemolysis (Dai et al., 2015), and enhances cellular uptake either by passive targeting or actively through endocytosis (Zhang et al., 2020). Combined, all these factors lead to an overall improvement therapeutic index. For example, the HepG2 cell line was tested by Liu and colleagues in 2017 using BA pegylated and non-pegylated liposomes. The study reported enhanced solubility and cytotoxicity compared to free BA (Liu et al., 2017). In their *in vivo* studies, the authors showed that the BA pegylated liposomes increased inhibition in tumour growth more than when free BA or non-pegylated liposomes were used (Liu et al., 2017). In all studies, the pegylated liposomes improved the effects of BA, which suggested that adding PEG was necessary to induce the enhanced permeability and retention effect (Liu et al., 2017). Table 1.3 is a summarised version of

other studies that analysed BA formulations and focused more on apoptosis and improved targeting.

Table 1.3: The potential anticancer mechanisms of BA formulations

Name of Formulation	Biological Model	Anticancer Mechanism or Findings	References
Poly (lactic-co-glycolic acid)-loaded nanoparticles of betulinic acid (BNP)	HepG2 liver cancer cell line Albino Wistar rats	Improved cytotoxic effect (GI_{50} < 10 µg/mL). Tumour growth inhibition. Normal liver enzyme levels. Decreased proinflammatory cytokines. Apoptosis induction (upregulation of caspase 3 and 8).	Kumar et al., 2018b
BA-loaded PLGA-mPEG nanoparticles (BA NPs)	MCF-7 breast cancer and PANC-1 pancreatic cancer cell lines. Ehrlich model	Improved cytotoxic effect (MCF-7 IC_{50}: 19.50 ± 1.06 vs 10.28 ± 0.72 µM and PANC-1 IC_{50}: 18.45 ± 2.34 vs 11.48 ± 2.70 µM). Higher induction of apoptosis via the mitochondrial pathway (change in mitochondrial membrane potential). Elevated reaction oxygen species (ROS). G_1/G_0 phase arrest. Tumour growth inhibition.	Saneja et al., 2017a
BA conjugated to methylated-polyethylene glycol (mPEG-BA)	Hep3b and Huh-7 liver cancer cell lines Ehrlich ascites tumour (EAT) model	Higher induction of apoptosis via the mitochondrial pathway (upregulation of Bax, downregulation of Bcl-2, elevated levels of activated PARP and caspase 3). Tumour growth inhibition.	Saneja et al., 2017b
Biosurfactant-coated BA liposomes	HepG2 liver cancer cell line	Improved cytotoxic effect (IC_{50}: 10.53 vs 3.11 g/mL). Higher induction of apoptosis via the mitochondrial pathway (change in mitochondrial membrane potential). G_1/G_0 phase arrest.	Shu et al., 2019

Betulinic acid derivative (2c) nanoparticle (2c-NP)	HT-29 colorectal cancer cell line	Improved cytotoxic effect (IC_{50}: 14.9 vs 1.81 µM). Apoptosis (upregulation of caspases 3, 8 and 9 and change in mitochondrial membrane potential). G_2/M and S phase arrests. Chromatin fragmentation.	Dutta et al., 2019
PEG and poly-L-lysine-graft-polyethylene glycol (PLL-g-PEG)-BA NPs	HEK293 normal, Caco-2 colorectal cancer, Hela cervical cancer, and MCF-7 breast cancer cell lines	Tumour-specific cytotoxic effect (Caco-2 IC_{50}: 9.74 vs 3.12 µM), Hela IC_{50}: 17.73 vs 3.26 µM) and MCF-7 IC_{50}: 36.31 vs 13.13 µM). Higher induction of apoptosis (change in mitochondrial membrane potential). G_1/G_0 phase arrest.	Oladimeji et al., 2021
PLGA-BA NPs	A549 lung cancer and L6 myoblast cell lines Balb/c mice	Tumour-specific cytotoxic effect (IC_{50}: 50 µg/mL). Sub-G_1 phase arrest Higher induction of apoptosis (upregulated PARP, Bax and caspase 3, downregulated Bcl-2). Crossed the blood-brain barrier	Das et al., 2016
Folic acid modified BA polymeric NP (FA-PEG-PBuOx/BA)	Hela cervical cancer and HT-29 colorectal cancer cell lines	Improved cytotoxic effect (Hela IC_{50} < 31 µg/mL and HT-29 IC_{50}: 43 µg/mL). Enhanced tumour targeting (via endocytosis)	Zhang et al., 2020
FA-8-arm-PEG-BA NPs	LLC and A549 lung cancer cell lines C57BL/6 mice Tumour xenograft model	Improved cytotoxic effect (LLC IC_{50}: 6.56 ± 0.43 vs 0.09 ± 0.00 µg/mL) and A549 IC_{50}: 8.31 ± 0.46 vs 0.08 ± 0.02 µg/mL). Enhanced tumour targeting (via endocytosis) Prolonged blood circulation Improved tumour growth inhibition and animal survival. Maintained IgE levels.	Dai et al., 2015

Two studies by Dai and colleagues (2014) and Lu and colleagues (2020) used pegylation to improve the efficacy of DHA, thereby forming multi-arm (4 and 8 arm) PEG-DHA and DHA/MPEG-PCL, respectively. Both studies showed improved cytotoxicity after conjugation specific to the cancerous cell lines. Furthermore, treating mice models with the conjugates resulted in tumour growth inhibition and animal survival (Dai et al., 2014; Lu et

al., 2020). In another study by Kumar and colleagues, hyaluronic (HA)-DHA conjugate was assessed against lung cancer cells, similar to the previously mentioned studies, and conjugation improved cytotoxicity. This was further associated with higher induction of apoptotic cell death compared to free DHA (Kumar et al., 2019). The findings of these studies are summarised in Table 1.4.

Table 1.4: The potential anticancer mechanisms of DHA formulations

Name of Formulation	Biological Model	Anticancer Mechanism or Findings	References
Multi-arm PEG-DHA	LLC and A549 lung cancer cell lines. Tumour xenograft model.	G_1/G_0 phase arrest. Longer blood circulation. Improved tumour growth inhibition and animal survival.	Dai et al., 2014
Poly (ethylene glycol) methyl ether-poly(e-caprolactone) loaded DHA nanoparticles (DHA/MPEG-PCL)	Hela cervical cancer cell line Female Balb/c nude mice	Improved cytotoxic effect (IC_{50} not reported). Enhanced cellular uptake. Higher induction of apoptosis. Improved induction of S-phase arrest. Improved tumour growth inhibition and animal survival. Reduced glucose uptake.	Lu et al., 2020
Hyaluronic acid (HA)-DHA	A549 lung cancer cell line	Improved cytotoxic effect (IC_{50} not reported). . Enhanced cellular uptake. Higher induction of apoptosis via the mitochondrial pathway (change in mitochondrial membrane potential).	Kumar et al., 2019
DHA-loaded magnetic nanoparticles (MNP-DHA)	MCF-7, MCF-7/ADR, MDA-MB-231, and MDA-MB-453 breast cancer cell lines	Improved cytotoxic effect and potency (IC_{50}: 26.10 vs 7.76 µg/mL). Elevated ROS.	Guo et al., 2019
PLGA-chitosan coated DHA NPs	KB cervical cancer (Hela) subline and HL-60 leukaemia cell line	Improved cytotoxic effect (KB IC_{50}: 2.79 ± 0.07 vs 0.24 ± 0.05 µg/mL and HL-60 IC_{50}: 2.90 ± 0.03 vs 0.22 ± 0.03 µg/mL). Higher induction of apoptosis	Nguyen et al., 2019
Pectin-DHA	4T1 and MCF-7	Improved cytotoxic effect (4TI	Liu et al., 2018

conjugate	breast cancer cell lines. Tumour bearing mice. Tumour xenograft model	IC_{50}: 6.19 ± 0.51 vs 0.77 ± 0.01 µg/mL and MCF-7 IC_{50}: 7.35 ± 0.77 vs 0.12 ± 0.03 µg/mL). Improved drug delivery to the cancer cells. Prolonged blood circulation Improved tumour growth inhibition and animal survival. Reduced IgE concentration.	
Eight-arm PEG-DHA NPs	LLC and A549 lung cancer cell lines. Normal mice Tumour xenograft model	Improved cytotoxic effect (IC_{50} not reported). Increased cellular uptake. Prolonged blood circulation Improved tumour growth inhibition and animal survival. Maintained IgE levels.	Liu et al., 2016
PLGA-PEG-DHA NPs	4T1 breast cancer and 3T3 fibroblast normal cell lines Sprague-Dawley rats Tumour bearing mice	Tumour-specific cytotoxic effect (IC_{50} not reported). Increased cellular uptake in the cancer cells. Prolonged blood circulation Enhanced drug accumulation in tumour. Improved tumour growth inhibition and tumour cell apoptosis.	Li et al., 2020
DHA magnetic liposomes	Hep-2 and Cal-27 head and neck squamous cell carcinoma cell lines. Male Balb/c nude mice	G_1/G_0, S, and G_2/M phase arrests. Higher induction of apoptosis Improved tumour growth inhibition. Higher induction of apoptosis (elevated caspase 3) Improved drug delivery	Li et al., 2019
Alkyl-glycoside DHA liposomes	HepG2 liver cancer and HL7702 normal liver cell lines	Tumour-specific cytotoxic effect. Enhanced tumour targeting.	Shen et al., 2020

	Tumour xenograft model	Improved tumour growth inhibition and animal survival. Prolonged blood circulation. Enhanced tumour targeting with no notable histological effect on surrounding tissues.	

1.2.3. Apoptosis evasion: a crucial hallmark of cancer

At least 14 cancer hallmarks have been identified, including evading cell death. This hallmark is discussed in detail in the following sections.

Introduction to cell death

Multicellular organisms require cell death for the physiological benefit of growth and development (Chen et al., 2018). It is also a necessary process to eliminate unwanted, damaged, or transformed cells and due to cell-specific signalling pathways (Green & Llambi, 2015). Morphologically, there are three modes of cell death, type I (apoptosis), type II (autophagy) and type III (necrosis) (Golstein & Kroemer, 2007; Chen et al., 2018). Type I or apoptotic cell death is important in this study. However, a brief overview of the characteristics associated with cell death types II and III is also provided.

Autophagy is a cell death mechanism that links proteins and organelles to lysosomes for degradation (Chen et al., 2018). Autophagy can be primarily seen in immune cells with an immune reaction against invaders such as whole pathogens, viral genome and/or microbial proteins presented as antigens to phagocytotic cells for clearance (D'Arcy, 2019). Under normal circumstances, autophagy is essential for recycling cellular components (Chen et al., 2018; D'Arcy, 2019). Three autophagic mechanisms have been documented in literature known as (1) *macroautophagy*: results in degradation and recycling of cellular material due to fusion of autophagosomes and lysosomes, (2) *microautophagy*: lysosomes directly engulf the cellular material without the need of vesicles and (3) *chaperone mediated autophagy*: involves the interaction of heat shock proteins and their chaperones which results in protein degradation and recycling (Gracio et al., 2017; Santana-Codina et al., 2017; Lim et al., 2021). Macroautophagy has been found to have a dual effect against cancer cells (Yang et al., 2011; Santana-Codina et al., 2017). In early stages of tumour formation, macroautophagy acts as a tumour suppressive process that inhibits cancer cell survival by discarding cells with damaged DNA, excessive ROS levels and mitochondrial dysfunction (Karakas and Gozuacik, 2014; Gracio et al., 2017; Santana-Codina et al., 2017). However, in later tumour stages, it

helps cells survive under unfavourable conditions (hypoxic, growth factor deprivation and reduced nutrient supply) through prevention of anoikis thereby promoting tumour invasion and metastasis (Yang et al., 2011; Karakas and Gozuacik, 2014; Gracio et al., 2017). For PDAC, which possesses a *KRAS* activating mutation, autophagy maintains tumour growth through provision of ATP under basal conditions (Yang et al., 2011; Gracio et al., 2017; Santana-Codina et al., 2017).

Necrosis is unregulated, accidental cell death due to non-specific cellular stressors. It is characterised by cell swelling, organelle expansion, random DNA degradation, rupturing of the plasma membrane and release of cellular contents, which trigger an inflammatory response and damages tissues (Syntichaki and Tavernarakis, 2002; Proskuryakov et al., 2003; Chen et al., 2018; D'Arcy, 2019).

Unlike necrosis, which is unregulated, apoptosis is a type of programmed cell death characterised by cell shrinkage, chromatin condensation, nuclear fragmentation, subsequent rounding up of the cell, and formation of apoptotic bodies, which eventually get engulfed by phagocytotic cells, thus preventing any inflammatory reaction (Chen et al., 2004; Jiao et al., 2007; Green & Llambi, 2015; Chen et al., 2018). There are two different pathways, namely the extrinsic (death receptor) and intrinsic (mitochondrial) pathways (Ali-Seyed et al., 2016). The extrinsic pathway of apoptosis is triggered by ligands such as Fas (FasL), tumour necrosis factor-alpha (TNF-α) or tumour necrosis factor-related apoptosis-inducing ligand (TRAIL) binding to their respective receptors, namely Fas, TNFR, death receptor 4 or 5 (DR4/5). Therefore, successful ligand-receptor interactions result in the recruitment of adaptor proteins, namely Fas-associated (FADD) or TNF-associated death domain (TRADD) and procaspase 8 (Ali-Seyed et al., 2016; Szegezdi & Leverkus, 2016; Lafont et al., 2018). Members of the **c**ysteine-**asp**artic acid prote**ase** (caspase) family are typically expressed as inactive forms (procaspase) and must be cleaved to become active (caspase). Therefore, activated caspase will produce an effect dependent on the cell type. In type I cells, sufficient caspase 8 is available to activate executioner caspases (3,6, and/or 7). The caspase 8 signal is low in type II cells and requires amplification to reach the executioner caspases. This occurs through the cleavage of Bid, a pro-apoptotic protein of the Bcl-2 family, to truncated Bid (tBid) that translocates to activate the mitochondrial pathway (Chen et al., 2018). Mice knockout studies have shown that lymphocytes within thymus glands are Type I cells while hepatocytes are Type II. Although this is still under debate, numerous cancer cell lines

possess Type I-like (SW480 and H460) or Type II-like (HCT116) characteristics as showed by Ozoren and El-Deiry (2002).

In the intrinsic pathway of apoptosis, a signal such as cellular stress, reactive oxygen species or DNA damage disrupts the mitochondrial membrane potential. This also aids the oligomerisation of Bax/Bak, forming a pore that releases mitochondrial components such as apoptosis-inducing factor (AIF), cytochrome c, and second mitochondria-derived activator of caspase/ direct inhibitor of apoptosis (IAP) binding protein with low pI (Smac/DIABLO) (Ali-Seyed et al., 2016; Zhang et al., 2019). Cytochrome c interacts with dATP, apoptosis protease activating factor 1 (Apaf-1) and procaspase 9, forming a complex known as the apoptosome that leads to the autoactivation of procaspase 9 to caspase 9, which then activates procaspase 3 to caspase 3, leading to apoptosis (Chen et al., 2018; D'Arcy, 2019). Figure 1.4 is a schematic diagram summarising both apoptosis pathways, showing the convergence of the extrinsic and intrinsic pathways at effector caspase 3, leading to apoptosis.

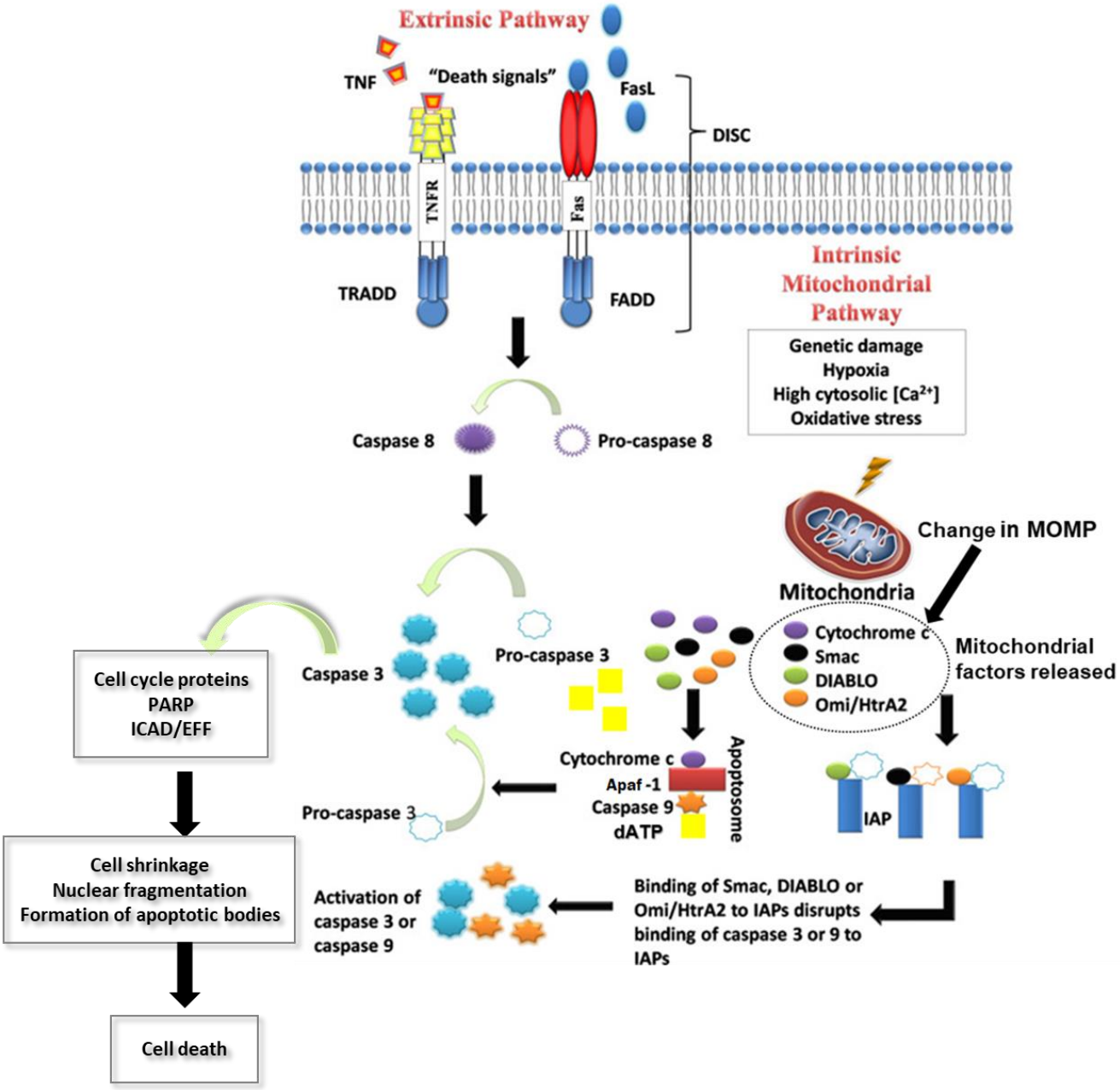

Figure 1.4: Death receptor and mitochondrial pathways of apoptotic cell death. In the death receptor pathway, ligands bind to their respective cell surface receptors leading to a DISC complex (ligated Fas/TNF to its receptor, adaptor molecules and procaspase initiator caspase 8) that activates caspase 8 protein. Intrinsic apoptosis occurs because of cellular stresses that disrupt the outer mitochondrial membrane potential, releasing factors residing in the inter-mitochondrial space, further activating caspases, and leading to apoptosis. (Obtained from Wong et al., 2011 – Open Access Article that permits using the original work under the Creative Commons BY 2.0 (https://creativecommons.org/licenses/by/2.0/). Modifications to this image include indication change in mitochondrial outer membrane permeabilisation (MOMP), inserting a dashed circle around cytochrome c, Smac, DIABLO, and Omi/HtrA2 and labelling them as mitochondrial factors released, and addition of dATP molecules to the apoptosome complex.

Evasion of apoptosis in cancer cells

Dysregulation of apoptosis has been reported in many diseases, where it can be excessive (neurodegenerative disorders and autoimmune diseases) or evaded (cancer) (Singh, 2007). Many mechanisms of evasion are employed by cancer cells to favour survival. The first mechanism is the disruption of the balance between pro- and anti-apoptotic proteins, where proteins that inhibit apoptosis will be upregulated while pro-apoptotic proteins are inhibited, favouring cell survival (Wong, 2011; Wagh & Bose, 2019). The B-cell lymphoma 2 (Bcl-2) family comprises structurally related proteins that interact to either inhibit or activate apoptosis (Wagh & Bose, 2019). The proapoptotic activators are made up of proteins that possess 3 of the four Bcl-2 homology domains, Bcl-2-associated X protein (Bax) and Bcl-2 homology antagonist/killer (Bak), and those that only have the third Bcl-2 homology domain (BH-3 only) which include p53 upregulated modulator of apoptosis (Puma), BH3 interacting-domain death agonist (Bid) and Bcl-2 associated agonist of cell death (Bad), among others (Farghadani & Naidu, 2022). Pro-apoptotic effectors, such as Bax and Bak, can form the pore in the outer mitochondrial membrane necessary for the intrinsic pathway (Wong, 2011). The anti-apoptotic proteins (possess all four Bcl-2 homology domains) include Bcl-2, B-cell lymphoma-extra large (Bcl-X_L) and myeloid leukaemia 1 (Mcl-1), which inhibit apoptosis (Wong, 2011). Wuillème-Toumi and colleagues assessed expression profiles of anti-apoptotic Mcl-1 protein in multiple myeloma (MM) patients (Wuillème-Toumi et al., 2005). Their results showed that Mcl-1 is overexpressed in MM patients. This correlated with progression, the severity of the diseases and poor clinical outcomes (reduced survival) (Wuillème-Toumi et al., 2005). Similar upregulation of anti-apoptotic Bcl-2 members associated with the downregulation of pro-apoptotic proteins has been reported in several tumour types (Taniai et al., 2004; Kelly & Strasser, 2011; Wong, 2011; Thomas et al., 2013; Delbridge & Strasser, 2015; Inoue-Yamauchi et al., 2017).

The mutation in *TP53* that leads to loss-of-function of the gene product (p53 protein) has been reported in more than 50% of cancers (Wang & Sun, 2010; Ge et al., 2019). The p53 protein is an important activator of the mitochondrial pathway of apoptosis as it is known to target and activate p53-regulated apoptosis-inducing protein 1 (AIP1), Puma, Noxa, and Bax, as a response mechanism to detected DNA damage. This triggers mitochondrial outer membrane permeabilisation (MOMP) disruption and release of cytochrome c (Ozaki & Nakagawara, 2011; Aubrey et al., 2018). The protein can also activate Apaf-1 and cytochrome c, members of the apoptosome complex crucial for initiating intrinsic apoptosis

by activating caspase proteins (Aubrey et al., 2018). In cancer, since the mutation in the gene results in a loss of function, all these processes are inhibited as an evasion mechanism of cancer cells (Feroz & Sheikh, 2020). Another set of anti-apoptotic proteins known as the inhibitors of apoptosis proteins (IAPs) directly prevents the functioning of caspase proteins by binding to them, inhibiting their interactions with target substrates necessary to induce apoptosis (Hunter et al., 2007). In several cancer types, overexpression of survivin, a type of IAP, leads to the survival and hence proliferation and progression of transformed cells (Nachmias et al., 2004; Liang et al., 2020).

Another evasion mechanism cancer cells employ is defective receptor signalling, either by overexpression of decoy receptors or solubilisation of the Fas ligand receptor (Wong, 2011; Wagh & Bose, 2019). The expression of the differentially spliced cellular-FLICE inhibitory protein (c-FLIP) inhibits the formation of the DISC by binding to the ligand-receptor complex. However, it lacks the death effector domain necessary for procaspase 8 and FADD or TRADD adaptor molecule binding (Thapa et al., 2022). Studies have shown that cFLIP overexpression in cancer cells is associated with the accumulation of procaspase 8 and 3, indicative of direct inhibition of apoptosis (Riley et al., 2013; Tenev et al., 2001). All these evasion strategies are summarised in Figure 1.5 below.

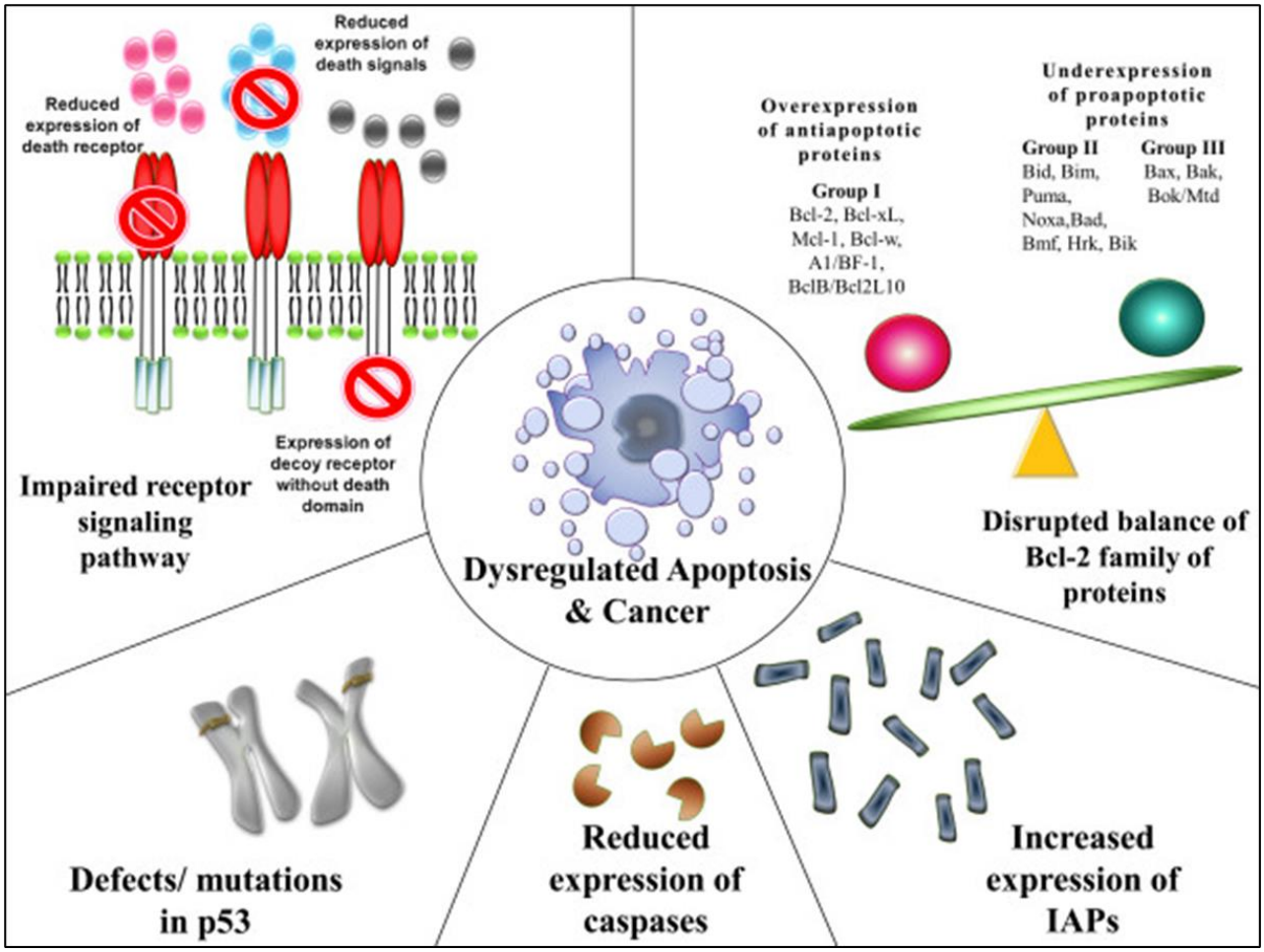

Figure 1.5: Apoptosis evasion mechanisms in cancer. Cancer cells exhibit several evasion mechanisms that aid survival (overexpression of anti-apoptotic factors and impaired death receptor signalling) and bypass necessary checkpoints that might repair damaged or mutated DNA (mutations in p53). Obtained from Wong et al., 2011 – Open Access Article that permits using the original work under the Creative Commons BY 2.0 (https://creativecommons.org/licenses/by/2.0/). No modifications were made to this figure.

1.3. Study Rationale

Despite an improved understanding of pancreatic cancer biology and the growing availability of different chemotherapeutic regimes for treatment, the rates of mortality closely parallel incidence (Puri & Saif, 2014). Furthermore, the disease is associated with a poor prognosis with a five-year survival of about 11% (Siegel et al., 2021). Most of the available chemotherapy is non-specific and cytotoxic for both normal and cancerous cells resulting in adverse side-effects (Brigger et al., 2012). The drugs have poor solubility due to their hydrophobic nature and differential pharmacokinetics (Wan et al., 2018). Furthermore, PC still proves resistant to these drugs. Natural compounds with promising anticancer and pro-apoptotic characteristics have been tested against this aggressive malignancy. Like synthetic

compounds, phytochemicals are associated with poor solubility, inability to cross the plasma membrane and reduced therapeutic indices. Polymer-drug conjugation promises to circumvent these limitations, thereby increasing the therapeutic index and potentially improving the apoptosis-induction of the free compounds (Kost & Langer, 2012; Wan et al., 2018). In a previous study in our laboratory, we showed dose-dependent cytotoxicity and a low IC_{50} value for PEG-BA treatment when compared to the free drug, BA, in MIA PaCa-2 cells. Apoptosis induction and anti-inflammatory activity were also improved due to conjugation (Fru et al., 2021). Although these results are promising for pancreatic cancer treatment, the mechanism by which these conjugates induced cell death was still unclear. Understanding the cell death mechanism can provide insight into the conjugates' potential targets and the improved activity of the free drug resulting from conjugation. This knowledge can be used modify the conjugate to be even more efficient. The present study seeks to elucidate the mechanism of cell death and potentially show how polymer-drug conjugates may affect cancer cell survival.

1.4. Aims and Objectives of the Study

1.4.1. Aim

The study aims to determine the mechanism of cell death induced after treating a pancreatic cancer cell line (MIA PaCa-2) with betulinic acid and dihydroartemisinin polymer-drug conjugates (PEG-BA and PEG-DHA).

1.4.2. Study objectives

- To determine cell death inducing effect of PEG-BA and PEG-DHA on pancreatic cancer (MIA-PaCa-2) and non-cancerous (Vero) cells using 3-(4,5-dimethylthiazol-2-yl)-2,5-diphenyltetrozolium bromide (MTT), 2,3-Bis-(2-methoxy-4-nitro5-sulfophenyl)-2H-tetrazolium-5-carboxanilide salt (XTT) and flow cytometry-based assays.
- To investigate the expression of apoptotic genes (*TNF, TNFSF10, BAX, BID, CASPASE 2, CASPASE 3, CASPASE 7* and *CASPASE 8)* involved in both the intrinsic and extrinsic pathways using real-time polymerase chain reaction (PCR) after treatment with BA and PEG-BA.
- To determine the antioxidant potential of the conjugated compounds using 2,2-diphenyl-1-picrylhydrazyl (DPPH) and N, N′-diethyl-1,4-phenylenediamine (DEPPD).
- To assess the effect of BA and PEG-BA treatment on the apoptosis evasion mechanism of MIA PaCa-2 cells using NF-κB/p65 enzyme-linked immunosorbent assay (ELISA).

Figure 1.6 shows the techniques used in this study, starting with cytotoxicity studies (MTT/XTT), from which 50% inhibitory concentrations were calculated for a range of concentrations (0.78-100 µM). Concentrations around the IC_{50} value (½ IC_{50}, IC_{50} or 2x IC_{50}) ranging from those obtained in this study and the study by Mthimkhulu et al (2019) were then used to determine the ROS status, mode of cell death induced by the compounds, the effect on cell cycling, apoptosis-related gene expression, morphological changes and the mechanism of apoptosis evasion relative to NF-κB post-treatment. The reason for this was to closely compare the results using the different assays used in the different projects to further delineate the effects of polymer conjugation against pancreatic cancer cells. It should be noted that most of these findings were recently published (Mosiane et al., 2023). These include the cell cycle, antioxidant, reactive oxygen species, real-time PCR and the NF-κB findings for BA and PEG-BA on MIA PaCa-2 cells.

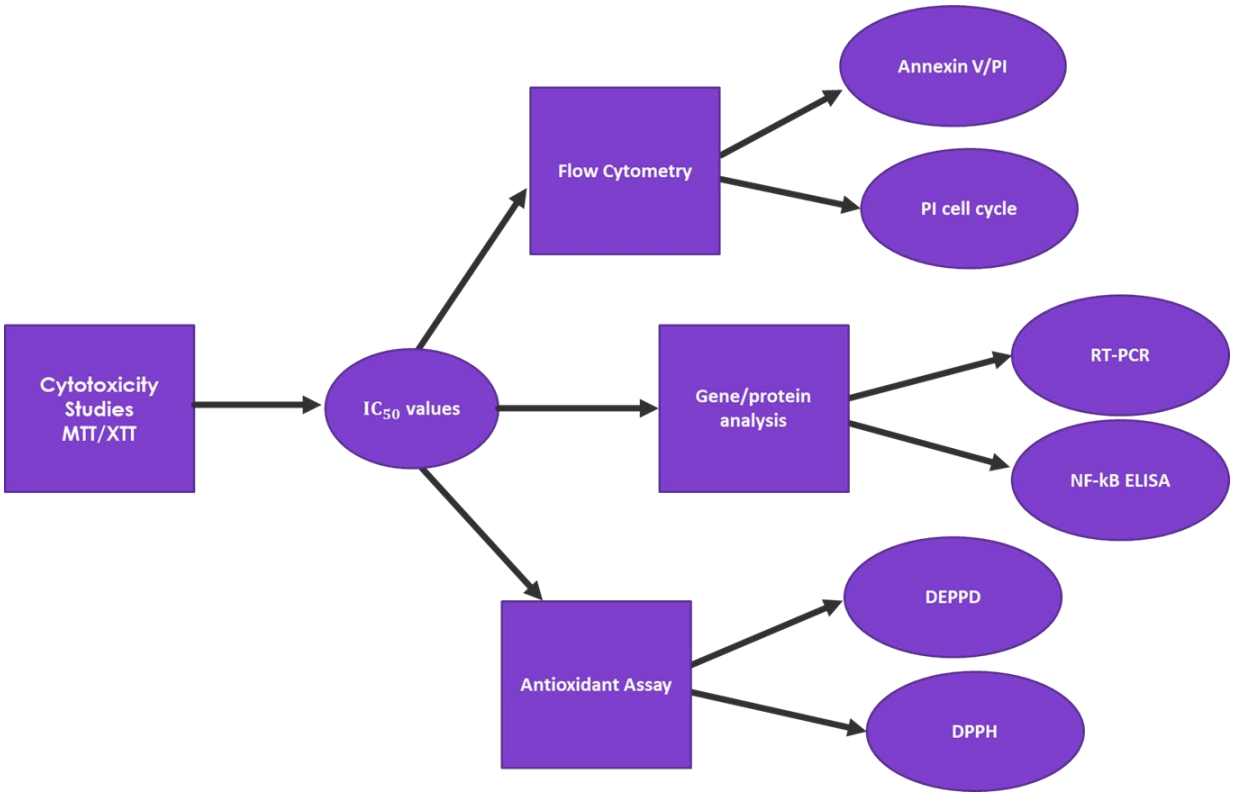

Figure 1.6: Schematic diagram representing the laboratory techniques used to determine the anticancer and cell death mechanisms of the free drugs and complimentary polymer conjugates. Certain assays were only performed for BA and PEG-BA which was generally more promising than DHA and PEG-DHA.

CHAPTER 2

DETERMINATION OF CYTOTOXICITY EFFECT AND ANTIOXIDANT POTENTIAL

2.1. Literature Review

Cytotoxicity is defined as the degree to which a substance can cause cellular damage (Mukherjee, 2019). Cytotoxic agents are used to treat cells with characteristic uncontrollable proliferation, such as cancer cells, to induce growth inhibition. After treatment with these agents, the cells may undergo various forms of cell death, including necrosis, apoptosis, and autophagy or stop actively growing and dividing to decrease cell proliferation (Çelik, 2018; Salih Istifli et al., 2019). The cytotoxic effect that has been induced can be measured to test the activation of cell death, and this is done using viability/cytotoxicity assays. These assays screen drugs based on their pharmacological activity to determine potency and specificity (Mukherjee, 2019). Betulinic acid has shown promising anticancer potential against cervical cancer, melanomas, carcinomas, leukaemia, and blastoma (Fulda, 2008; Ali-Seyed et al., 2016). A second drug, dihydroartemisinin, has also shown promising therapeutic indices against pancreatic and lung cancer cell lines (Mu et al., 2008; Wang et al., 2011). Both drugs have been conjugated to several polymers to improve their cytotoxic effect. These drugs and their complimentary polymer-drug conjugates were assessed using tetrazolium salts which are metabolic activity viability assays that detect the cellular redox potential using a colorimetric method (Weyermann et al., 2005). In addition to cytotoxicity, assessing morphological characteristics after treatment can be an important measure of cell death. Several features can be used to differentiate necrotic from apoptotic cells using microscopy (Hu et al., 2021). Apoptotic cells lose junctions with neighbouring cells, shrink, and become more rounded with an intact plasma membrane. Necrotic cells are characterised by cell swelling and plasma membrane rupture (Belashov et al., 2019; Hu et al., 2021). In this study, light microscopy was used to assess the morphology of MIA PaCa-2 cells after treatment.

Another vital feature assessed in promising chemotherapeutic drugs is their antioxidant potential. Antioxidants can be natural or synthetically derived, and they counter the effect of oxidants by impeding their interactions with biological molecules and by oxidation-repair mechanisms (Anggraini et al., 2019; Rubio & Cerón, 2021). Antioxidant inhibition can occur at any of the three levels of oxidative stress: initiation, propagation, and termination (Kedare & Singh, 2011). When the level of oxidants exceeds the level of antioxidants, it results in a phenomenon known as oxidative stress (Mantovani et al., 2002; Kilk et al., 2014). This state

damages membranes and cellular components such as nucleic acids, proteins, lipids, and polysaccharides and alters signalling transduction pathways (Kilk et al., 2014; Rubio & Cerón, 2021). Oxygen, carbon, nitrogen, and sulphur are known to produce species that play an essential role in oxidative stress (Rubio & Cerón, 2021). Of importance are unstable and highly reactive oxygen-derived free radicals called reactive oxygen species (ROS). These reactive oxygen species are known to play a dual role in cancer. ROS induction can be beneficial in cancer treatment, where a potential anticancer drug (prooxidative) can induce recruitment of DISCs and lead to activation of effector caspases (Perillo et al., 2020). Briefly, the elevated ROS has the potential of disrupting the mitochondrial membrane potential, thereby stimulating release of cytochrome c (via the Bax/Bak channel) which then reacts with Apaf-1 and procaspase 9, in the presence of dATP, forming the apoptosome (Perillo et al., 2020). This then results apoptosis. In addition, other modes of cell death such as autophagy and ferroptosis can also be triggered (Perillo et al., 2020). Therefore, prooxidative compounds take advantage of the already elevated ROS in cancer cells and induce a cytotoxic effect that leads to their demise (Kim et al., 2019). On the other hand, it is well-documented that elevated ROS levels are risk factors for many degenerative diseases, such as cancer (Kedare & Singh, 2011; Kilk et al., 2014). An anti-cancer drug with antioxidant potential can be ideal due to the added advantage of combatting inflammation (ROS), potentially blocking cancer progression (Mosiane et al., 2023). ROS, along with the antioxidant potential of the compounds and controls, will be assessed further in this chapter.

2.2. Methods and Materials

2.2.1. Background of compound synthesis

This project collaborated with chemists at the South African Council for Scientific and Industrial Research (CSIR), who synthesised and characterised the polymer-drug conjugates. A detailed synthesis of the compounds has been published (Mthimkhulu, 2019; Mvango et al., 2020). Briefly, the chemical synthesis was done by individually conjugating compounds (BA and DHA) to the polyethylene glycol (PEG) polymer by creating covalent bonds in the form of amide or ester bonds (Pearson & Li, 2017). The conjugates were purified by membrane dialysis, a technique that separates molecules in a solution by restricted diffusion through a semi-permeable membrane with a specific molecular weight cut-off (Cho et al., 2013). Further characterisation was done using proton nuclear magnetic resonance spectroscopy which confirmed the covalent linkage between the drug (either BA or DHA) and PEG and the degree of polymer functionalization (Mvango et al., 2020). The final

products (polymer-drug conjugates) that were formed are shown in Figure 2.1. PEG was chosen as the polymer of choice because its conjugates showed promise over chitosan in a previous project that was performed in our laboratory involving BA and DHA.

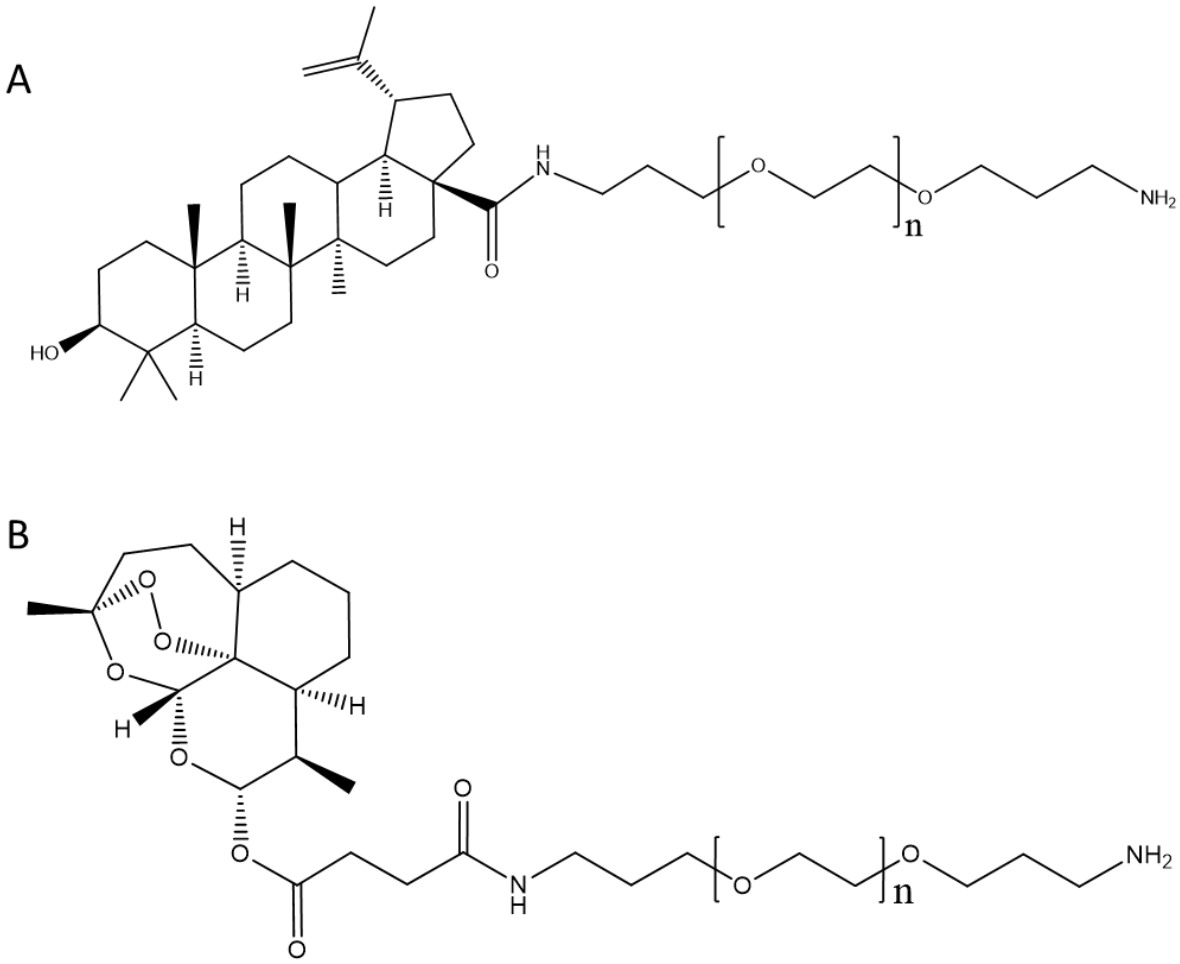

Figure 2.1: Chemical structures of the polymer drug conjugates used in this project. (A) Polyethylene glycol-betulinic acid (PEG-BA) and (B) polyethylene glycol-dihydroartemisinin (PEG-DHA). The structures were drawn using the ChemDraw Ultra software.

2.2.2. Preparation of the compounds for experiments

The compounds (free drugs and conjugates) were dissolved in dimethyl sulfoxide (DMSO) (Sigma-Aldrich, St. Louis, MO, USA) to a concentration of 20 mg/mL. All the compounds were aliquoted in single-use aliquots of 5 µL, 10 µL and 15 µL and stored at -20℃ until needed. For the experiments, each compound was made up of complete medium (Dulbecco's modified Eagle's medium supplemented with 10% foetal bovine serum) to a concentration of 1 mg/mL and further diluted to experimental concentrations of 0.78-100 µM. Different stock concentrations of doxorubicin (200 µg/mL) and gemcitabine (5 mg/mL) were used for the

positive controls. The final experimental control for doxorubicin was 0.2 µg/mL (manufacturer's concentration at which the drug induces apoptosis). In the case of gemcitabine, serially diluted concentrations similar to those used for the compounds (0.78-100 µM) were used. DMSO at a working concentration of 0.33% (similar to the final treated cells) was used as the vehicle control, and cells with media only as the negative control. Ethical clearance was obtained from the University's Human Research Ethics Committee (HREC) in the form of a waiver (W-CBP-200506-1). This is attached as Appendix II.

2.2.3. Cell lines

The cell lines used in this project were MIA PaCa-2 and Vero cells. The MIA PaCa-2 cells were obtained from the Japanese Collection of Research Bioresources (JCRB) Cell Bank (JCRB Cell Bank; Ibaraki, Japan). The MIA PaCa-2 cells are derived from a pancreatic adenocarcinoma found in the tail and body of the pancreas of a 65-year-old man (Deer et al., 2010). Gradiz and colleagues (2016) performed a characterisation study using the MIA PaCa-2 cells. They showed that this cell line has neurotensin and functional somatostatin receptors (SSTR2), which predominate in pancreatic tumours (Gradiz et al., 2016). Vero cells were used for normal cell comparison. Vero cells are derived from the kidney of an African green monkey (*Cercopithecus aethiops*). They are a continuous mammalian cell line used in research for over five decades (Ammerman et al., 2008).

2.2.3.1. Cell maintenance and treatment

Both cell lines were cultured in Dulbecco's modified Eagle's medium (DMEM) with slight modifications in terms of preparation. For the MIA PaCa-2 cells, the DMEM (Sigma-Aldrich, St Louis, MO, USA) was made up to a final concentration of 13.4 g/L with sodium bicarbonate (Sigma-Aldrich, St Louis, MO, USA) dissolved in double-distilled deionised water ($NAHCO_3$ – 3.7 g/L) and supplemented with 1% antibiotic antimycotic solution containing 10 000 units/mL of Penicillin, 10 000 µg/mL streptomycin and 25 µg/mL amphotericin B (Sigma-Aldrich, St Louis, MO, USA). The DMEM (13.4 g/L DMEM powder + 3.7 g/L NaHCO3) was dissolved in sterile double-distilled deionised water for the Vero cells. The medium was supplemented with 1.1 mM sodium pyruvate (Thermo Fischer Scientific, Waltham, MA, USA), 25 mM HEPES buffer (Thermo Fischer Scientific, Waltham, MA, USA), 250 µg/mL gentamicin (Sigma-Aldrich, St Louis, MO, USA), and 0.5% antibiotic antimycotic solution (Sigma-Aldrich, St Louis, MO, USA). The additional

reagents added to the DMEM enabled the Vero cell line to grow. Both media were supplemented with 10% heat-inactivated foetal bovine serum (Celtic Molecular Diagnostics (Pty)Ltd, Cape Town, South Africa).

The cells were cultured in 75 cm^2 vented flasks (Thermo Fischer Scientific, Waltham, MA, USA) and kept in a humidified incubator (95% humidity, 37℃, 5% CO_2). The cells were harvested every 2-4 days or when they reached an 80-90% confluency using trypsin-EDTA dissociation reagent (Sigma-Aldrich, St. Louis, MO, USA). The culture medium was discarded, and the adherent cells were washed using 1x phosphate-buffered saline (PBS: Sigma-Aldrich, St Louis, MO, USA). This was followed by adding trypsin-EDTA (Sigma-Aldrich, St. Louis, MO, USA) and incubating for 2-5 minutes until the cells detached from the flask. The trypsin was inactivated by adding complete culture medium at double the volume of trypsin. The cell suspension was then transferred to 50 mL falcon tubes for centrifugation (200x *g* for 5 minutes). This was followed by resuspension of the pellet with complete medium and cell counting using the trypan-blue exclusion method (Rosli et al., 2015). For experiments, cells were treated with the positive controls (gemcitabine and doxorubicin), DMSO (vehicle control), compounds (free drugs: BA and DHA) and conjugates: PEG-BA and PEG-DHA). The polymer polyethylene glycol (PEG) was only tested for cytotoxicity studies. The cells were incubated for 72 hours in a humidified incubator (95% humidity, 37℃, 5% CO_2).

2.2.4. Cytotoxicity studies using tetrazolium salts

To measure the viability of the cell lines during and after treatment, the 3-(4,5-dimethylthiazol-2-yl)-2,5-diphenyltetrozolium bromide (MTT) and 2,3-Bis-(2-methoxy-4-nitro-5-sulfophenyl)-2H-tetrazolium-5-carboxanilide salt (XTT) assays were used. These tetrazolium salt assays are based on the metabolic activity of viable cells since they affect the activity of the mitochondria, an organelle responsible for producing cellular energy necessary for powering several biochemical processes (Lee et al., 2014; Murphy et al., 2016). The MTT assay was performed as previously described by Hamada et al. (2006) with slight modifications (Hamada et al., 2006). Briefly, after counting cells with a haemocytometer, the cell concentration was adjusted using complete media to $1x10^5$ cells/mL, seeded at a volume of 100 µL in a 96-well plate and incubated overnight to allow the cells to attach before treatment. This was followed by treatment with the free drugs, conjugates, polymer, and standards diluted from the DMSO dissolved stocks with complete media to create serial dilutions from 0.78-100 µM, 0.2 µg/mL for doxorubicin and 0.33% for DMSO. The cells

were then incubated for 72 hours at 37℃ (95% humidity, 5% CO_2). The polymer is ordinarily non-toxic, as confirmed in the literature (Pinzaru et al., 2021) but was also tested separately to confirm this. PEG was assessed at 0.78-100 µM and incubated for 72 hours at 37℃ (95% humidity, 5% CO_2). After incubation, the cells were washed using an Eppendorf centrifuge 5810 R (Eppendorf, Hamburg, Germany) at 277x *g* for 5 minutes. The supernatant was discarded, and 110 µL of the MTT master mix consisting of 5 mg/mL of MTT working solution and complete media at a ratio of 1:10, was added to each well and incubated for 6 hours at 37℃ (95% humidity, 5% CO_2).

The MTT reagent is a yellow-coloured dye that enters the cell membrane and reaches the mitochondria. It is reduced to an insoluble and dark-purple formazan by succinate dehydrogenase (Lee et al., 2014; van Tonder et al., 2015; Mukherjee, 2019). This reduction reaction only occurs in living cells, meaning cell viability can be determined and the cytotoxic effect and potency of the tested compounds on the cells assessed (Lee et al., 2014; van Tonder et al., 2015). The insoluble product forms crystals, which are then solubilised using reagents such as isopropanol, DMSO or SDS in HCl (Lee et al., 2014; Salih Istifli et al., 2019). In this experiment, solubilisation was performed by replacing the MTT-containing media with 100 µL of a hydrochloric acid-isopropanol (1:9) solubilising reagent followed by further incubation at 37℃ (95% humidity, 5% CO_2) for at least 15 minutes. After the incubation, the plate absorbance was measured using a Multiscan Sky spectrophotometer (Thermo Fischer Scientific, Waltham, MA, USA) at a wavelength of 570 nm and a reference wavelength of 650 nm.

In the case of XTT (Sigma-Aldrich, St Louis, MO, USA), the spent media was discarded following centrifugation (200x *g* for 5 minutes) after the 72-hour incubation period, and 125 µL of the XTT master mix containing 100 µL of complete media and 25 µL of XTT working solution was added to each well before incubating for 4 hours at 37℃ (95% humidity, 5% CO_2). This assay did not need a solubilisation step because metabolically active cells convert the water-soluble XTT reagent into a water-soluble, orange-coloured formazan product (Salih Istifli et al., 2019). The intensity of the developed formazan was read using a Multiscan Sky spectrophotometer (Thermo Fischer Scientific, Waltham, MA, USA) at a wavelength of 450 nm and a reference wavelength of 690 nm.

Data analysis: For the cytotoxicity studies, individual assays were performed on different days to four experimental repeats unless stated otherwise. The absorbance data obtained from the plate reader was analysed using Microsoft Excel, and viability was calculated, followed by cytotoxicity determination as shown below in formulas 1 and 2. This was followed by calculating the IC_{50} values by plotting the log concentration against the triplicate readings using GraphPad Prism (v8.0.2.263). The IC_{50} value is the half-maximal inhibitory concentration and represents the concentration at which the compounds will inhibit cell viability by 50% (Aykul & Martinez-Hackert, 2016). The data (graphs and tables) are reported as mean ± standard error of the mean (SEM).

$$Viability = \frac{mean\ absorbance\ of\ sample}{mean\ absorbance\ of\ control} \times 100 \quad (1)$$

$$Cytotoxicity = 100 - viability \quad (2)$$

2.2.5. Microscopic analysis for determining cell death

Apoptosis is characterized by morphological changes such as cell shrinkage, detachment from neighbouring cells (breakdown of tight junctions) and subsequent rounding up of the cell (Green & Llambi, 2015; Chen et al., 2018). These features can be visualised using light microscopy, a technique that dates to the late 1800s and is based on the principle of vision via the lens of the human eye (Yang., 2013). The protocol used was developed after optimisation. Briefly, cells were seeded into 24-well plates at a concentration of $1x10^5$ cells/mL, followed by overnight incubation (37℃, 95% humidity, 5% CO_2). This was followed by treatment with complete DMEM, 0.33% DMSO, and varying concentrations (1, 2, 4 and 8 µM) of BA and PEG-BA only. The morphological changes were photographed after 24, 48 and 72 hours using the Olympus IX51 microscope (Olympus - Life Sciences Solutions, Tokyo, Japan) at 10 X magnification. Brightfield microscopy without phase contrast or differential interference contrast was used and served as a suitable tool to visualise only the structures or outlines of the cells to identify morphological changes (Thorn, 2016). An MTT assay was performed simultaneously to confirm the cytotoxic effect of BA and PEG-BA at 1, 2, 4 and 8 µM according to the protocol described above (Section 2.2.4.), with volumes adjusted to suit the size of a 24-well plate. After the incubation, the plates were analysed using a Multiscan

Sky spectrophotometer (Thermo Fischer Scientific, Waltham, MA, USA) at a wavelength of 570 nm and a reference wavelength of 650 nm. Data analysis commenced as described in Section 2.2.4.

2.2.6. Analysis of antioxidative potential and reactive oxygen species reduction

Although the aetiology of PC is not well-known, inflammation has been described as a significant risk factor. Two assays were used to assess the potential antioxidative capacities of BA and PEG-BA. They were performed using the 2,2-Diphenyl-1-picrylhydrazyl (DPPH) antioxidant assay for the compound activity and the N, N-Dimethyl-p-phenylenediamine (DEPPD) assay for ROS activity in MIA PaCa-2 cells.

2.2.6.1. DPPH Assay

The antioxidant activity of the compounds (BA, DHA, PEG-BA, and PEG-DHA) was assessed using the 2,2-Diphenyl-1-picrylhydrazyl (DPPH) assay. The assay measures the radical scavenging ability of the potential antioxidants (compounds). Unlike other radicals that are unstable and easily dimerise with neighbouring atoms, DPPH is a highly stable radical containing an unpaired valence electron on its nitrogen atom (Sharma & Bhat, 2009; Kedare & Singh, 2011; Anggraini et al., 2019). The delocalised electron gives off a deep violet colour when dissolved in organic solvents such as methanol, ethanol and DMSO (Sharma & Bhat, 2009; Kedare & Singh, 2011). This odd electron can be reduced if it receives a hydrogen atom from the antioxidants converting the DPPH radical to the corresponding hydrazine (Kedare & Singh, 2011). This antioxidant/DPPH radical interaction results in the loss of the violet colour (less violet → dull yellow) directly proportional to the overall antioxidant capacity or free radical scavenging capacity of the compounds (Kedare & Singh, 2011; Garcia et al., 2012; Alvares & Furtado, 2021). Several known antioxidants have been used as the standard for this assay, such as ascorbic acid (vitamin C), butylated hydroxyl toluene, tocopherol, butylated hydroxyl anisole, gallic acid and Trolox (de Menezes et al., 2021). The standard chosen for this assay is ascorbic acid ($AscH_2$). The compounds and standard were tested at varying concentrations of 0.78-100 µM.

The assay was performed with modifications from the protocol by Mistry and Shah (2014). Briefly, 180 µL of distilled water was added to the first nine rows of a 96 well-plate and 100 µL to the remaining wells. This was followed by adding 20 µL of the methanol-dissolved BA, DHA, PEG-BA, PEG-DHA, and $AscH_2$ in the appropriate wells under a fume hood to

prevent the evaporation of the methanol. A two times serial dilution was performed in the plates before adding 100 µL of freshly prepared methanolic DPPH solution (which was diluted to a final concentration of 60 µM) to all triplicate wells except the compound control wells in the dark. The plates were then covered in aluminium foil and shaken on a Titertek microplate shaker (Medical EXPO, Marseilles, France) for 10 minutes, followed by an additional 35-minute incubation in the dark. After incubation, absorbance was measured at 517 nm using a Multiscan Sky microplate reader (Thermo Fisher Scientific, Waltham, MA, USA).

Data analysis: Four experimental repeats were performed for the antioxidant activity (DPPH) assay on different days. The antioxidant potential (AP), which represents the percentage inhibition of DPPH radical of the compounds, was calculated using Formula 3 below. After obtaining the antioxidant potential of the free drugs, polymer-drug conjugates and standard in Microsoft Excel, non-linear regression analysis was performed in GraphPad Prism (v8.0.2.263) to produce dose-response curves to determine IC_{50} values.

$$A.P. = \frac{Absorbance_{control} - Absorbance_{sample}}{Absorbance_{control}} \times 100 \quad (3)$$

2.2.6.2. DEPPD reactive oxygen species activity studies

The ROS reduction potential and oxidative status of the Vero and MIA PaCa-2 cells was determined using the N, N-Dimethyl-p-phenylenediamine (DEPPD) assay. This assay is based on the Fenton reaction that measures the level of hydroperoxides which can be quantified from biological fluids such as serum, urine, plasma, and cell supernatants (Paltrinieri et al., 2010; Hitomi et al., 2022). The assay was performed according to the protocol by Williams with slight modifications (Williams, 2012). Briefly, 140 µL of 0.1 M sodium acetate buffer (pH 4.8) was added to the wells of a 96-well plate. This was followed by the addition of 10 µL of 0.39-50 µM of the standard (hydrogen peroxide (H_2O_2)) and cell supernatants [negative control (media only), vehicle control (DMSO), standard (doxorubicin) and 2xIC_{50} (selected after optimisation of the assay) of gemcitabine, BA, DHA, PEG-BA, and PEG-DHA]. Then, 100 µL of R_1/R_2 solution, made up of 100 µg/mL DEPPD (R_1) and 4.37 µM $FeSO_4$ (R_2) at a ratio of 1:25, was added to all wells, except the blank. The plate was

covered with aluminium foil paper for at least 1 minute, and absorbance readings were obtained using a Victor™ X3 model 2030 multilabel plate reader (PerkinElmer, Waltham, MA, USA) at a wavelength of 505 nm with a kinetic loop of 30 readings per well.

According to Fenton's reaction, proteins release transition metals such as iron at an acidic state that catalyses the conversion of hydroperoxides (ROOH) present in the sample to alkoxy (RO^-) and peroxy (ROO^-). These newly formed radicals can oxidise the alkyl-substituted aromatic amine (DEPPD radical), forming a stable radical cation that can be quantified using spectrophotometry (Cornelli et al., 2001). The intensity of the developed coloured radical is directly proportional to the concentration of hydroperoxides in the sample, following the Beer-Lambert Law (Fabjan et al., 2018; Hitomi et al., 2022).

Data analysis: Three experimental repeats were performed on different days for the DEPPD (ROS) assay. A hydrogen peroxide-derived standard curve was used to extrapolate the concentration of hydroperoxides present after each treatment. The formula was developed by introducing a linear trendline (MS Excel) on the standard curve using the formula of the trendline. The data is presented as mean ± SEM.

2.2.7. Statistical analysis

The distribution of the data was first assessed using the four normality tests (Shapiro-Wilk (W), Anderson–Darling (A2*), D'Agostino–Pearson omnibus (K2), and Kolmogorov–Smirnov (distance)) provided in the GraphPad Prism software (GraphPad, San Diego, CA, USA). Normality was assessed by plotting Q-Q plots assuming that predicted residual vs actual residual will form a roughly straight line for normally distributed data. The Student's t-test for normally distributed data (for comparing two groups) and two-way analysis of variance (ANOVA) for comparing three or more groups were used. Tukey's *post hoc* test was also performed where necessary. The Mann-Whitney test (for comparing two groups) and the Kruskal-Wallis test (for comparing three or more groups) were used for non-parametric data, followed by Dunn's *post hoc* test. A p-value of less than 0.05 was considered significant.

2.3. Results and Discussion

2.3.1. Cytotoxicity analysis of the compounds

Cytotoxicity assays performed using XTT or MTT reagents are usually detected using spectroscopy, where a specific wavelength measures the absorbance of the resulting product. The Beer-Lambert law applies, where absorbance is directly proportional to the concentration

of the sample, in this case, the formazan product produced (Kocsis et al., 2006; Abitan et al., 2008; Mayerhöfer et al., 2020). Therefore, the greater the number of live cells for each treatment, the higher the absorbance, suggesting a reduced cytotoxic effect. In this study, the cytotoxicity of the compounds and standard drugs was first assessed using the MTT assay.

Cytotoxicity of gemcitabine on normal and pancreatic cancer cells using MTT

Gemcitabine, a widely used drug for pancreatic cancer treatment, was used as a control. Treating the MIA PaCa-2 cells with gemcitabine (0.78-100 µM) resulted in a higher cytotoxic effect compared to the Vero cells, without statistical significance. (Figure 2.2). The analysis of the IC_{50} values showed that the drug was more potent on the normal cell line compared to the pancreatic cancer cells (7.26 ± 1.66 µM vs 7.63 ± 2.04 µM). This reflects the problems encountered when using gemcitabine as a chemotherapeutic agent for PDAC treatment. As mentioned before, gemcitabine is associated with adverse side effects due to requiring higher doses for therapeutic efficacy (Moysan et al., 2013; El-Sheikh et al., 2021). This is one major reason why alternatives to synthetic medicines, such as gemcitabine, that could potentially be cytotoxic to pancreatic cancer cells while being less toxic to normal cells, are currently being considered (Anderson et al., 2009).

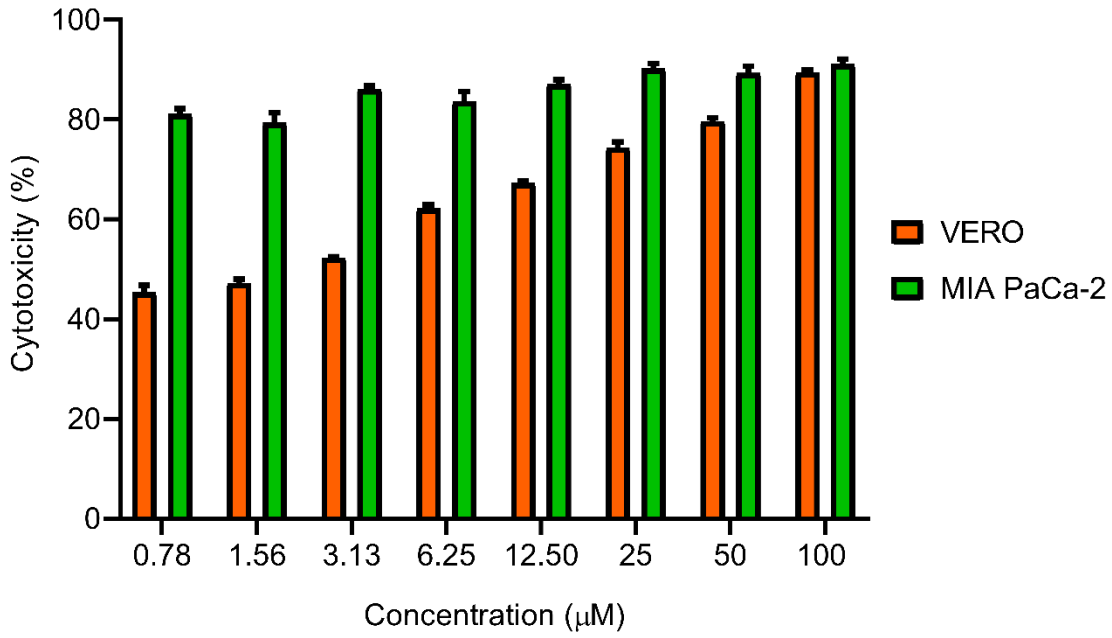

Figure 2.2: Cytotoxic effect of gemcitabine on Vero and MIA PaCa-2 cells after 72 hours using MTT assay. Treatment with varying concentrations (0.78-100 µM) of gemcitabine resulted in a dose-response cytotoxic effect only in the normal cell line. More than 80% cytotoxicity was observed in the

pancreatic cancer cell line at the lowest concentration. The Student's t-test showed no statistical significance ($p > 0.05$) between the two cell lines at the tested concentrations. The results are expressed as mean ± SEM, n=4.

Cytotoxicity of DHA and PEG-DHA using the MTT assay

Compared to the free drug DHA, the conjugate (PEG-DHA) had a dose-dependent cytotoxic effect on Vero cells after the 72-hour treatment. Treating the non-cancerous cells with 50 µM of PEG-DHA induced a cytotoxic effect of 83.21 ± 7.91%, 1.21-fold higher than the cytotoxicity induced by the free drug of (68.64 ± 3.49%; p = 0.0285) (Figure 2.3A). Comparing the IC_{50} values of the free drug and conjugate showed that PEG-DHA was more potent to the normal cell line with 16.96 ± 3.19 µM required to inhibit 50% cell growth (DHA IC_{50}: 20.64 ± 5.14 µM; p = 0.4714). A similar trend to the Vero cells was observed, but to a greater extent, where the conjugate induced a dose-dependent cytotoxicity on the MIA PaCa-2 cells compared to free DHA (Figure 2.3B). In addition, the IC_{50} of PEG-DHA was 10.51 ± 6.13 µM, which was 1.68-fold lower than that obtained for DHA (17.65 ± 6.71 µM; p = 0.4551). These results may suggest an increased potency of PEG-DHA compared to DHA, especially in the MIA PaCa-2 cells. This is not surprising because DHA is associated with low bioavailability, poor solubility, reduced half-life, and uncontrolled release, which affects its overall clinical efficacy. Polymer-conjugation aims to circumvent these issues.

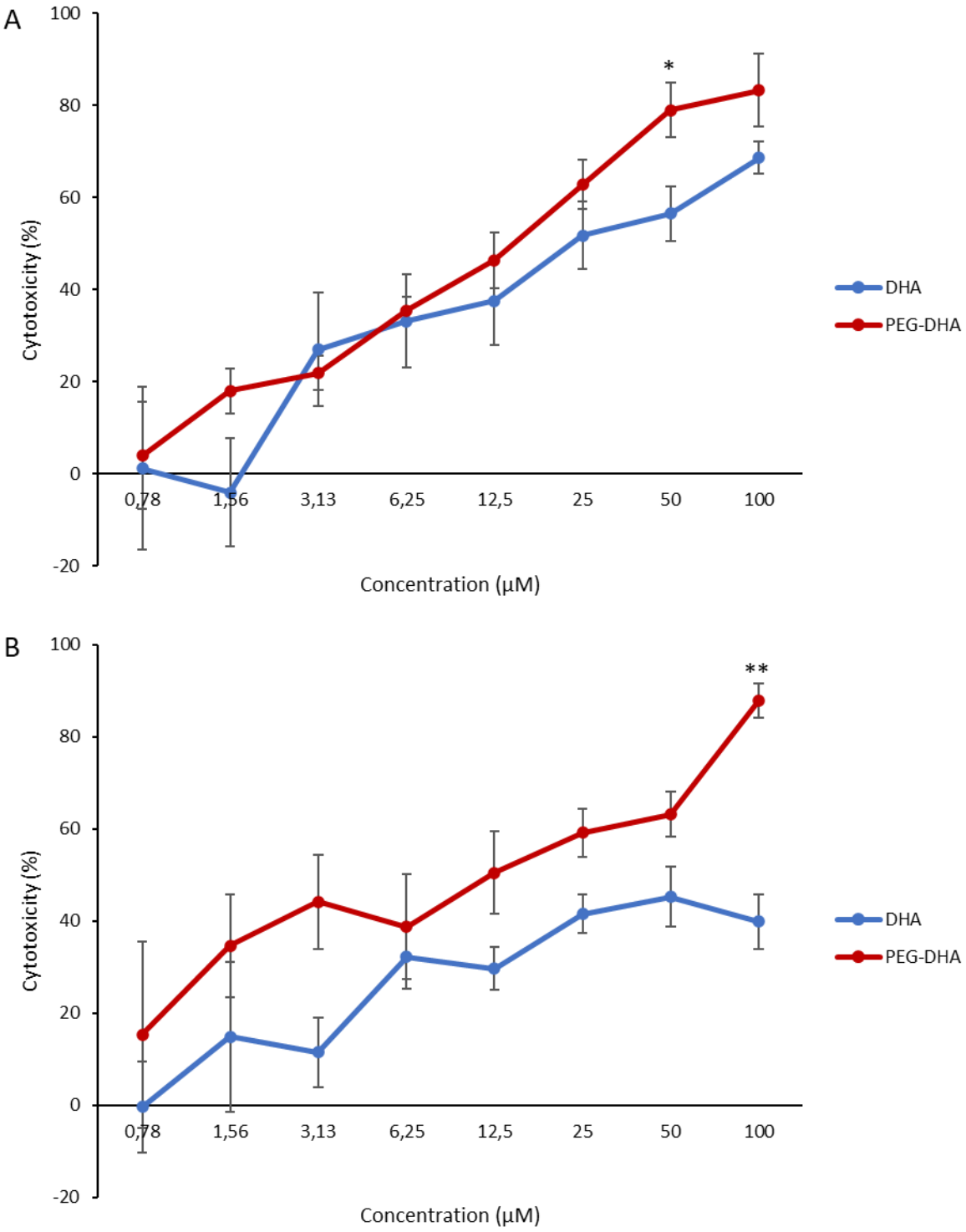

Figure 2.3: Cytotoxic effect of DHA and PEG-DHA on Vero and MIA PaCa-2 cells using the MTT assay. (**A**) Vero cells and (**B**) MIA PaCa-2 cells were treated with varying concentrations (0.78-100 µM) of DHA and PEG-DHA for 72 hours (95% humidity; 37°C; 5% CO_2). The conjugate (PEG-DHA) resulted in higher cytotoxicity than free DHA against both cell lines in a dose-dependent manner. The data are presented as mean ± SEM (n=4). A Student's t-test was used to assess the statistical significance in cytotoxicity between the two drugs: *$p < 0.05$ and **$p < 0.01$.

Other studies have also explored formulations aiming to improve the activity of DHA. Lu et al. (2021) analysed the *in vitro* and *in vivo* effects of DHA/MPEG-PCL nanoparticles against cervical cancer. They reported improved cellular uptake, cytotoxicity, apoptosis induction, cell cycle arrest, higher survival and reduced systemic toxicity in mice models (Lu et al., 2020). In a 2014 paper, Dai and colleagues tested multi-arm PEG-DHA polymer-drug conjugates against lung cancer cell lines (A549 and LLC) and *in vivo* on a C57BL/6 mouse model. Although cytotoxicity analysis showed similar IC_{50} values for DHA and the conjugates, the *in vivo* assays showed that the conjugates, especially the 8-arm PEG-DHA, had prolonged blood circulation and inhibited tumour growth at a higher rate compared to free DHA (Dai et al., 2014). In a previous study performed in our laboratory, similar results were obtained where free DHA had a higher IC_{50} value compared to PEG DHA on the MIA PaCa-2 and Vero cells, suggesting an improved cytotoxic effect and higher potency after conjugation of DHA to PEG (Mthimkulu, 2019).

Cytotoxicity of doxorubicin using XTT

Assessing the cytotoxicity of the second chemotherapeutic drug (doxorubicin), free drug (BA) and conjugate (PEG-BA) using the MTT assay resulted in an underestimation of the compounds' toxicities (as shown in Appendices III and IV). This may be attributed to well-known limitations associated with using the MTT assay to evaluate cytotoxicity (Berridge et al., 2005; Ghasemi et al., 2021). As per the principle of the assay, the disruption of the positively charged quaternary tetrazole ring core reduces the reagent to an insoluble violet formazan by the activity of mitochondrial enzymes (Berridge et al., 2005; Ghasemi et al., 2021). Other biomolecules, such as ascorbic acid, glutathione and its enzyme, azide, cysteine, cyanide, and tocopherols can also cause this reaction to take place (Berridge et al., 2005; Ghasemi et al., 2021; Sarı et al., 2021). This suggests that these compounds can potentially cross-react with the MTT to produce false positive results. The outcome is increased absorbance suggestive of increasing cell viability when the cytotoxicity of doxorubicin, BA and PEG-BA or compounds capable of reducing MTT are assessed (Berridge et al., 2005; van Tonder et al., 2015; Sarı et al., 2021). MTT has been modified by replacing some of the methyl groups in the three surrounding aromatic rings with negatively charged sulfonate groups leading to a better soluble alternative eliminating the need for a solubilising reagent and reducing nonspecific reduction reactions (Berridge et al., 2005). However, this modification influenced the ability of the reagent to cross the plasma membrane, which is

why assays such as the XTT, WST-1, and MTS are always used in conjunction with an electron coupling agent such as 1-methoxyPMS (mPMS) (Berridge et al., 2005).

The XTT assay was further used to assess the cytotoxic effect of doxorubicin, BA and PEG-BA on the Vero and MIA PaCa-2 cells. Treatment with doxorubicin (0.2 µg/mL) showed increased cytotoxicity to the MIA PaCa-2 cells compared to the Vero cell line, although this was not significant (Figure 2.4; $p = 0.819$). While the MTT results may have not shown that the data is more accurate, it is notable that further confirmatory assays using the annexin-V PI kit corroborated this. Doxorubicin is a well-known chemotherapeutic agent used to treat several tumours (Thorn et al., 2011). The recommended concentration (0.2-2 µg/mL) at which doxorubicin induces apoptosis was also obtained as an IC_{50} value by other studies that analysed the cytotoxic effect of doxorubicin on HL-60 human myeloid leukaemia (Faujan et al., 2010), breast cancer cells (Pilco-Ferreto & Calaf, 2016) and pancreatic cancer cells (Bai et al., 2014). These results showed that a low concentration of doxorubicin is required to inhibit the viability of the cells by 50% (Bai et al., 2014).

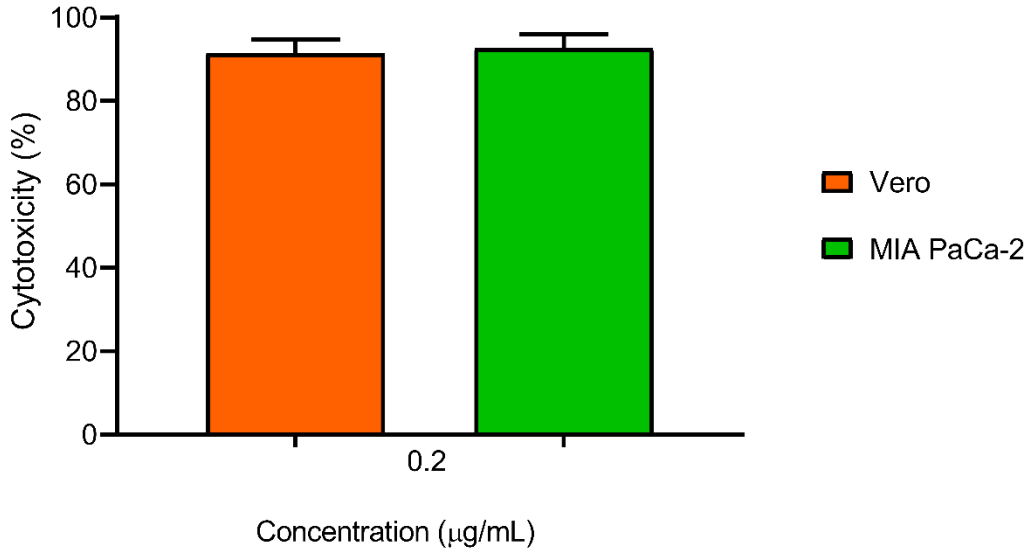

Figure 2.4: Cytotoxic effect of 0.2 µg/mL doxorubicin using the XTT assay. An increase in cytotoxicity was seen for the pancreatic cancer cells compared to the non-cancerous cells (92.58 ± 3.44% vs 91.43 ± 3.18%). However, there was no statistical significance ($p > 0.05$) when the cytotoxicity was compared using a Student's t-test. Results are expressed as mean ± SEM, n=4.

The cytotoxic effect of BA and PEG-BA using the XTT assay

Compared to free BA, the Vero cells were more sensitive to the conjugate PEG-BA, which induced dose-dependent cytotoxicity (Figure 2.5A). A relatively high concentration of 25 µM of BA only resulted in 15 ± 3.13% cytotoxicity on the Vero cells (Figure 2.5A). It was only at concentrations higher than 25 µM (50-100 µM) that a better cytotoxic effect was observed (50 µM: 32.69 ± 2.47% and 100 µM: 84.11 ± 1.27%). Analysis of the IC_{50} showed that 9.02 ± 0.79 µM of PEG-BA was required to kill 50% of the Vero cells, which was 5-fold lower than the IC_{50} obtained for free BA (45.06 ± 6.27 µM; p = 0.0005). Faujan and colleagues (2010) tested BA on normal human lymphocytes and found the IC_{50} was greater than 30 µg/mL (equivalent to 65.69 µM). Similarly, Zuco and colleagues (2002) tested BA on normal fibroblasts and found the IC_{50} was 10.2 µg/mL (equivalent to 22.33 µM). These studies and the present study suggest that BA is not toxic to non-cancerous cells. In contrast, Oladimeji and colleagues (2021) tested BA loaded nanocomplexes and found that free BA had a higher cytotoxic effect and reported an IC_{50} value of 32.4 µM which was more than 2.5-fold lower than that reported for the nanocomplexes on HEK293 (non-cancerous) cells.

The conjugate, PEG-BA, showed an increased dose-dependent cytotoxic effect on the pancreatic cancer cell line compared to free BA (Figure 2.5B). Similarly, a relatively high concentration of 25 µM of BA only resulted in 19.66 ± 5.56% cytotoxicity (Figure 2.5B). Treating the MIA PaCa-2 cells with 3.13 µM of PEG-BA resulted in 37.46 ± 0.23%, which was 13.43-fold higher than the effect induced by BA at the same concentration (2.79 ± 0.70%; p = 0.0229). This trend was observed with increasing concentration. In addition to cytotoxicity, the drug's ability to inhibit 50% MIA PaCa-2 cell growth (IC_{50}) was also assessed. The results showed that PEG-BA had an IC_{50} of 3.01 ± 0.62 µM, and a 13-fold higher concentration of the free BA was required to cause the same effect. Comparing the effect of PEG-BA treatment on the Vero and MIA PaCa-2 cells shows that the conjugate induced cytotoxicity in both cell lines, however to a greater extent in the pancreatic cancer cells, suggesting moderate selectivity.

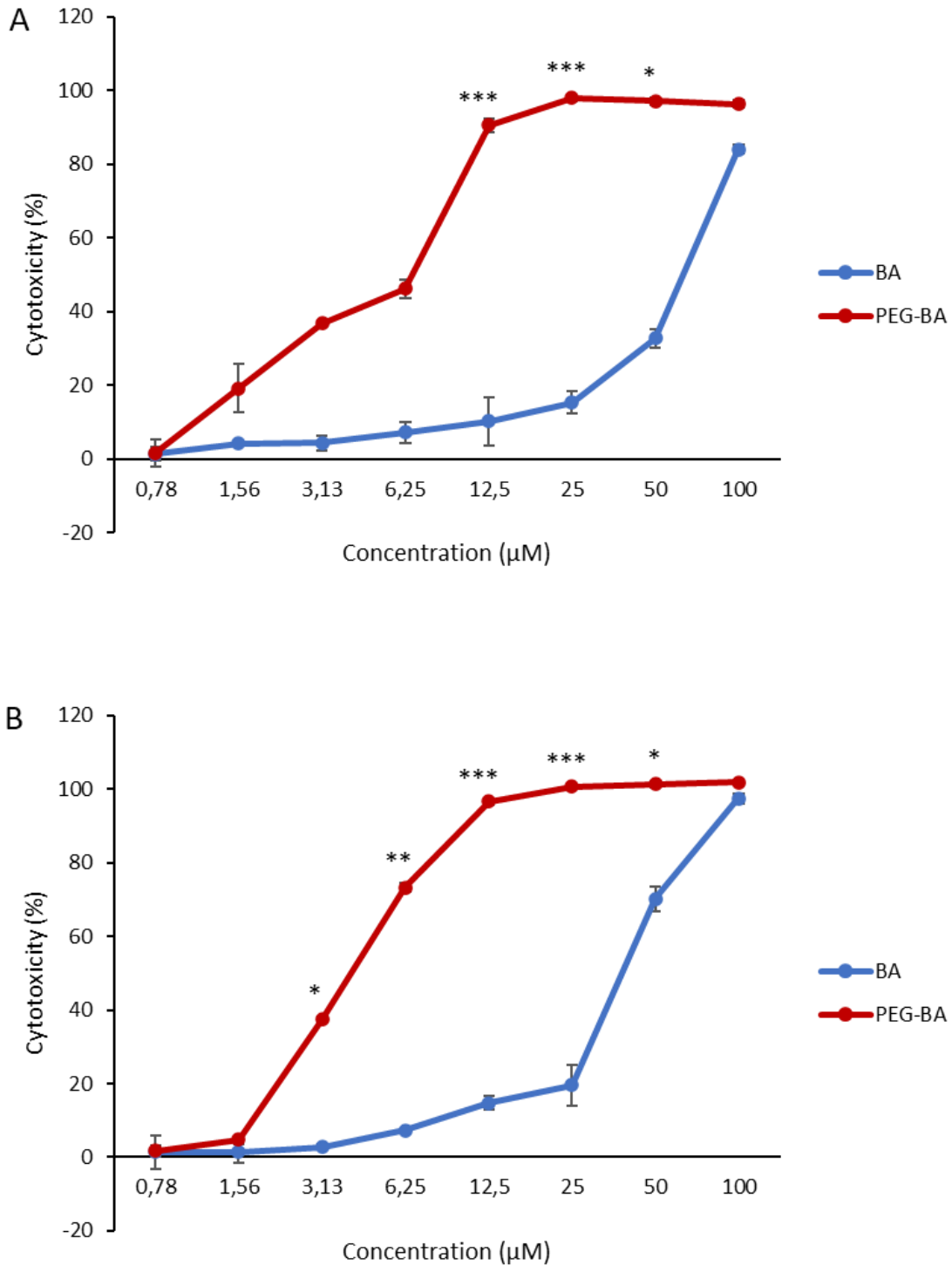

Figure 2.5: Cytotoxic effect of BA and PEG-BA on MIA PaCa-2 cells. (**A**) Vero cells and (**B**) MIA PaCa-2 cells were treated with varying concentrations (0.78-100 µM) of BA and PEG-BA for 72 hours. PEG-BA treatment resulted in dose-dependent cytotoxicity on both cell lines but, to a greater extent, on the pancreatic cancer cells. Furthermore, native BA only demonstrated reasonable cytotoxicity at concentrations greater than 50µM. The data are presented as mean ± SEM (n=4). A Student's t-test was used to assess the statistical significance in cytotoxicity between the two drugs: *$p < 0.05$, **$p < 0.01$ and ***$p < 0.001$.

Formulations that improved the cytotoxicity of BA against cancer cells have been reported in the literature. In 2020, Farcas and colleagues tested BA-magnetoliposomes against breast cancer cells. They found that the BA formulation induced a selective cytotoxic effect against the MDA-MB-231 breast cancer cells under hyperthermal conditions compared to the BA-liposome and free BA (Farcas et al., 2020). Furthermore, a study by Pinzaru and colleagues tested BA-loaded uncoated (SilCo_BA) and PEG-coated (PEG_SilCo_BA) silver nanocolloids against lung and liver cancer cells. The authors found that 10 µM of SilCo_BA induced higher cytotoxicity than PEG_SilCo_BA (33.56% vs 27.95%) on the liver cancer cells (Pinzaru et al., 2021) in a time-dependent manner.

Results from a previous study performed in our laboratory using BA and PEG-BA also showed improved cytotoxicity and potency to MIA PaCa-2 cells compared to the Vero cells (Fru et al., 2021). These studies support the hypothesis that coupling or conjugating BA to a drug delivery platform such as PEG improves its cytotoxicity and potency to cancer cells. In this study, the void polymer, PEG, did not induce any cytotoxic effect on either cell line (as shown in Appendix V), confirming the role of PEG was mainly to aid in drug delivery, which is required to improve the therapeutic index of the DHA and BA (Mathiyalagan et al., 2014; Kumar et al., 2018b; Pinzaru et al., 2021). A similar non-toxic effect has been reported in other studies that used PEG as a polymer (Righeschi et al., 2014; Lu et al., 2020). In addition, minimal to negligent cytotoxicity was observed after treatment with 0.33% DMSO for both assays (appendix VI).

In addition to improved cytotoxicity and potency, PEG-BA improved the selectivity and specificity of BA due to reduced toxicity to non-cancerous cells, a phenomenon that can be quantified using the selectivity index. The selectivity index is obtained by dividing the IC_{50} value of the normal (Vero) cells by the cancer cells (MIA PaCa-2) (Lica et al., 2021). This ratio was assessed for all the compounds and standards except for doxorubicin since only one concentration (0.2 µg/mL) was tested. In all instances, the conjugates had higher selectivity than the free compounds and standard (Table 2.1). Gemcitabine is the only drug that demonstrated undesirable toxicity against non-cancerous cells (SI < 1). BA, DHA, and PEG-DHA induced general toxicity against the cells (1 < SI < 2), and PEG-BA was the only drug that had a desirable and selective cytotoxic effect against the MIA PaCa-2 cells (SI > 2). This targeted cytotoxicity was desirable since an essential characteristic of an anticancer agent is

killing the desired cancer cells with a reduced effect on normal or neighbouring cells (Lica et al., 2021).

Table 2.1: Comparison of IC_{50} values (potency) and selectivity index of free compounds and conjugates against standard gemcitabine.

Test Compounds	50% Inhibitory Concentrations (IC_{50}) µM		Selectivity Index (SI)
	Vero	MIA PaCa-2	
Gem	7.26 ± 1.66	7.63 ± 2.04	0.95
BA	45.06 ± 6.27	40.29 ± 3.60	1.12
PEG-BA	9.02 ± 0.79	3.01 ± 0.62	3.00
DHA	20.64 ± 5.14	17.65 ± 6.71	1.17
PEG-DHA	16.96 ± 3.19	10.51 ± 6.13	1.61

Dose-response curves are attached to appendix VII and VIII.

2.3.2. Effect of BA and PEG-BA on the morphology of MIA PaCa-2 cells

The results obtained in the cytotoxicity analysis showed that PEG-BA was a potent cytotoxic drug against the pancreatic cancer cell line. The free drug, BA and polymer-drug conjugate PEG-BA were chosen for further testing using light microscopy and additional cytotoxicity analysis at 1, 2, 4 and 8 µM. The concentration choice was based on the range of IC_{50} values obtained for this study and previous study by Mthimkhulu and colleagues (2019).

The plated cells were visualised for any morphological changes after treatment with BA and PEG-BA at 24-, 48- and 72-hour intervals using an Olympus light microscope. Assessing the cells at 24 and 48 hours after treatment with 1, 2, 4 and 8 µM of BA showed no noticeable differences to the untreated cells, where most of the cells maintained the characteristic spindle-shape (elongated) of the MIA PaCa-2 cells indicative of viability (Sasaki et al., 2020) as shown in Appendix IX and X. However, the cells started to show some morphological changes, such as rounding or clumps at 2 and 4 µM after 72 hours (Figure 2.6C-D). Pinzaru and colleagues (2021) analysed the effect of BA loaded silver nanocolloids on morphology of liver and lung cancer cells at 10X magnification using brightfield microscopy. The authors presented cell changes characteristic of cell death (cell rounding, loss of adherence to neighbouring cells, and floating cells). Therefore, although most studies use 20 or 40x magnification, morphological changes can be visualised even at 10x magnification which was also used in the present study.

Most of the BA-treated MIA PaCa-2 cells (> 90%) were viable even after 72 hours incubation (2 µM: 4.88 ± 2.42% and 4 µM: 5.55 ± 3.85% cytotoxicity). Studies have shown cell rounding is associated with apoptosis because of the initial detachment from neighbouring cells and shrinkage (Wegert et al., 2011; Anaya-Eugenio et al., 2020). Treating the MIA PaCa-2 cells with 8 µM of BA induced minimal morphological changes in the photomicrographs as most of the cells were still viable. They were numerous attached elongated cells and an insignificant number of cells that were rounded (Figure 2.6E). This was supported by the concurrent MTT assay, which only indicated a marginal increase in cytotoxicity (15.70 ± 5.57%) (Figure 2.6J).

Compared to BA, the conjugate PEG-BA induced morphological changes from spindle-shaped cells to more rounded cells at the lowest concentration of 1 µM (Figure 2.6F). This was associated with a 3.6-fold higher cytotoxic effect when analysed using the MTT assay ($p = 0.0255$). The number of rounded cells increased with time (from 24 to 72 hours), suggesting that PEG-BA induced the formation of clumps of round cells and a cytotoxic effect in a dose and time-dependent manner. When assessing the morphological changes at 2 and 4 µM, most of the MIA PaCa-2 cells had detached from neighbouring cells resulting mainly in clumps of rounded cells (Figure 2.6G-H). Although two populations of elongated cells and clumps of rounded cells were still evident, most of the cells were dying from the treatment, unlike BA (2 µM: 85.72 ± 0.47% vs 4.88 ± 2.42%; $p < 0.0001$ and 4 µM: 93.72 ± 0.47% vs 5.55 ± 3.85%; $p < 0.0001$). At the highest concentration of 8 µM, the elongated cells were no longer visible; only clumps of shrunken, rounded, and detached cells were evident. This was confirmed by the MTT cytotoxicity finding, which was 100% (Figure 2.6I-J).

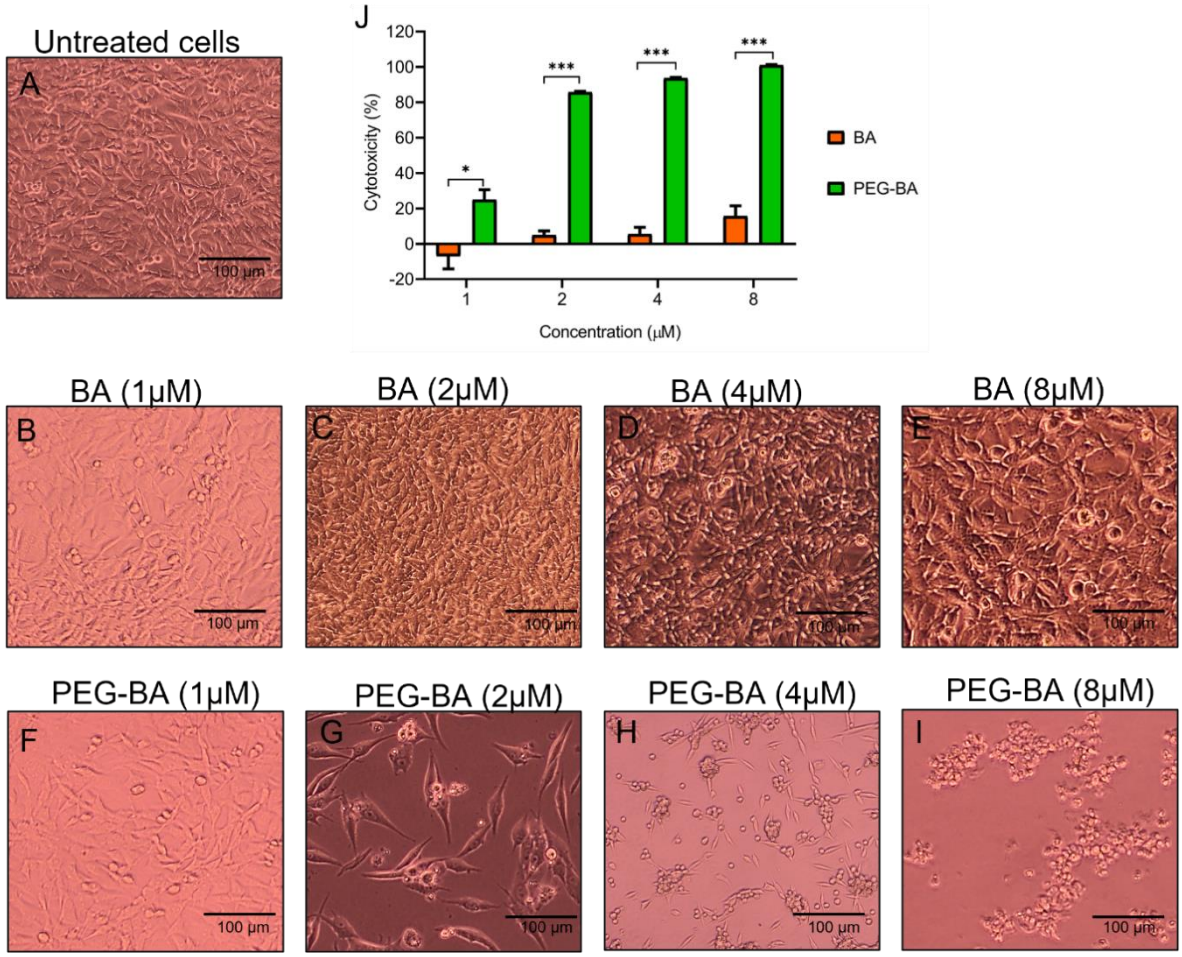

Figure 2.6: Microscopic and cytotoxic analysis of MIA PaCa-2 cells after treatment with BA and PEG BA. The cytotoxic effect was measured using MTT tetrazolium dye after 72 h. (A) Untreated MIA PaCa-2 cells were a reference for the morphological assessment in the MTT assay. (B–E) MIA PaCa-2 cells were treated with various concentrations (1–8 µM) of BA. The cells continued to grow, even at the highest concentration (8µM), although some formed clumps of rounded cells. (F–I) PEG-BA (1–8 µM) treated MIA PaCa-2 cells. The degree of cells rounding up was dose-dependent, where all the plated cells formed rounded clusters at 8 µM. Magnification: 10 X, scale bar: 100 µm. (J) A quantitative bar graph showing cytotoxicity of BA and PEG-BA relative to untreated cells at 72 h (mean ± SEM), n = 3. A Student's t-test was used to assess the statistical significance in cytotoxicity between the two drugs: *$p < 0.05$ and ***$p < 0.001$.

Coricovac and colleagues (2021) assessed the effect of BA (5, 10 and 50 µM) on a human melanoma cell line (A375 cells) after 24 hours by determining the cellular morphology using a light microscope. Their results showed no visible changes in morphology at the lowest tested concentration (5 µM). Increasing the concentration to 10 and 50 µM resulted in a higher percentage of rounded and detached cells, confirming cytotoxicity with increasing concentration (Coricovac et al., 2021). In another study by Xu and colleagues (2014), BA at 15, 30 and 50 µM was tested against cervical cancer (Hela) cells and at least 30 µM was

required to inhibit 50% and 70% of the Hela cells at 48 and 72 hours, respectively (Xu et al., 2014). Both these studies and the present study indicated that higher concentrations of BA are required to fully appreciate the cytotoxic effect of BA, especially at a morphological level.

At 24 and 48 hours, only one population of dead cells was visible (Appendix IX and X). Overall, these results suggested that PEG-BA improved the ability of BA to form clumps of rounded cells which is a crucial feature of apoptosis and not necrosis, evident from the intact plasma membrane and reduction in the size of the cytoplasm (Vorobjev et al., 2015).

2.3.3. Assessing the antioxidant potential of the compounds

In addition to assessing cytotoxicity, the antioxidant potential of the compounds was analysed using the DPPH assay. Medicinal plants are a good source of antioxidants with desirable radical scavenging abilities (Adesanwo et al., 2013; Sati et al., 2013). This property was demonstrated when BA was assessed using the DPPH assay, where the free drug inhibited the DPPH radical, although without any significant changes at all the tested concentrations (Figure 2.7). Comparing BA to PEG-BA showed the conjugate resulted in a dose-dependent inhibition of the DPPH radical (Figure 2.7). At 25 µM, PEG-BA reduced the DPPH radical by 29.17 ± 1.05%, which was 1.4-fold higher than BA (21.30 ± 2.13%, $p = 0.1291$). This trend was also observed at the remaining concentrations (50 µM: 39.57 ± 0.58% vs 24.27 ± 2.91%, $p = 0.0092$, and 100 µM: 36.56 ± 1.86% vs 24.26 ± 3.07%, $p = 0.0279$). The second free drug, DHA, also did not result in a significant change in inhibition of the DPPH radical, and the activity of the drug was improved when it was conjugated to PEG (Figure 2.7). At 6.25 and 12.5 µM, PEG-DHA reduced DPPH by 16.18 ± 1.49% and 19.34 ± 1.07%, which were 1.62-fold (9.98 ± 2.32%, $p = 0.0217$) and 2.71-fold (7.15 ± 2.11%) higher than free DHA. A similar trend was observed with the other concentrations tested with 100 µM of PEG-DHA, resulting in 40.68 ± 2.20% inhibition of DPPH compared to 4.12 ± 2.15% induced by DHA at the same concentration ($p < 0.0001$; Figure 2.7).

This may be due to the presence of phenolic groups, tocopherols or a hydroxyl functional group that can readily donate hydrogen atoms, an essential aspect of the DPPH assay based on the electron transfer ability of potential antioxidants (Adesanwo et al., 2013; Anggraini et al., 2019). Consequently, an increase in the number of hydroxyl groups (-OH) or other hydrogen donating groups (-NH, -SH and others) in the molecular structure can result in higher antioxidant activity (Adesanwo et al., 2013). This means that the antioxidant

properties arise from an increased reactivity of the compounds as electron donors, which give off their hydrogen to stabilise the unpaired electron on the DPPH radical (Adesanwo et al., 2013). An analysis of the molecular structure of ascorbic acid ($AscH_2$) has been reported to be a 2:1 stoichiometry against the DPPH radical, meaning that one vitamin molecule can scavenge two DPPH radicals at a time (Kedare & Singh, 2011; Boulebd, 2020). On the other hand, analysis of the chemical structure of the free drugs shows that DHA has a potential 1:1 stoichiometry against DPPH radical as it can readily give off one hydrogen atom, while BA has a 2:1 stoichiometry. This explains the weaker antioxidant potential of DHA compared to BA. Unfortunately, the scavenging ability can be affected by numerous factors, including poor aqueous solubility (Boulebd, 2020). Polymer drug conjugation can improve solubility without altering the chemical structure of the free drug, which can then result in enhanced antioxidant potential.

In an analysis to determine the compounds' ability to inhibit at least 50% of the initial DPPH concentration (IC_{50}), the free drugs demonstrated IC_{50} values greater than 100 µM, suggesting a lower antioxidant potential than $AscH_2$ (25.58 ± 0.44 µM). Adesanwo and colleagues (2013) made a similar observation where they assessed the antioxidant capacity of BA isolated from *Tetracera potatoria* roots and reported an IC_{50} value of 0.141 mg/ml (equivalent to 309 µM) which is greater than 100 µM. The conjugates resulted in improved antioxidant potential evident from the lower IC_{50} values (PEG-BA: 15.59 ± 0.64 µM and PEG-DHA: 34.65 ± 4.37 µM) compared to the free drugs. This indicates a higher radical scavenging potential for the complimentary polymer conjugates than the free drugs. Among the two conjugates, PEG-BA had a better scavenging ability than ascorbic acid (25.58 ± 0.44 µM; p =0.006). Therefore, the conjugates further improved antioxidant and cytotoxic potential against pancreatic cancer cells. This is an essential parameter for potential anticancer drugs.

It is worth noting that the antioxidant potential of PEG-only was not tested. This is because in polymer drug conjugates, the function of the polymer is to deliver the drug to the target site, protect it from degradation, release adequate amounts of the drug and rapid elimination to avoid systemic toxicity. Polymers that are used in drug delivery systems are usually non-toxic, non-antigenic and non-reactive (Feng and Tong, 2016). These are some of the characteristics of PEG (the polymer used in this study). This suggests that the polymer does not have any effect on any activity that is observed from the drug construct. Therefore, the

increased antioxidant potential is assumed to be due to the drug. The vehicle control induced a minimal antioxidant effect on both the Vero and MIA PaCa-2 cell lines (Appendix XI).

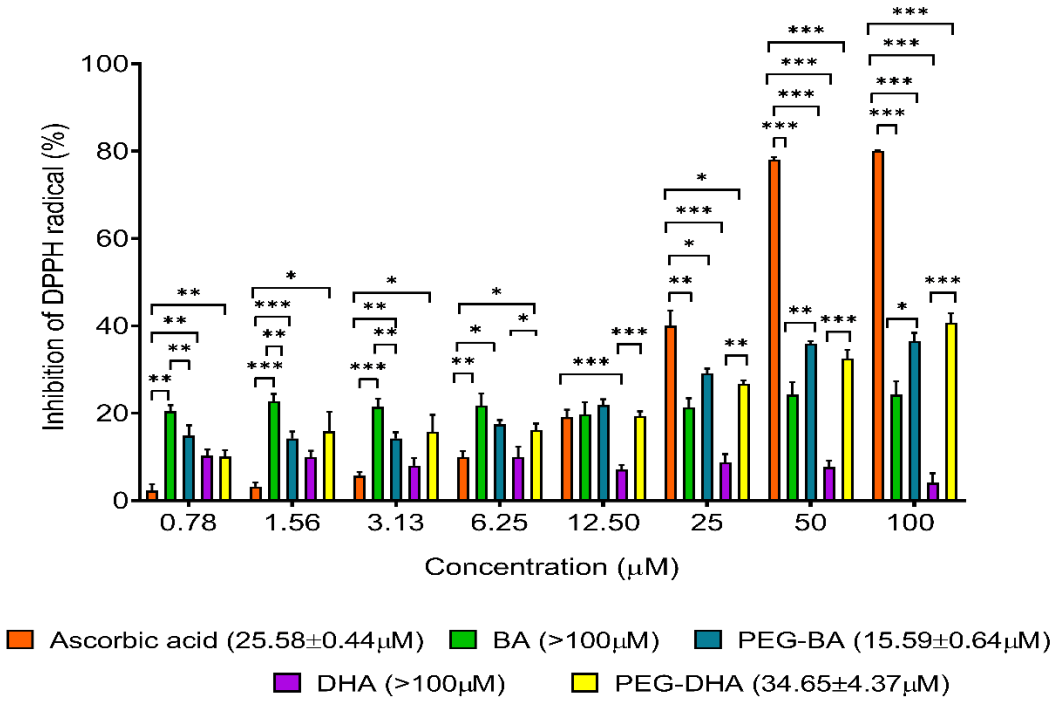

Figure 2.7: Antioxidant potential of the compounds using the DPPH assay. The antioxidant potential was assessed at varying concentrations (0.78-100 μM) for ascorbic acid, BA, PEG-BA, DHA, and PEG-DHA. Both conjugates (PEG-BA and PEG-DHA) resulted in dose-dependent antioxidant potential with a higher antioxidant effect (low $IC_{50,}$ as shown in the figure key). Data are shown as mean ± SEM (n=4), *p < 0.05, **p < 0.01 and ***p < 0.001.

DEPPD reactive oxygen species activity studies

The DEPPD assay directly quantifies ROS by analysing the reactive-oxygen metabolites (ROM) produced by these species (Wakabayashi et al., 2014). These are known as hydroperoxides which are relatively more stable than other free radicals and are formed by lipids and proteins that can oxidise molecules that contain sulphur groups (thiols) (Vassalle et al., 2006; Wakabayashi et al., 2014). The results from this assay showed there were significantly high concentrations of hydroperoxides in the pancreatic cancer cells compared to the non-cancerous cells indicating higher levels of ROS (74.73 ± 5.70 μM vs 546.96 ± 29.03 μM; p < 0.0001) (Figure 2.8). Other studies have reported similar results where the level of ROS in cancer cells exceeds that in non-cancerous cells (Zhou et al., 2014; Liu et al., 2018). At a physiological state, moderate levels of ROS are necessary for embryonic development, guiding tissue maintenance and immunity (Milkovic et al., 2019). An imbalance of ROS production and antioxidant defence systems results in a state known as

oxidative stress which has been shown to play a role in tumour initiation, growth, and progression (Liu et al., 2018; Milkovic et al., 2019; Snezhkina et al., 2019; Yang and Lian, 2020). ROS can interact with and modify macromolecules (Wakabayashi et al., 2014; Liu et al., 2018; Milkovic et al., 2019; Snezhkina et al., 2019). ROS can also result in DNA oxidation, affecting the stability of the genome and causing gene mutations, which facilitates carcinogenesis (Zhou et al., 2014; Milkovic et al., 2019).

Treating the Vero cells with the compounds resulted in a moderate increase in the concentrations of hydroperoxides, with the highest levels being observed when PEG-BA (112.32 ± 29.69 µM vs 74.73 ± 5.70 µM for untreated cells) and PEG-DHA (151.78 ± 54.87 µM vs 74.73 ± 5.70 µM) were used (Figure 2.8). The resulting production of hydroperoxides after treatment compared to the untreated cells suggested that the compounds acted as prooxidants to the non-cancerous cells (Cornelli et al., 2001). The results were different when the MIA PaCa-2 cells were treated with the compounds, showing a reduction in the hydroperoxide concentrations relative to the untreated sample (gemcitabine (433.34 ± 33.53 µM) > PEG-BA (518.80 ± 25.53 µM) > DHA (520.16 ± 16.66 µM) > PEG-DHA (531.16 ± 25.90 µM) > BA (542.43 ± 9.70 µM) vs untreated (546.96 ± 29.03 µM). This has also been documented in literature where cancer has been associated with high levels of ROS, which can be potentially reduced by treatment with promising antioxidants (Wakabayashi et al., 2014). Wakabayashi and colleagues (2014) used the same assay to quantify the ROM levels in serum samples obtained from lung cancer patients to predict the clinical response to chemotherapy. The authors detected elevated levels of ROMs before chemotherapy in the responders and the non-responders compared to the healthy controls. After 2-4 rounds of chemotherapy, the ROM levels were reduced to normal ranges in the responders. Therefore, results from this study suggest the compounds possess antioxidative potential against pancreatic cancer cells but not non-cancerous cells, where a prooxidative effect was noted (Figure 2.8).

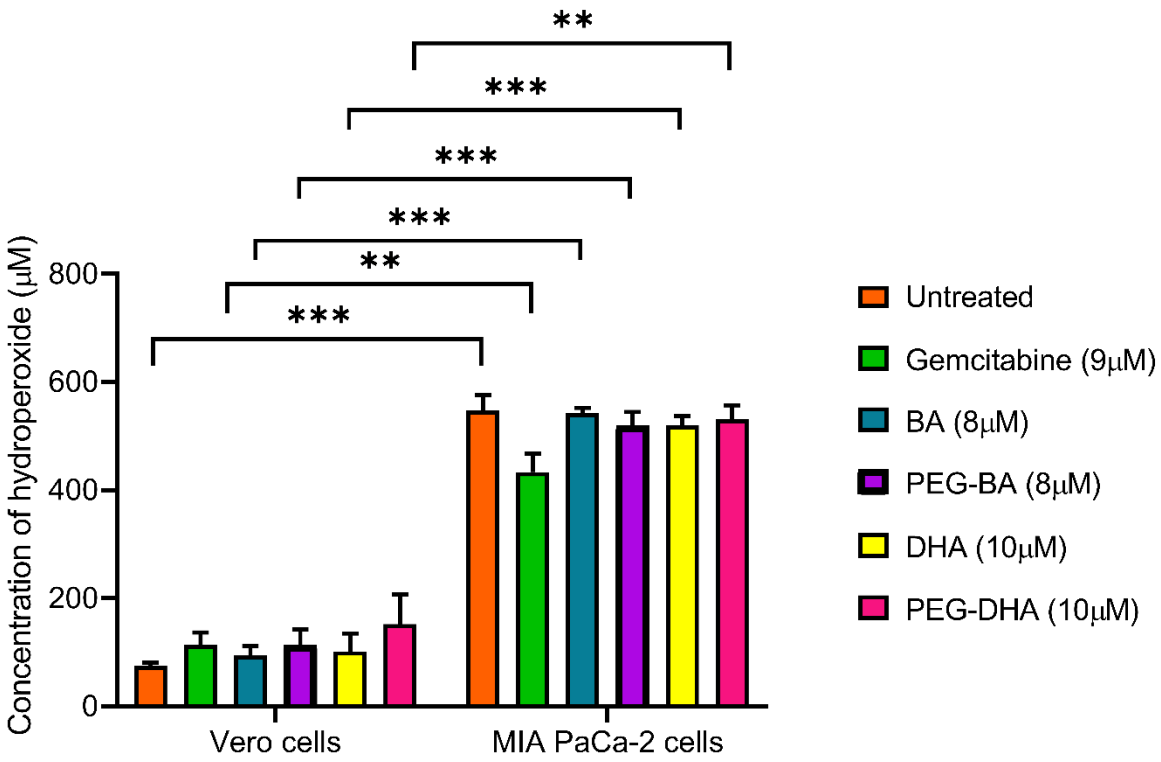

Figure 2.8: ROS status of cells pre-and post-treatment with the compounds. The concentration of hydroperoxides was assessed using the DEPPD assay. The untreated pancreatic cancer cells exhibited higher ROS status than the normal Vero cells. Treatment of the Vero and MIA PaCa-2 cells resulted in pro-oxidant and antioxidant capabilities, respectively. Data are shown as mean ± SEM (n=3), A two-way ANOVA was used to assess the change in the concentrations of hydroperoxides after treatment: **$p < 0.01$ and ***$p < 0.001$.

2.4. Summary of Cytotoxicity and Antioxidant Studies

Analysis of cytotoxicity, antioxidant potential and reactive oxygen species showed the conjugation of BA to PEG (PEG-BA), and DHA to PEG (PEG-DHA) improved overall activity. The IC_{50} value of PEG-BA against the MIA PaCa-2 cells was 3-times lower than that for the Vero cells (3.01 ± 0.62 µM vs 9.02 ± 0.79 µM), suggesting selectivity to the pancreatic cancer cells. Furthermore, the conjugate's cytotoxic ability and potency on MIA PaCa-2 cells were better than that of gemcitabine (7.63 ± 2.04 µM) and free BA (40.29 ± 3.60 µM). Morphological analysis after treatment with PEG-BA showed apoptosis was triggered in the MIA PaCa-2 cells. More rounding and detached cells were observed with increasing concentration. This was concurrent with the cytotoxic findings where the highest concentration of 8 µM resulted in 100% cytotoxicity. PEG-BA also possessed the highest antioxidant potential (15.59 ± 0.64 µM) compared to all the compounds in the DPPH assay. This suggests that, in addition to being selective against PC cells, it also possesses antioxidant activity, making it an ideal anticancer compound since some anticancer agents, such as

curcumin, exhibit their anti-cancer activity through antioxidant mechanisms (Singh et al., 2016). Two tetrazolium salt-based assays were used to assess the cytotoxic effect. This is because there are some limitations that have been reported about these assays. In the MTT assay, some compounds have the potential of cross-reacting with the MTT to produce false positive results thereby suggesting increased cell viability. Furthermore, cell culture medium exhaustion can lead to underestimation of cell cytotoxicity (Hu et al, 2021). Some studies have also disputed the use of media containing phenol red as it can also interfere with wavelength readings and lead to increased cell viability (Hu et al, 2021). In addition, XTT has also been reported to have the potential of overestimating viability of certain compounds (Aslantruk, 2018; Carreno et al, 2021). This is the reason why both assays were used for comparison first and foremost but also to determine which one is more effective for which drugs. In this regard, the drugs were further tested using flow cytometric techniques (Chapter 3) which further confirmed that PEG-BA is a more suitable compound than BA (free), DHA, and PEG-DHA against pancreatic cancer cells with the desirable low toxicity to the non-cancerous cells.

CHAPTER 3
MECHANISM OF CELL DEATH

3.1. Literature Review

Cell death is an essential process in cancer treatment as it aids in regulating the rate of uncontrollable proliferation, constant activation of oncogenes and survival mechanisms that promote tumour growth, progression, and metastasis (Wong, 2011; Grasso et al., 2012; Labi and Erlacher, 2015). Several biologists have studied the different mechanisms of cell death, and at least 34 modes have been identified to date (Liu et al., 2018). Two of the most studied forms of cell death are the focus of this section of the dissertation, namely, apoptosis and necrosis. Apoptosis, also called programmed cell death, is a process characterised by cell shrinkage, chromatin condensation, the collapse of the cytoskeleton, disassembly of the nuclear envelope, plasma membrane phospholipid disruption and formation of apoptotic bodies that eventually tag the cells for phagocytosis before eliciting an immune response (Green & Llambi, 2015; Manning & Zuzel, 2003). Necrosis, also known as accidental cell death, is characterised by increased cell size, plasma membrane rupture, loss of organelle structure, and expulsion of cellular contents, followed by inflammation (Manning & Zuzel, 2003).

The mammalian cell cycle comprises two main phases: interphase and mitosis (M). The Interphase is subdivided into three phases. S represents the phase in which the cell undergoes DNA synthesis in preparation for mitosis. The gap phases (G) are where the cell undergoes protein synthesis, accumulation of growth factors, organelle duplication, formation of centrosomal components and generation of ATP (Nunez, 2001). The main enzymes that drive progression in the cell cycle are cyclin-dependent kinases (CDKs) which activate their targets by phosphorylation (Barnum & O'Connell, 2014). The cell cycle undergoes tight regulation through three main checkpoints. The G_1 checkpoint assesses the presence of growth factors and nutrients, and DNA before it is replicated. The G_2 checkpoint occurs during the transition to mitosis. It assesses cell size and whether the DNA was replicated correctly to prepare for mitosis (cell division). Lastly, the metaphase checkpoint that occurs during mitosis ensures proper alignment of the chromosomes along the equatorial plane thereby preparing for cell division (Barnum & O'Connell, 2014). It is well-documented that the cell cycle is dysregulated in most cancer types, including pancreatic cancer (Chung et al., 2019). The tumour protein p53 (*TP53*) mutation allows cells with damaged DNA to bypass cell cycle checkpoints and leads to apoptosis evasion (Wang et al., 2021). The cyclin-dependent kinase

inhibitor 2A (*CDKN2A*) mutation disrupts the G_1 checkpoint leading to cell cycle dysregulation (Wang et al., 2021). These mutations are present in most pancreatic cancer. It is worth noting that any cell cycle arrest that can trigger cell death (i.e., lead to apoptosis when cells have damaged DNA) downstream its mechanism is sufficient to be developed as an anticancer agent. A well-documented example is gemcitabine which is a pyrimidine nucleoside analogue that has successfully treated many solid tumours, such as pancreatic cancer (Linskens, 2000; Dasanu, 2008; El-Sheikh et al., 2021). The drug functions by inhibiting progression through the cell cycle, specifically through the G_1/S checkpoint and kills cells synthesising DNA (S-phase), thereby inducing apoptosis (Tavil et al., 2007; Dasanu, 2008). Similarly, curcumin (a natural anti-inflammatory compound) is known to induce a S-phase arrest in colon cancer cells and induce apoptosis via p53 and Bax mediated mechanism (Li et al., 2022).

Annexin-V/PI was used to differentiate between live, apoptotic, and necrotic cells. The cell cycle status was determined using propidium iodide after 72 hours of treatment with BA, DHA, PEG-BA, PEG-DHA, and the standard chemotherapeutic drugs (doxorubicin and gemcitabine) on Vero and MIA PaCa-2 cells.

3.2. Methods and Materials

3.2.1. Annexin V/PI double staining

The annexin-V/PI apoptosis detection kit (BD Biosciences, Franklin Lakes, NJ, USA) was used to determine the type of cell death induced after treatment with the free drugs (BA and DHA), conjugates (PEG-BA and PEG-DHA), and controls (DMSO, doxorubicin and gemcitabine) on the MIA PaCa-2 and Vero cells. Under physiological conditions, the phospholipid bilayer of the plasma membrane has a general asymmetrical arrangement. Phospholipids, such as phosphatidylcholine and sphingomyelin, are found in the outer and phosphatidylserine (PS) on the inner leaflet of the plasma membrane (Baskic et al., 2006; Bahmani et al., 2011). During the early phases of apoptosis, this asymmetry is disrupted, and PS translocates from the cytosolic side of the cell membrane to the outer leaflet (Baskic et al., 2006; Bahmani et al., 2011). Annexin-V is a protein with a calcium-dependent high affinity for PS, so a fluorophore-labelled Annexin-V can detect early apoptosis using flow cytometry (Hingorani et al., 2011). As cell death progresses, the integrity of the cell membrane decreases, making it permeable to another component of the kit, PI. Membranes of dead cells

are permeable to PI, whereas viable cells exclude PI, making it possible to identify cells going through necrosis or apoptosis using flow cytometry (Vermes et al., 2000; Galluzzi et al., 2009).

The assay was carried out as described by Vermes and colleagues (2000). Briefly, 1 mL of cell suspension at a concentration of $1x10^5$ cells/mL was plated in 24-well plates and incubated overnight to allow them to recover from trypsinisation and adhere to the plate before treatment. The cells were then treated with the compounds shown in Table 3.1, and ½ IC_{50}, IC_{50} and 2x IC_{50} were selected as the concentrations. The concentration choice was based on the range of IC_{50} values obtained from cytotoxicity studies from this study and a previous study by Mthimkhulu and colleagues (2019). The same concentration was used for both cell lines to enable easier comparison. For the standard (gemcitabine), the median of the IC_{50} of PEG-BA and PEG-DHA was used to determine the type and percentage of cell death induced. The 24-well plates containing the treated cells were incubated for 72 hours (95% humidity, 37℃, 5% CO_2). The cells were harvested using trypsin EDTA (Sigma-Aldrich, St Louis, MO, USA) and washed at 200x *g* for 5 minutes. This was followed by a 30-minute resting phase, where the cells were allowed to recover from trypsinisation by resuspending the pellet in 2 mL complete DMEM.

Table 3.1: Chosen half-maximal inhibitory concentrations (IC_{50}) for flow cytometric analysis.

	Approximated IC_{50} (µM) for Downstream Analysis		
IC_{50} range	½ IC_{50}	IC_{50}	2x IC_{50}
Gemcitabine	2.25	4.5	9
BA and PEG-BA	2	4	8
DHA and PEG-DHA	2.5	5	10

The selected concentrations were similar to previous studies in our laboratory.

The cells were washed after resting using 2 mL of 1xPBS (200x *g* for 5 minutes). The concentration of annexin V and PI used for this study was based on pre-titred values from previous studies in our laboratory (Mthimkhulu, 2019). The pellet was resuspended with 100 µL of annexin binding buffer followed by the addition of 2 µL annexin-V/FITC fluorochrome-conjugated dye into the relevant Corning® round-bottom polypropylene tubes

(The Scientific Group, Johannesburg, South Africa). The mixture was incubated on ice for 15 minutes and protected from light. After the incubation, excess annexin-V/FITC was washed (200x *g* for 5 minutes) using 1 mL of the annexin-V binding buffer. The supernatant was discarded, and the pellet was resuspended in 100 µL of the binding buffer, followed by staining with 2 µL PI into the relevant Corning® round-bottom polypropylene tube (The Scientific Group, Johannesburg, South Africa). This was followed by 15 minutes of incubation on ice, protected from light. The reaction was stopped by adding 250 µL of binding buffer.

Data acquisition: The stained cells were analysed using a BD LSRFortessa Analyzer (BD Biosciences, Franklin Lakes, NJ, USA). The selected parameters for this assay were FITC detection using a 530/30 band filter and PI detection at a 610/20 band filter, acquiring at least 30 000 events per sample at a low to medium flow rate.

Compensation: A flow cytometer is an optic-related measuring device based on the principle of emission that occurs when light strikes particles moving linearly in a liquid medium (excitation) (Traganos, 1984; Adan et al., 2017). When using multiple fluorochromes simultaneously, their emission spectra might overlap, as in the case of FITC and PI, where light emitted by FITC spills over into the PI channel at the same wavelength. This is corrected using compensation calculated from controls with no stain and single stain to determine the percentage of interference of each fluorochrome relative to the other and subtract it from the samples (Adan et al., 2017).

Compensation controls were untreated cells prepared using similar conditions to the experimental samples. These cells were fixed with fixation/permeabilization buffer (BD Biosciences, Franklin Lakes, NJ, USA) and incubated on ice for 20 minutes to induce cell death. The fixed cells were washed (200x *g* for 5 minutes) using 2 mL of 1xPermWash solution (BD Biosciences, Franklin Lakes, NJ, USA). For the untreated and unstained compensation control, 350 µL of annexin V binding buffer was used to resuspend the pellet, and no staining was required. For the annexin-VFITC only compensation control, 100 µL was resuspended with annexin-V binding buffer, followed by adding 2 µL annexin-V/FITC fluorochrome-conjugated dye on ice for 15 minutes. After the incubation, excess annexin-V/FITC was washed (200x *g* for 5 minutes) using 1 mL annexin-V binding buffer, and the pellet was resuspended with 350 µL of annexin-V binding buffer. Lastly, for the PI-only compensation control, the pellet was resuspended with 100 µL of annexin-V binding buffer,

followed by adding 2 µL of PI stain on ice for 15 minutes. After staining, the reaction was stopped by adding 250 µL of annexin-V binding buffer. All the compensation controls were analysed using the same data acquisition parameters as the experimental samples on the BD LSRFortessa Analyzer (BD Biosciences, Franklin Lakes, NJ, USA).

Data analysis: Three independent experiments (n=3) were performed for the Annexin V-PI double staining technique and the cell cycle analysis using PI. Data obtained from the FACSDiva Software (BD Biosciences, Franklin Lakes, NJ, USA) on the flow cytometer was exported as flow cytometry standard (FCS) files and analysed in FlowJo version 10.8.1 (FlowJo, LLC, Ashland, KY, USA). The gating strategy for the annexin V-PI double staining to determine the mode of cell death involved identifying the population of interest and excluding cell debris based on forward scatter area (FSC-A), side scatter (SSC-A) characteristics and the appropriate instrument threshold values. The first gate after this was the FSC-A vs FSC-H to isolate the single cells (parent 1 or P1 population) and exclude doublets. The final gate was a quadrant gate to delineate cells undergoing the different modes of cell death (Figure 3.1). This was obtained by introducing curly quadrant plots, which are exponentially based quadrilateral gates that can separate the cells in terms of their fluorescent signals. A two-parameter analysis allowed the delineation of live or viable ($PE^-/FITC^-$), necrotic ($PE^+/FITC^-$), early apoptotic ($PE^-/FITC^+$) and late apoptotic or early necrotic cells ($PE^+/FITC^+$) (Crowley et al., 2016; Duensing and Watson, 2018). This data (percentages of the different subpopulations) was exported to MS Excel, and GraphPad software (v8.0.2.263) was used to analyse plot bar graphs (mean ± SEM). Figure 3.1 shows a simple schematic diagram to explain the two-parameter analysis used in the FlowJo software.

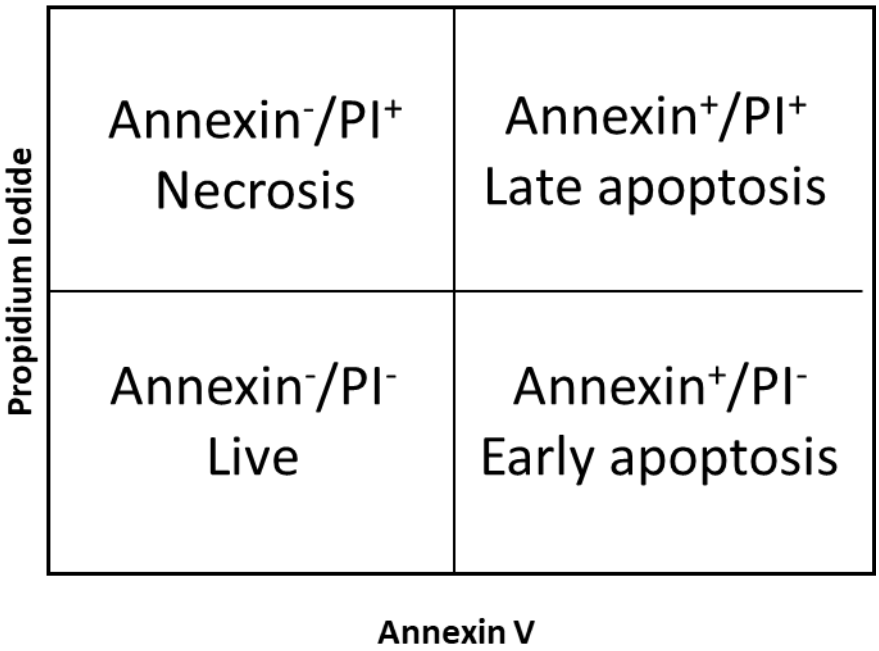

Figure 3.1: Schematic quadrant plot for Annexin V/PI double staining. This diagram explains the four quadrants used to delineate the different populations of cells using annexin V/FITC and PI. The first quadrant (Q1) represents the Annexin V^-/PI^+ cells that underwent necrosis. Q2 represents the Annexin V^+/PI^+ cells which underwent late apoptosis. Q3 represents the Annexin V^+/PI^- cells that underwent early apoptosis, and Q4 represents the viable Annexin V^-/PI^- cells.

3.2.2. Cell cycle analysis using propidium iodide

The cell cycle status of Vero and MIA PaCa-2 cells was analysed using propidium iodide after treatment with DMSO (0.33%), doxorubicin (0.2 µg/mL), gemcitabine, BA, DHA, PEG-BA, and PEG-DHA. This is a single parameter-based assay that analyses the cell cycle status of cells pre-and post-treatment. It is based on quantifying DNA content within cells directly proportional to the fluorescent intensity of stained cells (Jayat & Ratinaud, 1993; Nunez, 2001). The fluorescent signal is obtained from DNA-binding dyes that can intercalate into the grooves of DNA (propidium iodide and ethidium bromide) or possess a high binding affinity for specific areas of DNA, i.e., adenosine-tyrosine (Hoechst 33342/33258 or DAPI) and guanine-cytosine-rich areas (chromomycin A_3) (Traganos, 1984; Jayat & Ratinaud, 1993; Adan et al., 2017).

The cell cycle analysis was performed using propidium iodide according to the Moores cancer centre protocol (https://moorescancercenter.ucsd.edu/research/shared-resources/flow-cytometry/protocols.html#Cell-Cycle-Analysis-by-DNA-Cont). Briefly, the MIA PaCa-2 and Vero cells at a density of $2x10^6$ cells/mL were seeded in a 6-well plate and incubated

overnight for attachment. This was followed by treating the cells with the compounds at the IC_{50} and 2x IC_{50} for 72 hours and incubating at 37℃ (95% humidity, 5% CO_2). The cells were harvested using trypsin EDTA (Sigma-Aldrich, St Louis, MO, USA) and washed (200x *g* for 5 minutes). **Fixation and staining:** The pellet was resuspended in ice-cold (2 mL) 1xPBS followed by a wash step (200x *g*, 5 minutes, 4℃). After this step, the pellet containing cells was resuspended with 1 mL of ice-cold 1xPBS, followed by gentle vortexing and the dropwise addition of 70% ethanol (9 mL). The cells were fixed at -20℃ for at least 24 hours. The ethanol-fixed cells were centrifuged (200x *g*, 10 minutes, 4℃) to remove the ethanol. This formed a disc-shaped pellet necessitating careful disposal of the supernatant to avoid cell loss. The pellet was resuspended with 3 mL of ice-cold 1xPBS and centrifuged (200x *g*, 10 minutes, 4℃). A staining master-mix solution (500 µL) prepared by dissolving 2 mg of RNAse A in 10 mL of 0.1% Triton-X solution in PBS and containing 400 µL of 500 µg/mL of propidium iodide dye was added to the pellet. The cells were incubated for 30 minutes at room temperature. After incubation, the stained cells were placed on ice in a closed Styrofoam box to protect them from the light.

Data acquisition: At least 30 000 events were acquired and recorded for each sample at low flow rates using the FACSDiva Software on a BD LSRFortessa Analyzer (BD Biosciences, Franklin Lakes, NJ, USA). A low flow rate of below 400 events/second enables proper cell discrimination (Nunez, 2001).

Data analysis: Three independent experiments (n=3) were performed for the cell cycle analysis, and the data obtained from the FACSDiva Software (BD Biosciences, Franklin Lakes, NJ, USA) on the flow cytometer was exported as flow cytometry standard (FCS) files and further in FlowJo version 10.8.1 (FlowJo, LLC, Ashland, KY, USA). The analysis of the cell cycle data was based on two gating strategies. The first gate was to isolate cells of interest by introducing a gate on an SSC-H vs FSC-H scale. This was enough to gate out cells that are not to be analysed such as doublets. This was followed by drawing a histogram plot using the cell count vs phycoerythrin (PE) scales to quantify the DNA content in untreated and treated cells. The control (untreated) group was used as a baseline to determine the population of cells found in the different phases of the cell cycle. This is because the aim of analysing the data is to assess the effect of treatment had on the cell lines. Therefore, any variation from the untreated cells was interpreted as a shift from one phase to the other. The mathematical model chosen for allocating these constraints is the Watson (pragmatic) model, which approximates that the G_1/G_0 or G_2/M is normally distributed and that one of the peaks

can be identified (Watson et al., 1987). In addition, specific constraints on the coefficient of variance (CV) and root mean square (RMS) were applied to the data sets for reproducibility and reliability of cell cycle analysis for each experimental sample based on the untreated sample. The subpopulations (sub-G_1, G_1/G_0, S and G_2/M) obtained data from the DNA histograms (explained in Figure 3.2) were exported and further analysed in MS Excel, and the GraphPad software (v8.0.2.263) was used to plot bar graphs (mean ± SEM).

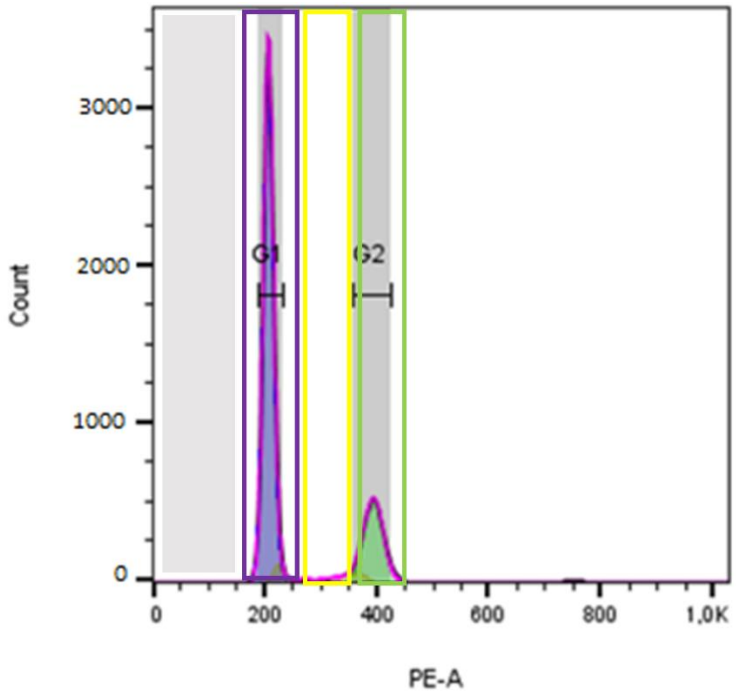

***Figure 3.2**:* Cell cycle histogram. This histogram serves as an explanatory diagram for the cell cycle analysis. The grey shaded area (usually indicated by a white peak in FlowJo) represents the sub-G_1 phase. The area highlighted in purple (usually indicated as a purple peak in a grey-shaded background) represents the G_1/G_0 phase. The area highlighted by yellow (usually indicated as a yellow-coloured peak) represents the S phase. The area highlighted in green (usually indicated as a green peak in a grey-shaded background) represents the G_2/M phase of the cell cycle.

3.2.3. Statistical analysis

Normality tests were first performed, followed by two-way ANOVA and Tukey's *post hoc* test since the data was normally distributed. Data with a p-value less than 0.05 was considered statistically significant.

3.3. Results and Discussion

3.3.1. Mode of cell death using Annexin V/PI

Light scattering properties of cells obtained as they pass through a light beam were used for the gating mechanisms of both assays. Forward scatter (FSC) is light diffraction along a

similar axis as the light beam, and this is used to measure cell size and surface area (Traganos, 1984; Wilkerson, 2012; Adan et al., 2017). Side scatter (SSC) is light reflected perpendicular to the light beam and is used to analyse cell granularity (Traganos, 1984; Wilkerson, 2012; Adan et al., 2017). Both properties allow the differentiation of a desired cellular subset in a heterogenous population (Adan et al., 2017). Figure 3.3 shows the gating strategy employed to analyse the mode of cell death induced before and after treatment with the compounds. The untreated MIA PaCa-2 and Vero cells stained with Annexin-V/FITC and propidium iodide showed some degree of cell death that could have been induced by trypsinisation and injury during pipetting. These values were subtracted when quantifying cell death to only reflect that induced following treatment with the compounds alone.

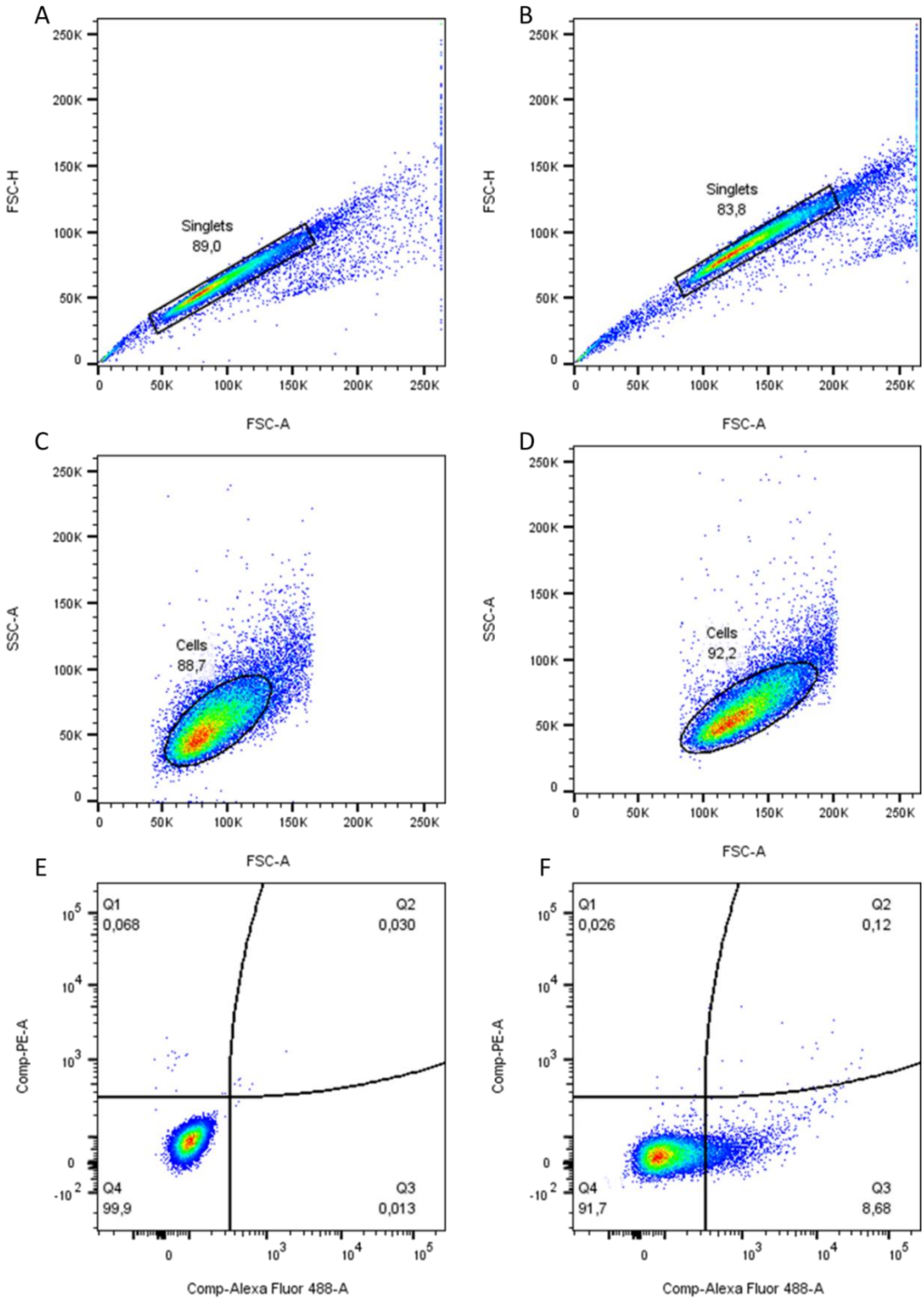

Figure 3.3: Gating strategy for determining the mode of cell death. The FCS files obtained from the flow cytometer on the FACSDiva software were gated using the FlowJo software. The representative dot plots indicate the necessary gating employed to identify cells positive for Annexin V/PI staining. The cells of interest were isolated from doublets using the FSC-H vs FSC-A (A-B) and SSC-A vs FSC-A (C-D). This was followed by differentiating the cell death modes using fluorescent signals from the FITC and PI dyes (E-F), where necrotic (Q1), late apoptotic (Q2), early apoptotic (Q3), and live cells (Q4) were identified. E represents untreated, unstained MIA PaCa-2 cells, and F represents MIA PaCa-2 cells treated with 8 µM of BA.

The induction of cell death after BA and PEG-BA treatment on Vero cells

The conjugate PEG-BA induced cell death in a dose-dependent manner, with most cell death being by apoptosis, both early and late phases (Figure 3.4). A similar trend was observed in the BA-treated Vero cells, but to a lesser extent than PEG-BA. At 4 µM, BA induced 25.83% of the cells that died, while 0.02 ± 0.01% underwent necrosis. Comparing this to PEG-BA (4 µM) showed that the conjugate resulted in a 2-fold higher induction of apoptosis (51.68%), and less than 1% of the cells underwent necrosis (0.73 ± 0.57%; $p = 0.1562$). Overall, BA resulted in higher cell viability than PEG-BA (74.13 ± 7.25% vs 47.67 ± 4.00; $p < 0.0001$), suggesting that the free drug was less toxic to the Vero cells at 4 µM. Compared to BA, most of the gemcitabine (56.83%) treated cells underwent apoptosis, and BA-treated cells were still viable. Well-known drugs such as gemcitabine are also toxic to non-cancerous cells and, therefore, cause side effects (Dasanu, 2008; Greco & Vicent, 2009). Rzeski and colleagues assessed the effect of BA on a human skin fibroblast cell line and found they underwent some apoptosis, but it was not as significant as on the other cancer cells that were tested (Rzeski et al., 2006). Other studies have shown that BA is non-toxic to non-cancerous cells; however, the authors only assessed cytotoxicity and did not include the non-cancerous cells in the apoptosis studies (Jung et al., 2007; Fulda, 2008; Xu et al., 2014; Ali-Seyed et al., 2016; Hordyjewska et al., 2018).

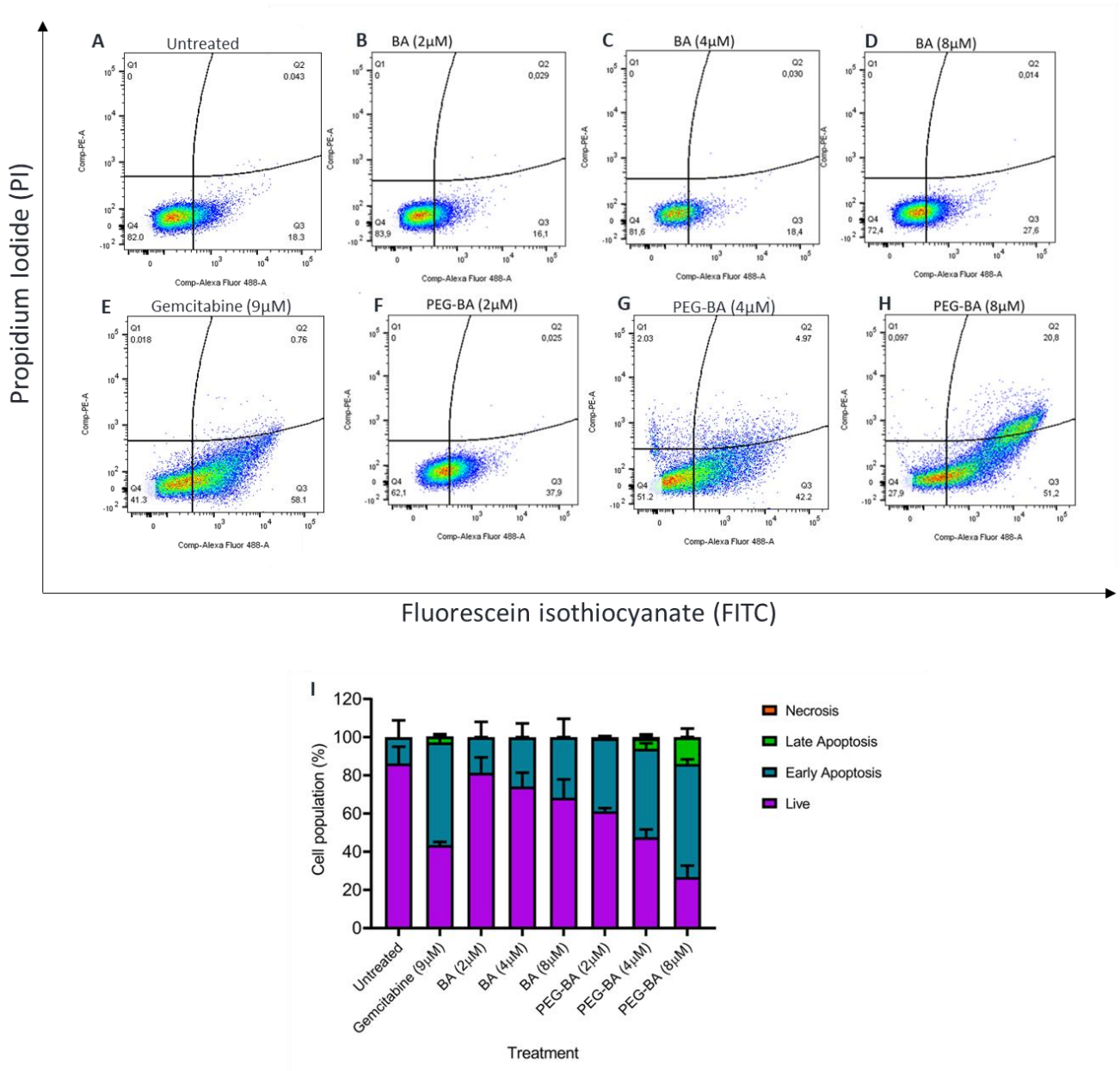

Figure 3.4: Cell death induction on the Vero cells after 72-hour treatment with BA and PEG-BA using the Annexin V/PI assay. (A-H) Representative dot plots demonstrating (Q1) necrotic cells, (Q2) late apoptotic cells, (Q3) early apoptotic cells and (Q4) live cells. Most BA-treated cells remained viable (Q4), while PEG-BA resulted in a dose-dependent induction of both early and late apoptosis. A minority of the cells underwent necrosis. Majority of the gemcitabine treating cells underwent early apoptosis and some of the cells were viable. (I) Quantitative bar graphs representing the four modes indicated because of treatment (mean ± SEM), n=3.

The induction of cell death after BA and PEG-BA treatment on MIA PaCa-2 cells

Treating the MIA PaCa-2 cells with PEG-BA resulted in a higher induction of cell death, compared to free BA, in a dose-dependent manner (Figure 3.5). At least 7.68% of the pancreatic cancer cells underwent apoptosis after treatment with 4 µM BA. Apoptotic cell

death induction was highly improved (6.91-fold) when the conjugate was used at the same concentration. These results correspond with the cytotoxicity studies where PEG-BA was a more potent construct producing the lowest IC_{50} value against the MIA PaCa-2 cells. Analysis of necrotic cell death after treatment with BA and PEG-BA on the MIA PaCa-2 cells showed that less than 1% of the cells underwent necrosis. In terms of viability, most of the BA-treated cells (92.30 ± 0.01%) were live after 4 µM of treatment compared to PEG-BA (46.87 ± 0.01%; $p < 0.0001$). Both gemcitabine and PEG-BA induced the highest level of apoptosis on MIA PaCa-2 cells compared to other cell death modes, with the conjugate causing higher levels of early apoptosis at 4 and 8 µM ($p = 0.1608$ and $p = 0.0002$, respectively).

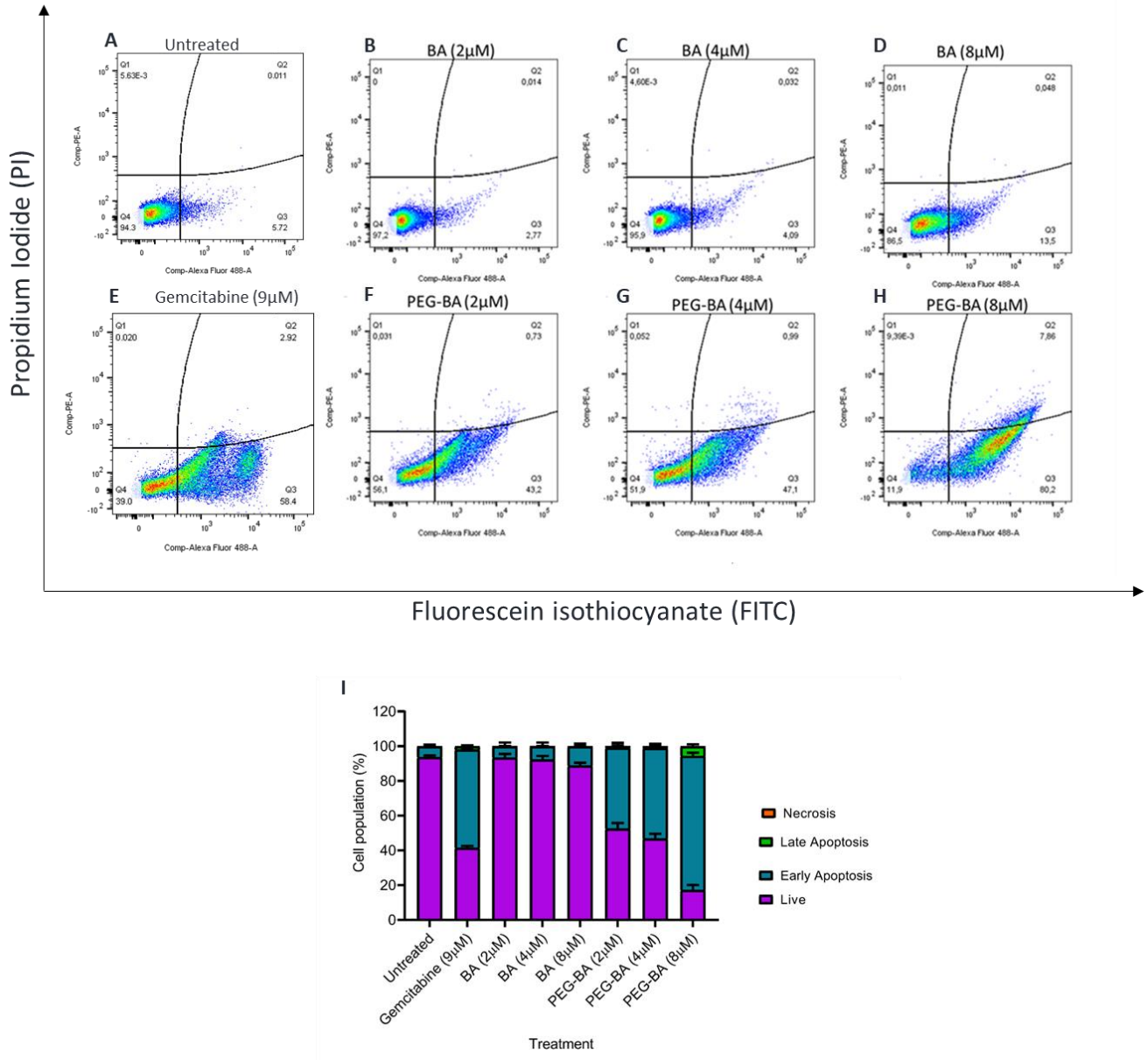

Figure 3.5: Cell death induction on the MIA PaCa-2 cells after 72-hour treatment with BA and PEG-BA using the Annexin V/PI assay. (A-H) Representative dot plots demonstrating (Q1) necrotic cells, (Q2) late apoptotic cells, (Q3) early apoptotic cells and (Q4) live cells. Most BA-treated cells remained viable (Q4), while PEG-BA resulted in a dose-dependent induction of both early and late apoptosis. A minority of cells underwent necrosis. Similarly, gemcitabine treatment induced high levels of early apoptosis and minimal necrosis. (I) Quantitative bar graphs representing the four modes indicated because of treatment (mean ± SEM), n=3.

Zhan and colleagues tested BA in H460 (lung cancer) cells and found that 100 µM induces apoptosis in 36.07% of the cell population (Zhan et al., 2018). Another study found 40 µM of BA resulted in 39.10% of the U937 (leukaemia) cells undergoing apoptosis (Park et al., 2021). Both studies showed that a high concentration of BA is required to induce apoptosis in

cancer cells (Xu et al., 2014; Yaozu et al., 2021; Yurasakpong et al., 2021). The lower levels of apoptosis induction from the current study could result from the lower concentrations of BA used. Vu and colleagues (2021) showed that BA co-treatment (20 µM BA + 1 µM doxorubicin) resulted in at least 97% of MOML-13, an acute myeloid leukaemia cell line, undergoing apoptosis. Notably, this finding, where a greater level of early apoptosis was notable compared to late apoptosis, is similar to the findings of this study. These findings showed that PEG-BA treatment resulted in a higher induction of apoptosis than necrosis in both the normal and the pancreatic cancer cell lines. Furthermore, performing statistical analysis to assess the effect of PEG-BA on Vero vs MIA PaCa-2 cells showed no statistical significance at 2 µM ($p = 0.0755$), 4 µM ($p = 0.8001$) and 8 µM ($p = 0.2226$). Therefore, this suggests that moderate selectivity was observed only in the conjugated drug, and the specificity factor reported by Zuco and colleagues was not apparent for free BA when this assay was used (Zuco et al., 2002).

The induction of cell death after DHA and PEG-DHA treatment on Vero cells

The conjugate PEG-DHA induced dose-dependent cell death in the normal cell line (Figure 3.6G). Treating the cells with 5 µM of PEG-DHA caused at least 86.57% of apoptotic cell death, which was 1.42-fold higher than the level of apoptosis induced after treatment with free DHA (Figure 3.6G). Both compounds caused less than 1% of necrosis in the Vero cells ($0.12 \pm 0.06\%$ vs $0.11 \pm 0.03\%$; $p > 0.9999$), suggesting these compounds induce apoptosis and not necrosis. More DHA-treated cells were viable after treatment compared to PEG-DHA ($38.77 \pm 2.85\%$ vs $13.31 \pm 2.12\%$; $p = 0.5293$). Analysing the effect of doxorubicin on cell death in Vero cells showed a greater induction of apoptosis (71.68%) compared to free DHA (60.94%) and this was associated with a 4.09-fold higher induction of necrosis (Figure 3.6E and I).

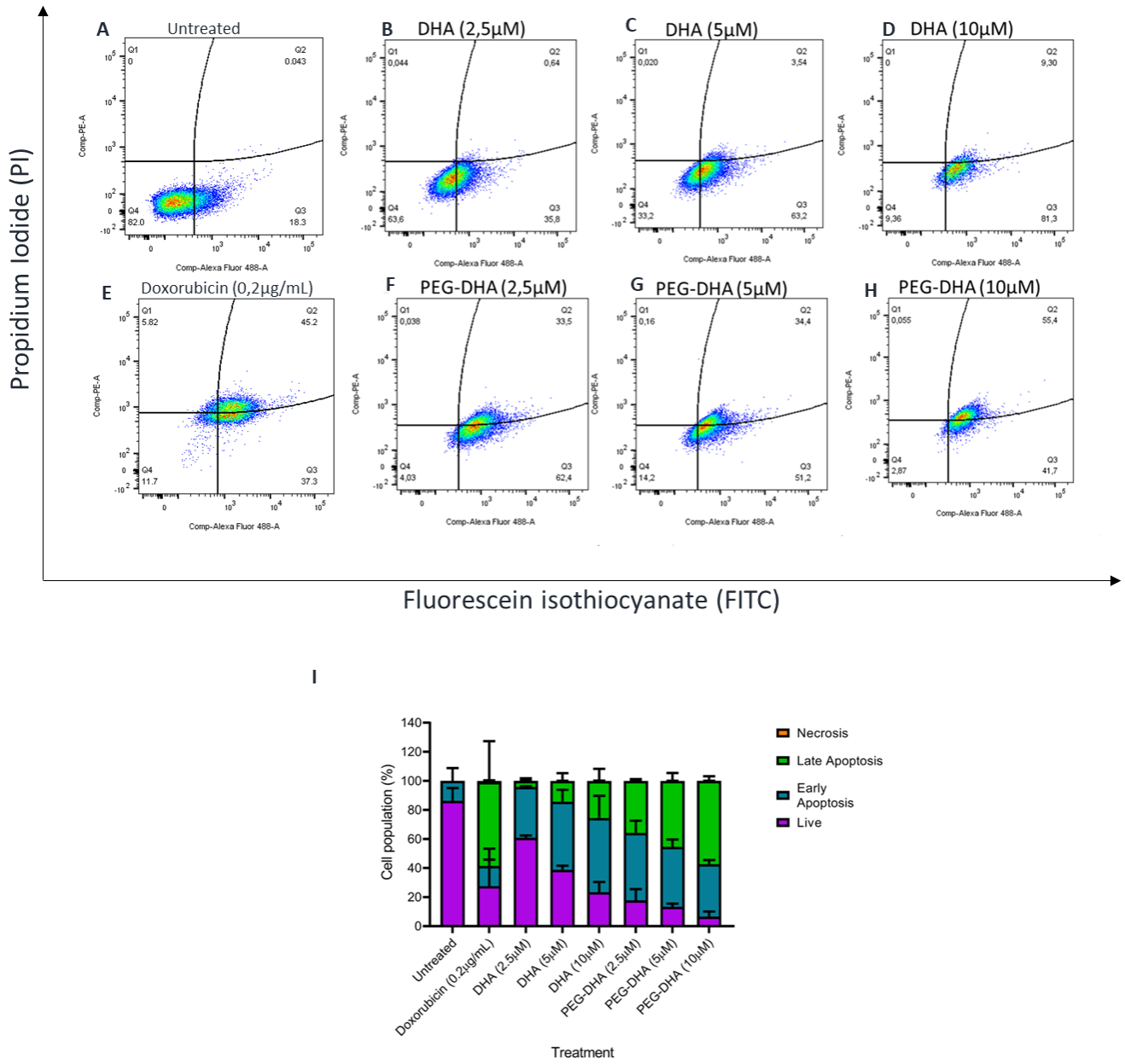

Figure 3.6: Level of cell death induction post-DHA and PEG-DHA treatment on Vero cells using the Annexin V/PI assay. (A-H) Representative dot plots demonstrating necrotic cells (Q1), late apoptotic cells (Q2), early apoptotic cells (Q3) and live cells (Q4). Overall, the DHA treatment resulted in a dose-dependent decline in viable cells associated with an increase in apoptotic cells, a similar trend observed when PEG-DHA was used. A few of the cells underwent necrosis. Treating the Vero cells with doxorubicin induced late apoptosis. (I) Quantitative bar graphs representing the four modes indicated because of treatment (mean ± SEM), n=3.

The induction of cell death after DHA and PEG-DHA treatment on MIA PaCa-2 cells

Similarly, treating the pancreatic cancer cells with PEG-DHA resulted in a dose-dependent induction of cell death (Figure 3.7I). Only 12.91% of the MIA PaCa-2 cells underwent apoptosis after treatment with 5 µM of DHA. This was improved when PEG-DHA was used,

and a 3.95-fold higher induction of apoptosis was observed. DHA and PEG-DHA resulted in less than 1% of the MIA PaCa-2 cells undergoing necrosis at all the tested concentrations (Figure 3.7I). PEG-DHA treatment resulted in a reduced percentage of viable cells compared to free DHA (48.97 ± 0.00% vs 87.07 ± 0.01%; p = 0.1503), suggesting cytotoxicity. This finding was comparable to the cytotoxicity findings reported in Chapter 2, where treating the MIA PaCa-2 cells with 100 µM only induced a cytotoxic effect of 39.92 ± 5.96%, indicating at least 60% viability at the high concentration. On the other hand, doxorubicin induced higher levels of apoptosis than PEG-DHA (79.39% vs 63.85%), with most of the cells undergoing the late phase (Figure 3.7I). The doxorubicin data was more like the XTT findings where 0.2 µg/mL induced a cytotoxic effect of 92.58 ± 3.44%, therefore, while the MTT results may have not show that the data is more accurate, it is notable that further confirmatory assays using the Annexin V/PI kit corroborated this. In addition, the highest level of necrosis induction was observed when the MIA PaCa-2 cells were treated with 0.2 µg/mL compared to all the tested drugs (3.10 ± 1.40% vs <1%).

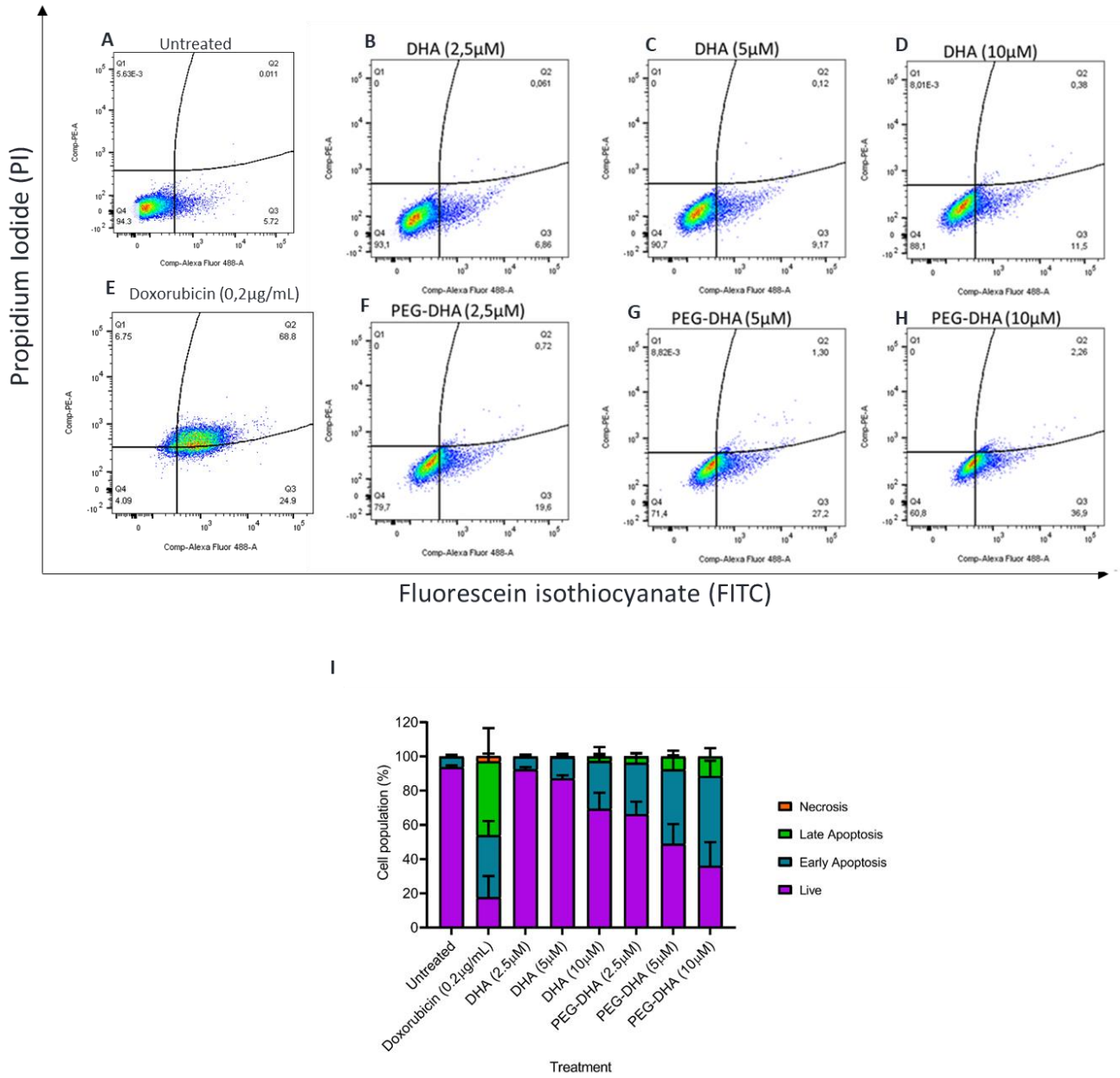

Figure 3.7: Level of cell death induction post-DHA and PEG-DHA treatment on MIA PaCa-2 cells using the Annexin V/PI assay. (A-H) Representative dot plots demonstrating necrotic cells (Q1), late apoptotic cells (Q2), early apoptotic cells (Q3) and live cells (Q4). The DHA treatment resulted in a dose-dependent decline in viable cells associated with an increase in apoptotic cells, a similar trend observed when PEG-DHA was used. A minority of the cells underwent necrosis. Doxorubicin treated cells populated the Q2 and Q3 indicating apoptosis is the main mode of cell death. (I) Quantitative bar graphs representing the four modes indicated because of treatment (mean ± SEM), n=3.

In a study by Lu and colleagues (2020), the authors synthesised DHA nanoparticles capable of self-assembling in aqueous solutions and tested them against the cervical cancer cells HeLa cells. Treating the HeLa cells with 25 µg/mL of DHA/MPEG-PCL resulted in 60.51 ± 5.39% apoptosis compared to the 43.68 ± 2.3% by free DHA, suggesting that the nanocarrier

system improved the apoptosis-inducing ability of DHA (Lu et al., 2020). Overall, an increased level of apoptosis was observed in the Vero cells compared to the MIA PaCa-2 cells after DHA and PEG-DHA treatment. When a comparison of the conjugates' apoptosis-inducing effect against MIA PaCa-2 cells was assessed, it was evident that PEG-BA was a more potent inducer of apoptosis at all the tested concentrations, which were significantly lower than those chosen for PEG-DHA, i.e., 2, 4, 8 µM vs 2.5, 5, 10 µM. The vehicle control (DMSO) was also tested for its potential apoptosis inducing ability. For both cell lines, more than 80% of the cells were viable, and cell death induction was reduced compared to the drugs (Appendix XII).

3.3.2. Cell cycle status

In the cell cycle studies with PI, using flow cytometry, the effect of the compounds BA, DHA, PEG-BA, PEG-DHA, and controls (DMSO, doxorubicin and gemcitabine) were analysed after a 72-hour incubation. Additional controls included an untreated, stained sample and one untreated and unstained. The gating strategy employed to determine the cycling characteristics of the MIA PaCa-2 and the Vero cells is shown below (Figure 3.8) in an untreated and treated sample.

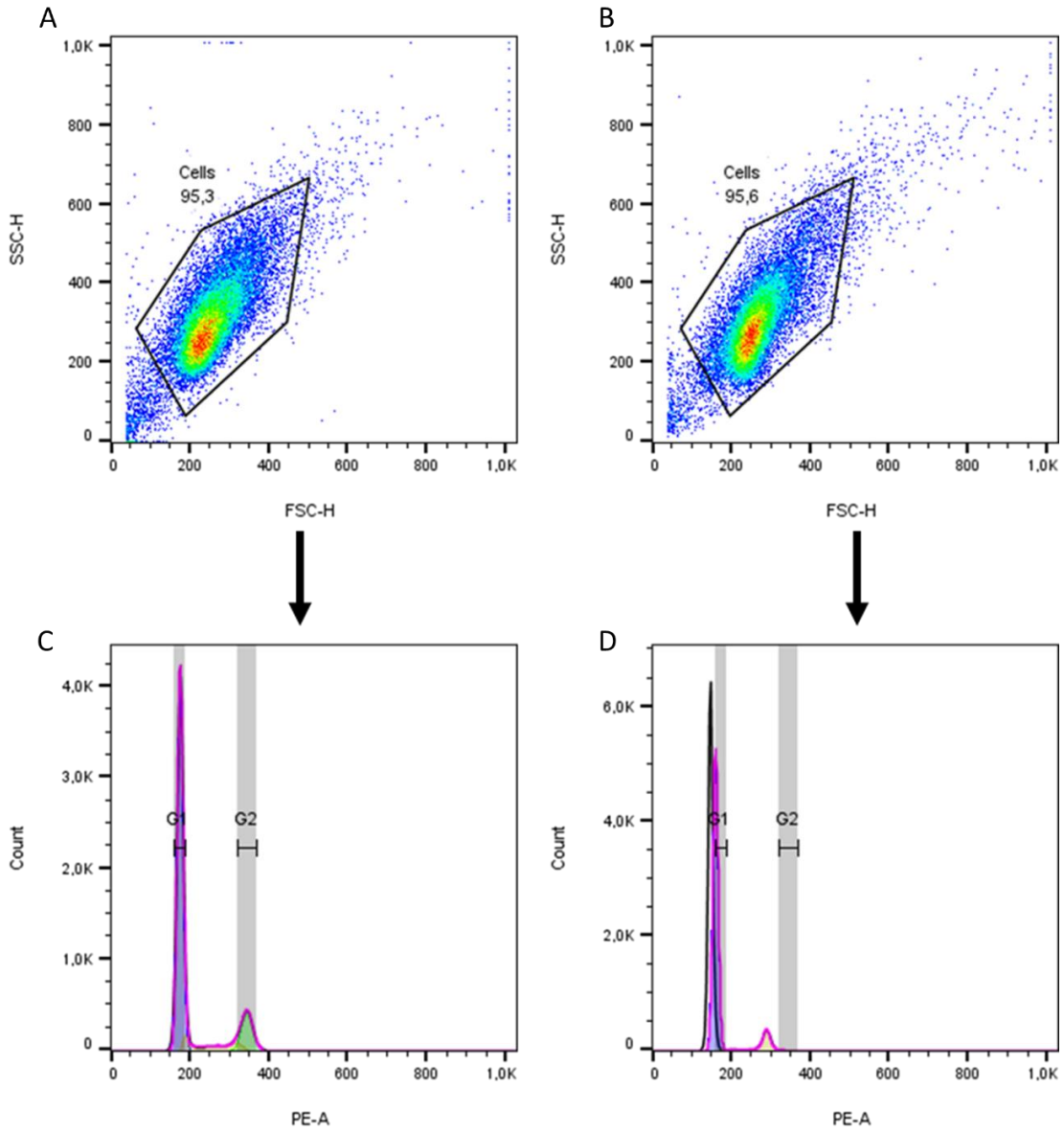

Figure 3.8: Gating strategy employed for cell cycle analysis. The FCS files obtained from the flow cytometer on the FACSDiva software were gated using the FlowJo software. The cells of interest were gated using SSC-H vs FSC-H (A-B), followed by cell cycle status analysis, represented in histograms indicating DNA content quantified by propidium iodide. C: Untreated MIA PaCa-2 cells and D: BA-treated cells.

Effect of BA and PEG-BA treatment on the cycling characteristics of the Vero cells

The untreated samples for each cell line were assessed as controls to determine baseline cycling so that the treatment effect could be extrapolated. Most of the untreated Vero cells were in the G_1/G_0 (68.67 ± 0.29%) compared to S (6.88 ± 0.02%) and G_2/M (20.50 ± 0.14%) phases (Figure 3.9A). It was found that at least 1.12 ± 0.82% of the untreated cells were in the sub-G_1 phase. Literature has shown that this sub-G_1 phase indicates apoptotic cells or induction of apoptosis because it represents hypodiploid cells with a DNA content lower than in the G_1 phase. Notably, the DNA content in the G_1 phase is half that of the G_2/M phase.

DNA degradation, a notable characteristic of apoptosis, can be one of the causes of the reduced DNA content, confirming that the cells found before G_1/G_0 are undergoing apoptosis (Wang et al., 2011; Crowley et al., 2016).

Treating the Vero cells with BA (4 µM) resulted in an S-phase arrest, indicated by an increase in the cell population relative to the untreated sample (6.88 ± 0.02% vs 10.83 ± 3.64%; p = 0.8012). Although 4 µM BA induced lower levels of apoptosis (sub-G_1), doubling the concentration resulted in a 7.67-fold increase in apoptosis compared to untreated cells (1.12 ± 0.82% vs 8.59 ±4.42%; *p* = 0.9351). Compared to BA, PEG-BA resulted in a dose-dependent induction of apoptosis. Furthermore, treating the Vero cells with 4 µM induced a higher S-phase arrest (10.83 ± 3.64% vs 19.11 ± 7.53%; p = 0.4364) associated with a 116.86-fold higher induction of apoptosis (0.36 ± 6.24% vs 42.06 ± 9.45%; p = 0.0749). In the XTT assay, 4 µM (found between 3.13 and 6.25 µM) of PEG-BA induced a cytotoxic effect that ranged between 36.82 and 46.27% in the Vero cells. Furthermore, in the annexin V/PI studies, 4 µM induced apoptosis in 51.68% of the cell population. This suggests that these findings (together with cell cycle studies) were correlated because they showed a similar trend.

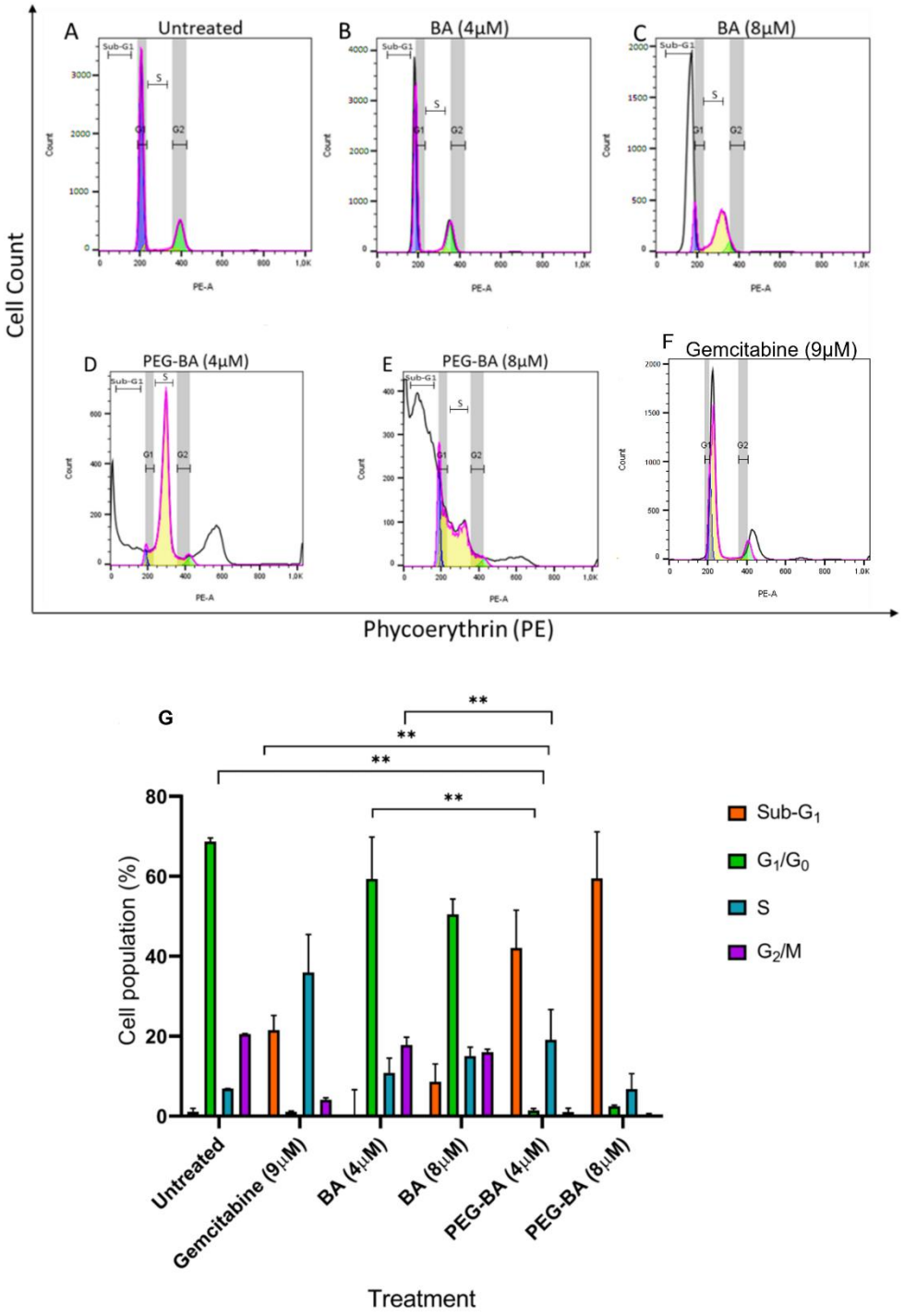

Figure 3.9: Cell cycle status of Vero cells after treatment with BA and PEG-BA. Representative histograms showing the different phases of the cell cycle indicated by the white (sub-G_1), purple (G_1/G_0), yellow (S) and green (G_2/M) peaks. Interval arrow lines were inserted to highlight the sub-G_1 and S phases. BA and PEG-BA resulted in a dose-dependent shift of cells from the G_1/G_0 to the sub-G_1 phase, indicating apoptosis induction associated with an S-phase arrest. Gemcitabine treatment induced a S phase and sub-G_1 arrests. (G) Quantitative bar graphs showing the overall cycling status of the pancreatic cancer cells (mean ± SEM), n=3, *$p < 0.05$, **$p < 0.01$.

Effect of BA and PEG-BA treatment on the cycling characteristics of the MIA PaCa-2 cells

In the untreated MIA PaCa-2 cells, most of the cells were in the G_1/G_0 (45.27 ± 4.70%) compared to S (17.67 ± 1.22%) and G_2/M (25.07 ± 2.44%) phases (Figure 3.10A). The sub-G_1 phase was also assessed, and it was found that at least 4.57 ± 0.82% of the untreated cells were in this phase. Treatment with PEG-BA resulted in a dose-dependent apoptotic effect on the pancreatic cancer cells, where most cells shift into the sub-G_1 phase relative to the untreated sample (Figure 3.10G). When the MIA PaCa-2 cells were treated with 4 µM BA, the cells shifted from the G_2/M phase (21.64 ± 4.07% vs 25.07 ± 2.44%; p = 0.9311) to the S (19.57 ± 1.51% vs 17.67 ± 1.22%; p = 0.9464), G_1/G_0 (50.93 ± 5.23% vs 45.27 ± 4.70%; p = 0.5372) and sub-G_1 (19.63 ± 4.49% vs 4.57 ± 0.82%; p = 0.5470) phases compared to the untreated sample. Therefore, at least 20% of the cell population was undergoing apoptosis, evidenced by the increase in the sub-G_1 population. Compared to free BA, when the MIA PaCa-2 cells were treated with 4 µM of PEG-BA, at least 39.50 ± 5.32% were in the sub-G_1 phase (19.36 ± 4.49%; p = 0.3846). PEG-BA reduced MIA PaCa-2 cells in the G_2/M, S, G_1/G_0 phases.

The XTT data showed that at 3.13-12.5 µM, PEG-BA resulted in a cytotoxicity range of 37.46-96.65% which further correlated with Annexin V/PI studies where the level of cell death induced was between 47.47% and 82.2% for 2-8 µM. Both assays showed that viability was inhibited, and apoptosis was observed as the mode of cell death post-PEG-BA treatment on the MIA PaCa-2 cells. This is a similar trend that was observed in the cell cycle studies as well. In addition, all assays showed the selectivity of PEG-BA against the MIA PaCa-2 cells which was associated with a greater cytotoxic effect, potency and apoptosis inducing ability than in the Vero cells.

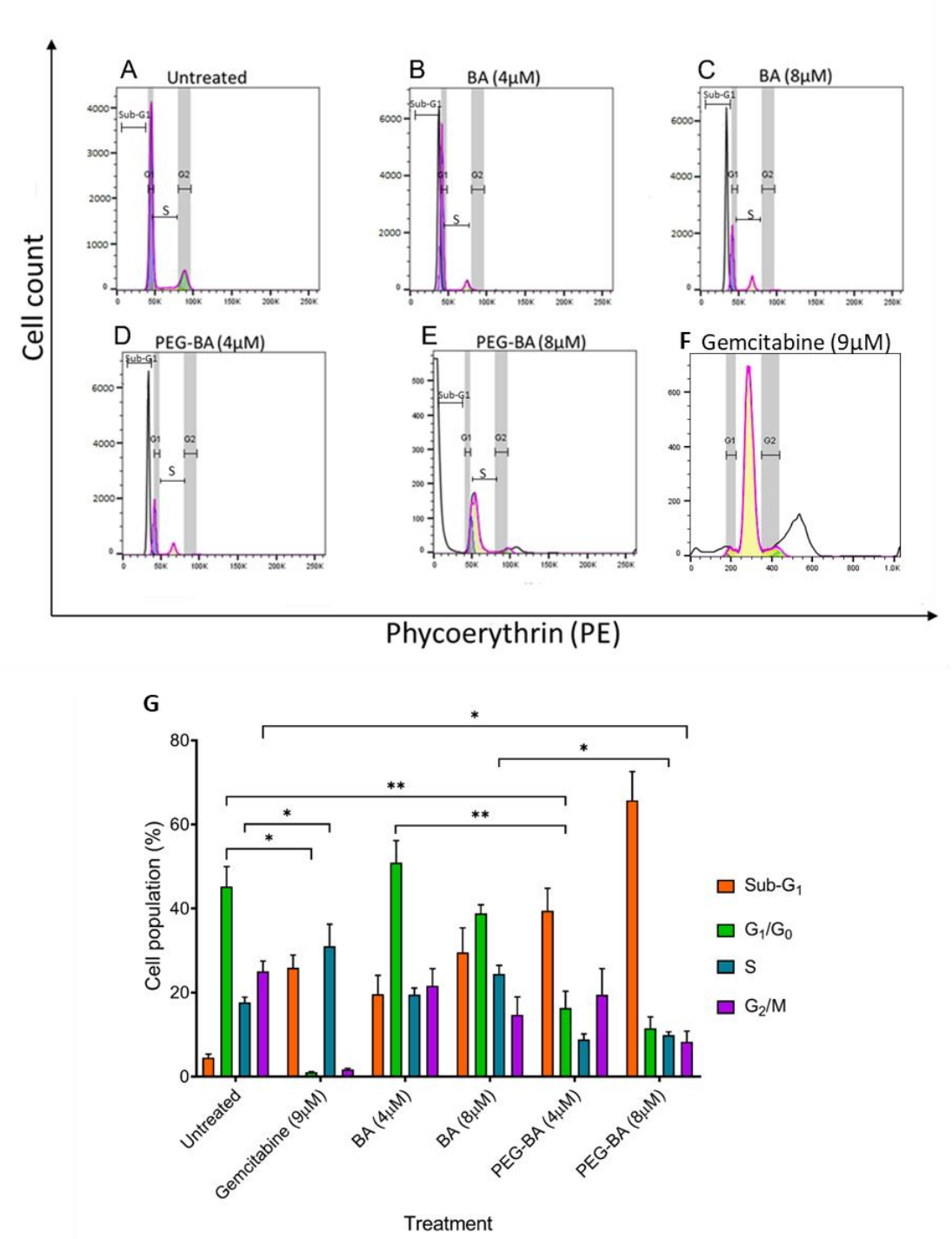

Figure 3.10: Cell cycle status of MIA PaCa-2 cells after treatment with BA and PEG-BA. (A-E) Representative histograms showing the different phases of the cell cycle indicated by the white (sub-G_1), purple (G_1/G_0), yellow (S) and green (G_2/M) peaks. Interval arrow lines were inserted to highlight the sub-G1 and S phases. Both BA and PEG-BA resulted in a dose-dependent shift of cells from the G_1/G_0 to the sub-G_1 phase, indicating apoptosis induction. (F) Quantitative bar graphs showing the overall cycling status of the pancreatic cancer cells (mean ± SEM), n=3, *$p < 0.05$, **$p < 0.01$.

The accumulation of cells in the G_1/G_0 phase due to BA treatment on cancer cells has been previously reported (Mullauer et al., 2011; Csuk, 2014; Saneja et al., 2017a). Zuco and

colleagues (2002) assessed the effect on cycling characteristics of ovarian carcinoma (INGROV-1) and metastatic melanoma cells (Me665/2/21) after BA and doxorubicin treatment. They found that, in the INGROV-1 cells, BA induced a sub-G_1 arrest. In the Me665/2/21 cells, BA treatment resulted in a G_1/G_0 arrest with no change in DNA content from cells found in the sub-G_1 phase relative to the untreated sample (Zuco et al., 2002). Faujan and colleagues (2010) analysed the effect of BA on human cancer cells (leukaemic, breast and cervical carcinoma, and glioblastomas) and murine melanoma cells PBMCs isolated from healthy controls. The authors observed an increase in the cells in sub-G_1 and a subsequent reduction of cells in the G_2/M. Interestingly, in their study, BA resulted in an S-phase arrest after 24-hour treatment with 2.6 µg/mL (5.69 µM) of free BA; however, the G_1/G_0 arrest was observed after a 72-hour treatment (Faujan et al., 2010). All these and the current study show BA induces a context-based cell cycle arrest where different cell lines present with different cycling characteristics. The most common arrests are the G_1/G_0 and sub-G_1 phases.

In a study by Saneja and colleagues in 2017, the authors assessed the effect of betulinic acid-loaded polylactide-co-glycolidemonomethoxy polyethylene glycol nanoparticles (PLGA-mPEG NPs) on PANC-1 cells and found a higher G_1/G_0 arrest compared to free BA (46.7% vs 68.4%; $p < 0.01$). Overall, cell cycle findings from these studies showed that conjugation improved the apoptosis-inducing ability of BA, specifically in pancreatic cancer cells.

Effect of DHA and PEG-DHA treatment on the cycling characteristics of the Vero cells

Treating the Vero cells with 5 µM DHA resulted in an S-phase arrest relative to the untreated sample (6.88 ± 0.02% vs 18.95 ± 1.40%; $p = 0.3465$), as shown in Figure 3.11. Surprisingly, this was elevated compared to the S-phase arrest induced by PEG-DHA at the same concentration (18.95 ± 1.40% vs 9.31 ± 1.36%; $p = 0.4781$), suggesting that the conjugate caused the non-cancerous cells to shift from the S-phase to the G_1/G_0 phase, although this was still lower than the untreated sample. Compared to the conjugate, the free DHA induced a higher level of apoptosis at the highest tested concentration of 10 µM (4.79 ± 2.75% vs 11.57 ± 6.21%; $p = 0.6810$). Therefore, it seems that conjugation maintained the G_1/G_0 phase arrest that was observed in the untreated cells. In addition, PEG-DHA also induced a G_2/M phase which is consistent with published literature (Jiao et al., 2007; Dai et al., 2014). Overall, DHA treatment resulted induced a cytotoxic effect ranging from 27% to 37.54% (3.13-12.5 µM) which was lower than the level of cell death that was induced (2.5 µM:

39.2%, 5 µM: 61.23%, and 10 µM: 76.61%) in the Annexin V/PI analysis. For PEG-DHA, the cytotoxicity range was 21.92% and 46.41% for the 3.13 to 12.5 µM concentration range. This was at least 2-fold lower than the level of cell death (2.5 µM: 82.19%, 5 µM: 86.69%, and 10 µM: 93.42%) in the apoptosis assay. Both studies suggests that PEG-DHA had a greater cytotoxic and death inducing effect on the Vero cells compared to free DHA, however the cell cycle analysis data did not correlate with these findings.

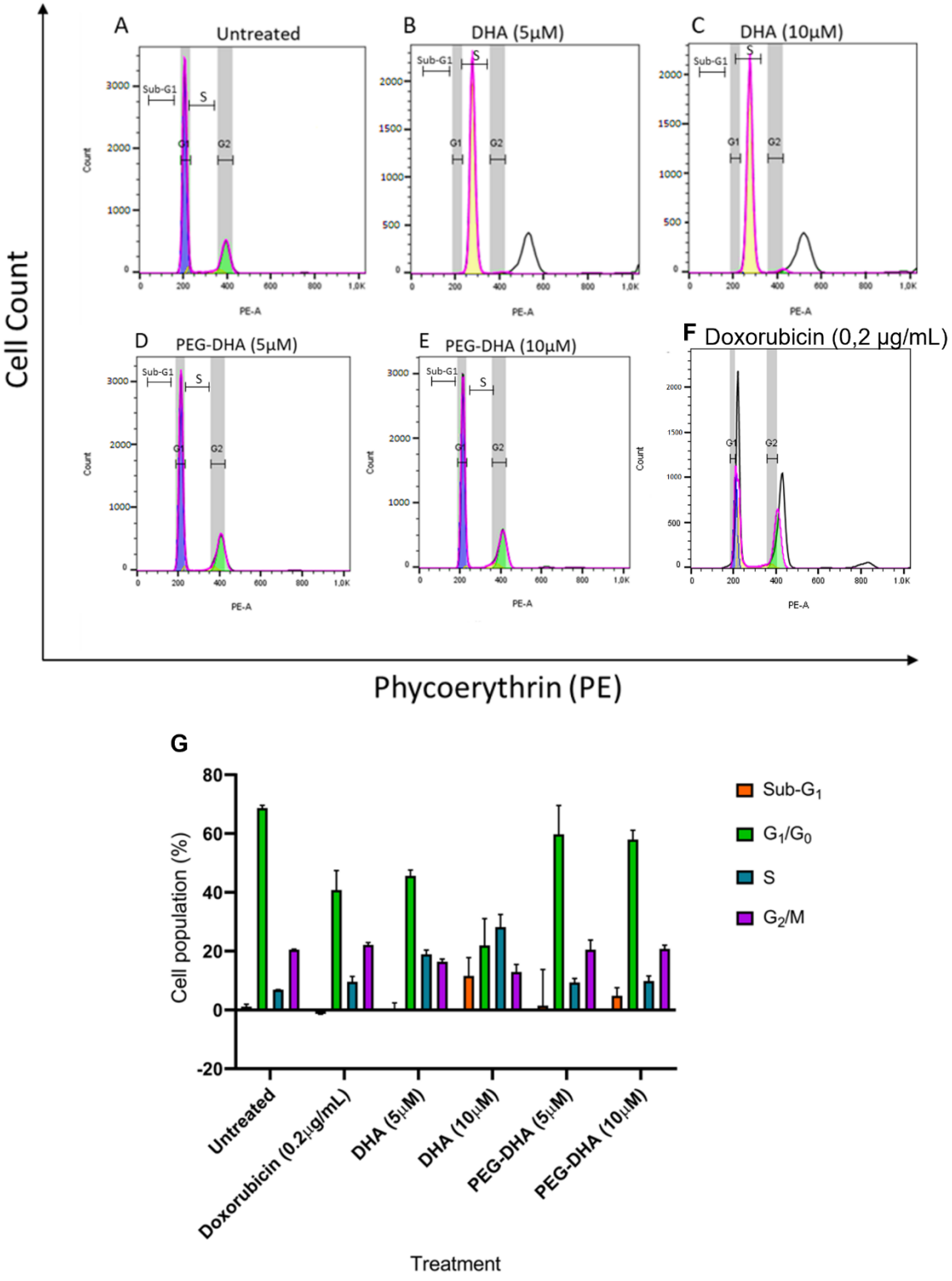

Figure 3.11: Cell cycling status of Vero cells post-treatment with DHA and PEG-DHA. (A-F) Representative histograms showing the different phases of the cell cycle indicated by the white (sub-G_1), purple (G_1/G_0), yellow (S) and green (G_2/M) peaks. Interval arrow lines were inserted to highlight the sub-G_1 and S phases. Overall, DHA resulted in a dose-dependent arrest in the S-phase associated with apoptosis induction, while PEG-DHA treatment resulted in a decline in the S and Sub-G_1 phases. (G) Quantitative bar graphs indicating the overall cycling status of the pancreatic cancer cells (mean ± SEM), n=3, $p > 0.05$.

Effect of DHA and PEG-DHA treatment on the cycling characteristics of the MIA PaCa-2 cells

When the MIA PaCa-2 cells were treated with DHA, a dose-dependent arrest in the sub-G_1 and G_1/G_0 was observed (Figure 3.12). At least 13.45 ± 2.69% (p = 0.8085) were arrested in the Sub-G_1 phase at 5 µM, indicating apoptosis. A G_1/G_0 arrest was also induced after DHA treatment (untreated vs 5µM DHA: 45.27 ± 4.70% vs 57.90 ± 2.92%; p = 0.4079) relative to the untreated pancreatic cancer cells. Comparing these results to PEG-DHA, a similar G_1/G_0 arrest was observed, although this decrease was marginal (G_1/G_0: 57.90 ± 2.92% vs 55.37 ± 2.00%; p = 0.9558. Furthermore, a slightly higher sub-G_1 arrest was observed after PEG-DHA treatment (13.45 ± 2.69% vs 20.05 ± 4.34%; p = 0.8863), suggesting that the conjugate enhanced the apoptosis-inducing ability of DHA (Figure 3.12). An additional G_2/M phase arrest was also observed due to PEG-DHA relative to the untreated sample (untreated vs 5µM PEG-DHA: 25.07 ± 2.44% vs 29.28 ± 5.54%; p = 0.8133).

Dai and colleagues (2014) assessed the cell cycle status in Lewis lung carcinoma (LLC) cells post-treatment with IC_{80} of non-conjugated DHA and its multi-arm-PEG-DHA conjugates after 24 hours. Their findings showed that all the compounds (DHA and its different multi-arm conjugates) could induce a G_1/G_0 arrest (Dai et al., 2014). Jiao and colleagues (2007) reported the effect of varying concentrations of DHA against ovarian cancer cells (OVCA-420) after 48 hours. Their findings showed that DHA induced a dose-dependent arrest of the OVCA-420 cells in the G_2/M and Sub-G_1 phases, further indicating that DHA has an apoptosis-inducing ability. Results from this study showed that PEG-DHA induced three phase arrests (G_1/G_0, G_2/M and sub-G_1), specifically in the MIA PaCa-2 cells, an observation reported in studies that used DHA (and a PEG-DHA formulation) on cancer cells. Therefore, this suggests that conjugation improved the level of arrest associated with the inhibition of DNA synthesis observed with a reduction in the cell population cycling in the S-phase.

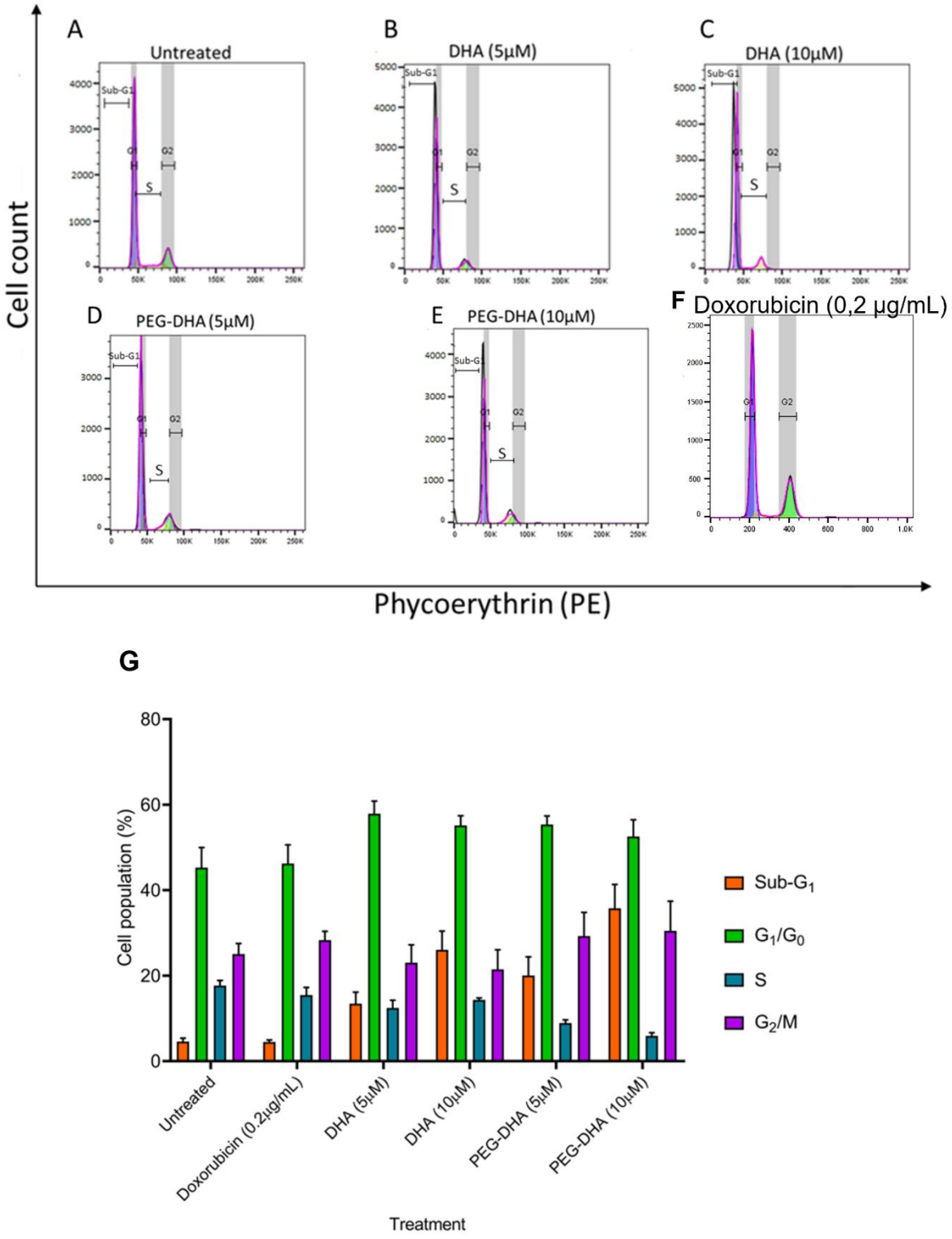

Figure 3.12: Cell cycling status of MIA PaCa-2 cells post-treatment with DHA and PEG-DHA. (A-F) Representative histograms showing the different phases of the cell cycle indicated by the white (sub-G_1), purple (G_1/G_0), yellow (S) and green (G_2/M) peaks. Interval arrow lines were inserted to highlight the sub-G1 and S phases. Overall, both DHA and PEG-DHA resulted in a dose-dependent arrest in the G_1/G_0 and an increment in apoptotic cells (sub-G_1). In addition, the conjugate arrested cells in the G_2/M phase. (G) Quantitative bar graphs indicating the overall cycling status of the pancreatic cancer cells (mean ± SEM), n=3, $p > 0.05$.

Overall, treating the non-cancerous cells with 0.33% DMSO resulted induced an S (25.15 ± 9.34%) and sub-G_1 phase arrests (3.50 ± 1.47%). In the MIA PaCa-2 cells, DMSO treatment only led to a G_1/G_0 phase arrest (67.77 ± 4.21%). These results can be found in Appendix XIII.

3.4. Summary of Flow Cytometry-based Studies

Apoptosis was the primary mode of cell death detected after treatment with the compounds. PEG-BA and PEG-DHA induced higher levels of apoptosis on the MIA PaCa-2 cells than the complementary free drugs. In the cell cycle studies, PEG-BA resulted in the highest sub-G_1 arrest. Both assays demonstrated that conjugation was necessary for improving the apoptosis-inducing ability of BA. Compared to all the compounds, PEG-BA presented as a potent inducer of apoptosis in pancreatic cancer cells, necessitating further testing.

CHAPTER 4
APOPTOSIS: MOLECULAR MECHANISM OF INDUCTION AND EVASION

4.1. Literature Review

Several studies have shown that BA has apoptosis-inducing potential in several tumours, including cervical (Wang et al., 2022), colon (Dutta et al., 2015), pancreatic cancer (Fru et al., 2021), leukaemia (Ehrhardt et al., 2004), multiple myeloma (Shen et al., 2019) and neuroblastoma (Schmidt et al., 1997; Fulda, 2008). There is consensus that the mechanism by which BA induces apoptosis is via the mitochondrial pathway (Fulda et al., 1998; Fulda, 2008; Csuk, 2014). Given that BA has limitations, as previously discussed, numerous formulations, such as nanoparticles (carbon, magnetic and polymeric), liposomes, and polymeric conjugates, have been tested to improve the anticancer properties of the compound (Saneja et al., 2018). However, the mechanisms of cell death associated with these formulations are not fully understood.

In this chapter, we explore the potential cell death mechanisms resulting from treating pancreatic cancer cells with PEG-BA only since it was the most promising of the two conjugates in the cytotoxicity and mode of cell death assays. This was done by quantifying apoptosis-related gene expression levels using real-time polymerase chain reaction. Tumour necrosis factor (*TNF*) and TNF-superfamily member 10 (*TNFSF10*) are genes that code for pro-inflammatory cytokines, which act as ligands that bind to death receptors, initiating the extrinsic pathway of apoptosis (Lafont et al., 2018). *CASPASE 2* codes for caspase 2, an initiator that can alter the mitochondrial membrane potential, activating the intrinsic apoptosis pathway. *CASPASE 8* codes for caspase 8, an initiator caspase of the extrinsic apoptosis pathway activated by the death-inducing signalling complex (DISC). *CASPASES 3* and *7* code for executioner caspases 3 and 7 that conveys the signal from initiator caspases and activates target proteins by cleavage, leading to apoptotic cell death (Miles & Hawkins, 2017). *BAX* codes for Bcl-2-associated X protein (Bax), a proapoptotic Bcl-2 (B-cell lymphoma 2) family member that homo-oligomerises with Bak forming a channel that leads to mitochondrial factors that activate the intrinsic apoptosis pathway (Karch et al., 2013). *BID* codes for BH3-interacting domain death agonist (Bid), also a proapoptotic member of the Bcl-2 family that functions in the extrinsic and intrinsic pathways of apoptosis and activates disruption of the mitochondrial outer membrane potential. All these genes are essential for

this study because they are usually downregulated in cancers, favouring survival over apoptosis.

The mechanism of apoptosis evasion was investigated by performing an ELISA to measure the protein level of NF-kB/p65 during PEG-BA treatment. It is well-documented that NF-κB protein subunits play an important role in inflammation, cell differentiation, proliferation, and death (Xia et al., 2014; Xia et al., 2018; Zinatizadeh et al., 2021). Mediation of inflammation by NF-κB takes place by the regulation of pro-inflammatory cytokines such as interleukins, transforming growth factor beta and tumour necrosis factor-alpha (Mosiane et al., 2023). In addition, NF-κB is continuously transcribed in pancreatic cancer, leading to transcriptional and translational upregulation of genes involved in angiogenesis, apoptosis induction, tissue invasion and growth factors, thus activating survival pathways (Mosiane et al., 2023).

4.2. Methods and Materials

4.2.1. Gene expression analysis of proapoptotic genes

Quantification of expression of the apoptotic and reference genes was performed before and after treatment with BA (4 µM), PEG-BA (4 µM) and gemcitabine (4.5 µM) on the MIA PaCa-2 and Vero cells, using real-time quantitative polymerase chain reaction (qPCR). This assay is based on the amplification of cDNA using intercalating DNA binding dyes such as SYBR green or probes specific to a particular DNA sequence such as a TaqMan probe mimicking the *in vivo* process of DNA replication. In qPCR, the amplification is monitored in real-time after every PCR cycle by detecting fluorescence emitted by the amplicon. We used the SYBR green-based qPCR method that binds to double-stranded DNA after detecting the target sequence. Although this increases the chances of non-specific binding, a melting curve is added at the end of the amplification to produce a dissociation curve to differentiate non-specific binding from the target amplicons (Chauhan, 2019).

Total RNA extraction

The RNA extraction step was done according to the manufacturer's guidelines, using the E.Z.N.A® Total RNA Kit I (Omega Bio-Tek, Norcross, GA, USA). Briefly, cells were seeded into 6-well plates at a concentration of 5×10^6 cells/mL and incubated overnight (95% humidity, 37℃, 5% CO_2). This was followed by treatment and incubation (95% humidity, 37℃, 5% CO_2) for 72 hours with complete DMEM, gemcitabine, BA, and PEG-BA. The cells were harvested using trypsin-EDTA dissociation reagent (Sigma-Aldrich, St Louis, MO, USA) and washed (200x *g* for 5 minutes). The centrifugation step was followed by

completely removing the media (supernatant). To lyse the cells, 700 µL of guanidium thiocyanate (GTC)-lysis buffer containing 2% β-mercaptoethanol was added to the pellet. The addition of the β-mercaptoethanol allows the inactivation of potential RNAses that might break down the required extract. This mixture was then transferred to an RNA Homogenizer Mini Column contained in a lid-free 2 mL collection tube and centrifuged for 60 seconds at 13 000x *g*. Freshly prepared 70% ethanol (700 µL) was added to the filtrate and gently vortexed, then transferred to a HiBind®RNA Mini Column in a collection tube. The mixture was centrifuged at 10 000x *g* for 60 seconds. The bound RNA was washed (30 seconds at 10 000x *g*) using 500 µL of RNA Wash Buffer I. The filtrate was discarded, and the RNA was rewashed (60 seconds at 10 000x *g*) using a second buffer (RNA Wash Buffer II containing 100% ethanol). This step was performed twice to ensure proper washing of the RNA before drying the HiBind®RNA Mini Column to remove any residual ethanol by centrifugation at 15 000x *g* for 2 minutes. The HiBind®RNA Mini Column was transferred to a 1.5 mL Eppendorf tube, followed by adding 60 µL of nuclease-free water and a centrifugation step (15 000x *g* for 120 seconds) to elute the RNA. The Nanodrop 2000 (Thermo Fischer Scientific, Waltham, MA, USA) was used to assess the purity and concentration of the samples. All RNA samples had A_{260}/A_{280} and A_{260}/A_{230} readings above 1.8 and 2.0, respectively. The RNA was stored in aliquots at -80℃ until required.

Complementary DNA synthesis

Two-step real-time PCR was used in this study. The first step is to convert the RNA to a complementary double-stranded DNA to be used as a template in the polymerase chain reaction. This is done by a transcriptase enzyme that reverses transcription from the normal DNA to RNA during protein synthesis into RNA to DNA. The ProtoScript II First Strand cDNA Synthesis Kit (New England BioLabs Inc, Ipswich, MA, USA) was used for this aspect of the assay. The manufacturer's protocol was followed. Briefly, 250 ng/µL of the RNA was thawed on ice for at least 30 minutes (or until the samples melted), and all the other reagents were kept on ice. The following components were mixed to make up the reaction required for cDNA synthesis: 2 µL of $d(T)_{23}$ VN (50 µM) primers that initiate cDNA synthesis by annealing to the poly-A tail of the RNA sample, 10 µL of the ProtoScript II Reaction Mix (2X) containing dNTPs in an optimised buffer, 2 µL of the Protoscript II Enzyme Mix (10X), a combination of ProtoScript II Reverse Transcriptase and Murine RNase inhibitor, and 6 µL of the RNA template diluted with the required amount of nuclease-free water to have a uniform final cDNA concentration of all the samples at 1000 ng/mL. The

PCR Eppendorf tubes containing 20 µL of the reaction components were then processed in a SimpliAmp Thermal Cycler (Thermo Fischer Scientific, Waltham, MA, USA) at the following conditions: 42℃ for one hour, enzyme inactivation at 80℃ for 5 minutes and an infinite hold at 4℃. Aliquots of 4 µL were made for each sample and kept at -80℃ for further use to avoid multiple freeze-thaw cycles.

Quantitative Polymerase Chain reaction

Quantitative PCR (qPCR) can be used to determine the expression levels of target genes. The assay was performed in a 96-well plate (on ice) according to the MIQE guidelines (Bustin et al., 2009). In summary, 5 µL of the PowerUp™ SYBR™ Green Master Mix (2X) containing Dual-Lock™ Taq DNA polymerase enzyme, uracil-DNA glycosylase (UGD) and 2'-deoxyuridine,5'-triphosphate (dUTP), was added to each well, in duplicate. This was followed by the addition of 0.5 µL each of the in-house designed reverse and forward primers (Table 4.1) of the apoptosis-related genes and the reference genes, β-Actin (*ACTB*) and mitochondrial ribosomal protein L19 (*MRPL19*), to the respective wells. The reference genes were chosen because they have been identified as suitable in pancreatic cancer gene expression studies (Hustinx et al., 2004; Rubie et al., 2005; Cherubini et al., 2021; de Koning et al., 2021).

The cDNA template (2 µL) was added to the plate, followed by 2 µL of nuclease-free water, forming 10 µL for each well. The QuantStudio™1 System thermocycler (Thermo Fischer Scientific, Waltham, MA, USA) was used to process the reaction under the conditions mentioned in Table 4.2. The .eds files obtained from the thermocycler were further analysed in MS Excel.

Table 4.1: List of genes used for real-time PCR and their primer sequences.

Gene Name	***Forward Primer Sequence***	***Reverse Primer Sequence***
TNF	5′-TGCACTTTGGAGTGATCGGC-3′	5′-TTGTCACTCGGGGTTCGAGA-3′
TNFSF10	5′-TTGGGACCCCAATGACGAAGA-3′	5′-TGGTCCCAGTTATGTGAGCTG-3′
BAX	5′-CCAGCAAACTGGTGCTCAAGG-3′	5′-ACAGGGACATCAGTCGCTTCA-3′
BID	5′-GACCCTGGGAGAGCTCTGAAGC-3′	5′-CTCCGACTCACTCCTGGTTCAC-3′
CASPASE 2	5′-TACTCCCACCGTTGAGCTGT-3′	5′-TGCCAGCTGGAAGTGTGTTTG-3′
CASPASE 3	5′-TTGGAACCAAAGATCATACATGGAA-3′	5′-TGAGGTTTGCTGCATCGACA-3′
CASPASE 7	5′-AGTGGATGCTAAGCCAGACCG-3′	5′-TCGAACGCCCATACCTGTCA-3′
CASPASE 8	5′-ATAGGC CTGTGACGAAGGTGC-3′	5′-GCGGAATGTAGTCCAGGCTCA-3′
ACTB[1]	5′-CTTCGCGGGCGACGAT-3′	5′-CCACATAGGAATCCTTCTGACC-3′
MRPL19[1]	5′-CCTAGGCCGGAGTTTCCAA-3′	5′-GACTCAAGAACCTGCGTTCC-3′

[1] The reference genes used to normalise fold expression.

Table 4.2: The PCR cycling conditions employed on the Thermocycler 1

	Process	***Temperature (℃)***	***Time (seconds)***
Hold	UGD activation	50	120
(1X)	Dual-lock DNA polymerase	95	120
PCR	Denaturation	95	15
(40X)	Annealing	50-60	15
	Extension	72	60
	Melting Curve	95	1
	(∞)	60	20
		95	1

Data Analysis

The .eds files obtained after the experiment were exported from the QuantStudio™1 thermocycler (Thermo Fischer Scientific, Waltham, MA, USA) into the Design & Analysis (2.6.0) Real-Time PCR System software for primary analysis, which involved the generation of the cycle threshold (C_t) values. The values were then exported to .xls files and analysed in MS Excel. The relative gene expression levels before and after treatment were analysed using the comparative C_t method. The fold changes were determined using the $2^{-\Delta\Delta C_t}$ method (Livak & Schmittgen, 2001). The data were plotted as mean ± SD to represent the relative fold change normalised by an average of the reference genes (*ACTB* and *MRPL19*).

4.2.2. NF-κB/p65 ELISA

The human nuclear factor kappa-B p65 subunit (NF-κB/p65) enzyme-linked immunosorbent assay (ELISA) kit (Elabscience Biotechnology Inc, Houston, Texas, USA) was used to determine the concentration of NF-kB/p65 present in cellular samples after treatment with complete DMEM, BA, PEG-BA, and gemcitabine. The assay is based on exploiting the specificity of antigen-antibody interactions that detect target proteins (antigens). An antigen containing the sample or standard is added to wells coated with a capture antibody. This is followed by adding a biotinylated detection antibody that will bind to its specific antigen epitope. The subsequent antibody-antigen-antibody interaction forms the "sandwich" ELISA (Sakamoto et al., 2018). A secondary antibody conjugated to an enzyme probe, such as alkaline phosphatase (ALP) or horseradish peroxidase (HRP), detects the biotinylated primary antibody. The substrate solution (containing 3,3',5,5'-tetramethylbenzidine (TMB)) will be converted to a chromogenic signal (blue) by the enzyme. The reaction is stopped producing a yellow-coloured solution which is then quantified (Burguillos, 2013; Sakamoto et al., 2018).

The assay was performed according to the manufacturer's protocol with slight modifications. Briefly, cells at a density of 2×10^6 cells/mL were seeded into a 6-well plate and incubated at 37℃ (95% humidity, 5% CO_2) for overnight attachment. This was followed by treatment with media only, 4.5 µM gemcitabine, 4 µM BA and 4 µM PEG-BA, followed by a 72-hour incubation period (95% humidity, 37℃, 5% CO_2). For this assay, the cell lysates were used.

Collection of cell lysates: After incubation, the cells were harvested using trypsin-EDTA dissociation solution (Sigma-Aldrich, St Louis, MO, USA) and washed (200x *g* for 5 minutes). The supernatant was discarded, and the pellet (containing cells) was washed (2500x *g* for 5 minutes at 4℃) using ice-cold 1xPBS. This step was repeated to remove any residual media. After the second centrifugation step, the pellet was resuspended in radioimmunoprecipitation assay (RIPA) lysis buffer (Thermo Fisher Scientific, Waltham, MA, USA), and the mixture was placed on ice for 15 minutes. The cell mixture was washed (14 000x *g* for 15 minutes at 4℃) to pellet the cell debris. The supernatant (containing the lysed cells) was aliquoted (110 µL) and stored at -20℃ until further use.

Sandwich ELISA procedure: Following the manufacturer's protocol, 100 µL of the kit standard (0-10 ng/mL) and lysates (diluted 2X with sample diluent) were added in duplicate to respective wells of the protein-coated 96-well plate, sealed and incubated at 37℃ (95% humidity, 5% CO_2) for 1.5 hours. The liquid was discarded, and 100 µL of the biotinylated detection antibody working solution was added to each well. The plate was sealed and incubated at the same conditions for an hour. This was followed by washing three times by adding 350 µL of the wash buffer, soaking for at least 60 seconds and aspirating the waste. Then 100 µL of HRP conjugate working solution was added to each well, sealed and incubated (95% humidity, 37℃, 5% CO_2) for 30 minutes. The liquid was decanted, followed by five washes. This was followed by adding the substrate reagent (90 µL) to the wells; the plate was sealed and covered in aluminium foil to protect it from light. The plate was incubated for at least 15 minutes (95% humidity, 37℃, 5% CO_2), followed by adding 50 µL of stop solution. The optical density was measured at 450 nm using the Multiscan Sky spectrophotometer (Thermo Fisher Scientific, Waltham, MA, USA).

Data analysis: Experimental repeats for the cell lysates (n=3) were performed for each sample in duplicate for the NF-κB ELISA. The data files obtained from the SkanIT Sky multi-plate reader software (Thermo Fischer Scientific, Waltham, MA, USA) were exported as .xls files for analysis in MS Excel. A standard curve (Appendix XIV) was used to

extrapolate the concentration of NF-κB/p65 in each sample after treatment. The results were plotted as bar graphs (mean ± SEM) using GraphPad Prism software (v8.0.2.263).

4.2.3. Statistical Analysis

Normality tests were followed by two-way ANOVA and Tukey's *post hoc* test for normally distributed data for the statistical analysis. The Kruskal-Wallis test, followed by Dunn's *post hoc* test, was done for non-parametric data. Data with $p < 0.05$ was considered statistically significant.

4.3. Results and Discussion

4.3.1. Gene expression profiles of apoptosis-related genes

Following results obtained by the apoptosis assay using flow cytometry where PEG-BA resulted in a dose-dependent induction of apoptotic cell death, the current study investigated the molecular mechanism by profiling genes associated with apoptosis (*BAX, BID, CASPASES (2, 3, 7* and *8), TNF* and *TNFSF10*). According to the Central Dogma of molecular biology, DNA serves as the genetic material that is transcribed into messenger RNA and translated into proteins which are essential for cellular functioning (Zhao and Krishnan, 2014). Therefore, a link exists between mRNA and protein levels. A study by Vogel and Marcotte (2013) showed that there is a 40% correlation between gene expression (mRNA quantification) and protein levels (Vogel and Marcotte, 2013). Hence, in this study, the real-time PCR results were compared with literature findings based on proteins that function in apoptosis to try and predict the potential apoptotic mechanism of PEG-BA in PC cells.

Relative to the untreated MIA PaCa-2 cells, BA treatment resulted in a moderate increase in *TNF* (3.47 ± 1.95; p = 0.3048) and *CASPASE 3* expression (4.02 ± 1.93; p = 0.1712), which was associated with downregulation of *CASPASE 8* (0.40 ± 1.93; $p = 0.0401$) (Figure 4.1A). Studies have shown that, in most cancers, there is overexpression of anti-apoptotic genes coupled with downregulation or silencing (inactivation) of pro-apoptotic genes (Wong, 2011; Hong-Duck, 2016). A contradictory finding was made in melanoma cells where "cell-free" mitochondrial studies using BA demonstrated that the drug could activate caspase 8 and 3 without needing the TNF-receptor (since it is found on the cell-free surface), suggesting that the apoptosis-inducing ability of BA may be cell-type specific (Fulda, 2008; Csuk, 2014). Compared to BA, treating the MIA PaCa-2 cells with PEG-BA resulted in the non-significant upregulation of *TNF* (3.47 ± 1.95 vs 23.72 ± 1.03; p = 0.3048) and *TNFSF10* (1.24 ± 1.93 vs

4.87 ± 1.94; p > 0.9999) (Figure 4.1A). The products of *TNF* and *TNFSF10* can be inhibited by binding to decoy receptors such as cellular-FLICE inhibitory protein (cFLIP), which aid cell proliferation and are overexpressed and differentially spliced in several cancer types' (Tenev et al., 2001; Riley et al., 2013). The inhibition occurs because of the absence of a death effector domain (DED), used by tumour necrosis factor receptor type 1-associated DEATH domain (TRADD) adaptor molecules and procaspase 8 to form the DISC, whose inhibition disrupts the extrinsic pathway of apoptosis (Thapa et al., 2022). Studies have shown that cFLIP overexpression in cancer cells is associated with the accumulation of procaspase 8 and 3, suggesting direct inhibition of apoptosis (Tenev et al., 2001; Riley et al., 2013).

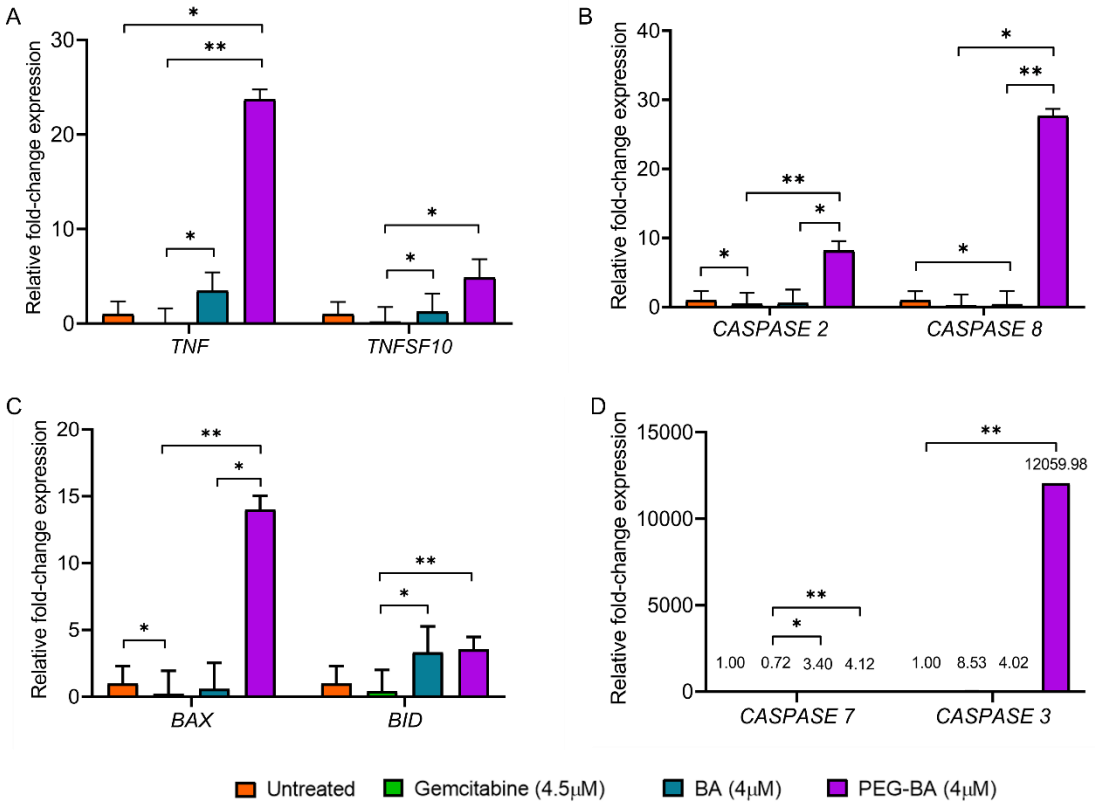

Figure 4.1: Fold change expression of apoptosis-related genes in treated and untreated MIA PaCa-2 cells. MIA PaCa-2 cells were treated with PEG-BA and BA (4 μM), and the expression of (A) TNF and TNFSF10 (B), CASPASE 2 and CASPASE 8 (C) BAX and BID (D) CASPASE 7 and CASPASE 3. Treatment with PEG-BA showed the most significant fold change of TNF (23.72 ± 1.03), TNSF10 (4.87 ± 1.94), BAX (14.01 ± 3.55), CASPASE 3 (12059.98 ± 1.74), CASPASE 2 (8.16 ± 1.40) and CASPASE 8 (27.69 ± 0.99). Expression values are shown as the mean ± SD, *p < 0.05 and **p < 0.01.

Furthermore, comparing BA to PEG-BA treatment showed overexpression of *CASPASE 2* (0.58 ± 1.93 vs 8.16 ± 1.40; p = 0.0401), *CASPASE 8* (0.40 ± 1.93 vs 27.69 ± 0.99; p = 0.0021), *CASPASE 3* (4.02 ± 1.93 vs 12059.98 ± 1.74; p = 0.0872) and *CASPASE 7* (3.40 ± 1.97 vs 4.12 ± 1.74; p = 0.9092) (Figures 4.1 B and D). The initiator caspases (2 and 8) are activated by forming complexes that facilitate their hydrolysis, which is necessary for caspase function (Chen et al., 2018). The activated initiators then activate the executioner caspases (3 and 7), resulting in apoptosis activation. Both types of caspases are inhibited by the inhibitors of apoptosis (IAPs), which directly prevent functioning by binding to them and inhibiting their interactions with target substrates necessary to induce apoptosis (Hunter et al., 2007). In several cancer types, overexpression of survivin, a type of IAP, leads to the survival, proliferation, and progression of transformed cells (Nachmias et al., 2004; Liang et al., 2020). The function of Bid protein in type 2 cells with low caspase signal is necessary for the activation of the mitochondrial pathway, either by direct inhibitory binding to the Bcl-2 protein, allowing Bax/Bak oligomerisation, or directly triggering the release of cytochrome c (Desagher et al., 1999; Korsmeyer et al., 2000; Gu et al., 2005). In this study, PEG-BA resulted in the overexpression of *BAX* (0.60 ± 1.93 vs 14.01 ± 3.55; p = 0.0401) and *BID* (3.34 ± 1.93 vs 3.55 ± 0.93; p = 0.9092) in the MIA PaCa-2 cells (Figure 4.1C). In most cancers, including pancreatic cancer, both proapoptotic proteins are inhibited by high expression of Bcl-2 antiapoptotic proteins, facilitating the evasion of apoptosis (Chipuk et al., 2008). A study by Naseri and colleagues (2015) showed that apoptosis could be restored in cancer cells such as HepG2, T47D and HCT116 by activating Bax (Naseri et al., 2015).

Overall, these results demonstrated that PEG-BA improved the apoptosis-inducing ability of BA by leading to transcription of pro-apoptotic genes involved in the intrinsic and extrinsic apoptosis pathways. These results correlated with the previously discussed flow cytometry results, which showed high levels of apoptosis (Fru et al., 2021). Relative to the untreated MIA PaCa-2 cells, treatment with gemcitabine resulted in an increased fold-change expression of *CASPASE* 3 (8.53 ± 1.55; p = 0.0872), and all the other genes were downregulated. This may suggest that gemcitabine possibly induces apoptosis using other genes not tested in this study. Treatment with PEG-BA in comparison with gemcitabine showed an increased expression of *TNF* (23.72 ± 1.03 vs 0.20 ± 1.54; p = 0.0021), *CASPASE 8* (27.69 ± 0.99 vs 0.49 ± 1.54; p = 0.0401), BID (3.55 ± 0.93 vs 0.42 ± 1.59; p = 0.0087), *CASPASE 2* (8.16 ± 1.40 vs 0.26 ± 1.55; p = 0.0021), *CASPASE 7* (4.12 ± 1.74 vs 0.72 ±

1.55; p = 0.0087), *TNFSF10* (4.87 ± 1.94 vs 0.06 ± 1.55; p = 0.0166) and *BAX* (14.01 ± 3.55 vs 0.23 ± 1.71; p = 0.0021). Furthermore, even though there was overexpression of *CASPASE 3* (12059.98 ± 1.74 vs 8.53 ± 1.55; p = 0.1712), it was not statistically significant (p > 0.05). These results show that PEG-BA may have a higher potential for inducing apoptosis in the MIA PaCa-2 cells than gemcitabine. The fold-change expression levels obtained after treatment with BA, PEG-BA and gemcitabine on the normal cell line are shown in Appendix XV.

4.3.2. Analysis of NF-κB expression with drug treatments

The human nuclear factor kappa light chain enhancer of B cells p65 subunit (NF-κB/p65) enzyme-linked immunosorbent assay (ELISA) kit was used to assess the apoptosis evasion mechanism of pancreatic cancer cells pre-and post-treatment with BA and PEG-BA. At rest, NF-κB is inactivated by the bound inhibitor IKB protein family, preventing its translocation to the nucleus (Xia et al., 2018). Phosphorylation inhibits IKBs and releases NF-κB, leading to dimerization of its subunits (canonical: p50 and p65 or non-canonical: p100 and p52), which translocate to the nucleus and activate transcription of their target genes (Xia et al., 2018; Zinatizadeh et al., 2021). Some of the NF-κB targets (such as cytokines) can induce changes in the mitochondrial function resulting in ROS necessary to change the permeability of the outer membrane (Carra et al., 2022). This has been associated with release of mitochondrial components such as apoptosis-inducing factor (AIF), cytochrome c, and second mitochondria-derived activator of caspase/ direct inhibitor of apoptosis (IAP) binding protein with low pI (Smac/DIABLO) (Ali-Seyed et al., 2016; Zhang et al., 2019), initiating the intrinsic pathway of apoptosis. Furthermore, some studies have shown the presence of NF-κB components within the mitochondria which can further influence changes in mitochondrial outer membrane potential after a stimulus (Albensi et al., 2019). It is still unclear how NF-κB translocates to the mitochondria, however hypotheses have been made that NF-κB may permanently reside in the organelle and that it requires certain stimulus for activation (Carra et al., 2022).

It is worth noting that quantifying protein level using an ELISA does not provide information on the location of the protein but is based on exploring the specificity of antigen-antibody interactions that detect target proteins (in this case NFkB-p65). However, given that cell lysates were collected, it is safe to assume that intracellular (nuclear + cytosolic) NFkB-p65

was measured and that disruption of the plasma membrane was necessary to release adequate amounts of the protein (Xia et al., 2018).

Overall, treatment with BA resulted in a moderate increase in NF-κB concentration (Figure 4.2) relative to the untreated sample (2.78 ± 0.27 vs 2.70 ± 0.21 ng/mL; p = 0.9484). Studies have shown that BA can activate NF-κB by inducing phosphorylation of the IKBs (Zuco et al., 2002; Fulda, 2008; Kumar et al., 2018a). Compared to BA treatment (p = 0.2863) and the untreated sample (p = 0.1521), PEG-BA (3.09 ± 0.42 ng/mL) resulted in an even higher concentration of NF-κB (Figure 4.2). This finding is not surprising given that we also showed an increased expression of *TNF* (23.72 ± 1.03), a well-documented activator of NF-κB (Xia et al., 2018; Zinatizadeh et al., 2021), with PEG-BA treatment further supporting a potential activation of the NF-κB pathway. The control drug, gemcitabine led to a reduction of NF-κB concentration compared to the untreated sample (2.67 ± 0.19 ng/mL vs 2.70 ± 0.21 ng/mL; p = 0.9981).

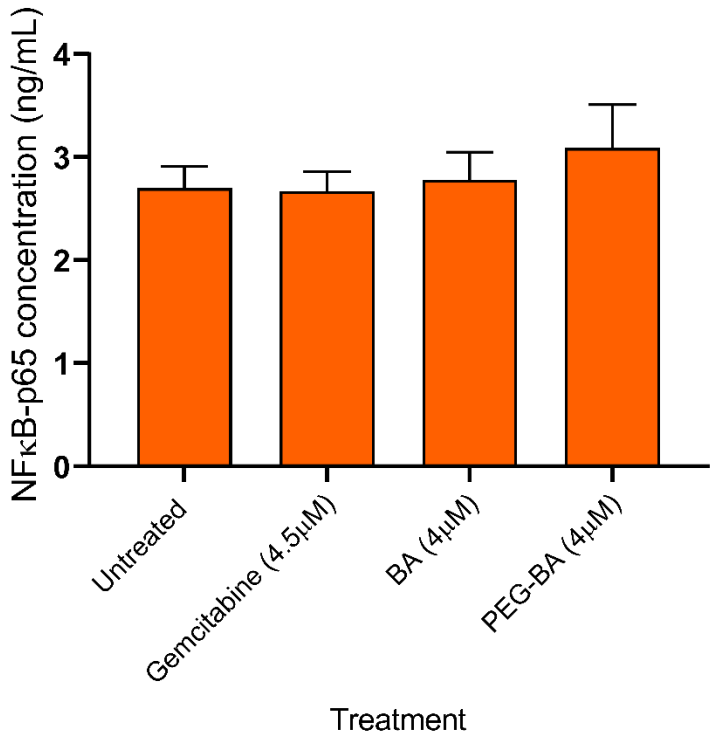

Figure 4.2: NF-κB protein levels from untreated cell lysates, BA, and PEG-BA treated MIA PaCa-2 cells. Treatment with PEG-BA (3.09 ± 0.42 ng/mL) and BA (2.78 ± 0.27 ng/mL) resulted in moderately increased NF-κB levels compared with other groups (untreated: 2.70 ± 0.21 ng/mL and gemcitabine: 2.67 ± 0.19 ng/mL). The data is represented as the mean ± SEM.

Although NF-κB has always been regarded as an active inducer of survival pathways in several malignancies (Xia et al., 2014), studies have shown a positive link between NF-κB signalling and apoptosis, specifically its p65 subunit (Lin et al., 1999; Xia et al., 2018; Zinatizadeh et al., 2021). Furthermore, the protein has been shown to be necessary to induce BA-associated apoptotic cell death (Zuco et al., 2002). Additionally, introducing NF-κB inhibitors in cells reduced BA-related apoptosis, reiterating that NF-κB activation is necessary for BA to induce its apoptotic effect on cancer cells (Zuco et al., 2002). Ryan and colleagues demonstrated the proapoptotic role of NF-κB in Soas-2 cells. The authors found that p53 (a protein also increased in MIA PaCa-2 cells) induces translocation of NF-κB to the nucleus, thereby activating binding to DNA (Ryan et al., 2000). In addition, inhibiting NF-κB reduced apoptosis, suggesting that NF-κB may be crucial in the induction of apoptosis by doxorubicin in Soas-2 cells (Ryan et al., 2000). Another study showed that the activation of the NF-κB/p65 by aspirin resulted in the induction of Bax-dependent apoptosis in human colorectal carcinoma cells (Khandelwal et al., 2011). It is worth noting that, in this study, PEG-BA treatment resulted in overexpression of *BAX* (14.01 ± 3.55) in the MIA PaCa-2 cells. These findings may suggest that NF-κB plays an important proapoptotic role, which may be improved by PEG-BA treatment.

4.4. Summary of the Apoptosis Induction and Evasion Mechanism

In the pancreatic cancer cells, the polymer-drug conjugate, PEG-BA, resulted in the overexpression of apoptotic genes with involvement in both the extrinsic and intrinsic pathways. This showed that polymer conjugation was necessary to improve the apoptosis-inducing ability of BA. One of the reasons why a low level of statistical significance was observed may be due to the limited number of repeats that were performed for this assay. This is because limited repeats have the potential of reducing the statistical power which can result in p values that are greater than alpha ($p > 0.05$) (Vaux et al, 2012; Faber and Fonseca, 2014; Leppink et al., 2016). This means that during hypothesis testing, the null hypothesis was accepted, suggesting that the different effects of treatment may have been caused by chance (Grabowski, 2016). In addition, high variability in the reported data for BA treatment may be another reason. Therefore, when the standard deviation is high, the data is more spread out and hypothesis tests can produce imprecise estimates of the drugs' effect. Therefore, more repeats are required to confirm these findings.

It is worth noting that several studies in literature have shown that certain drugs (such as BA) possess the ability to not only lead to the transcription and translation of pro-apoptotic genes and proteins, but also to their activation (Janyst et al., 2017; Kuo et al., 2018). Because caspases are enzymes that require cleavage for activation, protein analysis studies are necessary to validate caspase activity post treatment (Yurasakpong et al., 2021). Furthermore, treatment with BA and PEG-BA led to a moderate increase in NF-κB concentration (without statistical significance), suggesting that it is safe to hypothesize that BA and PEG-BA have the potential of activating NF-κB, however, more studies are required to determine how this occurs. In addition, its noteworthy to state that NF-κB activation is not the only role player of BA-related apoptosis, hence it is still being studied further to confirm whether absence of NF-κB results in complete inhibition of apoptosis.

CHAPTER 5

CONCLUDING DISCUSSIONS

This chapter provides general comments based on the different study objectives, considerations for future work, study limitations, and the conclusion.

5.1. Summary of Findings

5.1.1. Does conjugation improve anti-cancer activity by improving cytotoxicity and antioxidant potential?

In this study, prodrug constructs, PEG-BA, and PEG-DHA, revealed better anticancer properties than the free drugs, BA, and DHA. Treatment with PEG-BA improved the cytotoxicity profile of BA, where the viability of the Vero and MIA PaCa-2 cells decreased dose-dependently, as shown in Chapter 2 (Figure 2.5). Furthermore, half-maximal concentrations (IC_{50}) required to inhibit at least 50% of the cell population for PEG-BA treated cells were significantly improved (Chapter 2; Table 2.1), whereas a 13.39-fold higher concentration of BA was required, indicating improved potency on conjugation. Cytotoxicity alone in cancer therapy is not enough. Most treatments are effective for killing tumours but also affect the viability of normal or neighbouring cells, making specificity an imperative factor to consider. PEG-BA resulted in a selectivity index of 3.00, suggesting that the conjugate selectively targeted the MIA PaCa-2 cells. A similar improvement was observed when analysing the cytotoxic effect of DHA and its complementary conjugate on the cell lines (Chapter 2; Figure 2.5), although comparatively lower than BA and PEG-BA effects. The potency of PEG-DHA was higher than the free drug, where a 1.68-fold higher concentration of DHA was required to kill 50% of the MIA PaCa-2 cells. Moreover, the selectivity index of DHA was 1.12, and 1,61 for PEG-DHA (Table 2.1), indicating improved targeting.

Light microscopy was used to assess the morphological effect of PEG-BA treatment on MIA PaCa-2 cells. The result was the formation of smaller clumps of detached and rounded cells, a morphological feature of apoptosis induction and progression (Chapter 2; Figure 2.6). Analysis of the antioxidant potential of the compounds using the DPPH assay revealed that PEG-BA could reduce the DPPH radical at lower concentrations than BA, DHA, PEG-DHA and the ascorbic acid standard or control (Chapter 2; Figure 2.7). The level of hydroperoxide and ROS metabolites before and after treatment was assessed using a DEPPD assay. The free drugs showed minimal response compared to the conjugates, suggesting that pegylation by conjugation with PEG was necessary to improve the antioxidant potential of the free drugs

against the pancreatic cancer cell line (Chapter 2; Figure 2.8). Overall, the conjugates improved the ability of BA and DHA to scavenge radicals, another important hallmark in cancer treatment, but this was more prominent for PEG-BA than PEG-DHA.

5.1.2. Does conjugation improve anti-cancer activity by induction of apoptotic cell death mechanisms?

Flow cytometric analysis confirmed that BA and DHA are apoptosis-inducing compounds. In the annexin-V/PI staining technique, when PEG-BA was used to treat the MIA PaCa-2 cells, high levels of early apoptosis were induced compared to other modes of cell death and in a dose-dependent manner (Chapter 3; Figure 3.5). This was an improvement from the low levels of apoptosis observed when only BA was used as treatment. Furthermore, cell cycle analysis confirmed that PEG-BA improved the apoptosis-inducing ability of free BA by inducing a sub-G_1 phase arrest (Chapter 3; Figure 3.10). Early apoptosis ($Annexin^+/PI^-$) induction was higher in the DHA-treated cells than in the MIA PaCa-2 cells treated with BA. However, conjugating DHA to PEG resulted in lower levels of apoptosis induction than PEG-BA. Despite this, overall, conjugation improved the apoptosis-inducing ability of DHA, which was confirmed in the cell cycle studies (Chapter 3; Figures 3.7 and 3.12). Given that one of the main aims of this project was to determine the potential mechanism of dihydroartemisinin polymer-drug conjugate (PEG-DHA) on pancreatic cancer cells, Figure 5.1 was developed to summarise the findings.

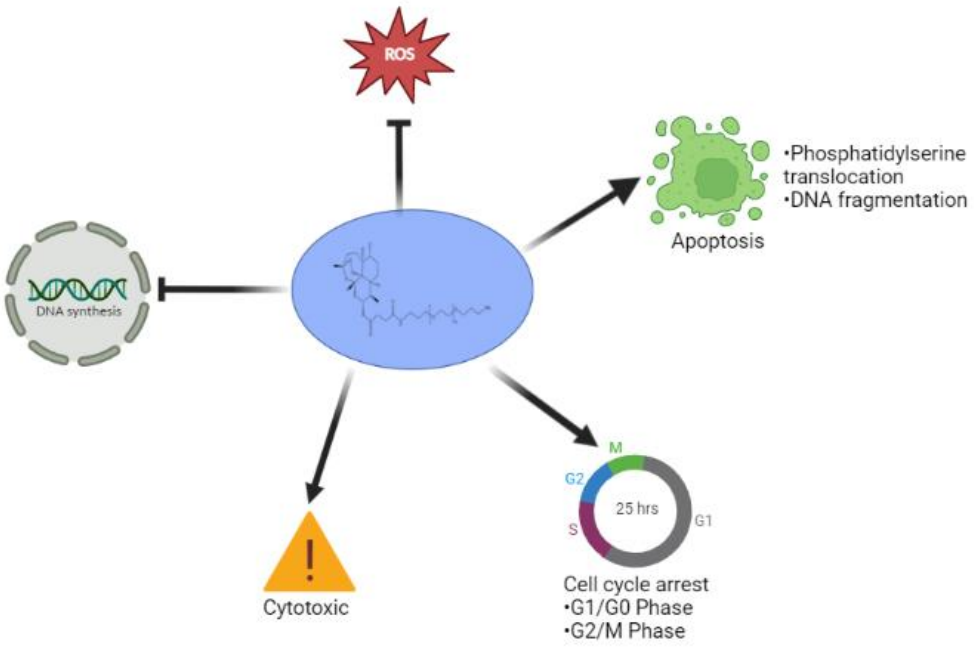

Figure 5.1: Schematic diagram of the proposed cell death mechanism of PEG-DHA on pancreatic cancer cells. Compared to DHA, PEG-DHA showed improved selective cytotoxicity to pancreatic cancer cells. The conjugate also possessed promising ROS-reducing capacity and, therefore, antioxidant potential. Apoptosis was the primary mode of cell death induced in the pancreatic cancer cell line. It was characterised by two features: (1) the flip of phosphatidylserine (PS) in the outer leaflet of the plasma membrane, which was bound by annexin-v and allowed for quantification in the annexin V/PI studies, and (2) the accumulation of cells in the sub-G_1 phase of the cell cycle. Furthermore, PEG-DHA induced G_1/G_0 and G_2/M arrests after 72 h treatment (inhibiting the MIA PaCa-2 cells from cycling into the other phases of the cell cycle). Lastly, the conjugate inhibited DNA synthesis at all tested concentrations.

5.1.3. Does conjugation improve the expression of apoptotic-related genes and related proteins?

This part of the study was only performed on BA and PEG-BA with gemcitabine as the control drug on the MIA PaCa-2 cells. The conjugate improved the apoptosis-inducing ability of BA as it resulted in upregulation and overexpression of *TNF*, *TNFSF10*, *BID*, *BAX*, *CASPASE 2*, *CASPASE 3*, *CASPASE 7*, and *CASPASE 8*, proapoptotic genes involved in both extrinsic and intrinsic pathways of apoptosis (Chapter 4; Figure 4.1). BA and PEG-BA activated NF-κB, an inflammatory protein involved in the evasion of apoptosis by cancer cells. The protein did not affect apoptosis because it is necessary to induce BA-related apoptosis (Chapter 4; Figure 4.2). Determining the potential mechanism of betulinic acid polymer-drug conjugate (PEG-BA) on MIA PaCa-2 (pancreatic cancer) cells was one of the main aims of this study. Therefore, Figure 5.2 was developed to summarise all the findings.

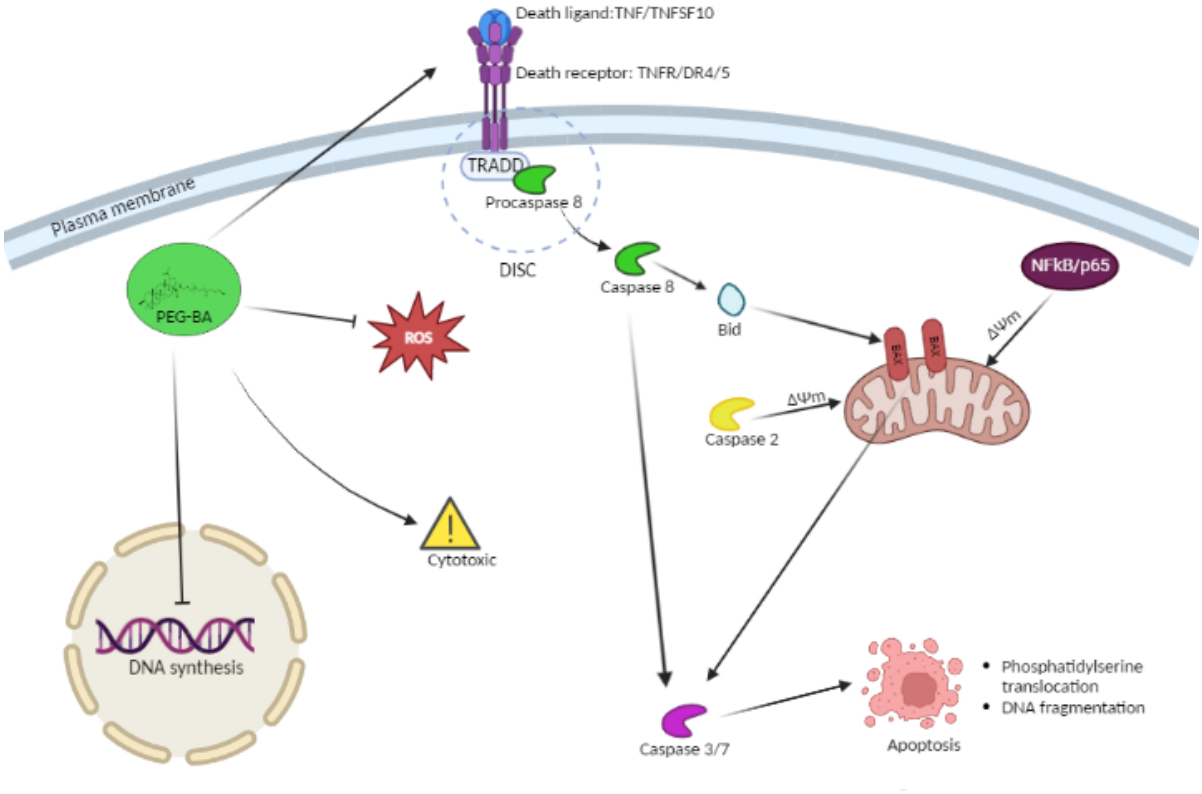

Figure 5.2: The proposed mechanism by which PEG-BA induces cell death in pancreatic cancer cells. PEG-BA (green oval) inhibits DNA synthesis of the MIA PaCa-2 cells, observed as a reduction in the cells cycling in the S-phase. The conjugate also exhibits selective cytotoxicity to the pancreatic cancer cells, indicated by a low IC_{50} and higher selectivity index. PEG-BA prevents the accumulation of reactive oxygen species (ROS), indicative of the antioxidant potential of the PEG-BA. Regarding cell death, the conjugate induces apoptosis in the cancer cells. This might be through the extrinsic pathway where a death signal induces ligation of tumour necrosis factor (TNF) or TNF superfamily member 10 (TNSFS10) to their respective receptors (TNF receptor (TNFR) or death receptor 4 or 5 (DR4/5) as shown at the membrane level. This allows for the potential recruitment of adaptor proteins such as TNFR type 1-associated DEATH domain protein (TRADD), which eventually leads to the binding of inactive caspase 8 (procaspase 8), forming the death-inducing signalling complex (DISC), leading to autoactivation of procaspase 8. Therefore, caspase 8 can directly activate procaspase 3/7 or require amplification of the death signal via cleavage of Bid. The cleaved Bid can activate Bax (intrinsic pathway), which leads to downstream activation of caspase 3/7. In addition, PEG-BA also leads to an increase in NF-kB, which suggests that the target of NF-κB (represented as NFkB/p65) can induce cellular damage enough to disrupt the mitochondrial membrane potential (ΔΨm), leading to further mitochondrial perturbations. PEG-BA can potentially activate caspase 2, which also leads to ΔΨm. After the caspase 3/7 effector is activated, it leads to apoptosis, observed by the characteristic phosphatidylserine translocation and potential DNA fragmentation. This schematic diagram is based on deductions from the literature and findings from this study.

5.2. Future Work

5.2.1. Three-dimensional cell culture and in vivo studies

In this study, two-dimensional cell culture was used to assess the effect of PEG-BA and PEG-DHA on pancreatic cancer and normal cell lines. However, this type of cell culture does not

fully reflect the complex processes and interactions in living organisms (Jensen & Teng, 2020; Baruffaldi et al., 2021). A potential solution is to use three-dimensional (3D) cell culture, which mimics *in vivo* cell growth (Langhans, 2018). This is because 3D cell culture has an ECM (scaffold of hydrogels or organoids), cell-cell and cell-ECM interactions, and preserves the natural morphology of the cells (Jensen & Teng, 2020). 3D cell culture can reflect the heterogenous microenvironment of cancer cells (Baruffaldi et al., 2021). Lastly, *in vivo* studies are crucial in discovering new drugs that can be used for cancer treatment to understand the drug effects in living organisms fully (Brake et al., 2017).

5.2.2. Analysis of the effect of PEG-BA on MOMP

Several studies have shown that BA can induce apoptosis via the mitochondrial pathway. This confirmation was made by analysing the effect of BA on the mitochondrial outer membrane potential (MOMP), which is usually disrupted in the early stages of intrinsic apoptosis. The results obtained in this study indicate that PEG-BA induces apoptosis using both pathways; however, analysis of MOMP using dyes such as JC-1 could offer specific data on how PEG-BA induces apoptosis via the mitochondrial pathway. Data from such an assay could be crucial in developing a list of targets for PEG-BA, especially in pancreatic cancer cells.

5.2.3. Protein expression assays

It is well-documented that not all transcribed mRNA gets translated into proteins. This means that further studies are required to properly delineate the mechanism of apoptotic cell death caused by PEG-BA on the MIA PaCa-2 cells. Western blotting techniques of the initiator caspases (2, 8 and 9), executioner caspases (3 and 7), anti- and proapoptotic proteins (Bcl-2, Bax etc.), and poly adenosine diphosphate-ribose polymerase (PARP) could add more information on the pathway of PEG-BA induced apoptosis in pancreatic cancer cells. In addition, combined immunofluorescences that focus on combining direct and indirect antigen detection via antigen-antibody interactions could be used to quantify protein expression of the initiator and executioner caspases. Enzyme-linked immunosorbent assays (ELISAs) could also be considered for protein quantification.

5.2.4. Metabolomic analysis

Studies have shown that dysregulated metabolism is an important factor supporting the needs of cancer cells for uncontrolled proliferation and differentiation (Beger, 2013; DeBerardinis and Chandel, 2016). The importance of metabolomic studies in cancer treatment is that they

can help elucidate potential drug targets while enhancing the understanding of mechanisms of action employed by the tested drug (Cuperlovic-Culf & Culf, 2016). Therefore, a metabolic platform such as mass spectrometry or nuclear magnetic resonance (NMR) spectroscopy could quantify the apoptosis-related metabolites produced in pancreatic cancer cells in response to PEG-BA (Halama et al., 2013).

5.2.5. Specialised polymer-drug conjugation

Polymer-drug conjugation is a potential alternative to the plethora of downsides associated with current chemotherapeutic drugs. Advanced nanomedical synthesis, such as dual co-polymers, conjugating more than one drug, substituting different functional groups of currently known anticancer phytochemicals and conjugating them to smart materials that could exhibit conformational changes because of external stimuli could be considered in the future. They all serve as the basis of the evolution of polymer-drug conjugation for advanced and specialised targeting of cancer cells.

5.3. Study Limitations

The effect of the stroma on treatment with polymer-drug conjugates

The tumour microenvironment (TME) in pancreatic cancer is one of the critical determinants of treatment response because PC is characterised by a desmoplastic stroma (Wang et al., 2021). The stroma component assists the tumour cells with growth and progression into invasion and metastasis to distant sites (Baghban et al., 2020). Therefore, stromal cells can influence response to treatment by limiting access to the tumour cells (Hirata & Sahai, 2017). The theory behind polymer-drug conjugates offers a potential solution to this problem via the enhanced permeability and retention (EPR) effect (Mthimkhulu et al., 2021). This phenomenon exploits the leaky vasculature of tumour cells and the lack of a defined lymphatic system by allowing the drug to permeate and be retained in the TME (Mthimkhulu et al., 2021). Polymer-drug conjugates may be modified to consist of a targeting moiety in addition to the basic units of a polymer, drug, and a linker to fully benefit from the EPR effect (Alven et al., 2020). No targeting moiety was used in this study; therefore, this may have limited the ability of the conjugates to target the tumour cells selectively. In the cytotoxicity studies, PEG-BA induced a highly selective cytotoxic effect against pancreatic cancer cells. However, in the flow cytometry assays, the conjugate also induced apoptotic cell death in the non-cancerous cells although this was not as significant as the standard chemotherapeutic drugs.

5.4. Overall Conclusion

This study showed that polymer-drug conjugation is a promising alternative for improving the activity of potential phytochemicals for cancer treatment. This was demonstrated using two existing natural-based drugs, BA, and DHA. Conjugation of both drugs to PEG improved cytotoxicity, potency, and selectivity to MIA PaCa-2 compared to normal Vero cells. The concurrent improvement in reducing reactive oxygen species activity and the observed antioxidative potential after conjugation, especially of PEG-BA, makes the conjugate an 'ideal' anti-cancer agent. Furthermore, there was an improvement in apoptosis induction, a critical cell death mechanism evaded in most cancer types. Taken together, the findings from this study suggest that conjugation is a viable approach to improving anticancer potential. It is recommended that PEG-BA be explored further for consideration in pancreatic cancer treatment.

REFERENCES

Abitan, H., Bohr, H. and Buchhave, P. (2008). Correction to the Beer-Lambert-Bouguer law for optical absorption. *Applied Optics*, 47(29), 5354-5357. https://doi.org/10.1364/AO.47.005354

Abu-Odah, H., Molassiotis, A. and Liu, J. (2020). Challenges on the provision of palliative care for patients with cancer in low- and middle-income countries: a systematic review of reviews. *BMC Palliative Care*, 19(55), 1-16. https://doi.org/10.1186/s12904-020-00558-5

Adan, A., Alizada, G., Kiraz, Y., et al. (2017). Flow cytometry: basic principles and applications. *Critical Reviews in Biotechnology*, 37(2), 163–176. https://doi.org/10.3109/07388551.2015.1128876

Adesanwo, J.K., Makinde, O.O. and Obafemi, C.A. (2013). Phytochemical analysis and antioxidant activity of methanol extract and betulinic acid isolated from the roots of Tetracera potatoria. *Journal of Pharmacy Research*, 6, 903–907. https://doi.org/10.1016/j.jopr.2013.09.003

Ahmed, S., Bradshaw, A.-D., Gera, S., et al. (2017). The TGF-β/Smad4 Signaling Pathway in Pancreatic Carcinogenesis and Its Clinical Significance. *Journal of Clinical Medicine*, 6(5), 1-11. https://doi.org/10.3390/jcm6010005

Aiken, C. and Chen, C. (2005). Betulinic acid derivatives as HIV-1 antivirals. *Trends in Molecular Medicine*, 11(1), 31–36. https://doi.org/10.1016/j.molmed.2004.11.001

Albensi, B.C. (2019). What is nuclear factor kappa B (NFkB) doing in and to the mitochondrion. *Frontiers in Cell and Developmental Biology*, 7:154. https://doi.org/10.3389/fcell.2019.00154

Ali-Seyed, M., Jantan, I., Vijayaraghavan, K., et al. (2016). Betulinic Acid: Recent Advances in Chemical Modifications, Effective Delivery, and Molecular Mechanisms of a Promising Anticancer Therapy. *Chemical Biology & Drug Design*, 87, 517–536. https://doi.org/10.1111/cbdd.12682

Alvares, J.J. and Furtado, I.J. (2021). Kinetics of DPPH• scavenging by bacterioruberin from Haloferax alexandrinus GUSF-1 (KF796625). *Journal of Analytical Science and Technology*, 12(44), 1-11. https://doi.org/10.1186/s40543-021-00293-3

Alven, S., Nqoro, X., Buyana, B., et al (2020). Polymer-Drug Conjugate, a Potential Therapeutic to Combat Breast and Lung Cancer. *Pharmaceutics*, 12(406), 1-24. https://doi.org/10.3390/pharmaceutics12050406

Ammerman, N.C., Beier-Sexton, M. and Azad, A.F. (2008). Growth and Maintenance of Vero Cell Lines. *Current Protocols on Microbiology*, 11, 1-10. https://doi.org/10.1002/9780471729259.mca04es11

Anaya-Eugenio, G.D., Eggers, N.A., Ren, Y., et al. (2020). Apoptosis Induced by (+)-Betulin Through NF-κB Inhibition in MDA-MB-231 Breast Cancer Cells. *Anticancer Research*, 40, 6637–6647. https://doi.org/10.21873/anticanres.14688

Anderson, L.N., Cotterchio, M. and Gallinger, S. (2009). Lifestyle, dietary, and medical history factors associated with pancreatic cancer risk in Ontario, Canada. *Cancer Causes Control*, 20, 825–834. https://doi.org/10.1007/s10552-009-9303-5

Anggraini, T., Wilma, S., Syukri, D., et al. (2019. Total Phenolic, Anthocyanin, Catechins, DPPH Radical Scavenging Activity, and Toxicity of Lepisanthes alata (Blume) Leenh. *International Journal of Food Science*, 2019, 1–7. https://doi.org/10.1155/2019/9703176

Ansari, D., Gustafsson, A. and Andersson, R. (2015). Update on the management of pancreatic cancer: Surgery is not enough. *World Journal of Gastroenterology*, 21(11), 3157–3165. https://doi.org/10.3748/wjg.v21.i11.3157

Antolovich, M., Prenzler, P.D., Patsalides, E., et al. (2002). Methods for testing antioxidant activity. *Analyst*, 127, 183-198.

Aslanturk, O.S. (2018). In vitro cytotoxicity and cell viability assays: principles, advantages and disadvantages. *IntechOpen Chapter 1*, 1-17. https://doi.org/10.5772/intechopen.71923

Asombang, A., Madsen, R., Simuyandi, M., et al. (2016). Pancreatic Cancer: Patterns in a Low- to Middle-Income Population, Zambia: 1032. *Medical Journal of Zambia*, 111, S449. https://doi.org/10.14309/00000434-201610001-01032

Aubrey, B.J., Kelly, G.L., Janic, A., et al. (2018). How does p53 induce apoptosis and how does this relate to p53-mediated tumour suppression? *Cell Death and Differentiation*. 25, 104–113. https://doi.org/10.1038/cdd.2017.169

Aykul, S. and Martinez-Hackert, E. (2016). Determination of half-maximal inhibitory concentration using biosensor-based protein interaction analysis. *Analytical Biochemistry*, 508, 97–103. https://doi.org/10.1016/j.ab.2016.06.025

Baghban, R., Roshangar, L., Jahanban-Esfahlan, R., et al. (2020). Tumor microenvironment complexity and therapeutic implications at a glance. *Cell Communication and Signaling*, 18(59), 1-19. https://doi.org/10.1186/s12964-020-0530-4

Bahmani, P., Schellenberger, E., Klohs, J., et al. (2011). Visualization of Cell Death in MICE with Focal Cerebral Ischemia using Fluorescent Annexin A5, Propidium Iodide, and Tunel Staining. *Journal of Cerebral Blood Flow & Metabolism*, 31, 1311–1320. https://doi.org/10.1038/jcbfm.2010.233

Bai, X., Zhi, X., Zhang, Q., et al. (2014). Inhibition of protein phosphatase 2A sensitizes pancreatic cancer to chemotherapy by increasing drug perfusion via HIF-1α-VEGF mediated angiogenesis. *Cancer Letter*, 355, 281–287. https://doi.org/10.1016/j.canlet.2014.09.048

Barnum, K.J. and O'Connell, M.J. (2014). Cell Cycle Regulation by Checkpoints, In: Noguchi, E., Gadaleta, M.C. eds. Cell Cycle Control, Methods in Molecular Biology. Springer New York, New York, NY, pp. 29–40. https://doi.org/10.1007/978-1-4939-0888-2_2

Baruffaldi, D., Palmara, G., Pirri, C., et al. (2021). 3D Cell Culture: Recent Development in Materials with Tunable Stiffness. *ACS Applied Bio Materials*, 4, 2233–2250. https://doi.org/10.1021/acsabm.0c01472

Baskic, D., Popovic, S., Ristic, P., et al. (2006). Analysis of cycloheximide-induced apoptosis in human leukocytes: Fluorescence microscopy using annexin V/propidium iodide versus acridin orange/ethidium bromide. *Cell Biology International*, 30, 924–932. https://doi.org/10.1016/j.cellbi.2006.06.016

Beganovic, S. (2010). Clinical Significance of the KRAS Mutation. *Bosnian Journal of Basic Medical Sciences*, 9, S17–S20. https://doi.org/10.17305/bjbms.2009.2749

Beger, H.G., Rau, B., Gansauge, F., et al. (2003). Treatment of Pancreatic Cancer: Challenge of the Facts. *World Journal of Surgery*, 27(10), 1075–1084. https://doi.org/10.1007/s00268-003-7165-7

Beger, R. (2013). A Review of Applications of Metabolomics in Cancer. *Metabolites*, 3, 552–574. https://doi.org/10.3390/metabo3030552

Belashov, A.V., Zhikhoreva, A.A., Belyaeva, T.N., et al. (2019). Quantitative assessment of changes in cellular morphology at photodynamic treatment in vitro by means of digital holographic microscopy. *Biomedical Optics Express*, 10(1), 4975-4986. https://doi.org/10.1364/BOE.10.004975

Berridge, M.V., Herst, P.M. and Tan, A.S. (2005). Tetrazolium dyes as tools in cell biology: New insights into their cellular reduction, in: Biotechnology Annual Review. Elsevier, pp. 127–152. https://doi.org/10.1016/S1387-2656(05)11004-7

Blakney, A., Jiang, Y., Woodrow, K., et al. (2014). Delivery of multipurpose prevention drug combinations from electrospun nanofibers using composite microarchitectures. *International Journal of Nanomedicine*, 2967-2978. https://doi.org/10.2147/IJN.S61664

Bonifácio, B.V., Silva, P.B. da, Ramos, M.A. et al. (2013). Nanotechnology-based drug delivery systems and herbal medicines: a review [WWW Document]. *International Journal of Nanomedicine*, URL https://www.dovepress.com/nanotechnology-based-drug-delivery-systems-and-herbal-medicines-a-revi-peer-reviewed-fulltext-article-IJN (accessed 8.12.20).

Boon, S.S., Luk, H.Y., Xiao, C., et al. (2022). Review of the Standard and Advanced Screening, Staging Systems and Treatment Modalities for Cervical Cancer. *Cancers*, 14, 2913-2939. https://doi.org/10.3390/cancers14122913

Boulebd, H. (2020). Comparative study of the radical scavenging behavior of ascorbic acid, BHT, BHA and Trolox: Experimental and theoretical study. *Journal of Molecular Structure*, 1201, 127210. https://doi.org/10.1016/j.molstruc.2019.127210

Brake, K., Gumireddy, A., Tiwari, A., et al. (2017). In vivo Studies for Drug Development via Oral Delivery: Challenges, Animal Models and Techniques. *Pharmaceutica Analytica* Acta, 8(9), 1-12. https://doi.org/10.4172/2153-2435.1000560

Brigger, I., Dubernet, C. and Couvreur, P. (2012). Nanoparticles in cancer therapy and diagnosis. *Advanced Drug Delivery Reviews*, 64, 24–36. https://doi.org/10.1016/j.addr.2012.09.006

Bryant, K.L., Stalnecker, C.A., Zeitouni, D., et al. (2019). Combination of ERK and autophagy inhibition as a treatment approach for pancreatic cancer. *Nature Medicine*, 25(4), 628–640. https://doi.org/10.1038/s41591-019-0368-8

Burguillos, M.A. (2013). Use of Meso-Scale Discovery™ to Examine Cytokine Content in Microglia Cell Supernatant, in: Joseph, B., Venero, J.L. eds. Microglia, Methods in Molecular Biology. Humana Press, Totowa, NJ, pp. 93–100. https://doi.org/10.1007/978-1-62703-520-0_11

Bustin, S.A., Benes, V., Garson, J.A., et al. (2009). The MIQE Guidelines: Minimum Information for Publication of Quantitative Real-Time PCR Experiments. *Clinical Chemistry*, 55(4), 611–622. https://doi.org/10.1373/clinchem.2008.112797

Camacho, K.M., Menegatti, S. and Mitragotri, S. (2016). Low-molecular-weight polymer–drug conjugates for synergistic anticancer activity of camptothecin and doxorubicin combinations. *Nanomedicine*, 11(9), 1139–1151. https://doi.org/10.2217/nnm.16.33

Carreno, E.A., Alberto, A.V.P., de Souza, C.A.M., et al. (2021). Considerations and technical pitfalls in the employment of the MTT assay to evaluate photosensitizers for photodynamic therapy. 11, 2603. https://doi.org/10.3390/app11062603

Carra, G., Avalle, L., Secli, L. (2021). Shedding light on NF-kB Functions in Cellular Organelles. *Frontiers in Cell Developmental Biology*, 10, 1-9. https://doi.org/10.3389/fcell.2022.841646

Çelik, T.A. (2018). Introductory Chapter: Cytotoxicity, in: Çelik, T.A. (Ed.), Cytotoxicity. InTech. https://doi.org/10.5772/intechopen.77244

Chamberlin, S.R., Blucher, A., Wu, G., et al. (2019). Natural Product Target Network Reveals Potential for Cancer Combination Therapies. *Frontiers in Pharmacology*, 10(557), 1-16. https://doi.org/10.3389/fphar.2019.00557

Chan, C.K., Aimagambetova, G., Ukybassova, T., et al. (2019). Human Papillomavirus Infection and Cervical Cancer: Epidemiology, Screening, and Vaccination—Review of Current Perspectives. *Journal of Oncology*. 2019, 1–11. https://doi.org/10.1155/2019/3257939

Chen, H.-H., Zhou, H.-J., Wang, W.-Q., et al. (2004). Antimalarial dihydroartemisinin also inhibits angiogenesis. *Cancer Chemotherapy and Pharmacology*, 53, 423–432. https://doi.org/10.1007/s00280-003-0751-4

Chen, H., Sun, B., Pan, S., et al. (2009). Dihydroartemisinin inhibits growth of pancreatic cancer cells in vitro and in vivo. *Anticancer Drugs*, 20(2), 131–140. https://doi.org/10.1097/CAD.0b013e3283212ade

Chen, T., Li, M., Zhang, R., et al. (2009). Dihydroartemisinin induces apoptosis and sensitizes human ovarian cancer cells to carboplatin therapy. *Journal of Cellular and Molecular Medicine*, 13(7), 1358–1370. https://doi.org/10.1111/j.1582-4934.2008.00360.x

Chen, T., Chen, M. and Chen, J. (2013). Ionizing Radiation Potentiates Dihydroartemisinin-Induced Apoptosis of A549 Cells via a Caspase-8-Dependent Pathway. *PLoS ONE*, 8(3), e59827. https://doi.org/10.1371/journal.pone.0059827

Chen, Q., Kang, J. and Fu, C. (2018). The independence of and associations among apoptosis, autophagy, and necrosis. *Signal Transduction and Targeted Therapy*, 3, 18-29. https://doi.org/10.1038/s41392-018-0018-5

Chen, Y., Mi, Y., Zhang, X., et al. (2019). Dihydroartemisinin-induced unfolded protein response feedback attenuates ferroptosis via PERK/ATF4/HSPA5 pathway in glioma cells. Journal of Experimental & Clinical Cancer Research, 38(402), 1-16. https://doi.org/10.1186/s13046-019-1413-7

Cherubini, A., Rusconi, F. and Lazzari, L. (2021). Identification of the best housekeeping gene for RT-qPCR analysis of human pancreatic organoids. *PLOS ONE*, 16(12), e0260902. https://doi.org/10.1371/journal.pone.0260902

Chintharlapalli, S., Papineni, S., Ramaiah, S.K., et al. (2007). Betulinic Acid Inhibits Prostate Cancer Growth through Inhibition of Specificity Protein Transcription Factors. *Cancer Research*, 67(6), 2816–2823. https://doi.org/10.1158/0008-5472.CAN-06-3735

Chintharlapalli, S., Papineni, S., Lei, P., et al. (2011). Betulinic acid inhibits colon cancer cell and tumor growth and induces proteasome-dependent and -independent downregulation of specificity proteins (Sp) transcription factors. *BioMedCentral Cancer*, 11(371), 1-12. https://doi.org/10.1186/1471-2407-11-371

Chipuk, J.E., Fisher, J.C., Dillon, C.P., et al. (2008). Mechanism of apoptosis induction by inhibition of the anti-apoptotic BCL-2 proteins. *Proceedings of the National Academy of Sciences* 105(51), 20327–20332. https://doi.org/10.1073/pnas.0808036105

Cho, H., Lai, T.C. and Kwon, G.S. (2013). Poly(ethylene glycol)-block-poly(ε-caprolactone) micelles for combination drug delivery: Evaluation of paclitaxel, cyclopamine and gossypol in intraperitoneal xenograft models of ovarian cancer. *Journal of Controlled Release*, 166, 1–9. https://doi.org/10.1016/j.jconrel.2012.12.005

Chung, S., Vail, P., Witkiewicz, A.K., et al. (2019). Coordinately Targeting Cell-Cycle Checkpoint Functions in Integrated Models of Pancreatic Cancer. *Clinical Cancer Research*, 25(7), 2290–2304. https://doi.org/10.1158/1078-0432.CCR-18-1620

Cichewicz, R.H. and Kouzi, S.A. (2004). Chemistry, biological activity, and chemotherapeutic potential of betulinic acid for the prevention and treatment of cancer and HIV infection. *Medicinal Research Reviews*, 24(1), 90–114. https://doi.org/10.1002/med.10053

Clyburn, R.D., Reid, P., Evans, C.A., et al. (2010). Increased anti-tumour effects of doxorubicin and zoledronic acid in prostate cancer cells in vitro: supporting the benefits of combination therapy. *Cancer Chemotherapy and Pharmacology*, 65, 969–978. https://doi.org/10.1007/s00280-009-1106-6

Cook, J.H., Melloni, G.E.M., Gulhan, D.C., et al. (2021). The origins and genetic interactions of KRAS mutations are allele- and tissue-specific. *Nature Communications*, 12(1808), 1-14. https://doi.org/10.1038/s41467-021-22125-z

Coricovac, D., Dehelean, C.A., Pinzaru, I., et al. (2021). Assessment of Betulinic Acid Cytotoxicity and Mitochondrial Metabolism Impairment in a Human Melanoma Cell Line. *International Journal of Molecular Sciences*, 22, 4870. https://doi.org/10.3390/ijms22094870

Cornelli, U., Terranova, R., Luca, S., et al. (2001). Bioavailability and Antioxidant Activity of Some Food Supplements in Men and Women Using the D-Roms Test as a Marker of Oxidative *Journal of Nutrition*, 131, 3208–3211. https://doi.org/10.1093/jn/131.12.3208

Crowley, L.C., Scott, A.P., Marfell, B.J., et al. (2016). Measuring Cell Death by Propidium Iodide Uptake and Flow Cytometry. *Cold Spring Harbour Protocols*, 2016, 905-910. https://doi.org/10.1101/pdb.prot087163

Csuk, R. (2014). Betulinic acid and its derivatives: a patent review (2008 – 2013). *Expert Opinions on Therapy Patents*, 24(8), 913–923. https://doi.org/10.1517/13543776.2014.927441

Cuperlovic-Culf, M. and Culf, A.S. (2016). Applied metabolomics in drug discovery. *Expert Opinions on Drug Discovery*, 11, 759–770. https://doi.org/10.1080/17460441.2016.1195365

da Costa, M.P., Tato Marinho, R., Cortez-Pinto, H., et al. (2020). Twenty-Five Years of Increasing Mortality from Pancreatic Cancer in Portugal. *Pancreas*, 49, e2–e3. https://doi.org/10.1097/MPA.0000000000001446

Dai, L., Wang, L., Deng, L., et al. (2014). Novel Multiarm Polyethylene glycol-Dihydroartemisinin Conjugates Enhancing Therapeutic Efficacy in Non-Small-Cell Lung Cancer. *Scientific Reports*, 4, 5871. https://doi.org/10.1038/srep05871

Dai, L., Cao, X., Liu, K.-F., et al. (2015). Self-assembled targeted folate-conjugated eight-arm-polyethylene glycol–betulinic acid nanoparticles for co-delivery of anticancer drugs. *Journal of Material Chemistry B*, 3, 3754–3766. https://doi.org/10.1039/C5TB00042D

D'Arcy, M.S. (2019). Cell death: a review of the major forms of apoptosis, necrosis and autophagy. *Cell Biology International*, 43, 582–592. https://doi.org/10.1002/cbin.11137

Das, J., Samadder, A., Das, S., et al. (2016). Nanopharmaceutical Approach for Enhanced Anti-cancer Activity of Betulinic Acid in Lung-cancer Treatment via Activation of PARP: Interaction with DNA as a Target: -Anti-cancer Potential of Nano-betulinic Acid in Lung Cancer-. Journal of Pharmacopuncture 19, 37–44. https://doi.org/10.3831/KPI.2016.19.005

Dasanu, C.A. (2008). Gemcitabine: vascular toxicity and prothrombotic potential. *Expert Opinion on Drug Safety*, 7(6), 703–716. https://doi.org/10.1517/14740330802374262

de Koning, W., Latifi, D., Li, Y., et al. (2021). Identification, Validation, and Utilization of Immune Cells in Pancreatic Ductal Adenocarcinoma Based on Marker Genes. *Frontiers in Immunology*, 12, 649061. https://doi.org/10.3389/fimmu.2021.649061

de Menezes, B.B., Frescura, L.M., Duarte, R., et al. (2021). A critical examination of the DPPH method: Mistakes and inconsistencies in stoichiometry and IC50 determination by UV–Vis spectroscopy. *Analytica Chimica Acta*, 1157, 338398. https://doi.org/10.1016/j.aca.2021.338398

de Sá, M.S., Costa, J.F.O., Krettli, A.U., et al. (2009). Antimalarial activity of betulinic acid and derivatives in vitro against Plasmodium falciparum and in vivo in P. berghei-infected mice. *Parasitology Research*, 105, 275–279. https://doi.org/10.1007/s00436-009-1394-0

DeBerardinis, R.J. and Chandel, N.S. (2016). Fundamentals of cancer metabolism. *Scientific Advances*, 2, e1600200. https://doi.org/10.1126/sciadv.1600200

Deer, E.L., González-Hernández, J., Coursen, J.D., et al. (2010). Phenotype and Genotype of Pancreatic Cancer Cell Lines. *Pancreas*, 39(4), 425–435. https://doi.org/10.1097/MPA.0b013e3181c15963

Delbridge, A.R.D. and Strasser, A. (2015). The BCL-2 protein family, BH3-mimetics and cancer therapy. *Cell Death and Differentiation*, 22, 1071–1080. https://doi.org/10.1038/cdd.2015.50

Demir, I.E. (2012). Nerve-cancer interactions in the stromal biology of pancreatic cancer. Frontiers in Physiology, 3, 1-11. https://doi.org/10.3389/fphys.2012.00097

Desagher, S., Osen-Sand, A., Nichols, A., et al. (1999). Bid-induced Conformational Change of Bax Is Responsible for Mitochondrial Cytochrome c Release during Apoptosis. *The Journal of Cell Biology*, 144(5), 891–901. https://doi.org/10.1083/jcb.144.5.891

Distler, M., Aust, D., Weitz, J., et al. (2014). Precursor Lesions for Sporadic Pancreatic Cancer: PanIN, IPMN, and MCN. *BioMed Research International*, 2014, 1–11. https://doi.org/10.1155/2014/474905

Doi, T., Ishikawa, T., Okayama, T., et al. (2017). The JAK/STAT pathway is involved in the upregulation of PD-L1 expression in pancreatic cancer cell lines. *Oncology Reports*, 37, 1545–1554. https://doi.org/10.3892/or.2017.5399

Duan, X., Wang, W., Pan, Q., et al. (2021). Type 2 Diabetes Mellitus Intersects with Pancreatic Cancer Diagnosis and Development. Front. Oncol. 11, 1-9. https://doi.org/10.3389/fonc.2021.730038

Duensing, T.D. and Watson, S.R. (2018). Assessment of Apoptosis (Programmed Cell Death) by Flow Cytometry. *Cold Spring Harbour Protocols*, 38-40. https://doi.org/10.1101/pdb.prot093807

Dutta, D., Sarkar, A., Chakraborty, B., et al. (2015). Induction of apoptosis by a potent Betulinic acid derivative in Human colon carcinoma HT-29 cells, *International Journal of Scientific and Research Publications*, 5(2), 1-7.

Dutta, D., Paul, B., Mukherjee, B., et al. (2019). Nanoencapsulated betulinic acid analogue distinctively improves colorectal carcinoma in vitro and in vivo. Scientific Reports, 9, 1-20. https://doi.org/10.1038/s41598-019-47743-y

Ehrhardt, H., Fulda, S., Führer, M., et al. (2004). Betulinic acid-induced apoptosis in leukemia cells. *Leukemia*, 18, 1406–1412. https://doi.org/10.1038/sj.leu.2403406

El-Sheikh, S.M.A., Khairy, M.H., Osama, E., et al. (2021). Nanotechnology improves the therapeutic efficacy of gemcitabine against a human hepatocellular carcinoma cell line and minimizes its in vivo side effects. *Naunyn-Schmiedeberg's Archives of Pharmacology*, 394, 631–643. https://doi.org/10.1007/s00210-020-02004-y

Faber, J. and Fonseca, L.M. (2014). How sample size influences research outcomes. *Evidence-based Orthodontics*, 19(4), 27-29. https://doi.org/10.1590/2176-951.19.4.027-029.ebo

Fabjan, T., Vrtačnik-Bokal, E., Kumer, K., et al. (2018). Determination of oxidative stress balance in follicular fluid. *Laboratoriums Medizin*, 42(1-2), 51–58. https://doi.org/10.1515/labmed-2017-0106

Fan, Z., Fan, K., Yan, C., et al. (2018). Critical role of KRAS mutation in pancreatic ductal adenocarcinoma. *Translational Cancer Research*, 7(6), 1728–1736. https://doi.org/10.21037/tcr.2018.10.19

Farcas, C.G., Dehelean, C., Pinzaru, I.A., et al. (2020). Thermosensitive Betulinic Acid-Loaded Magnetoliposomes: A Promising Antitumor Potential for Highly Aggressive Human Breast Adenocarcinoma Cells Under Hyperthermic Conditions. *International Journal of Nanomedicine*, 15, 8175–8200. https://doi.org/10.2147/IJN.S269630

Farghadani, R. and Naidu, R. (2022). The Role of Apoptosis as a Double-Edge Sword in Cancer, in: Tutar, Y. ed. Regulation and Dysfunction of Apoptosis. IntechOpen. https://doi.org/10.5772/intechopen.97844

Faujan, N.H., Alitheen, N.B., Yeap, S.K., et al. (2010). Cytotoxic effect of betulinic acid and betulinic acid acetate isolated from Melaleuca cajuput on human myeloid leukemia (HL-60) cell line. *African Journal of Biotechnology*, 9(38), 6387–6396.

Feng, Q and Tong, R. (2016). Anticancer nanoparticulate polymer-drug conjugate. *AIChE Bioengineering & Translational Medicine*, 1, 277-296. https://doi.org/10.1002/btm2.10033

Feroz, W. and Sheikh, A.M.A. (2020). Exploring the multiple roles of guardian of the genome: P53. *Egyptian Journal of Medical Human Genetics*, 21(49), 1-23. https://doi.org/10.1186/s43042-020-00089-x

Fontanay, S., Grare, M., Mayer, J., et al. (2008). Ursolic, oleanolic and betulinic acids: Antibacterial spectra and selectivity indexes. *Journal of Ethnopharmacology*, 120, 272–276. https://doi.org/10.1016/j.jep.2008.09.001

Foulkes, W.D., Flanders, T.Y., Pollock, P.M., et al. (1997). THE CDKN2A (pl6) GENE AND. *Molecular Medicine*, 3(1), 5-20.

Fru, P.N., Nweke, E.E., Mthimkhulu, N., et al. (2021). Anti-Cancer and Immunomodulatory Activity of a Polyethylene Glycol-Betulinic Acid Conjugate on Pancreatic Cancer Cells. *Life*, 11, 1-15. https://doi.org/10.3390/life11060462

Fulda, S., Scaffidi, C., Susin, S.A., et al. (1998). Activation of Mitochondria and Release of Mitochondrial Apoptogenic Factors by Betulinic Acid. *Journal of Biological Chemistry*, 273(51), 33942–33948. https://doi.org/10.1074/jbc.273.51.33942

Fulda, S. (2008). Betulinic Acid for Cancer Treatment and Prevention. *International Journal of Molecular Sciences*, 9, 1096–1107. https://doi.org/10.3390/ijms9061096

Galluzzi, L., Aaronson, S.A., Abrams, J., et al. (2009). Guidelines for the use and interpretation of assays for monitoring cell death in higher eukaryotes. *Cell Death and Differentiation*. 16, 1093–1107. https://doi.org/10.1038/cdd.2009.44

Garcia, E.J., Oldoni, T.L.C., Alencar, S.M., et al. (2012). Antioxidant activity by DPPH assay of potential solutions to be applied on bleached teeth. *Brazilian Dental Journal*, 23(1), 22–27. https://doi.org/10.1590/S0103-64402012000100004

Garcia-Gil, M., Turri, B., Gabriele, M., et al. (2021). Protopine/Gemcitabine Combination Induces Cytotoxic or Cytoprotective Effects in Cell Type-Specific and Dose-Dependent Manner on Human Cancer and Normal Cells. *Pharmaceuticals*, 14, 1-17. https://doi.org/10.3390/ph14020090

Ge, Y., Wu, S., Zhang, Z., et al. (2019). Inhibition of p53 and/or AKT as a new therapeutic approach specifically targeting ALT cancers. *Protein & Cell*, 10(11), 808–824. https://doi.org/10.1007/s13238-019-0634-z

Ghasemi, M., Turnbull, T., Sebastian, S., et al. (2021). The MTT Assay: Utility, Limitations, Pitfalls, and Interpretation in Bulk and Single-Cell Analysis. *International Journal of Molecular Sciences*, 22, 1-30. https://doi.org/10.3390/ijms222312827

Golstein, P. and Kroemer, G. (2007). Cell death by necrosis: towards a molecular definition. *TRENDS in Biochemical Sciences*, 32(1), 37–43. https://doi.org/10.1016/j.tibs.2006.11.001

Grabowski, B. (2016). P<0.05 might not mean what you think: American Statistical association clarifies p values. *Journal of National Cancer Institute*, 108(8), 4-5.

Gracio, D., Margo, F., Lima, R.T., et al. (2017). An overview on the role of autophagy in cancer. *Hematology & Medical Oncology*, 2(1): 1-4. https://doi.org/10.5761/HMO.1000117

Gradiz, R., Silva, H.C., Carvalho, L., et al. (2016). MIA PaCa-2 and PANC-1 – pancreas ductal adenocarcinoma cell lines with neuroendocrine differentiation and somatostatin receptors. Scientific Reports, 6, 1-14. https://doi.org/10.1038/srep21648

Grapin-Botton, A. (2005). Ductal cells of the pancreas. *The International Journal of Biochemistry & Cell Biology*, 37, 504–510. https://doi.org/10.1016/j.biocel.2004.07.010

Grasso, S., Piedad, M., Carrasco-Garca, E., et al. (2012). Cell Death and Cancer, Novel Therapeutic Strategies, in: Ntuli, T. ed. Apoptosis and Medicine. InTech. https://doi.org/10.5772/51285

Greco, F. and Vicent, M.J. (2009). Combination therapy: Opportunities and challenges for polymer–drug conjugates as anticancer nanomedicines. *Advanced Drug Delivery Reviews*, 61(13), 1203–1213. https://doi.org/10.1016/j.addr.2009.05.006

Green, D.R. and Llambi, F. (2015). Cell Death Signaling. *Cold Spring Harbour Perspectives in Biology*, 7(12), 1-24. https://doi.org/10.1101/cshperspect.a006080

Gu, Q., Wang, J.D., Xia, H.H.X., et al. (2005). Activation of the caspase-8/Bid and Bax pathways in aspirin-induced apoptosis in gastric cancer. *Carcinogenesis* 26(3), 541–546. https://doi.org/10.1093/carcin/bgh345

Guo, S., Yao, X., Jiang, Q., et al. (2019). Dihydroartemisinin-loaded Magnetic Nanoparticles for Enhanced Chemodynamic Therapy. *Frontiers in Pharmacology*, 11, 1-11.

Guo, Y., Zhu, H., Weng, M., et al. (2020). Chemopreventive effect of Betulinic acid via mTOR -Caspases/Bcl2/Bax apoptotic signaling in pancreatic cancer. *BMC Complementary Medicine and Therapies*, 20(178), 1-11. https://doi.org/10.1186/s12906-020-02976-7

Halama, A., Riesen, N., Möller, G., et al. (2013). Identification of biomarkers for apoptosis in cancer cell lines using metabolomics: tools for individualized medicine. *Journal of Internal Medicine*, 274(5), 425–439. https://doi.org/10.1111/joim.12117

Hamada, M., Sumi, T., Iwai, S., et al. (2006). Induction of endonuclease G-mediated apopotosis in human oral squamous cell carcinoma cells by protein kinase C inhibitor safingol. *Apoptosis*, 11(1), 47–56. https://doi.org/10.1007/s10495-005-3348-z

Handrick, R., Ontikatze, T., Bauer, K.-D., et al. (2010). Dihydroartemisinin Induces Apoptosis by a Bak-Dependent Intrinsic Pathway. *Molecular Cancer Therapeutics*, 9(9), 2497–2510. https://doi.org/10.1158/1535-7163.MCT-10-0051

Haque, S., Nawrot, D.A., Alakurtti, S., et al. (2014). Screening and Characterisation of Antimicrobial Properties of Semisynthetic Betulin Derivatives. *PLoS ONE* 9(7), 1-9. https://doi.org/10.1371/journal.pone.0102696

Hashem, S., Ali, T.A., Akhtar, S., et al. (2022). Targeting cancer signaling pathways by natural products: Exploring promising anti-cancer agents. *Biomedicine & Pharmacotherapy*, 150, 1-12. https://doi.org/10.1016/j.biopha.2022.113054

Hidalgo, M. (2010). Pancreatic Cancer. *New England Journal of Medicine*, 362(17), 1605–1617. https://doi.org/10.1056/NEJMra0901557

Hingorani, R., Deng, J., Elia, J., et al. (2011). Detection of Apoptosis Using the BD Annexin V FITC Assay on the BD FACSVerse™ System, 1-12.

Hirata, E. and Sahai, E. (2017). Tumor Microenvironment and Differential Responses to Therapy. *Cold Spring Harbor Perspectives in Medicine*, 7, 1-14. https://doi.org/10.1101/cshperspect.a026781

Hitomi, Y., Masaki, N., Ishinoda, et al. (2022). Effectiveness of the d-ROMs oxidative stress test to predict long-term cardiovascular mortality. *International Journal of Cardiology*, 354, 43–47. https://doi.org/10.1016/j.ijcard.2022.03.001

Hong-Duck, U. (2016). Bcl-2 family proteins as regulators of cancer cell invasion and metastasis: a review focusing on mitochondrial respiration and reactive oxygen species. *Oncotarget*, 7(5), 5193–5203. https://doi.org/10.18632/oncotarget.6405

Hordyjewska, A., Ostapiuk, A. and Horecka, A. (2018). Betulin and betulinic acid in cancer research. *Journal of Pre-Clinical and Clinical Research*, 12(2), 72–75. https://doi.org/10.26444/jpccr/92743

Hoyer, K., Hablesreiter, R., Inoue, Y., et al. (2021). A genetically defined signature of responsiveness to erlotinib in early-stage pancreatic cancer patients: Results from the CONKO-005 trial. *EBioMedicine*, 66, 1-11. https://doi.org/10.1016/j.ebiom.2021.103327

Hruban, R.H., Maitra, A., Kern, S.E., et al. (2007). Precursors to Pancreatic Cancer. *Gastroenterology Clinics of North America*, 36(4), 831–849. https://doi.org/10.1016/j.gtc.2007.08.012

Hu, J.-X., Zhao, C.-F., Chen, W.-B., et al. (2021). Pancreatic cancer: A review of epidemiology, trend, and risk factors. *World Journal of Gastroenterology*, 27(27), 4298–4321. https://doi.org/10.3748/wjg.v27.i27.4298

Hu, X., Li, Z., Lin, R., et al. (2021). Guidelines for Regulated Cell Death Assays: A Systematic Summary, A Categorical Comparison, A Prospective. *Frontiers in Cell and Developmental Biology*, 9, 1-28. https://doi.org/10.3389/fcell.2021.634690

Huang, L., Guo, Z., Wang, F., et al. (2021). KRAS mutation: from undruggable to druggable in cancer. *Signal Transduction and Targeted Therapy*, 6(1), 1-20. https://doi.org/10.1038/s41392-021-00780-4

Huang, M., Lu, J.J., Ding, J., et al. (2021). Natural Products in Cancer Therapy: Past, Present and Future. *Natural Products and Bioprospecting*, 11(1), 5–13. https://doi.org/10.1007/s13659-020-00293-7

Huang, X.J., Ma, Z.-Q., Zhang, W.P., et al. (2007). Dihydroartemisinin exerts cytotoxic effects and inhibits hypoxia inducible factor-1α activation in C6 glioma cells. *Journal of Pharmacy and Pharmacology*, 59(6), 849–856. https://doi.org/10.1211/jpp.59.6.0011

Hunter, A.M., LaCasse, E.C. and Korneluk, R.G. (2007). The inhibitors of apoptosis (IAPs) as cancer targets. *Apoptosis*, 12(9), 1543–1568. https://doi.org/10.1007/s10495-007-0087-3

Hustinx, S.R., Cao, D., Maitra, A., et al. (2004). Differentially expressed genes in pancreatic ductal adenocarcinomas identified through serial analysis of gene expression. *Cancer Biology & Therapy*, 3(12), 1254–1261. https://doi.org/10.4161/cbt.3.12.1238

Hymowitz, S.G., and Malek, S. (2018). Targeting the MAPK Pathway in RAS Mutant Cancer. *Cold Spring Harbor Perspectives in Medicine*, 8:a031492. https://doi.org/10.1101/cshperspect.a031492

Iglesias, J. (2009). S1 Identifying and assessing women at high risk for breast cancer. *Breast Cancer Research*, 11, S21. https://doi.org/10.1186/bcr2282

Ilic, M. and Ilic, I. (2016). Epidemiology of pancreatic cancer. *World Journal of Gastroenterology*, 22(44), 9694-9705. https://doi.org/10.3748/wjg.v22.i44.9694

Inoue-Yamauchi, A., Jeng, P.S., Kim, K., et al. (2017). Targeting the differential addiction to anti-apoptotic BCL-2 family for cancer therapy. *Nature Communications*, 8(1), 1-14. https://doi.org/10.1038/ncomms16078

Iwatate, Y., Hoshino, I., Ishige, F., et al. (2020). Prognostic significance of p16 protein in pancreatic ductal adenocarcinoma. *Molecular and Clinical Oncology*, 13(1), 83–91. https://doi.org/10.3892/mco.2020.2047

Janyst, K., Janyst, M., Siernicka, M. et al. (2017). Synergistic antitumour effects of histone deacetylase inhibitor scriptaid and bortezomib against ovarian cancer cells. *Oncology Reports*, 39, 1999-2005. https://doi.org/10.3892/or.2018.6248

Jayat, C. and Ratinaud, M.-H. (1993). Cell cycle analysis by flow cytometry: Principles and applications. *Biology of the Cell*, 78(1-2), 15–25. https://doi.org/10.1016/0248-4900(93)90110-Z

Jensen, C. and Teng, Y. (2020). Is It Time to Start Transitioning From 2D to 3D Cell Culture? *Frontiers in Molecular Biosciences*, 7, 1-15. https://doi.org/10.3389/fmolb.2020.00033

Jiao, Y., Ge, C., Meng, Q., et al. (2007). Dihydroartemisinin is an inhibitor of ovarian cancer cell growth. *Acta Pharmacologica Sinica*, 28(7), 1045–1056. https://doi.org/10.1111/j.1745-7254.2007.00612.x

Jung, G.-R., Kim, K.-J., Choi, C.-H., et al. (2007). Effect of Betulinic Acid on Anticancer Drug-Resistant Colon Cancer Cells. *Basic & Clinical Pharmacology & Toxicology*, 101(4), 277–285. https://doi.org/10.1111/j.1742-7843.2007.00115.x

Karakas, H.E., and Gozuacik, D. (2014). Autophagy and cancer. *Turkish Journal of Biology,* 38: 1-20. https://doi.org/10.3906/biy-1408-16

Karch, J., Kwong, J.Q., Burr, A.R., et al. (2013). Bax and Bak function as the outer membrane component of the mitochondrial permeability pore in regulating necrotic cell death in mice. *eLife*, 2, 1-21. https://doi.org/10.7554/eLife.00772

Kedare, S.B. and Singh, R.P. (2011). Genesis and development of DPPH method of antioxidant assay. *Journal of Food Science and Technology*, 48(4), 412–422. https://doi.org/10.1007/s13197-011-0251-1

Kelly, P.N. and Strasser, A. (2011). The role of Bcl-2 and its pro-survival relatives in tumourigenesis and cancer therapy. *Cell Death and Differentiation*, 18(9), 1414–1424. https://doi.org/10.1038/cdd.2011.17

Khan, A.K., Jain, A.G., Afridi, S., et al. (2019). Latest developments in chemotherapy for metastatic pancreatic cancer, in: Theranostic Approach for Pancreatic Cancer. Elsevier, pp. 111–139. https://doi.org/10.1016/B978-0-12-819457-7.00006-2

Khandelwal, N., Simpson, J., Taylor, G., et al. (2011). Nucleolar NF-κB/RelA mediates apoptosis by causing cytoplasmic relocalization of nucleophosmin. *Cell Death and Differentiation*, 18(12), 1889–1903. https://doi.org/10.1038/cdd.2011.79

Khdair, A., Di Chen, Patil, Y., et al. (2010). Nanoparticle-mediated combination chemotherapy and photodynamic therapy overcomes tumor drug resistance. *Journal of Controlled Release*, 141, 137–144. https://doi.org/10.1016/j.jconrel.2009.09.004

Khorana, A.A., Mangu, P.B., Berlin, J., et al. (2017). Potentially Curable Pancreatic Cancer: American Society of Clinical Oncology Clinical Practice Guideline Update. *Journal of Clinical Oncology*, 35(20), 2324–2328. https://doi.org/10.1200/JCO.2017.72.4948

Kilk, K., Meitern, R., Härmson, O., et al. (2014). Assessment of oxidative stress in serum by d-ROMs test. *Free Radical Research*, 48(8), 883–889. https://doi.org/10.3109/10715762.2014.919390

Kim, J.Y. and Hong, S.M. (2018). Precursor Lesions of Pancreatic Cancer. *Oncology Research and Treatment*, 41(10), 603–610. https://doi.org/10.1159/000493554

Kim, S.J., Hyun, S.K., and Young, R.S. (2019). Understanding Strategy in Anticancer Therapy. *Oxidatice Medicine and Cellular Longevity*, 1-12.

Kim S.Y., Hwangbo, H., Kim, M.Y. et al (2021). Betulinic Acid Restricts Human Bladder Cancer Cell Proliferation In Vitro by Inducing Caspase-Dependent Cell Death and Cell Cycle Arrest and Decreasing Metastatic Potential. *Molecules.* 26(1381), 1-18. https://doi.org/10.3390/molecules26051381

Kleeff, J., Korc, M., Apte, M., et al. (2016). Pancreatic cancer. *Nature Reviews Disease Primers*, 2(1), 1-22. https://doi.org/10.1038/nrdp.2016.22

Kocsis, L., Herman, P. and Eke, A. (2006). The modified Beer–Lambert law revisited. *Physics in Medicine and Biology*, 51(5), N91–N98. https://doi.org/10.1088/0031-9155/51/5/N02

Korsmeyer, S.J., Wei, M.C., Saito, M., et al. (2000). Pro-apoptotic cascade activates BID, which oligomerizes BAK or BAX into pores that result in the release of cytochrome c. *Cell Death and Differentiation*. 7(12), 1166–1173. https://doi.org/10.1038/sj.cdd.4400783

Kost, J. and Langer, R. (2012). Responsive polymeric delivery systems. *Advanced Drug Delivery Reviews*, 64, 327–341. https://doi.org/10.1016/j.addr.2012.09.014

Kumar, P., Bhadauria, A.S., Singh, A.K., et al. (2018a). Betulinic acid as apoptosis activator: Molecular mechanisms, mathematical modeling and chemical modifications. *Life Sciences*, 209, 24–33. https://doi.org/10.1016/j.lfs.2018.07.056

Kumar, P., Singh, A.K., Raj, V., et al. (2018b). Poly(lactic-co-glycolic acid)-loaded nanoparticles of betulinic acid for improved treatment of hepatic cancer: characterization, in vitro and in vivo evaluations. *International Journal of Nanomedicine*, 13, 975–990. https://doi.org/10.2147/IJN.S157391

Kumar, R., Singh, M., Meena, J., et al. (2019). Hyaluronic acid - dihydroartemisinin conjugate: Synthesis, characterization and in vitro evaluation in lung cancer cells. *International Journal of Biological Macromolecules*, 133, 495–502. https://doi.org/10.1016/j.ijbiomac.2019.04.124

Kuo, H., Tseng, C., Chen, N. (2018). MSP-4, an antimicrobial peptide, induces apoptosis via activation of extrinsic Fas/FasL- and intrinsic mitochondria-mediated pathways in one osteosarcoma cell line. *Marine drugs*, 16(8), 1-19. https://doi.org/10.3390/md16010008

Labi, V. and Erlacher, M. (2015). How cell death shapes cancer. Cell Death & Disease, 6(3), 1-11. https://doi.org/10.1038/cddis.2015.20

Labrie, F., Dupont, A., Giguere, M., et al. (1988). Benefits of Combination Therapy with Flutamide in Patients Relapsing after Castration. *British Journal of Urology*, 61(4), 341–346. https://doi.org/10.1111/j.1464-410X.1988.tb13971.x

Lafont, E., Hartwig, T. and Walczak, H. (2018). Paving TRAIL's Path with Ubiquitin. *Trends in Biochemical Sciences*, 43(1), 44–60. https://doi.org/10.1016/j.tibs.2017.11.002

Langhans, S.A. (2018). Three-Dimensional in Vitro Cell Culture Models in Drug Discovery and Drug Repositioning. *Frontiers in Pharmacology*, 9, 1-6. https://doi.org/10.3389/fphar.2018.00006

Larsen, F.O. and Hansen, S.W. (2004). Severe neurotoxicity caused by gemcitabine treatment. *Acta Oncologica*, 43(6), 590–591. https://doi.org/10.1080/02841860410018494

Lee, G.H., Chang, Y. and Kim, T.-J. (2014). Characterization, in: Ultrasmall Lanthanide Oxide Nanoparticles for Biomedical Imaging and Therapy. Elsevier, pp. 43–67. https://doi.org/10.1533/9780081000694.43

Lee, S.-H., Lee, S.-J., Jung, Y.S., et al. (2009). Blocking of p53-Snail Binding, Promoted by Oncogenic K-Ras, Recovers p53 Expression and function. *Neoplasia*, 11(1), 22-31. https://doi.org/10.1593/neo.81006

Lee, S.H. and Park, B.J. (2011). p53 Activation by Blocking Snail: A Novel Pharmacological Strategy for Cancer. *Current Pharmaceutical Design*, 17(6), 610–617. https://doi.org/10.2174/138161211795222658

Leppink, J., Winston, K., and O'Sullivan. (2016). Statistical significance does not imply a real effect. *Perspective Medical Education*, 5, 122-124. https://doi.org/10.1007/s40037-016-0256-6

Li, H., Li, X., Shi, X., et al. (2019). Effects of magnetic dihydroartemisinin nano-liposome in inhibiting the proliferation of head and neck squamous cell carcinomas. *Phytomedicine*, 56, 215–228. https://doi.org/10.1016/j.phymed.2018.11.007

Li, Z., Zhu, J., Wang, Y., et al. (2020). In situ apolipoprotein E-enriched corona guides dihydroartemisinin-decorating nanoparticles towards LDLr-mediated tumor-homing chemotherapy. *Asian Journal of Pharmaceutical Sciences*, 15(4), 482–491. https://doi.org/10.1016/j.ajps.2019.05.002

Li, P., Pu, S., Lin, C., et al. (2022). Curcumin selectivity induces colon cancer cell apoptosis and S cell cycle arrest by regulates Rb/E2F/p53 pathway. *Journal of Molecular Structure*, 1263: 1-9. https://doi.org/10.1016/jmolstruc.2022.133180

Liang, Jianfeng, Zhao, W., Tong, P., et al. (2020). Comprehensive molecular characterization of inhibitors of apoptosis proteins (IAPs) for therapeutic targeting in cancer. *BMC Medical Genomics*, 13(1),1-7. https://doi.org/10.1186/s12920-020-0661-x

Lica, J.J., Wieczór, M., Grabe, G.J., et al. (2021). Effective Drug Concentration and Selectivity Depends on Fraction of Primitive Cells. *International Journal of Molecular Sciences*, 22(9), 1-24. https://doi.org/10.3390/ijms22094931

Lim, S.O., Kim, H. and Jung, G. (2010). p53 inhibits tumor cell invasion via the degradation of snail protein in hepatocellular carcinoma. *FEBS Letters*, 584(11), 2231–2236. https://doi.org/10.1016/j.febslet.2010.04.006

Lim, S.M., Mohamad, E.A., and Chin, S. (2021). Is targeting autophagy mechanism in cancer a good approach? The possible double-edge sword effect. *Cell & Bioscience.* 11(56): 1-13. https://doi.org/10.1186/s13578-021-0057-z

Lin, B., Williams-Skipp, C., Tao, Y., et al. (1999). NF-kB functions as both a proapoptotic and antiapoptotic regulatory factor within a single cell type, *Cell death and Differentiation*, 6, 570-582.

Lin, L.-H., Chang, K.-W., Cheng, H.-W., et al. (2019). SMAD4 Somatic Mutations in Head and Neck Carcinoma Are Associated with Tumor Progression. *Frontiers in Oncology*, 9, 1-12. https://doi.org/10.3389/fonc.2019.01379

Linskens, R. (2000). Severe acute lung injury induced by gemcitabine. *The Netherlands Journal of Medicine*, 56(6), 232–235. https://doi.org/10.1016/S0300-2977(00)00029-2

Liu, K., Dai, L., Li, C., et al. (2016). Self-assembled targeted nanoparticles based on transferrin-modified eight-arm-polyethylene glycol–dihydroartemisinin conjugate. *Scientific Reports*, 6(1), 1-12. https://doi.org/10.1038/srep29461

Liu, X., Yang, W., Guan, Z., Yu, W., Fan, B., Xu, N., Liao, D.J., 2018. There are only four basic modes of cell death, although there are many ad-hoc variants adapted to different situations. *Cell & Bioscience*, 8(1), 1-6. https://doi.org/10.1186/s13578-018-0206-6

Liu, Y., Zhang, X., Liu, Z., et al. (2017). Gold nanoshell-based betulinic acid liposomes for synergistic chemo-photothermal therapy. *Nanomedicine: Nanotechnology, Biology and Medicine*, 13(6), 1891–1900. https://doi.org/10.1016/j.nano.2017.03.012

Liu, Y., Zheng, D., Ma, Y., et al. (2018). Self-Assembled Nanoparticles Platform Based on Pectin-Dihydroartemisinin Conjugates for Codelivery of Anticancer Drugs. *ACS Biomaterials Science & Engineering*, 4, 1641-1650. https://doi.org/10.1021/acsbiomaterials.7b00842

Liu, Z., Ren, Z., Zhang, J., et al. (2018). Role of ROS and Nutritional Antioxidants in Human Diseases. *Frontiers in Physiology*, 9, 1-14. https://doi.org/10.3389/fphys.2018.00477

Livak, K.J. and Schmittgen, T.D. (2001). Analysis of Relative Gene Expression Data Using Real-Time Quantitative PCR and the 2−ΔΔCT Method. *Methods*, 25(4), 402–408. https://doi.org/10.1006/meth.2001.1262

Loveday, B.P., Lipton, L. and Thomson, B.N. (2019). Pancreatic cancer: An update on diagnosis and management. *Australian Journal of General Practice*, 48(12), 826–831. https://doi.org/10.31128/AJGP-06-19-4957

Lowenfels, A.B. and Maisonneuve, P. (2005). Risk factors for pancreatic cancer. *Journal of Cellular Biochemistry*, 95(4), 649–656. https://doi.org/10.1002/jcb.20461

Lu, J.-J., Meng, L.-H., Shankavaram, U.T., et al. (2010). Dihydroartemisinin accelerates c-MYC oncoprotein degradation and induces apoptosis in c-MYC-overexpressing tumor cells. *Biochemical Pharmacology*, 80(1), 22–30. https://doi.org/10.1016/j.bcp.2010.02.016

Lu, Y., Chen, T. and Qu, J.-L. (2009). Bax translocation into mitochondria during dihydroartemisinin (DHA)-induced apoptosis in human lung adenocarcinoma cells, in: Chen, W.R. ed. Presented at the SPIE BiOS: Biomedical Optics, San Jose, CA, p. 71780J. https://doi.org/10.1117/12.807255

Lu, Y.-Y., Chen, T.-S., Wang, X.-P., et al. (2010). Single-cell analysis of dihydroartemisinin–induced apoptosis through reactive oxygen species–mediated caspase-8 activation and mitochondrial pathway in ASTC-a-1 cells using fluorescence imaging techniques. *Journal of Biomedical Optics*, 15(4), 046028-1-040628-16. https://doi.org/10.1117/1.3481141

Lu, Y., Wen, Q., Luo, J., et al. (2020). Self-assembled dihydroartemisinin nanoparticles as a platform for cervical cancer chemotherapy. *Drug Delivery*, 27(1), 876–887. https://doi.org/10.1080/10717544.2020.1775725

Maisonneuve, P. (2019). Epidemiology and burden of pancreatic cancer. *La Presse Médicale*, 48(3), e113–e123. https://doi.org/10.1016/j.lpm.2019.02.030

Majolo, F., de Oliveira Becker Delwing, L.K., Marmitt, D.J., et al. (2019). Medicinal plants and bioactive natural compounds for cancer treatment: Important advances for drug discovery. *Phytochemistry Letters*, 31, 196–207. https://doi.org/10.1016/j.phytol.2019.04.003

Manning, F. and Zuzel, K. (2003). Comparison of types of cell death: apoptosis and necrosis. *Journal of Biological Education*, 37(3), 141–145. https://doi.org/10.1080/00219266.2003.9655870

Mantovani, G., Macciò, A., Madeddu, C., et al. (2002). Reactive oxygen species, antioxidant mechanisms and serum cytokine levels in cancer patients: impact of an antioxidant treatment. *Journal of Cellular and Molecular Medicine*, 6(4), 570–582. https://doi.org/10.1111/j.1582-4934.2002.tb00455.x

Mathiyalagan, R., Subramaniyam, S., Kim, Y.J., et al. (2014). Synthesis and pharmacokinetic characterization of a pH-sensitive polyethylene glycol ginsenoside CK (PEG-CK) conjugate. *Bioscience, Biotechnology, and Biochemistry*, 78(3), 466–468. https://doi.org/10.1080/09168451.2014.885827

Mayerhöfer, T.G., Pahlow, S. and Popp, J. (2020). The Bouguer-Beer-Lambert Law: Shining Light on the Obscure. *ChemPhysChem*, 21(18), 2029–2046. https://doi.org/10.1002/cphc.202000464

McGuigan, A., Kelly, P., Turkington, R.C., et al. (2018). Pancreatic cancer: A review of clinical diagnosis, epidemiology, treatment and outcomes. *World Journal of Gastroenterology*, 24(43), 4846–4861. https://doi.org/10.3748/wjg.v24.i43.4846

Miles, M.A. and Hawkins, C.J. (2017). Executioner caspases and CAD are essential for mutagenesis induced by TRAIL or vincristine. *Cell Death & Disease*, 8(10), e3062–e3062. https://doi.org/10.1038/cddis.2017.454

Milkovic, L., Cipak Gasparovic, A., Cindric, M., et al. (2019). Short Overview of ROS as Cell Function Regulators and Their Implications in Therapy Concepts. *Cells*, 8(8), 1-14. https://doi.org/10.3390/cells8080793

Mistry, S. and Shah, S. (2014). Anti-oxidant activity of methanolic extract of Ficus religiosa linn bark by using DPPH ((1, 1-Diphenyl-2-Picrylhydrazyl. *International Journal of Phytopharmacy*. 4(2), 57–58.

Mokhtari, R.B., Homayouni, T.S., Baluch, N., et al. (2017). Combination therapy in combating cancer. *Oncotarget*, 8(23), 38022–38043. https://doi.org/10.18632/oncotarget.16723

Mosiane, K.S., Nweke, E.E., Balogun, M., et al. (2023). Polyethyleneglycol-Betulinic Acid (PEG-BA) Polymer-Drug Conjugate Induces Apoptosis and Antioxidation in a Biological Model of Pancreatic Cancer. *Polymers*, 15(2), 448. https://doi.org/10.3390/polym15020448

Motomura, K., Natsume, A., Kishida, Y., et al. (2011). Benefits of interferon-β and temozolomide combination therapy for newly diagnosed primary glioblastoma with the unmethylated MGMT promoter: A multicenter study. *Cancer*, 117(8), 1721–1730. https://doi.org/10.1002/cncr.25637

Moysan, E., Bastiat, G. and Benoit, J.-P. (2013). Gemcitabine versus Modified Gemcitabine: A Review of Several Promising Chemical Modifications. *Molecular Pharmaceutics*, 10(2), 430–444. https://doi.org/10.1021/mp300370t

Mthimkhulu, N. (2019). Bio-screening of Polymer Conjugates of the Drugs Betulinic Acid and Dihydroartemisinin against Pancreatic Cancer Cells (Masters Dissertation). University of the Witwatersrand, Johannesburg, South Africa.

Mthimkhulu, N., Mosiane, K.S., Nweke, E.E., et al. (2021). Prospects of Delivering Natural Compounds by Polymer-Drug Conjugates in Cancer Therapeutics. *Anti-Cancer Agents in Medicinal Chemistry*, 22(9), 1699–1713. https://doi.org/10.2174/1871520621666210419094623

Mu, D., Zhang, W., Chu, D., et al. (2008). The role of calcium, P38 MAPK in dihydroartemisinin-induced apoptosis of lung cancer PC-14 cells. *Cancer Chemotherapy & Pharmacology*, 61(4), 639–645. https://doi.org/10.1007/s00280-007-0517-5

Mukherjee, P.K. (2019). Bioassay-Guided Isolation and Evaluation of Herbal Drugs, in: Quality Control and Evaluation of Herbal Drugs. Elsevier, pp. 515–537. https://doi.org/10.1016/B978-0-12-813374-3.00013-2

Mullauer, F.B., van Bloois, L., Daalhuisen, J.B., et al. (2011). Betulinic acid delivered in liposomes reduces growth of human lung and colon cancers in mice without causing systemic toxicity. *Anticancer Drugs*, 22(3), 223–233. https://doi.org/10.1097/CAD.0b013e3283421035

Murphy, E., Ardehali, H., Balaban, R.S., et al. (2016). Mitochondrial Function, Biology, and Role in Disease: A Scientific Statement From the American Heart Association. *Circulation Research*, 118(12), 1960–1991. https://doi.org/10.1161/RES.0000000000000104

Mvango, S., Mthimkhulu, N., Fru, P.N., et al. (2020). Physico-chemical characterization of polyethylene glycol-conjugated betulinic acid. Presented at the FRACTURE AND DAMAGE MECHANICS: Theory, Simulation and Experiment, Mallorca, Spain, p. 020039. https://doi.org/10.1063/5.0028479

Nachmias, B., Ashhab, Y. and Ben-Yehuda, D. (2004). The inhibitor of apoptosis protein family (IAPs): an emerging therapeutic target in cancer. *Seminars in Cancer Biology*, 14, 231-243.

Naseri, M.H., Mahdavi, M., Davoodi, J., et al. (2015). Up regulation of Bax and down regulation of Bcl2 during 3-NC mediated apoptosis in human cancer cells. *Cancer Cell International*,15(1), 1-9. https://doi.org/10.1186/s12935-015-0204-2

Neureiter, D. (2014). Epigenetics and pancreatic cancer: Pathophysiology and novel treatment aspects. *World Journal of Gastroenterology*, 20(24), 1-20. https://doi.org/10.3748/wjg.v20.i24.7830

Nguyen, C.N., Tran, B.N., Thi, H.N., et al. (2019). Physical Absorption of Folic Acid and Chitosan on Dihydroartemisinin-Loaded Poly-Lactic-Co-Glycolic Acid Nanoparticles via Electrostatic Interaction for Their Enhanced Uptake and Anticancer Effect. *Journal of Nanomaterials*, 2019, 1–14. https://doi.org/10.1155/2019/6808530

Noel, B., Singh, S.K., Lillard, J.W., et al. (2020). Role of natural compounds in preventing and treating breast cancer. *Frontiers of Biosciences (School edition)*, 12, 137-160.

Nunez, R. (2001). DNA Measurement and Cell Cycle Analysis by Flow Cytometry. *Current Issues in Molecular Biology*, 3(3): 67-70.

Oladimeji, O., Akinyelu, J., Daniels, A., et al. (2021). Modified Gold Nanoparticles for Efficient Delivery of Betulinic Acid to Cancer Cell Mitochondria. *International Journal of Molecular Sciences*, 22(10), 1-14. https://doi.org/10.3390/ijms22105072

Oliveira-Costa, J.F., Meira, C.S., Neves, M.V.G. et al. (2022). Anti-Inflammatory Activities of Betulinic Acid: A Review. *Frontiers in Pharmacology*, 13, 1-9. https://doi.org/10.3389/fphar.2022.883857

Orth, M., Metzger, P., Gerum, S., et al. (2019). Pancreatic ductal adenocarcinoma: biological hallmarks, current status, and future perspectives of combined modality treatment approaches. *Radiation Oncology*, 14(1), 1-20. https://doi.org/10.1186/s13014-019-1345-6

O'Shaughnessy, J., Miles, D., Vukelja, S., et al. (2002). Superior Survival With Capecitabine Plus Docetaxel Combination Therapy in Anthracycline-Pretreated Patients With Advanced Breast Cancer: Phase III Trial Results. *Journal of Clinical Oncology*, 20(12), 2812–2823. https://doi.org/10.1200/JCO.2002.09.002

Ozaki, T. and Nakagawara, A. (2011). Role of p53 in Cell Death and Human Cancers. *Cancers*, 3(1), 994–1013. https://doi.org/10.3390/cancers3010994

Ozoren, N. and El-Deiry, W.S. (2002). Defining characteristics of Types I and II apoptotic cells in response to TRAIL. *Neoplasia*, 4(6), 551-557. https://doi.org/10.1038/sj.neo.7900270

Paltrinieri, S., Ravicini, S., Rossi, G., et al. (2010). Serum concentrations of the derivatives of reactive oxygen metabolites (d-ROMs) in dogs with leishmaniosis. *The Veterinary Journal*, 186(3), 393–395. https://doi.org/10.1016/j.tvjl.2009.08.019

Park, C., Jeong, J.-W., Han, M.H., et al. (2021). The anti-cancer effect of betulinic acid in u937 human leukemia cells is mediated through ROS-dependent cell cycle arrest and apoptosis. *Animal Cells and Systems*, 25(2), 119–127. https://doi.org/10.1080/19768354.2021.1915380

Parveen, S., Arjmand, F. and Tabassum, S. (2019). Clinical developments of antitumor polymer therapeutics. *RSC Advances*, 9(43), 24699–24721. https://doi.org/10.1039/C9RA04358F

Pearson, D. and Li, H. (2017). Conjugates toward medicines. *Journal of Pharmacology and Medical Chemistry*, 1(1), 32-39.

Pereira, N.P. and Corrêa, J.R. (2018). Pancreatic cancer: treatment approaches and trends. *Journal of Cancer Metastasis and Treatment*, 4(6), 1-14. https://doi.org/10.20517/2394-4722.2018.13

Perillo, B., Di Donato, M., Pezone, A. (2020). ROS in cancer therapy: the bright side of the moon. *Experimental & Molecular Medicine*, 52, 192-203. https://doi.org/10.1038/s12276-020-0384-2

Petitjean, A., Achatz, M.I.W., Borresen-Dale, et al. (2007). TP53 mutations in human cancers: functional selection and impact on cancer prognosis and outcomes. *Oncogene*, 26(15), 2157–2165. https://doi.org/10.1038/sj.onc.1210302

Pilco-Ferreto, N. and Calaf, G.M. (2016). Influence of doxorubicin on apoptosis and oxidative stress in breast cancer cell lines. *International Journal of Oncology*, 49(2), 753–762. https://doi.org/10.3892/ijo.2016.3558

Pinzaru, I., Sarau, C., Coricovac, D., et al. (2021). Silver Nanocolloids Loaded with Betulinic Acid with Enhanced Antitumor Potential: Physicochemical Characterization and In Vitro Evaluation. *Nanomaterials*, 11(1), 1-14. https://doi.org/10.3390/nano11010152

Proskuryakov, S.Y. a, Konoplyannikov, A.G. and Gabai, V.L. (2003). Necrosis: a specific form of programmed cell death? *Experimental Cell Research*, 283(1), 1–16. https://doi.org/10.1016/S0014-4827(02)00027-7

Puri, A., Saif, M.W., 2014. Pharmacogenomics Update in Pancreatic Cancer. *Journal of the Pancreas*, 15(2):114-117.

Rawla, P., Sunkara, T. and Gaduputi, V. (2019). Epidemiology of Pancreatic Cancer: Global Trends, Etiology and Risk Factors. *World Journal of Oncology*, 10(1), 10–27. https://doi.org/10.14740/wjon1166

Righeschi, C., Coronnello, M., Mastrantoni, A., et al. (2014). Strategy to provide a useful solution to effective delivery of dihydroartemisinin: Development, characterization and in vitro studies of liposomal formulations. *Colloids and Surfaces B: Biointerfaces*, 116: 121-127. https://.doi.org/10.1016/j.colsurfb.2013.12.019

Riley, J.S., Hutchinson, R., McArt, D.G., et al. (2013). Prognostic and therapeutic relevance of FLIP and procaspase-8 overexpression in non-small cell lung cancer. *Cell Death & Disease*, 4(12), e951–e951. https://doi.org/10.1038/cddis.2013.481

Ríos, J. and Máñez, S. (2018). New Pharmacological Opportunities for Betulinic Acid. *Planta Medica*, 84(1), 8–19. https://doi.org/10.1055/s-0043-123472

Rubie, C., Kempf, K., Hans, J., et al. (2005). Housekeeping gene variability in normal and cancerous colorectal, pancreatic, esophageal, gastric and hepatic tissues. *Molecular and Cellular Probes*, 19(2), 101–109. https://doi.org/10.1016/j.mcp.2004.10.001

Rubio, C.P. and Cerón, J.J. (2021). Spectrophotometric assays for evaluation of Reactive Oxygen Species (ROS) in serum: general concepts and applications in dogs and humans. *BioMedCentral Veterinary Research*, 17(1), 1-13. https://doi.org/10.1186/s12917-021-02924-8

Ruess, D.A., Görgülü, K., Wörmann, S.M., et al. (2017). Pharmacotherapeutic Management of Pancreatic Ductal Adenocarcinoma: Current and Emerging Concepts. *Drugs & Aging*, 34(5), 331–357. https://doi.org/10.1007/s40266-017-0453-y

Ryan, K., Ernst, M., Rice, N., et al. (2000). Role of NF-kB in p53-mediated programmed cell death. *Letter to Nature*, 404, 892-897.

Rzeski, W., Stepulak, A., Szymański, M., et al. (2006). Betulinic acid decreases expression of bcl-2 and cyclin D1, inhibits proliferation, migration and induces apoptosis in cancer cells. *Naunyn-Schmiedeberg's Archives of Pharmacology*, 374(1), 11–20. https://doi.org/10.1007/s00210-006-0090-1

Saeed, M.E.M., Mahmoud, N., Sugimoto, Y., et al. (2018). Betulinic Acid Exerts Cytotoxic Activity Against Multidrug-Resistant Tumor Cells via Targeting Autocrine Motility Factor Receptor (AMFR). *Frontiers in Pharmacology*, 9, 1-13. https://doi.org/10.3389/fphar.2018.00481

Sakamoto, S., Putalun, W., Vimolmangkang, S., et al. (2018). Enzyme-linked immunosorbent assay for the quantitative/qualitative analysis of plant secondary metabolites. *Journal of Natural Medicines*, 72(1), 32–42. https://doi.org/10.1007/s11418-017-1144-z

Salih Istifli, E., Tahir Hüsunet, M. and Basri Ila, H. (2019). Cell Division, Cytotoxicity, and the Assays Used in the Detection of Cytotoxicity, in: Salih Istifli, E., Basri Ila, H. (Eds.), Cytotoxicity - Definition, Identification, and Cytotoxic Compounds. IntechOpen. https://doi.org/10.5772/intechopen.88368

Saman, H., Raza, S.S., Uddin, S., et al. (2020). Inducing Angiogenesis, a Key Step in Cancer Vascularization, and Treatment Approaches. *Cancers*, 12(5), 1172. https://doi.org/10.3390/cancers12051172

Santana-Codina, N., Mancias, J.D., and Kimmelman, A.C. (2017). The role of autophagy in cancer. *The Annual Reviews of Cancer Biology*. 1:19-39. https://doi.org/10.1146/annurev-cancerbio-041816-122338

Saneja, A., Arora, D., Kumar, R., et al. (2018). Therapeutic applications of betulinic acid nanoformulations: Betulinic acid nanoformulations. *Annals of the New York Academy of Sciences*, 1421(1), 5–18. https://doi.org/10.1111/nyas.13570

Saneja, A., Kumar, R., Singh, A., et al. (2017a). Development and evaluation of long-circulating nanoparticles loaded with betulinic acid for improved anti-tumor efficacy. *International Journal of Pharmaceutics*, 531(1), 153–166. https://doi.org/10.1016/j.ijpharm.2017.08.076

Saneja, A., Sharma, L., Dubey, R.D., et al. (2017b). Synthesis, characterization and augmented anticancer potential of PEG-betulinic acid conjugate. *Materials Science and Engineering: C*, 73, 616–626. https://doi.org/10.1016/j.msec.2016.12.109

Saputra, E.C., Huang, L., Chen, Y., Tucker-Kellogg, L., 2018. Combination Therapy and the Evolution of Resistance: The Theoretical Merits of Synergism and Antagonism in Cancer. *Cancer Research*, 78(9), 2419–2431. https://doi.org/10.1158/0008-5472.CAN-17-1201

Sarı, C., Kolaylı, S. and Eyüpoğlu, F.C. (2021). A Comparative Study of MTT and WST-1 Assays in Cytotoxicity Analysis. *Haydarpaşa Numune Medical Journal*, 61(3), 281–288. https://doi.org/10.14744/hnhj.2019.16443

Sati, P., Pandey, A., Rawat, S., et al. (2013). Phytochemicals and antioxidants in leaf extracts of Ginkgo biloba with reference to location, seasonal variation and solvent system. Journal of Pharmacy Research, 7(9), 804–809. https://doi.org/10.1016/j.jopr.2013.09.001

Schmidt, M.L., Kuzmanoff, K.L. and Ling-Indeck, L. (1997). Betulinic acid induces apoptosis in human neuroblastoma cell lines. European Journal of Cancer, 33(12), 2007–2010. https://doi.org/10.1016/S0959-8049(97)00294-3

Schwarte-Waldhoff, I., Volpert, O.V., Bouck, N.P., et al. (2000). Smad4/DPC4-mediated tumor suppression through suppression of angiogenesis. *Proceedings of the National Academy of Sciences*, 97(17), 9624–9629. https://doi.org/10.1073/pnas.97.17.9624

Sellam, F., Harir, N., Khaled, M.B., et al. (2015). Delayed diagnosis of pancreatic cancer reported as more common in a population of North African young adults. *Journal of Gastrointestinal Oncology*, 6(5), 505-510.

Sharma, O.P. and Bhat, T.K. (2009). DPPH antioxidant assay revisited. *Food Chemistry*, 113(4), 1202–1205. https://doi.org/10.1016/j.foodchem.2008.08.008

Shen, M., Hu, Y., Yang, Y., et al. (2019). Betulinic Acid Induces ROS-Dependent Apoptosis and S-Phase Arrest by Inhibiting the NF- κ B Pathway in Human Multiple Myeloma. *Oxidative Medicine and Cellular Longevity*, 2019, 1–14. https://doi.org/10.1155/2019/5083158

Shen, S., Du, M., Liu, Q., et al. (2020). Development of GLUT1-targeting alkyl glucoside-modified dihydroartemisinin liposomes for cancer therapy. *Nanoscale*, 12(42), 21901–21912. https://doi.org/10.1039/D0NR05138A

Shu, Q., Wu, J. and Chen, Q. (2019). Synthesis, Characterization of Liposomes Modified with Biosurfactant MEL-A Loading Betulinic Acid and Its Anticancer Effect in HepG2 Cell. *Molecules*, 24(21), 1-17. https://doi.org/10.3390/molecules24213939

Siegel, R.L., Miller, K.D., Fuchs, H.E., et al. (2021). Cancer Statistics, 2021. *CA: A Cancer Journal for Clinicians*, 71(1), 7–33. https://doi.org/10.3322/caac.21654

Singh, N. (2007). Apoptosis in health and disease and modulation of apoptosis for therapy: An overview. *Indian Journal of Clinical Biochemistry*, 22(2), 6–16. https://doi.org/10.1007/BF02913307

Singh, N.P. and Lai, H. (2001). Selective toxicity of dihydroartemisinin and holotransferrin toward human breast cancer cells. *Life Sciences*, 70(1), 49–56. https://doi.org/10.1016/S0024-3205(01)01372-8

Singh, S., Sharma, B., Kanwar, S.S., et al. (2016). Lead Phytochemicals for Anticancer Drug Development. *Frontiers in Plant Science*, 7, 1-13. https://doi.org/10.3389/fpls.2016.01667

Singh, V.K., Arora, D., Ansari, M.I., et al. (2019). Phytochemicals based chemopreventive and chemotherapeutic strategies and modern technologies to overcome limitations for better clinical applications. *Phytotherapy Research*, 33(12), 3064–3089. https://doi.org/10.1002/ptr.6508

Snezhkina, A.V., Kudryavtseva, A.V., Kardymon, O.L., et al. (2019). ROS Generation and Antioxidant Defense Systems in Normal and Malignant Cells. *Oxidative Medicine and Cellular Longevity*, 2019, 1–17. https://doi.org/10.1155/2019/6175804

Şoica, C.M., Dehelean, C.A., Peev, C., et al. (2012). Physico-chemical comparison of betulinic acid, betulin and birch bark extract and *in vitro* investigation of their cytotoxic effects towards skin epidermoid carcinoma (A431), breast carcinoma (MCF7) and cervix adenocarcinoma (HeLa) cell lines. *Natural Product Research*, 26(10), 968–974. https://doi.org/10.1080/14786419.2010.545352

Sousa, J.L.C., Gonçalves, C., Ferreira, R.M., et al. (2021). Functionalization of Betulinic Acid with Polyphenolic Fragments for the Development of New Amphiphilic Antioxidants. *Antioxidants*, 10(2), 148. https://doi.org/10.3390/antiox10020148

Stark, A. and Eibl, G. (2015). Pancreatic Ductal Adenocarcinoma. *Pancreapedia*, 14, 1-9. https://doi.org/10.3998/panc.2015.14

Straume, O., Sviland, L. and Akslen, L.A. (2000). Loss of Nuclear p16 Protein Expression Correlates with Increased Tumor Cell Proliferation (Ki-67) and Poor Prognosis in Patients with Vertical Growth Phase Melanoma. *Clinical Cancer Research*, 6, 1845–1853.

Syntichaki, P. and Tavernarakis, N. (2002). Death by necrosis: Uncontrollable catastrophe, or is there order behind the chaos? *EMBO reports*, 3(7), 604–609. https://doi.org/10.1093/embo-reports/kvf138

Szegezdi, E. and Leverkus, M. (2016). Guiding the Killer and Bringing in Accomplices: Bispecific Antibody Treatment for Malignant Melanoma. *Journal of Investigative Dermatology*, 136(2), 362–364. https://doi.org/10.1016/j.jid.2015.12.002

Takacs, T., Kudlik, G., Kurilla, A., et al. (2020). The effects of mutant Ras proteins on the cell signalome. *Cancer and Metastasis Reviews*, 39:1051-1065. https://doi.org/10.1007/s10555-020-09912-8

Taniai, M., Grambihler, A., Higuchi, H., et al. (2004). Mcl-1 Mediates Tumor Necrosis Factor-Related Apoptosis-Inducing Ligand Resistance in Human Cholangiocarcinoma Cells. *Cancer Research*, 64(10), 3517–3524. https://doi.org/10.1158/0008-5472.CAN-03-2770

Tavil, Y., Arslan, U., Okyay, K., et al. (2007). Atrial Fibrillation Induced by Gemcitabine Treatment in a 65-Year-Old Man. *Oncology Research and Treatment*, 30(5), 253–255. https://doi.org/10.1159/000100930

Tenev, T., Marani, M., McNeish, I., et al. (2001). Pro-caspase-3 overexpression sensitises ovarian cancer cells to proteasome inhibitors. *Cell Death & Differentiation*, 8(3), 256–264. https://doi.org/10.1038/sj.cdd.4400808

Thapa, S.A., Rather, R.K., Singh, et al. (2022). Insights into the Role of Defective Apoptosis in Cancer Pathogenesis and Therapy, in: Tutar, Y. ed, Regulation and Dysfunction of Apoptosis. IntechOpen. https://doi.org/10.5772/intechopen.97536

Thomas, S., Quinn, B.A., Das, S.K., et al. (2013). Targeting the Bcl-2 family for cancer therapy. *Expert Opinion on Therapeutic Targets*, 17(1), 61–75. https://doi.org/10.1517/14728222.2013.733001

Thorn, C.F., Oshiro, C., Marsh, S., et al. (2011). Doxorubicin pathways: pharmacodynamics and adverse effects. *Pharmacogenetics and Genomics*, 21(7), 440–446. https://doi.org/10.1097/FPC.0b013e32833ffb56

Traganos, F. (1984). Flow Cytometry: Principles and Applications. I. *Cancer Investigation*, 2(2), 149–163. https://doi.org/10.3109/07357908409020296

van Tonder, A., Joubert, A.M. and Cromarty, A.D. (2015). Limitations of the 3-(4,5-dimethylthiazol-2-yl)-2,5-diphenyl-2H-tetrazolium bromide (MTT) assay when compared to three commonly used cell enumeration assays. *BMC Research Notes*, 8(1), 47. https://doi.org/10.1186/s13104-015-1000-8

Vassalle, C., Boni, C., Di Cecco, P., et al. (2006). Automation and validation of a fast method for the assessment of in vivo oxidative stress levels. *Clinical Chemistry and Laboratory Medicine (CCLM)*, 44(11),1-4. https://doi.org/10.1515/CCLM.2006.243

Vaux, D.I., Fidler, F., and Cumming, G. (2012). Replicates and repeats – what is the difference and is it significant? *European Molecular Biology Organization reports*, 13(4), 291-296.

Vendramini, E., Bomben, R., Pozzo, F., et al. (2022). KRAS and RAS-MAPK Pathway Deregulation in Mature B Cell Lymphoprofilerative Disorders. *Cancers*, 14, 666. https://doi.org/10.3390/cancers14030666

Vermes, I., Haanen, C. and Reutelingsperger, C. (2000). Flow cytometry of apoptotic cell death. *Journal of Immunological Methods*, 243(1-2), 167–190. https://doi.org/10.1016/S0022-1759(00)00233-7

Vincent, A., Herman, J., Schulick, R., et al. (2011). Pancreatic cancer. The Lancet 378, 607–620. https://doi.org/10.1016/S0140-6736(10)62307-0

Vincenzi, B., Stacchiotti, S., Collini, P., et al (2017). Human equilibrative nucleoside transporter 1 gene expression is associated with gemcitabine efficacy in advanced leiomyosarcoma and angiosarcoma. Br. J. Cancer 117, 340–346. https://doi.org/10.1038/bjc.2017.187

Vogel, C. and Marcotte, E.M. (2013). Insights into the regulation of protein abundance from proteomic and transcriptomic analyses. *Nature Reviews in Genetics*, 13, 227–232. https://doi.org/10.1038/nrg3185

Wagh, A.R. and Bose, K. (2019). Apoptosis in Cancer Cell Signaling and Current Therapeutic Possibilities, in: Bose, K., Chaudhari, P. eds. Unravelling Cancer Signaling Pathways: A Multidisciplinary Approach. Springer Singapore, Singapore, pp. 113–129. https://doi.org/10.1007/978-981-32-9816-3_5

Wakabayashi, T., Kawashima, T. and Matsuzawa, Y. (2014). Evaluation of reactive oxygen metabolites in patients with non-small cell lung cancer after chemotherapy 6.

Walko, C.M. and Lindley, C., 2005. Capecitabine: A review. Clin. Ther. 27, 23–44. https://doi.org/10.1016/j.clinthera.2005.01.005

Wan, X., Min, Y., Bludau, H., et al. (2018). Drug Combination Synergy in Worm-like Polymeric Micelles Improves Treatment Outcome for Small Cell and Non-Small Cell Lung Cancer. ACS Nano 12, 2426–2439. https://doi.org/10.1021/acsnano.7b07878

Wang, D., Xu, M., Li, F., et al. (2022). Target Identification-Based Analysis of Mechanism of Betulinic Acid-Induced Cells Apoptosis of Cervical Cancer SiHa. Nat. Prod. Commun. 17, 1934578X2211155. https://doi.org/10.1177/1934578X221115528

Wang, H.M., Chiu, C.C., Wu, P.F., et al. (2011). Subamolide E from Cinnamomum subavenium Induces Sub-G1 Cell-Cycle Arrest and Caspase-Dependent Apoptosis and Reduces the Migration Ability of Human Melanoma Cells. J. Agric. Food Chem. 59, 8187–8192. https://doi.org/10.1021/jf2018929

Wang, S., Zheng, Y., Yang, F., et al. (2021). The molecular biology of pancreatic adenocarcinoma: translational challenges and clinical perspectives. Signal Transduct. Target. Ther. 6, 249. https://doi.org/10.1038/s41392-021-00659-4

Wang, S.J., Sun, B., Cheng, Z.X., et al. (2011). Dihydroartemisinin inhibits angiogenesis in pancreatic cancer by targeting the NF-κB pathway. Cancer Chemother. Pharmacol. 68, 1421–1430. https://doi.org/10.1007/s00280-011-1643-7

Wang, Z., Dabrosin, C., Yin, X., et al. (2015). Broad targeting of angiogenesis for cancer prevention and therapy. Semin. Cancer Biol. 35, S224–S243. https://doi.org/10.1016/j.semcancer.2015.01.001

Wang, Z., Li, Y., Zhan, S., et al. (2019). SMAD4 Y353C promotes the progression of PDAC. BMC Cancer 19, 1037. https://doi.org/10.1186/s12885-019-6251-7

Wang, Z. and Sun, Y. (2010). Targeting p53 for Novel Anticancer Therapy. Transl. Oncol. 3, 1–12. https://doi.org/10.1593/tlo.09250

Watson, J.V., Chambers, S.H., and Smith, P.J. (1987). A pragmatic approach to the analysis of DNA histograms with a definable G1 peak. Cytometry 8, 1–8. https://doi.org/10.1002/cyto.990080101

Wegert, J., Bausenwein, S., Kneitz, S., et al. (2011). Retinoic acid pathway activity in wilms tumors and characterization of biological responses in vitro. Mol. Cancer 10, 136. https://doi.org/10.1186/1476-4598-10-136

Weyermann, J., Lochmann, D., and Zimmer, A. (2005). A practical note on the use of cytotoxicity assays. Int. J. Pharm. 288, 369–376. https://doi.org/10.1016/j.ijpharm.2004.09.018

Wilkerson, M.J. (2012). Principles and Applications of Flow Cytometry and Cell Sorting in Companion Animal Medicine. Vet. Clin. North Am. Small Anim. Pract. 42, 53–71. https://doi.org/10.1016/j.cvsm.2011.09.012

Williams, A.A. (2012). Metabonomics profile and corresponding immune parameters of HIV infected individuals (Doctrate Thesis). University of Pretoria, Pretoria, South Africa.

Wong, R.S. (2011). Apoptosis in cancer: from pathogenesis to treatment. J. Exp. Clin. Cancer Res. 30, 87. https://doi.org/10.1186/1756-9966-30-87

Wuillème-Toumi, S., Robillard, N., Gomez, P., et al. (2005). Mcl-1 is overexpressed in multiple myeloma and associated with relapse and shorter survival. Leukemia 19, 1248–1252. https://doi.org/10.1038/sj.leu.2403784

Xia, L., Tan, S., Zhou, Y., et al. (2018). Role of the NFκB-signaling pathway in cancer. OncoTargets Ther. Volume 11, 2063–2073. https://doi.org/10.2147/OTT.S161109

Xia, Y., Shen, S. and Verma, I.M. (2014). NF-κB, an Active Player in Human Cancers. Cancer Immunol. Res. 2, 823–830. https://doi.org/10.1158/2326-6066.CIR-14-0112

Xu, T., Pang, Q., Zhou, D., et al. (2014). Proteomic Investigation into Betulinic Acid-Induced Apoptosis of Human Cervical Cancer HeLa Cells. PLoS ONE 9, e105768. https://doi.org/10.1371/journal.pone.0105768

Yang, C., Li, Y., Fu, L., et al. (2018). Betulinic acid induces apoptosis and inhibits metastasis of human renal carcinoma cells in vitro and in vivo. J. Cell. Biochem. 119, 8611–8622. https://doi.org/10.1002/jcb.27116

Yang, S. and Lian, G. (2020). ROS and diseases: role in metabolism and energy supply. Mol. Cell. Biochem. 467, 1–12. https://doi.org/10.1007/s11010-019-03667-9

Yang, Z.Y., Yuan, J.Q., Di, M.Y., et al. (2013). Gemcitabine Plus Erlotinib for Advanced Pancreatic Cancer: A Systematic Review with Meta-Analysis. PLoS ONE 8, e57528. https://doi.org/10.1371/journal.pone.0057528

Yaozu, Z., Liu, Y., Zhao, H., et al. (2021). Betulinic acid inhibits glioma cell viability by downregulation of NF-κB and enhancement of apoptosis. Trop. J. Pharm. Res. 19, 2545–2551. https://doi.org/10.4314/tjpr.v19i12.9

Yogeeswari, P. and Sriram, D. (2005). Betulinic Acid and Its Derivatives: A Review on their Biological Properties. Curr. Med. Chem. 12, 657–666. https://doi.org/10.2174/0929867053202214

Yurasakpong, L., Nantasenamat, C., Nobsathian, S., et al. (2021). Betulinic Acid Modulates the Expression of HSPA and Activates Apoptosis in Two Cell Lines of Human Colorectal Cancer. Molecules 26, 6377. https://doi.org/10.3390/molecules26216377

Zhan, X., Li, J., Zhang, S., et al. (2018). Betulinic acid exerts potent antitumor effects on paclitaxel-resistant human lung carcinoma cells (H460) via G2/M phase cell cycle arrest and induction of mitochondrial apoptosis. Oncol. Lett. https://doi.org/10.3892/ol.2018.9097

Zhang, A., Sun, H., Xu, H., et al. (2013). Cell Metabolomics. OMICS J. Integr. Biol. 17, 495–501. https://doi.org/10.1089/omi.2012.0090

Zhang, E., Lu, X., Yin, S., et al. (2019). The functional role of Bax/Bak in palmitate-induced lipoapoptosis. Food Chem. Toxicol. 123, 268–274. https://doi.org/10.1016/j.fct.2018.11.011

Zhang, H., Zhou, T., Yu, Q., et al. (2020). pH-Sensitive betulinic acid polymer prodrug nanoparticles for efficient and targeted cancer cells treatment. Int. J. Polym. Mater. Polym. Biomater. 69, 659–668. https://doi.org/10.1080/00914037.2019.1596916

Zhang, Q., Zeng, L., Chen, Y., et al. (2016). Pancreatic Cancer Epidemiology, Detection, and Management. Gastroenterol. Res. Pract. 2016, 1–10. https://doi.org/10.1155/2016/8962321

Zhang, R., Yang, J., Sima, M., et al. (2014). Sequential combination therapy of ovarian cancer with degradable *N* -(2-hydroxypropyl)methacrylamide copolymer paclitaxel and gemcitabine conjugates. Proc. Natl. Acad. Sci. 111, 12181–12186. https://doi.org/10.1073/pnas.1406233111

Zhang, Y., Zhou, H., Zhang, Z., et al. (2021). Redox/NIR dual-responsive PEG-betulinic acid/pluronic-cypate prodrug micelles for chemophotothermal therapy. Colloids Surf. Physicochem. Eng. Asp. 609, 125662. https://doi.org/10.1016/j.colsurfa.2020.125662

Zhao, Y., and Krishnan, J. (2014). mRNA translation and protein synthesis: An analysis of different modelling methodologies and a new PBN based approach. *BMC Systems Biology*, 8, 1–24.

Zheng, Y., Liu, P., Wang, N., et al. (2019). Betulinic Acid Suppresses Breast Cancer Metastasis by Targeting GRP78-Mediated Glycolysis and ER Stress Apoptotic Pathway. Oxid. Med. Cell. Longev. 2019, 1–15. https://doi.org/10.1155/2019/8781690

Yang, Z.J., Chee, C.E., Huang, S., et al. (2011). The role of autophagy in cancer: therapeutic implications. *Molecular Cancer Therapeutics,* 10(9), 1533-1541. https://doi.org/10.1158/1535-7163-MCT-11-0047

Zhou, D., Shao, L. and Spitz, D.R. (2014). Reactive Oxygen Species in Normal and Tumor Stem Cells, in: Advances in Cancer Research. Elsevier, pp. 1–67. https://doi.org/10.1016/B978-0-12-420117-0.00001-3

Zinatizadeh, M.R., Schock, B., Chalbatani, G.M., et al. (2021). The Nuclear Factor Kappa B (NF-kB) signaling in cancer development and immune diseases. Genes Dis. 8, 287–297. https://doi.org/10.1016/j.gendis.2020.06.005

Zuco, V., Supino, R., Righetti, S.C., et al. (2002). Selective cytotoxicity of betulinic acid on tumor cell lines, but not on normal cells. Cancer Lett. 175, 17–25. https://doi.org/10.1016/S0304-3835(01)00718-2

Appendices

Appendix I: Publications

The review paper was not provided in this section because it was published in a subscription-based journal.

polymers

MDPI

Article

Polyethyleneglycol-Betulinic Acid (PEG-BA) Polymer-Drug Conjugate Induces Apoptosis and Antioxidation in a Biological Model of Pancreatic Cancer

Karabo Sekopi Mosiane [1], Ekene Emmanuel Nweke [1], Mohammed Balogun [2] and Pascaline Nanga Fru [1,*]

[1] Department of Surgery, School of Clinical Medicine, Faculty of Health Sciences, University of the Witwatersrand, 7 York Road, Parktown, Johannesburg 2193, South Africa
[2] Biopolymer Modification and Therapeutics Lab, Materials Science & Manufacturing, Council for Scientific and Industrial Research, Meiring Naude Road, Brummeria, Pretoria 0001, South Africa
* Correspondence: pascaline.fru@wits.ac.za; Tel.: +27-11-717-2476; Fax: +27-11-484-2117

Abstract: Pancreatic cancer (PC) is one of the most aggressive solid malignancies with poor treatment response and low survival rates. Herbal medicines such as betulinic acid (BA) have shown potential in treating various solid tumours, but with limitations that can be circumvented by polymer-drug conjugation. Polyethylene glycol-BA (PEG-BA) polymer-drug conjugate has previously shown selective anticancer activity against PC cells. Here, we elucidate the mechanism of cell death and the cell death pathway, anti-inflammatory and antioxidant activities of PEG-BA. PEG-BA induced apoptotic cell death by arresting MIA-PaCa-2 cells in the Sub-G_1 phase of the cell cycle compared with BA and untreated cells (39.50 ± 5.32% > 19.63 ± 4.49% > 4.57 ± 0.82%). NFκB/p65 protein expression was moderately increased by PEG-BA (2.70 vs. 3.09 ± 0.42 ng/mL; $p = 0.1521$). However, significant ($p < 0.05$) overexpression of the proapoptotic genes *TNF* (23.72 ± 1.03) and *CASPASE 3* (12,059.98 ± 1.74) compared with untreated cells was notable. The antioxidant potential of PEG-BA was greater (IC_{50} = 15.59 ± 0.64 μM) compared with ascorbic acid (25.58 ± 0.44 μM) and BA-only (>100 μM) and further confirmed with the improved reduction of hydroperoxide levels compared with BA-only (518.80 ± 25.53 μM vs. 542.43 ± 9.70 μM). In conclusion, PEG-BA activated both the intrinsic and extrinsic pathways of apoptosis and improved antioxidant activities in PC cells, suggesting enhanced anticancer activity upon conjugation.

Keywords: Polyethyleneglycol-betulinic acid; conjugation; apoptosis; antioxidation; reactive oxygen species

Citation: Mosiane, K.S.; Nweke, E.E.; Balogun, M.; Fru, P.N. Polyethyleneglycol-Betulinic Acid (PEG-BA) Polymer-Drug Conjugate Induces Apoptosis and Antioxidation in a Biological Model of Pancreatic Cancer. *Polymers* **2023**, *15*, 448. https://doi.org/10.3390/polym15020448

Academic Editors: Kalim Deshmukh, Kishor Kumar Sadasivuni and Tomáš Kovářík

Received: 26 October 2022
Revised: 5 January 2023
Accepted: 9 January 2023
Published: 14 January 2023

1. Introduction

Pancreatic cancer (PC) is a lethal solid malignancy with increasing incidence and mortality worldwide [1]. Most patients present with advanced stages of the disease, in which case the tumour is inoperable and has metastasised to other sites or both [2]. Currently, the best curative option is surgery using adjuvant chemotherapy, with only 15% of patients presenting with resectable or early-stage disease [2]. Combination chemotherapy regimens, including gemcitabine and FOLFIRINOX (oxaliplatin, irinotecan, fluorouracil and leucovorin), are used as the first-line therapy for PC and have shown improved patient survival [3]. Although survival has improved, this is still insufficient as the survival rate is still abysmal compared with other cancers. Furthermore, studies have demonstrated that the administration of chemotherapy could lead to adverse side effects suggesting the need to develop potent drugs against PC but with reduced side effects, including toxicity to normal cells [4].

Betulinic acid (3β-hydroxy-lup-20(29)-en-28-oic acid), the carboxylic acid derivative of betulin, is a naturally occurring, widely distributed pentacyclic triterpene sourced from the outer bark of the Betula alba tree [5]. Betulinic acid (BA) has shown promising anticancer

efficacy against several tumours, including cervical cancer, melanomas, leukaemia, blastomas and PC [6–8]. However, like any other natural compound, BA is associated with several limitations, including a high molecular weight, which inhibits passage through the lipid bilayer of cells, and poor solubility, which reduces biodistribution, bioavailability and overall therapeutic index [9].

Using nanoparticles in chemotherapy provides an efficient and selective drug delivery system for targeting tumour cells [10]. An example of this type of platform is polymer-drug conjugates, macromolecular constructs covalently linked to a polymeric carrier. Drug conjugation is known to maximise efficacy, reduce adverse side effects, prolong blood circulation, passively deliver drugs to tumours via the enhanced permeability and retention (EPR) effect and overcome tumour resistance [11,12]. In a recent study from our laboratory, conjugation of polyethylene glycol (PEG) to BA showed selective toxicity to PC cells compared with BA alone, resulting in increased apoptotic cell death [8]. However, the specific mechanism of apoptotic cell death and possible evasion strategies employed by the cancer cells were not investigated.

Apoptosis occurs via two different pathways, namely the extrinsic (death receptor) and intrinsic (mitochondrial) pathways [7]. The extrinsic pathway involves the formation of the death-inducing signalling complex (DISC) and subsequent activation of procaspase 8 to caspase 8 [13]. In type 1 cells, the signal from caspase 8 is strong enough to activate procaspase 3 to caspase 3 and leads to apoptosis [14,15]. In type 2 cells, the signal is weak and requires amplification via cleavage of Bid (truncated Bid), which is translocated to the mitochondria [7,15,16]. The intrinsic pathway is caused by cellular stress that disrupts the mitochondrial membrane potential, leading to leakage of cytochrome c (Cyt C) into the cytosol via the Bak/Bax channel [7,17,18]. CytC interacts with deoxyadenosine triphosphate (dATP), apoptotic proteinase-activating factor-1 (Apaf-1) and procaspase 9, forming a complex known as the apoptosome, which leads to the autoactivation of procaspase 9 to caspase 9, which in turn activates procaspase 3 to caspase 3, leading to apoptosis [13].

Cancer cells have developed mechanisms to evade apoptosis, a major hallmark of carcinogenesis [19]. One such mechanism is the dysregulation of pro- and antiapoptotic genes or proteins [20,21]. For example, the B-cell lymphoma 2 (Bcl-2) family, which includes both pro (including puma, Bid, Bad, Bax and Bak) and anti (such as Bcl-2, Bcl-XL and Mcl-1)-apoptotic members, are frequently dysregulated in carcinogenesis [21]. Unlike some tumours, PC is associated with the downregulation of the Bcl-2 protein [22–24]. This suggests that evasion of apoptosis is induced by the other antiapoptotic proteins (Bcl-X_L and Mcl-1). These proteins have been associated with the nuclear factor kappa-light chain enhancer of activated B cells (NF-κB), a mediator of inflammation, which is overexpressed in tumours [22]. Like other cancers, PC is known to downregulate the expression of Bax and Bak, favouring survival over cell death [22,25]. Furthermore, other studies have shown that cancer cells inhibit the activation of caspase proteins by overexpressing the inactive forms compared with the activated caspases [26–28].

In the case of cellular injury, the immune system is activated in an attempt to alleviate any resulting potential damage [29,30]. One of the response mechanisms used by the innate immune system is inflammation [29], with reactive oxygen species (ROS) playing a significant role. ROS are necessary for embryonic development at moderate levels, guiding tissue maintenance and immunity [31]. Consequently, chronic inflammation and subsequent overproduction of ROS can result in the induction of DNA oxidation, affecting the stability of the genome and causing gene mutations, which in turn facilitate cancer initiation [29,31–34]. Furthermore, inflammation aids in the formation of the tumour-promoting microenvironment and can cause chemoresistance in many cancer types, including PC [29,35]. NF-κB mediates inflammation by regulating pro-inflammatory cytokines such as interleukins, transforming growth factor beta and tumour necrosis factor-alpha [29,30,36]. In addition, NF-κB is continuously transcribed in PC, leading to transcriptional and translational upregulation of genes involved in angiogenesis, apoptosis inhibition, tissue invasion and growth factors, activating survival pathways [36–38].

In this study, PEG-BA was assessed for its effect on apoptosis by measuring DNA content, proapoptotic gene expression, and NF-κB protein activity on MIA PaCa-2 treated cells. Its effect on the inflammation induced by ROS was also assessed. The findings demonstrated that PEG-BA induces apoptosis by arresting cells in the sub-G_1 phase of the cell cycle, activates proapoptotic genes of the extrinsic and intrinsic pathways and inhibits ROS formation. Overall, there was cell growth inhibition, apoptosis induction and ROS activity inhibition in PC cells treated with PEG-BA, suggesting that apoptosis is the primary anticancer mechanism.

2. Materials and Methods

2.1. Compound Preparation

The compounds were synthesised and characterised as previously described [8,39]. The free compound (BA), conjugate (PEG-BA) and standard (gemcitabine) were dissolved to 20 mg/mL in tissue culture grade dimethylsulfoxide (DMSO) (Sigma-Aldrich, St. Louis, MO, USA) and stored in single-use aliquots at −20 °C until required for experiments.

2.2. Cell Culture Models and Maintenance

The biological model for PC used in this study was the MIA PaCa-2 cells obtained from the Japanese Collection of Research Bioresources (JCRB) Cell Bank (JCRB Cell Bank; Ibaraki, Japan). These cells were derived from a 65-year-old man with pancreatic adenocarcinoma located in the tail and body of the pancreas [40]. Vero cells, derived from the kidney of the African green monkey (Cercopithecus aethiops), were used as a model for normal cells to compare with the PC cells in the cytotoxicity and antioxidant activity assays.

Both cell lines were cultured in Dulbecco's modified Eagle's medium (DMEM) (Sigma-Aldrich, St. Louis, MO, USA) with slight modifications. The DMEM used for the MIA PaCa-2 cells was made up to a final concentration of 13.4 g/L with sodium bicarbonate ($NAHCO_3$—3.7 g/L) and 1% antibiotic antimycotic solution (10,000 units/mL of penicillin, 10,000 µg/mL streptomycin and 25 µg/mL amphotericin B). In the case of the Vero cells, the standard DMEM (13.4 g/L DMEM powder + 3.7 g/L $NaHCO_3$) was supplemented with 1.1 mM sodium pyruvate, 25 mM HEPES buffer, 250 µg/mL gentamicin, and 0.5% antibiotic antimycotic solution. Both media were further supplemented with 10% heat-inactivated foetal bovine serum (FBS). The cells were cultured in 75 cm^2 vented flasks (Thermo Fischer Scientific, Waltham, MA, USA) at 37 °C (95% humidity and 5% CO_2). The cells were harvested every 2–4 days or when they reached 80–90% confluency using a trypsin-EDTA (Sigma-Aldrich, St. Louis, MO, USA) dissociation reagent. Cell counting was performed using the trypan blue exclusion method [41].

2.3. Cell Treatment

For experimental purposes, the cells were allowed to adhere for 24 h and then treated with controls and test compounds diluted with DMEM. DMSO ($\geq$0.33%) was used as the vehicle control, 0.4 µM doxorubicin and 0.78–100 µM gemcitabine as control drugs, and 0.78–100 µM BA (free compound) and PEG-BA (polymer-drug conjugate) for 72 h in a humidified incubator (95% humidity, 37 °C and 5% CO_2).

2.4. Microscopic Analysis

MIA PaCa-2 cells exposed to varying concentrations (1, 2, 4 and 8 µM) of BA and PEG-BA were analysed using light microscopy. The morphological changes were photographed after 24, 48 and 72 h using the Olympus IX51 microscope (Olympus—Life Sciences Solutions, Tokyo, Japan) at 10 X magnification.

2.5. Cytotoxicity Analysis

Cytotoxicity assays were performed using tetrazolium dyes as previously described [8]. The IC_{50} value, the half-maximal inhibitory concentration representing the concentration at which the compounds will inhibit cell viability by 50% [42], was calculated using GraphPad

Prism (v8.0.2.263). This was followed by analysing the ratio between the IC_{50} on Vero and MIA PaCa-2 cells, defined as the selectivity index (SI).

2.6. Cell Cycle Status Determination with Propidium Iodide Dye

The single parameter-based propidium iodide staining technique was used to assess the cell cycle status of the cells, pre-and post-treatment with vehicle control (0.33% DMSO), 4 µM of BA and PEG-BA and 4.5 µM of gemcitabine following 72 h of treatment (37 °C; 95% humidity, 5% CO_2). The cells were harvested using trypsin EDTA and washed (200× *g*). The cell pellet was resuspended with ice-cold 1X PBS followed by dropwise addition of ice-cold 70% ethanol for fixation at −20 °C for at least 24 h before staining. A total of 500 µL of the staining mixture, prepared by dissolving 2 mg of RNase A in 0.1% Triton-X100 reagent in PBS and containing 400 µL of 500 µg/mL propidium iodide dye, was added to each sample and incubated at room temperature for 30 min. Data acquisition commenced at low flow rates (< 300 events/sec) for improved resolution and adequate DNA quantification on the BD LSRFortessa™ Analyser and FACSDiva software (BD Biosciences, Franklin Lakes, NJ, USA). At least 30,000 events were recorded per sample. The fluorescent signal from the samples was detected using the 610/20 band filter pass filter. The generated Flow Cytometry Standard (FCS) files in FACSDiva were imported and analysed using FlowJo v10.8.1 (FlowJo, LLC, Ashland, KY, USA).

2.7. Gene Expression Analysis of Apoptotic Genes

2.7.1. Extraction of Total RNA

Total RNA was extracted using the E.Z.N.A.® Total RNA Kit I (Omega Bio-Tek, Norcross, GA, USA) according to the manufacturer's guidelines. Briefly, 700 µL of guanidium thiocyanate (GTC)-lysis buffer containing 2% β-mercaptoethanol was added to the pelleted cells previously treated with 4 µM BA and PEG-BA and 4.5 µM gemcitabine for 72 h. This mixture was then transferred to an RNA homogeniser mini-column and centrifuged for 60 s at 13,000× *g*. This was followed by adding 700 µL of freshly prepared 70% ethanol and transferring to a HiBind®RNA mini-column. The mixture was centrifuged at 10,000× *g* for 60 s until the RNA in-solution was bound to the column. The bound RNA was washed (30 s at 10,000× *g*) with 500 µL of RNA Wash Buffer I. The filtrate was discarded, and the RNA was rewashed (60 s at 10,000× *g*) using a second buffer (RNA Wash Buffer II containing 100% ethanol). This step was repeated once to ensure proper washing of the RNA before drying the HiBind®RNA mini-column to remove any residual ethanol (15,000× *g* for 120 s). The HiBind®RNA mini-column was transferred to a 1.5 mL Eppendorf tube, and 60 µL of nuclease-free water was added, followed by centrifugation (15,000× *g* for 120 s) to elute the RNA. The eluted RNA was assessed for purity, and the concentration was determined using the Nanodrop 2000 (Thermo Fischer Scientific, Waltham, MA, USA).

2.7.2. Complementary DNA (cDNA) Synthesis

Total RNA (250 ng/µL) was used to make the cDNA template for each sample. The cDNA synthesis step was performed using the ProtoScript II First Strand cDNA Synthesis Kit (New England BioLabs Inc, Ipswich, MA, USA) following the manufacturer's protocol. Briefly, 20 µL of the reaction mixture was added to respective Eppendorf tubes: 2 µL of d(T)23 VN (50 µM) primers, 10 µL of the ProtoScript II reaction mix (2X), 2 µL of the Protoscript II enzyme mix (10 X) and 6 µL of the RNA template diluted with the required amount of nuclease-free water to have a uniform final cDNA concentration for all the samples of 1000 ng/µL. The samples were then incubated in a SimpliAmp Thermal Cycler (Thermo Fischer Scientific, Waltham, MA, USA) under the following conditions: 42 °C for one hour, enzyme inactivation at 80 °C for 5 min, and an infinite hold at 4 °C.

2.7.3. Quantitative Real-Time Polymerase Chain Reaction Analysis

Real-time PCR was performed in a 96-well plate format (on ice) according to the MIQE guidelines [43]. Briefly, 5 µL of the PowerUp™ SYBR™ Green Master Mix (2X),

0.5 µL each of forward and reverse primer (sequences shown in Table 1), 2 µL of the cDNA template, and 2 µL of nuclease-free water were added to each well of a 96-well PCR plate, in duplicate. The universal PCR conditions used entailed a UDG activation at 50 °C for 2 min, Dual-lock DNA polymerase activation at 95 °C for 2 min, PCR cycling (40 cycles) of denaturation (95 °C for 15 s), annealing primer-specific temperature range of 50–60 °C for 15 s and extension (72 °C for 60 s). Two reference genes: β-Actin (ACTB) and mitochondrial ribosomal protein L19 (MRPL19), were used to normalise relative fold expression. Fold changes were determined using the $2^{-\Delta\Delta CT}$ method [44].

Table 1. List of genes used for real-time polymerase chain reaction.

Gene Name	Forward Primer Sequence	Reverse Primer Sequence
TNF	5′-TGCACTTTGGAGTGATCGGC-3′	5′-TTGTCACTCGGGGTTCGAGA-3′
TNFSF10	5′-TTGGGACCCCAATGACGAAGA-3′	5′-TGGTCCCAGTTATGTGAGCTG-3′
BAX	5′-CCAGCAAACTGGTGCTCAAGG-3′	5′-ACAGGGACATCAGTCGCTTCA-3′
BID	5′-GACCCTGGGAGAGCTCTGAAGC-3′	5′-CTCCGACTCACTCCTGGTTCAC-3′
CASPASE 2	5′-TACTCCCACCGTTGAGCTGT-3′	5′-TGCCAGCTGGAAGTGTGTTTG-3′
CASPASE 3	5′-TTGGAACCAAAGATCATACATGGAA-3′	5′-TGAGGTTTGCTGCATCGACA-3′
CASPASE 7	5′-AGTGGATGCTAAGCCAGACCG-3′	5′-TCGAACGCCCATACCTGTCA-3′
CASPASE 8	5′-ATAGGCCTGTGACGAAGGTGC-3′	5′-GCGGAATGTAGTCCAGGCTCA-3′
ACTB [1]	5′-CTTCGCGGGCGACGAT-3′	5′-CCACATAGGAATCCTTCTGACC-3′
MRPL19 [1]	5′-CCTAGGCCGGAGTTTCCAA-3′	5′-GACTCAAGAACCTGCGTTCC-3′

[1] The housekeeping genes used to normalise fold expression.

2.8. NF-κB/p65 Transcription Factor Assay

The human nuclear factor kappa-B p65 subunit (NF-κB/p65) enzyme-linked immunosorbent assay (ELISA) kit from Elabscience Biotechnology Inc. (Houston, TX, USA) was used to determine the concentration of NF-kB/p65 present in cellular samples after treatment with complete DMEM, 4 µM of BA and PEG-BA, and 4.5 µM gemcitabine (72 h incubation). Cell supernatants and lysates derived from these samples were used to perform the ELISA according to the manufacturer's protocol with slight modifications. Briefly, 100 µL of the standards (0–10 ng/mL), lysates (diluted 2X with sample diluent), and supernatants were added to respective wells in the protein-coated 96-well plate, in duplicate, sealed, and incubated at 37 °C for 1.5 h. The samples were discarded, and 100 µL of the biotinylated detection antibody working solution was added and incubated for an hour. A wash step was employed by adding 350 µL of the wash buffer, soaking for at least 60 s, and aspirating three times. Horseradish peroxidase (HRP) conjugate working solution (100 µL) was added to each well, sealed, and incubated for 30 min. The plate was washed five times, and 90 µL of the substrate reagent was added to the wells. The plates were sealed and covered in foil to protect them from light. The plate was incubated for at least 15 min, followed by adding 50 µL of the stop solution. The optical density was measured at 450 nm using a Multiscan Sky microplate reader (Thermo Fischer Scientific, Waltham, MA, USA).

2.9. ROS Reduction and Potential Antioxidant Analysis

Although the aetiology of PC is not well-known, inflammation has been described as an important risk factor [2,45]. Two assays were used to assess the potential antioxidative capacities of BA and PEG-BA. This was performed using the 2,2-Diphenyl-1-picrylhydrazyl (DPPH) antioxidant assay for the compound activity and the N,N-Dimethyl-p-phenylenediamine (DEPPD) assay for ROS activity in MIA PaCa-2 cells.

2.9.1. DPPH Assay

BA, PEG-BA, and the ascorbic acid standard were tested in the antioxidant activity assay at concentrations in the range 0.78–100 µM. This assay was modified from the 2014 protocol by Mistry and Shah [46]. Briefly, 180 µL of distilled water was added to the first

nine rows of a 96 well-plate and 100 µL to the remaining wells. This was followed by adding 20 µL of BA, PEG-BA and ascorbic acid (dissolved in methanol) in the appropriate wells in a fume hood to prevent evaporation of the methanol. A two times serial dilution was performed before adding 100 µL of freshly prepared methanolic DPPH solution to triplicate wells, except for the compound control wells, in the dark. The plates were covered in foil and shaken on a Titertek microplate shaker (Medical EXPO, Marseilles, France) for 10 min. This was followed by an additional 35 min incubation period in the dark. After the incubation, absorbance readings were obtained at 517 nm using a Multiscan Sky microplate reader (Thermo Fisher Scientific, Waltham, MA, USA).

2.9.2. DEPPD Assay

The DEPPD assay was used to determine reactive oxygen metabolites (hydroperoxide) produced by reactive oxygen species (ROS) in PC cells. The oxidative status and ROS reduction potential of the MIA PaCa-2 cells pre- and post-treatment (72 h) with 0.33% DMSO and optimised working concentrations: 8 µM for BA and PEG-BA and 9 µM gemcitabine, were determined using the DEPPD assay. The assay was performed according to the protocol by William (2012), with modifications to accommodate using cell supernatants instead of the standard urine or blood samples [47]. Briefly, 140 µL of 0.1 M sodium acetate buffer (pH 4.8) was added to a 96-well plate. This was followed by adding 10 µL of 0.39–50 µM hydrogen peroxide standard and cell supernatants of negative control of (media only), vehicle control, BA and PEG-BA and standard gemcitabine. One hundred microlitres of R_1/R_2 solution (100 µg/mL DEPPD (R_1) and 4.37 µM FeSO4 (R_2) at a ratio of 1:25) was added to all wells except the blank. The plate was covered with foil for at least 1 min and analysed using a Victor™ X3 model 2030 multilabel plate reader (PerkinElmer, Waltham, MA, USA) at a wavelength of 505 nm with a kinetic loop of 30 readings per well.

2.10. Statistical Analysis

The GraphPad Prism Version 8 software (GraphPad, San Diego, CA, USA) was used to determine the statistical significance of the data. To assess whether the data were normally distributed, normality tests such as the Shapiro–Wilk (W), Anderson–Darling (A2*), D'Agostino–Pearson omnibus (K2), and Kolmogorov–Smirnov (distance) that are available in the GraphPad Prism (version 8) software were used. It was assumed that a *p*-value greater than α (0.05) meant that the null hypothesis (H_0) was accepted, and the data were classified as following a normal distribution. Furthermore, quantile-quantile (Q-Q) plots were assessed with the assumption that plotting predicted residual vs. actual residual forms a roughly straight line for normally distributed data. For two groups (passed normality tests and Q-Q plots), an unpaired Student t-test was performed. A two-way analysis of variance (ANOVA) was performed for more than two groups, followed by multiple comparisons using the Tukey post hoc test, if the data passed the normality tests and Q-Q plots. For data that only passed the normality tests but not the Q-Q plots, the non-parametric Kruskal–Wallis was performed followed by Dunn's post hoc test. A *p*-value of less than 0.05 was considered statistically significant.

3. Results

3.1. PEG-BA Causes Cell Rounding in a Dose and Time-Dependent Manner

At least 100,000 cells/mL were visualised for morphological changes before and after treatment using light microscopy. Figure 1A–I show representative micrographs of the effect of BA and PEG-BA on MIA PaCa-2 cells at 72 h only. Quantitative graphs showing percentage cytotoxicity using MTT are shown in Figure 1J. The results showed that, compared with untreated cells (Figure 1A), 2 and 4 µM BA started to induce minimal cell rounding or clumps. However, most plated cells were still viable even at 72 h (4.88 ± 2.42% and 5.55 ± 3.85% cytotoxicity—Figure 1C,D). Cell rounding is associated with apoptosis due to the initial detachment from neighbouring cells and shrinkage [48]. At the highest tested concentration (8 µM), there was a slightly increased cytotoxic effect (15.70 ± 5.70%)

that was not visible in the photomicrographs as the cells continued to grow (Figure 1E). On the other hand, the conjugated compound (PEG-BA) resulted in the formation of cell clumps at the lowest tested concentration (1 µM—Figure 1F) and a cytotoxic effect higher than that induced by BA at the same concentration ($p = 0.0255$). Therefore, PEG-BA induced increased cell clumping and cytotoxicity in a concentration and time-dependent manner. At 72 h, 8 µM of PEG-BA resulted in clumping of the cells forming clusters, indicating high toxicity towards the PC cells. This was also observed at 24 and 48 h (Figures S1 and S2). This is further confirmed with a 100% cytotoxicity after 72 h.

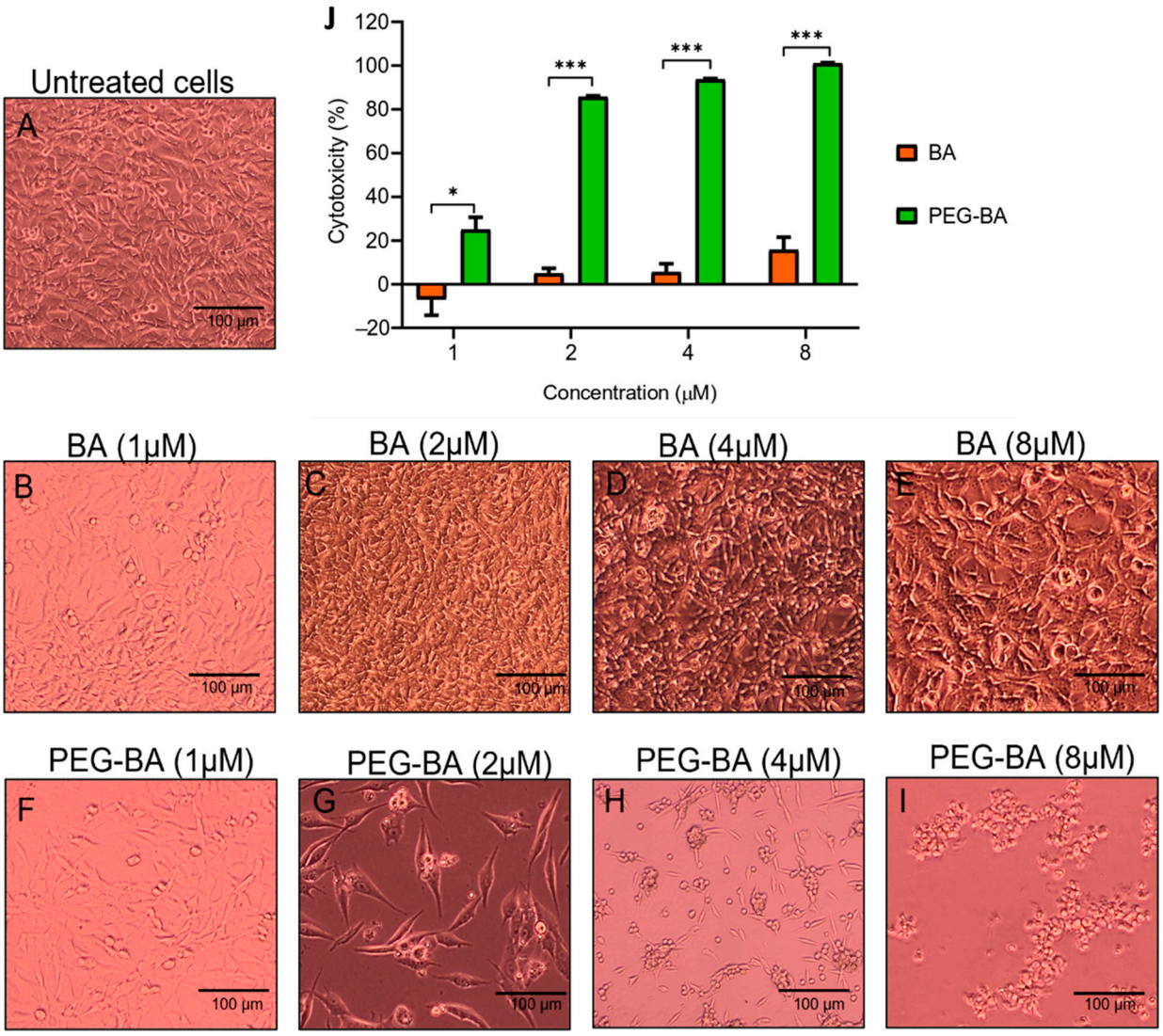

Figure 1. Microscopic and cytotoxic analysis of MIA PaCa-2 cells after treatment with BA and PEG-BA. The cytotoxic effect was measured using MTT tetrazolium dye after 72 h. (**A**) Untreated MIA PaCa-2 cells served as a reference for the morphology of the cells before treatment. (**B**–**E**) MIA PaCa-2 cells were treated with various concentrations (1–8 µM) of BA. The cells continued to grow, even at the highest concentration, although some formed clusters of rounded cells. (**F**–**I**) PEG-BA (1–8 µM) treated MIA PaCa-2 cells. The degree of cells rounding up was dose-dependent, where all the plated cells formed rounded clusters at 8 µM. Magnification: 10 X, scale bar: 100 µm. (**J**) Quantitative bar graph showing cytotoxicity of BA and PEG-BA relative to untreated cells at 72 h (mean ± SEM), n = 3, *: $p < 0.05$ and ***: $p < 0.001$.

3.2. PEG-BA Induces a Sub-G_1 Arrest in Pancreatic Cancer Cells

The cell cycle status of the MIA PaCa-2 cells before and after treatment was performed using propidium iodide dye on 4 μM of BA and PEG-BA treated cells. This is a concentration in the IC_{50} range from this (Figure S3) and a previous study [8]. The untreated MIA PaCa-2 cells showed a high percentage of cells in the G_1/G_0 (45.27 ± 4.70%) compared with cells undergoing DNA synthesis (S: 17.67 ± 1.22%) and those preparing to enter mitotic division or already in the phases of mitosis (G_2/M: 25.07 ± 2.44%) (Figure 2). The remaining cells, which were a minority (4.57 ± 0.82%), were in the area termed the sub-G_1 phase, which is the phase to the left of the G_1/G_0 phase. These results served as baseline populations for comparison after treatment, where a reduction or increase in cells from one phase to another was regarded as due to treatment [49]. At 4 μM, BA shifted the MIA PaCa-2 cells into sub-G_1 (19.63 ± 4.49%) and induced cell cycle arrest in the G_1/G_0 phase relative to the untreated MIA PaCa-2 cells (Figure 2B,D). PEG-BA (4 μM) treatment resulted in a more significant shift of cells into the sub-G_1 compared with the untreated sample and BA-only (PEG-BA: 39.50 ± 5.32% vs. untreated: 4.57 ± 0.82% and BA: 19.63 ± 4.49%) as shown in Figure 2C,D. Both compounds (PEG-BA and BA-only) inhibited entry into the S and G_2/M phases.

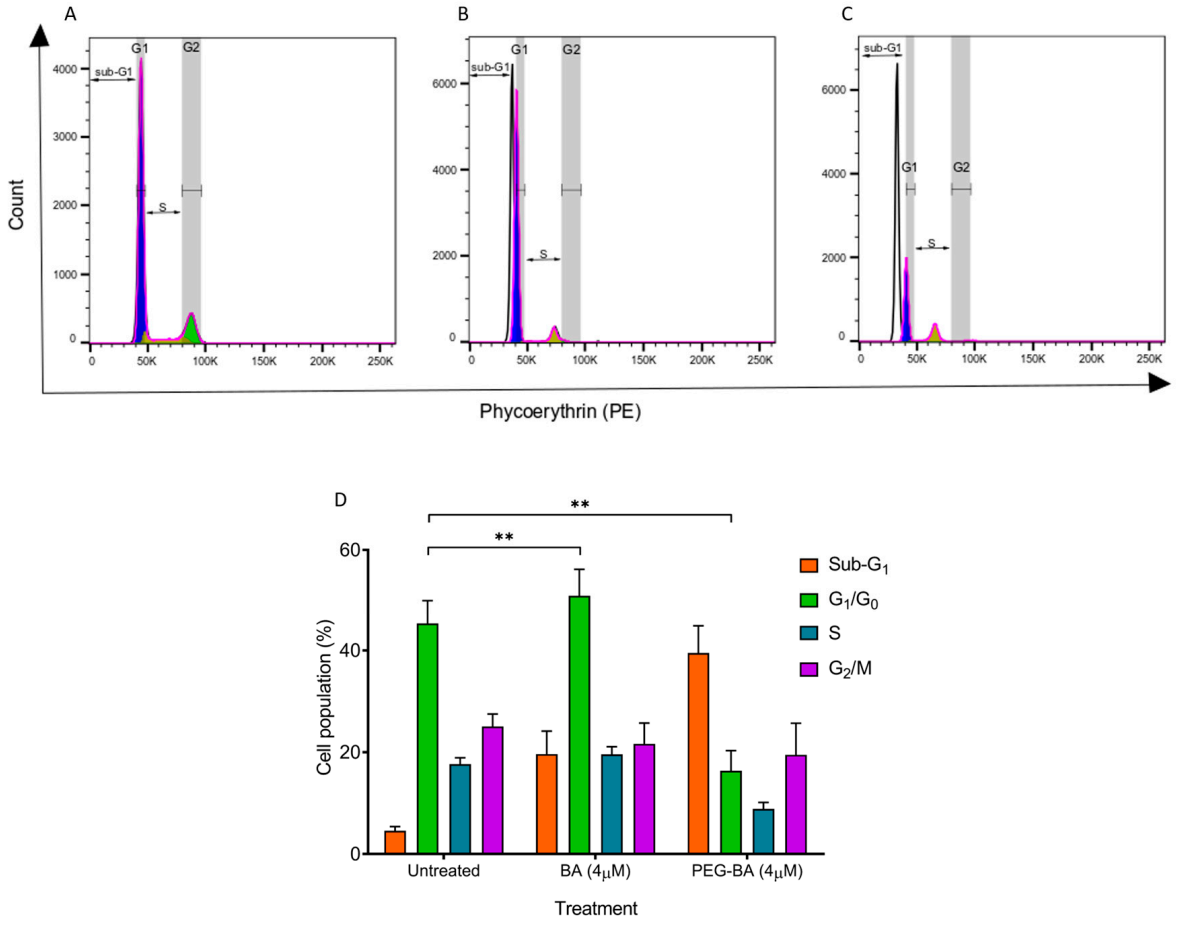

Figure 2. The cell cycle status was monitored using propidium iodide after 72 h of treatment. (**A**–**C**) Representative histograms showing the different phases of the cell cycle indicated by the white (sub-G_1), purple (G_1/G_0), yellow (S) and green (G_2/M) peaks. Double-sided arrows were inserted to highlight the sub-G_1 and S phases. Overall, both BA and PEG-BA resulted in a shift of cells from the G_1/G_0 to the sub-G_1 phase, indicating apoptosis induction. (**D**) Quantitative plots representing the overall cycling status of the PC cells (mean ± SEM), n = 3, **: $p < 0.01$. The Inkscape software (Version 1.1) was used to edit Figure 2A–C for clarity.

3.3. PEG-BA Elevates the Expression of Proapoptotic Genes

The cell cycle data reported here and the apoptosis assay performed previously [8] suggest that the anticancer activity of PEG-BA is via apoptosis. We then further investigated the potential mechanism by assessing the expression of key apoptotic genes (*TNF*, *TNFSF10*, *CASPASES* (*2, 3, 7, 8*), *BID* and *BAX*) of the extrinsic and intrinsic pathways of apoptosis using quantitative real-time PCR. Compared with BA, PEG-BA treatment in PC cells resulted in a significant increase in the proapoptotic genes, *CASPASE 2* (0.58 ± 1.93 vs. 8.16 ± 1.40; $p = 0.0401$), *CASPASE 8* (0.40 ± 1.93 vs. 27.69 ± 0.99; $p = 0.0021$) and BAX (0.60 ± 1.93 vs. 14.01 ± 3.55; $p = 0.0401$). Although not significant, *TNF* (3.47 ± 1.95 vs. 23.72 ± 1.03; $p = 3048$), *TNFSF10* (1.24 ± 1.93 vs. 4.87 ± 1.94; $p > 0.9999$), *BID* (3.34 ± 1.93 vs. 3.55 ± 0.93; $p = 0.9092$), *CASPASE 7* (3.40 ± 1.97 vs. 4.12 ± 1.74; $p = 0.9092$) and *CASPASE 3* (4.02 ± 1.93 vs. 12,059.98 ± 1.74; $p = 0.0872$) were also elevated (Figure 3). A reduced expression ($p > 0.05$) of apoptotic genes was observed when the PC cells were treated with gemcitabine, except for the non-significant overexpression of *CASPASE 3* ($p = 0.0872$). Comparing PEG-BA to gemcitabine showed high expression of *TNF* (23.72 ± 1.03 vs. 0.20 ± 1.54; $p = 0.0021$), CASPASE 8 (27.69 ± 0.99 vs. 0.49 ± 1.54; $p = 0.0401$), *BID* ($p = 0.0087$), *CASPASE 2* (8.16 ± 1.40 vs. 0.26 ± 1.55; $p = 0.0021$), *CASPASE 7* (4.12 ± 1.74 vs. 0.72 ± 1.55; $p = 0.0087$), *TNFSF10* (4.87 ± 1.94 vs. 0.06 ± 1.55; $p = 0.0166$) and *BAX* (14.01 ± 3.55 vs. 0.23 ± 1.71; $p = 0.0021$). Furthermore, non-significant overexpression of *CASPASE 3* (12,059.98 ± 1.74 vs. 8.53 ± 1.55; $p = 0.1712$) was also observed.

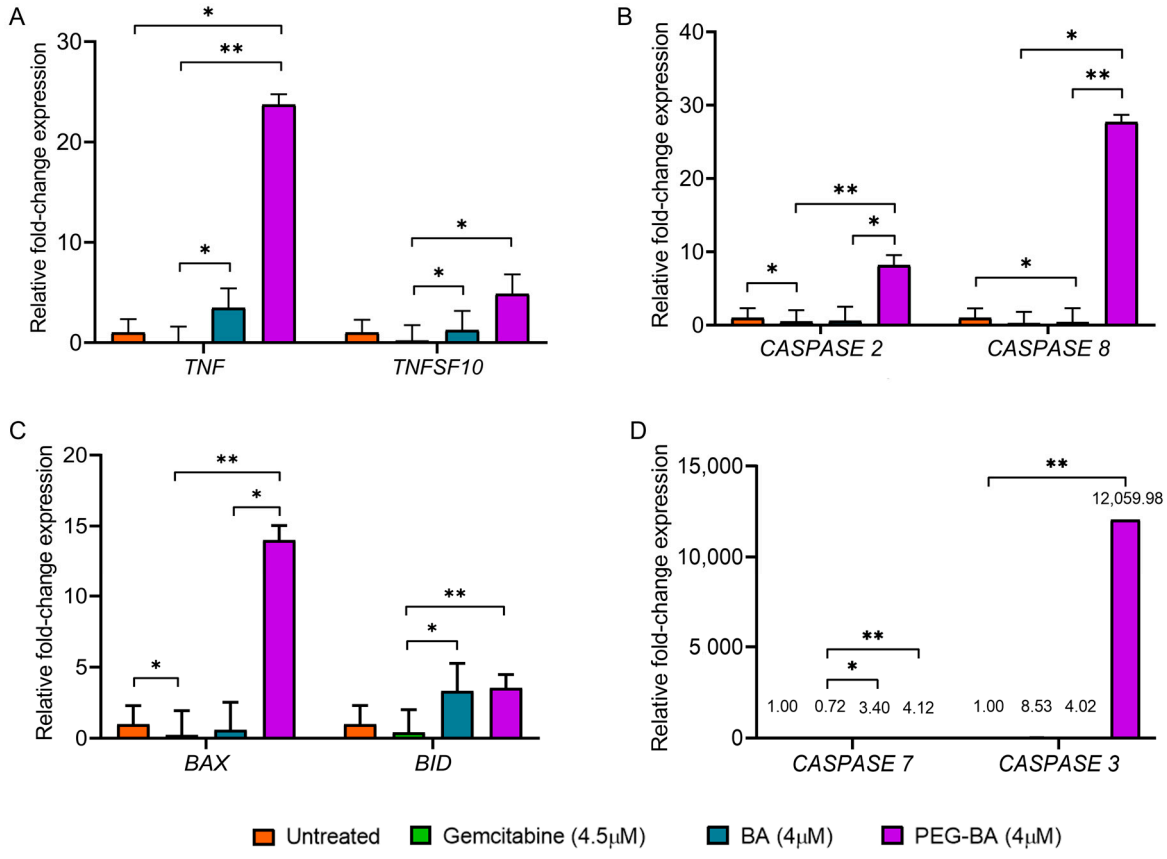

Figure 3. Fold change expression of apoptosis-related genes in treated and untreated MIA PaCa-2 cells. MIA PaCa-2 cells were treated with PEG-BA and BA (4 μM), and the expression of (**A**) *TNF* and *TNFSF10* (**B**), *CASPASE 2* and *CASPASE 8* (**C**) *BAX* and *BID* (**D**) *CASPASE 7* and *CASPASE 3*. Treatment with PEG-BA showed the biggest fold change of *TNF* (23.72 ± 1.03), *TNSF10* (4.87 ± 1.94), *BAX* (14.01 ± 3.55), *CASPASE 3* (12,059.98 ± 1.74), *CASPASE 2* (8.16 ± 1.40) and *CASPASE 8* (27.69 ± 0.99). Expression values are represented as mean ± SD, *: $p < 0.05$ and **: $p < 0.01$.

3.4. PEG-BA Treatment May Result in NF-κB Expression in Pancreatic Cancer Cells

The protein expression levels of nuclear factor kappa B (p65-subunit) in both lysate and supernatant of treated (PEG-BA, BA only and gemcitabine) MIA PaCa-2 cells were quantified using a sandwich ELISA. A higher level of NF-κB was observed in the lysate of the untreated and treated MIA PaCa-2 cells compared with the corresponding supernatant (Figure 4). NF-κB levels remained unchanged in the supernatant (untreated: 1.12 ± 0.06 ng/mL; gemcitabine: 1.09 ± 0.03 ng/mL; BA: 1.13 ± 0.06 ng/mL and PEG-BA: 1.17 ± 0.07 ng/mL), whereas the lysate showed moderate increases with the treatment of PEG-BA (3.09 ± 0.42 ng/mL; $p = 0.1521$) and BA (2.78 ± 0.27 ng/mL; $p = 0.9981$) compared with the untreated sample (2.70 ± 0.21 ng/mL). Gemcitabine resulted in a slight but insignificant decrease (2.67 ± 0.19 ng/mL; $p = 0.9484$).

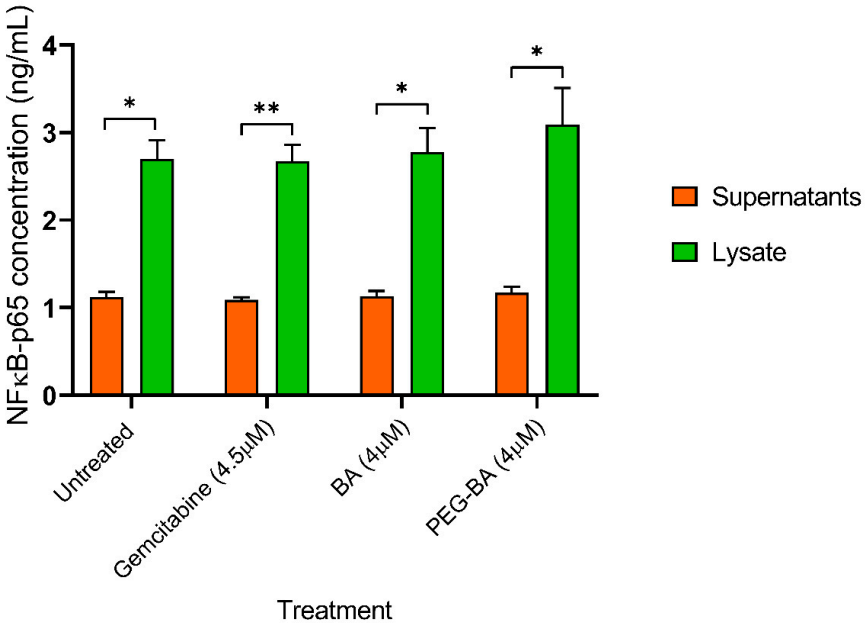

Figure 4. NF-κB protein levels from untreated cell lysates, supernatants, BA and PEG-BA treated MIA PaCa-2 cells. NF-κB levels were higher in the lysate compared with the supernatant. In the lysate, treatment with PEG-BA (3.09 ± 0.42 ng/mL) and BA (2.78 ± 0.27 ng/mL) moderately increased NF-κB levels compared with other groups (untreated: 2.70 ± 0.21 ng/mL and gemcitabine: 2.67 ± 0.19 ng/mL). The date is represented as mean ± SEM, *: $p < 0.05$ and **: $p < 0.01$.

3.5. PEG-BA Treatment Induces Antioxidant Activities in Pancreatic Cancer Cells

Antioxidant analysis using the DPPH assay showed that PEG-BA treatment induced a dose-dependent inhibition of DPPH compared with BA-only (Figure 5). BA treatment did not result in any significant changes in DPPH inhibition for all tested concentrations. At 25 μM, PEG-BA reduced the DPPH radical by 29.17 ± 1.05%, 1.4-fold higher than BA (21.30 ± 2.13%; $p = 0.1291$). This trend was also observed at the remaining concentrations (50 μM: 39.57 ± 0.58 vs. 24.27 ± 2.91% ($p = 0.0092$) and 100 μM: 36.56 ± 1.86% vs. 24.26 ± 3.07%, $p = 0.0279$). In an analysis to determine the compound's ability to inhibit at least 50% of the initial concentration of the DPPH radical (IC_{50}), PEG-BA was found to have the lowest IC_{50} (15.59 ± 0.64 μM) compared with BA-only (>100 μM) and ascorbic acid (25.58 ± 0.44; $p = 0.006$).

The level of ROS, specifically hydroperoxides, in the MIA PaCa-2 cells before and after treatment with PEG-BA, BA only and gemcitabine was assessed using the DEPPD assay. Overall, the results showed that there was a significantly ($p < 0.0001$) higher concentration of hydroperoxides (7.32-fold) in untreated cancer cells compared with the normal cells and treated cells (Figure 6). Treating the MIA PaCa-2 cells with PEG-BA resulted in a moderate reduction in hydroperoxide levels compared with the untreated (Figure 6), with no statisti-

cal significance (p = 0.5066). Notably, gemcitabine treatment reduced hydroperoxide levels (433.34 ± 33.53 μM) compared with untreated (546.96 ± 29.03 μM; p = 0.0451), PEG-BA treated (518.80 ± 25.53 μM; p = 0.2011) and BA-only (542.43 ± 9.70 μM; p = 0.0581) treated cancer cells.

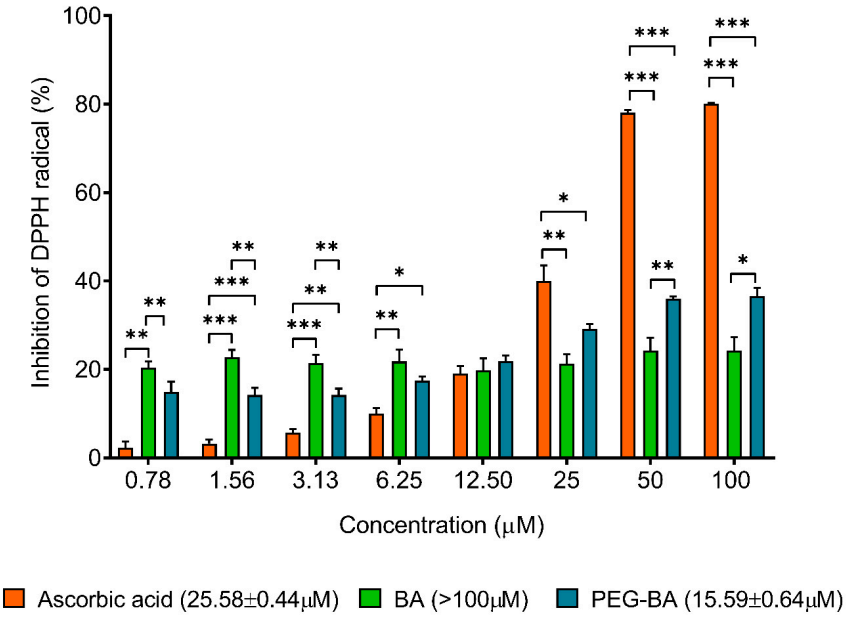

Figure 5. The antioxidant activity of PEG-BA and BA using the DPPH assay. The antioxidant potential was assessed at varying concentrations (0.78–100 μM). The conjugate, PEG-BA, exhibited a dose-dependent antioxidant effect resulting in the highest antioxidant potential compared with ascorbic acid and BA-only. This was indicated by the IC_{50} values shown in brackets on the graph. Data are shown as mean ± SEM (n = 4), *: $p < 0.05$, **: $p < 0.01$ and ***: $p < 0.001$.

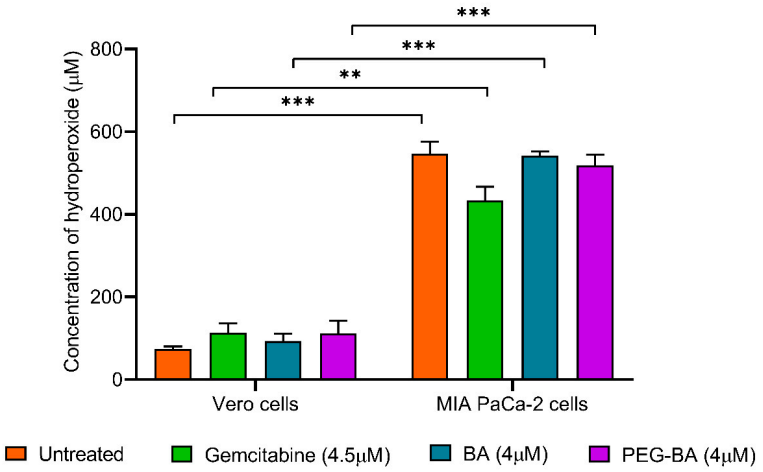

Figure 6. Reactive oxygen species levels were measured as hydroperoxides in MIA PaCa-2 and Vero cells before and after treatment with PEG-BA, BA only and gemcitabine using the DEPPD assay. MIA PaCa-2 cells generally showed higher levels of hydroperoxides compared with the normal cells (546.96 ± 29.03 μM vs. 74.73 ± 5.70 μM, p = 0.001). The effect of treatment on the normal cells resulted in a moderate increase in hydroperoxides, especially by gemcitabine (113.65 ± 22.77 μM) and PEG-BA (112.32 ± 29.69 μM) compared with free-BA (93.83 ± 17.43 μM). Conversely, treating the MIA PaCa-2 cells with gemcitabine (433.34 ± 33.53 μM), PEG-BA (518.80 ± 25.53 μM) and free-BA (542.43 ± 9.70 μM) resulted in hydroperoxide reduction compared with the untreated sample. Data are shown as mean ± SEM (n = 3), **: $p < 0.01$ and ***: $p < 0.001$.

4. Discussion

Pancreatic cancer is associated with chemoresistance. The conjugation of PEG to BA has been shown to kill PC cells effectively and selectively and could circumvent chemoresistance [8]. Analysing critical cellular processes such as apoptosis, inflammation and antioxidation during treatment with PEG-BA can help delineate the molecular mechanisms associated with treatment with the conjugated drug. In this study, PC cells were treated with PEG-BA and its proapoptotic and antioxidative characteristics were demonstrated compared with the free compound, BA and relevant controls.

MIA PaCa-2 cells were assessed using light microscopy to determine the effect of treatment on morphology. In this study, the characteristic spindle-shaped (elongated) morphology of MIA PaCa-2 cells was observed in the untreated sample [50]. Similarly, most BA-treated cells retained that morphology and the cells continued to grow and were still attached to neighbouring cells. A second population of smaller, rounded-up cells was also observed. It is well-documented that the rounding up and shrinkage of cells are critical characteristic features of initiation and progression into apoptosis [51,52]. This is also associated with an intact plasma membrane with reduced cytoplasm, further indicating an earlier phase of apoptosis and not necrosis [53]. Coricovac and colleagues (2021) tested the effect on the morphology of A375 human melanoma cells using BA (5–50 μM). Their results showed that apoptotic cells (smaller and rounded up) were present in a high percentage at 10 and 50 μM, suggesting that a high concentration of BA is required to visualise sufficient morphological differences to the untreated sample [54]. A similar finding was reported by Xu and colleagues (2014), where at least 30 μM of BA was required to inhibit 50% of Hela cells [55]. In contrast, PEG-BA resulted in a dose-dependent induction of cell rounding and shrinkage, which was confirmed by the cytotoxicity results even at 2 μM, suggesting that conjugation improved not only cytotoxicity but also apoptosis induction (confirmed in the downstream analysis performed in this study).

Cell cycle analysis studies, represented by the DNA content, showed an arrest of the cancer cells in the sub-G_1 phase after treatment with PEG-BA, relative to the untreated and BA-treated cells, suggesting an increase in apoptosis. Studies have shown that the presence of cells in the sub-G_1 phase indicates apoptotic cells or the induction of apoptosis [56]. This is because this phase represents hypodiploid cells with a DNA content less than that in the G_1 phase [56,57]. DNA degradation, a notable characteristic of apoptosis, can be one of the causes of the reduced DNA content, indicating that the cells found in the peak before the G_1/G_0 are undergoing apoptosis [56,57]. BA has been shown to induce apoptosis in various tumours, including leukaemia [58], neuroblastoma [59,60], cervical cancer [61], colon cancer [62], multiple myeloma [63] and PC [8]. In this study, both PEG-BA and BA induced a reduction of cancer cells in the S-phase, suggesting inhibition of DNA synthesis. The compounds also reduced the population of cells in the G_2/M phase, indicative of diminished cell proliferation and viability. Similar findings have been reported using PANC-1 and IGROV-1 cells treated with BA, resulting in either a sub-G_1 or a G_1/G_0 phase arrest [64,65]. Taken together, the findings from this study suggest that the drug conjugate PEG-BA induced increased apoptosis compared with free BA, and inhibited DNA synthesis, reduced cell proliferation and viability of PC cells.

Similar to the cell cycle findings, gene expression analysis further suggested a possible apoptosis-inducing ability of PEG-BA. PEG-BA induced the overexpression of proapoptotic genes of the extrinsic and intrinsic pathways, compared with free BA. According to the Central Dogma of molecular biology, DNA serves as the genetic material that is transcribed into messenger RNA and translated into proteins which are essential for cellular functioning [66]. Therefore, a link exists between mRNA and protein levels. A study by Vogel and Marcotte (2013) showed that there is a 40% correlation between gene expression (mRNA quantification) and protein levels [67]. Hence, in this study, the real-time PCR results were compared with literature findings based on proteins that function in apoptosis to try and predict the potential apoptotic mechanism of PEG-BA in PC cells. In cancer, the expression of antiapoptotic genes is elevated, and proapoptotic genes are downregulated [20,21]. *TNF*

and *TNFSF10* were upregulated post-PEG-BA treatment in PC cells (Figure 3A). These genes code for pro-inflammatory cytokines, which act as ligands that bind to death receptors, initiating the extrinsic pathway of apoptosis [15]. The products of *TNF* and *TNFSF10* can be inhibited by binding to decoy receptors such as cFLIP, which are overexpressed in several cancer types and aid cell proliferation, growth and survival [26,27]. The inhibition occurs because of the absence of a death effector domain (DED), used by tumour necrosis factor receptor type 1-associated DEATH domain (TRADD) adaptor molecules and procaspase 8 to form the DISC, whose inhibition disrupts the extrinsic pathway of apoptosis [26,27]. *CASPASE 2* and *8*, which code for initiator caspases 2 and 8, and *CASPASE 3* and *7*, which code for executioner caspases 3 and 7, were also overexpressed after PEG-BA treatment (Figure 3B,D). The initiator caspases are activated by forming complexes that facilitate their hydrolysis, which is necessary for caspase function [13]. The activated initiators then activate the executioner caspases, resulting in apoptosis activation. Both types of caspases are inhibited by the inhibitors of apoptosis (IAPs), which are generally overexpressed in cancer cells to favour survival and evade cell death [68,69]. The function of Bid protein in type 2 cells with low caspase signal is necessary for the activation of the mitochondrial pathway, either by direct inhibitory binding to the Bcl-2 protein, allowing Bax/Bak oligomerisation or directly triggering the release of Cyt C [70–72]. In this study, PEG-BA resulted in the overexpression of *BAX* and *BID* in the MIA PaCa-2 cells. In most cancers, including PC, both proapoptotic proteins are inhibited by high expression of Bcl-2 antiapoptotic proteins, facilitating the evasion of apoptosis [73]. A study by Naseri and colleagues (2015) showed apoptosis could be restored in cancer cells such as HepG2, T47D and HCT116 by activating Bax [74]. Conjugating PEG to BA improved the apoptosis-inducing ability of the free drug by activating proapoptotic genes.

It is well-documented that NF-κB protein subunits play an important role in inflammation, cell differentiation, proliferation, and death [75–77]. At rest, NF-κB is inactivated by the bound inhibitor IKB protein family preventing its translocation to the nucleus [76]. Phosphorylation inhibits IKBs and releases NF-κB, leading to dimerisation of its subunits (canonical: p50 and p65 or non-canonical: p100 and p52), which is translocated to the nucleus and activates transcription of their target genes [76,78]. In this study, NF-κB levels in the cell lysate were higher than in the supernatant, confirming its intracellular location and that disruption of the plasma membrane was necessary to release adequate amounts of the protein [76]. A slight but insignificant increase in NF-κB was observed after treatment with PEG-BA compared with untreated cancer cells. BA has been shown to activate NF-κB by inducing phosphorylation of the IKBs [6,65]. Notably, the present study showed an upregulation of TNF, an activator of NF-κB [74,75], with PEG-BA treatment. Although some studies have demonstrated the role of NF-κB in inducing cell survival pathways in several malignancies [73], several others have determined its role in apoptosis, specifically its p65 subunit [74–77]. NF-κB is necessary for BA-induced apoptotic cell death [65]. Ryan et al. (2000) demonstrated the proapoptotic role of NF-κB in Soas-2 cells. They found that p53 (a protein also increased in MIA PaCa-2 cells) induces translocation of NF-κB to the nucleus, thereby activating binding to DNA [79]. In addition, inhibiting NF-κB reduced apoptosis, suggesting that NF-κB may be crucial in the induction of apoptosis by doxorubicin in Soas-2 cells [79]. Another study showed that the activation of the NF-κB/p65 by aspirin resulted in the induction of Bax-dependent apoptosis in human colorectal carcinoma cells [80]. It is worth noting that in this study, PEG-BA treatment resulted in overexpression of *BAX* in the PC cells. These findings may suggest that NF-κB plays an important proapoptotic role, which may be improved by PEG-BA treatment.

PEG-BA treatment further improved antioxidant potential, demonstrated by a lower IC_{50} (15.59 ± 0.64 μM), suggesting a higher radical scavenging potential than ascorbic acid and BA. On the other hand, treatment with BA resulted in an IC_{50} greater than 100 μM, suggesting a lower antioxidant potential than ascorbic acid with an IC_{50} of 25.58 ± 0.44 μM. A similar observation was made by Adesanwo and colleagues (2013), where they assessed the antioxidant capacity of BA isolated from Tetracera potatoria roots and reported an

even higher IC_{50} value of 309 μM [81]. Several studies have reported that medicinal plants possess antioxidant activities with desirable radical scavenging abilities [81,82]. This is due to the presence of phenolic groups and tocopherols that can readily donate hydrogen atoms, which is an essential aspect of the DPPH assay, as it is based on the electron transfer ability of potential antioxidants [81,83]. Therefore, with an increase in the number of hydroxyl groups (-OH) or other hydrogen donating groups (-NH, -SH, etc.) in the molecular structure of a compound, the higher the antioxidant activity [81]. Our results, therefore, demonstrate that conjugating PEG to BA improves antioxidant activities due to the inherent anti-inflammatory property of BA, but also with added advantages such as improved solubility associated with conjugation.

The DEPPD assay confirmed significantly high concentrations of hydroperoxides in the PC cells compared with the normal cells (Figure 6), which has also been shown in other studies [32]. A moderate decrease in hydroperoxide concentrations was observed in PEG-BA-treated cancer cells compared with untreated cells. The reduction may be indicative of antioxidant activities [84]. Anticancer compounds possessing antioxidant potential are ideal due to the added advantage of combatting inflammation (ROS), potentially blocking cancer progression [31–33]. Our group has previously shown that PEG-BA downregulates the expression of Th1/Th2/Th17 cytokines involved in inflammatory processes, further confirming the anti-inflammatory ability of the conjugate [8,9].

5. Conclusions

This study has demonstrated that the potential therapeutic efficacy of betulinic acid on PC cells improved following polymer conjugation. It also showed at the morphological and molecular level that this increased efficacy is due to its ability to upregulate proapoptotic genes and, consequently, induce apoptosis while exhibiting antioxidation properties. These findings suggest that PEG-BA is further investigated as a treatment for PC using models such as 3D culture or animal models.

Supplementary Materials: The following supporting information can be downloaded at: https://www.mdpi.com/article/10.3390/polym15020448/s1, Figure S1: Microscopic analysis of BA and PEG-BA treatment on MIA PaCa-2 cells at 24 h. Figure S2: Microscopic analysis of BA and PEG-BA treatment on MIA PaCa-2 cells at 48 h. Figure S3: Cytotoxic effect of BA and PEG-BA on Vero and MIA PaCa-2 cells.

Author Contributions: Conceptualisation and administration of the study and experimental planning were done by E.E.N., M.B. and P.N.F. The conjugate synthesis and characterisation were done by M.B. The experiments were performed, and the data analysis and writing of the original manuscript draft were done by K.S.M., guided by E.E.N. and P.N.F. The principal investigator and primary grant holder was P.N.F. All authors have read and agreed to the published version of the manuscript.

Funding: This work is based on the research supported in part by the National Research Foundation of South Africa (Grant 105942), the University of the Witwatersrand Faculty Research Committee Individual Grant, No. 00140784411015121105514 2. Furthermore, the research reported in this publication was supported by the South African Medical Research Council under a Self-Initiated Research Grant. The views and opinions expressed are those of the author(s) and do not necessarily represent the official views of the SAMRC.

Institutional Review Board Statement: Ethical review and approval was waived for this study because no animal or human subjects were involved. A waiver was obtained from the Human Research Ethics Committee of the University of Witwatersrand (protocol code: W-CBP-200506-1, approved 6 May 2020).

Informed Consent Statement: Not applicable.

Data Availability Statement: The data presented in this study are available on request from the corresponding author.

Acknowledgments: The authors would like to acknowledge the input of Sindisiwe Mvango, who was involved in the synthesis and characterisation of the drug conjugate as well as Marietha Nel for cell culture support and final proofreading.

Conflicts of Interest: The authors declare no conflict of interest.

References

1. Siegel, R.L.; Miller, K.D.; Fuchs, H.E.; Jemal, A. Cancer statistics, 2021. *CA Cancer J. Clin.* **2021**, *71*, 7–33. [CrossRef] [PubMed]
2. Maisonneuve, P. Epidemiology and burden of pancreatic cancer. *Presse Médicale* **2019**, *48*, e113–e123. [CrossRef]
3. Kleeff, J.; Korc, M.; Apte, M.; La Vecchia, C.; Johnson, C.D.; Biankin, A.V.; Neale, R.E.; Tempero, M.; Tuveson, D.A.; Hruban, R.H.; et al. Pancreatic cancer. *Nat. Rev. Dis. Primer.* **2016**, *2*, 16022. [CrossRef]
4. Kim, A.; Ha, J.; Kim, J.; Cho, Y.; Ahn, J.; Cheon, C.; Kim, S.; Ko, S.; Kim, B. Natural products for pancreatic cancer treatment: From traditional medicine to modern drug discovery. *Nutrients.* **2021**, *13*, 3801. [CrossRef]
5. Yogeeswari, P.; Sriram, D. Betulinic acid and its derivatives: A review on their biological properties. *Curr. Med. Chem.* **2005**, *12*, 657–666. [CrossRef]
6. Fulda, S. Betulinic acid for cancer treatment and prevention. *Int. J. Mol. Sci.* **2008**, *9*, 1096–1107. [CrossRef]
7. Ali-Seyed, M.; Jantan, I.; Vijayaraghavan, K.; Bukhari, S.N.A. Betulinic acid: Recent advances in chemical modifications, effective delivery, and molecular mechanisms of a promising anticancer therapy. *Chem. Biol. Drug. Des.* **2016**, *87*, 517–536. [CrossRef]
8. Fru, P.N.; Nweke, E.E.; Mthimkhulu, N.; Mvango, S.; Nel, M.; Pilcher, L.A.; Balogun, M. Anti-cancer and immunomodulatory activity of a polyethylene glycol-betulinic acid conjugate on pancreatic cancer cells. *Life* **2021**, *11*, 462. [CrossRef] [PubMed]
9. Mthimkhulu, N.; Mosiane, K.S.; Nweke, E.E.; Balogun, M.; Fru, P.N. Prospects of delivering natural compounds by polymer-drug conjugates in cancer therapeutics. *Anticancer. Agents Med. Chem.* **2021**, *22*, 1699–1713. [CrossRef] [PubMed]
10. Vaidya, B.; Kulkarni, N.S.; Shukla, S.K.; Parvathaneni, V.; Chauhan, G.; Damon, J.K.; Sarode, A.; Garcia, J.V.; Kunda, N.; Mitragotri, S.; et al. Development of inhalable quinacrine loaded bovine serum albumin modified cationic nanoparticles: Repurposing quinacrine for lung cancer therapeutics. *Int. J. Pharm.* **2020**, *557*, 118995. [CrossRef] [PubMed]
11. Alven, S.; Nqoro, X.; Buyana, B.; Aderibigbe, B.A. Polymer-drug conjugate, a potential therapeutic to combat breast and lung cancer. *Pharmaceutics* **2020**, *12*, 406. [CrossRef]
12. Ekladious, I.; Colson, Y.L.; Grinstaff, M.W. Polymer-drug conjugate therapeutics: Advances, insights and prospects. *Nat. Rev. Drug Discov.* **2018**, *18*, 273–294. [CrossRef] [PubMed]
13. Chen, Q.; Kang, J.; Fu, C. The independence of and associations among apoptosis, autophagy, and necrosis. *Signal Transduct. Target Ther.* **2018**, *3*, 18. [CrossRef]
14. Samm, N.; Werner, K.; Rückert, F.; Saeger, H.D.; Grützmann, R.; Pilarsky, C. The role of apoptosis in the pathology of pancreatic cancer. *Cancers* **2010**, *3*, 1–16. [CrossRef]
15. Lafont, E.; Hartwig, T.; Walczak, H. Paving TRAIL's path with Ubiquitin. *Trends Biochem. Sci.* **2018**, *43*, 44–60. [CrossRef] [PubMed]
16. Szegezdi, E.; Leverkus, M. Guiding the killer and bringing in accomplices: Bispecific antibody treatment for malignant melanoma. *J. Investig. Dermatol.* **2016**, *136*, 362–364. [CrossRef] [PubMed]
17. Chen, H.H.; Zhou, H.J.; Wang, W.Q.; Wu, G.D. Antimalarial dihydroartemisinin also inhibits angiogenesis. *Cancer Chemother. Pharmacol.* **2004**, *53*, 423–432. [CrossRef]
18. Zhang, E.; Lu, X.; Yin, S.; Yan, M.; Lu, S.; Fan, L.; Hu, H. The functional role of Bax/Bak in palmitate-induced lipoapoptosis. *Food Chem. Toxicol.* **2019**, *123*, 268–274. [CrossRef] [PubMed]
19. Hanahan, D. Hallmarks of cancer: New dimensions. *Cancer Discov.* **2022**, *12*, 31–46. [CrossRef] [PubMed]
20. Wong, R.S. Apoptosis in cancer: From pathogenesis to treatment. *J. Exp. Clin. Cancer Res.* **2011**, *30*, 87. [CrossRef]
21. Hong-Duck, U.M. Bcl-2 family proteins as regulators of cancer cell invasion and metastasis: A review focusing on mitochondrial respiration and reactive oxygen species. *Oncotarget* **2015**, *7*, 5193–5203.
22. Evans, J.D.; Cornford, P.A.; Dodson, A.; Greenhalf, W.; Foster, C.S.; Neoptolemos, J.P. Detailed tissue expression of bcl-2, bax, bak and bcl-x in the normal human pancreas and in chronic pancreatitis, ampullary and pancreatic ductal adenocarcinomas. *Pancreatology* **2001**, *1*, 254–262. [CrossRef]
23. Virkajärvi, N.; Pääkkö, P.; Soini, Y. Apoptotic index and apoptosis influencing proteins bcl-2, mcl-1, bax and caspases 3, 6 and 8 in pancreatic carcinoma: Apoptosis influencing proteins in pancreatic carcinoma. *Histopathology* **1998**, *33*, 432–439. [CrossRef]
24. Campani, D.; Esposito, I.; Boggi, U.; Cecchetti, D.; Menicagli, M.; De Negri, F.; Colizzi, L.; Del Chario, M.; Mosca, F.; Fornaciari, G.; et al. Bcl-2 expression in pancreas development and pancreatic cancer progression. *J. Pathol.* **2001**, *194*, 444–450. [CrossRef]
25. Rajabi, S.; Maresca, M.; Yumashev, A.V.; Choopani, R.; Hajimehdipoor, H. The most competent plant-derived natural products for targeting apoptosis in cancer therapy. *Biomolecules* **2021**, *11*, 534. [CrossRef]
26. Riley, J.S.; Hutchinson, R.; McArt, D.G.; Crawford, N.; Holohan, C.; Paul, I.; Van Schaeybroeck, S.; Salto-Tellez, M.; Johnston, P.G.; Fennell, D.A.; et al. Prognostic and therapeutic relevance of FLIP and procaspase-8 overexpression in non-small cell lung cancer. *Cell Death Dis.* **2013**, *4*, e951. [CrossRef] [PubMed]
27. Tenev, T.; Marani, M.; McNeish, I.; Lemoine, N.R. Pro-caspase-3 overexpression sensitises ovarian cancer cells to proteasome inhibitors. *Cell Death Differ.* **2001**, *8*, 256–264. [CrossRef]
28. Jakubowska, K.; Guzińska-Ustymowicz, K.; Famulski, W.; Cepowicz, D.; Jagodzińska, D.; Pryczynicz, A. Reduced expression of caspase-8 and cleaved caspase-3 in pancreatic ductal adenocarcinoma cells. *Oncol. Lett.* **2016**, *11*, 1879–1884. [CrossRef] [PubMed]

29. Sharma, R.; Dua, J.S.; Prasad, D.N.; Hira, S.; Monika. Advancement in Novel Drug Delivery System: Niosomes. *JDDT* **2019**, *9*, 995–1001. [CrossRef]
30. Greten, F.R.; Grivennikov, S.I. Inflammation and cancer: Triggers, mechanisms, and consequences. *Immunity* **2019**, *51*, 27–41. [CrossRef]
31. Milkovic, L.; Cipak Gasparovic, A.; Cindric, M.; Mouthuy, P.A.; Zarkovic, N. Short overview of ROS as cell function regulators and their implications in therapy concepts. *Cells* **2019**, *8*, 793. [CrossRef]
32. Liu, Z.; Ren, Z.; Zhang, J.; Chuang, C.C.; Kandaswamy, E.; Zhou, T.; Zuo, L. Role of ROS and nutritional antioxidants in human diseases. *Front. Physiol.* **2018**, *9*, 477. [CrossRef] [PubMed]
33. Snezhkina, A.V.; Kudryavtseva, A.V.; Kardymon, O.L.; Savvateeva, M.V.; Melnikova, N.V.; Krasnov, G.S.; Dmitriev, A.A. ROS generation and antioxidant defence systems in normal and malignant cells. *Oxid. Med. Cell. Longev.* **2019**, *2019*, 1–17. [CrossRef] [PubMed]
34. Adhami, V.M. Pancreatic cancer and inflammation. *Am. J. Biomed. Sci.* **2010**, *2*, 322–328. [CrossRef]
35. Algül, H.; Treiber, M.; Lesina, M.; Schmid, R.M. Mechanisms of disease: Chronic inflammation and cancer in the pancreas—A potential role for pancreatic stellate cells? *Nat. Clin. Pract. Gastroenterol. Hepatol.* **2007**, *4*, 454–462. [CrossRef] [PubMed]
36. Hoesel, B.; Schmid, J.A. The complexity of NF-κB signaling in inflammation and cancer. *Mol. Cancer.* **2013**, *12*, 86. [CrossRef] [PubMed]
37. McKay, C.J.; Glen, P.; McMillan, D.C. Chronic inflammation and pancreatic cancer. *Best Pract. Res. Clin. Gastroenterol.* **2008**, *22*, 65–73. [CrossRef]
38. Tak, P.P.; Firestein, G.S. NF-κB: A key role in inflammatory diseases. *J. Clin. Investig.* **2001**, *107*, 7–11. [CrossRef]
39. Mvango, S.; Mthimkhulu, N.; Fru, P.N.; Pilcher, L.A.; Balogun, M.O. *Physico-Chemical Characterisation of Polyethylene Glycol-conjugated Betulinic Acid*; AIP Publishing: Mallorca, Spain, 2020; p. 020039. Available online: http://aip.scitation.org/doi/abs/10.1063/5.0028479 (accessed on 3 September 2022).
40. Deer, E.L.; González-Hernández, J.; Coursen, J.D.; Shea, J.E.; Ngatia, J.; Scaife, C.L.; Firpo, M.A.; Mulvihill, S.J. Phenotype and genotype of pancreatic cancer cell lines. *Pancreas* **2010**, *39*, 425–435. [CrossRef]
41. Strober, W. Trypan blue exclusion test of cell viability. *Curr. Protoc. Immunol.* **2019**, *111*, A3.B.1–A3.B.3.
42. Aykul, S.; Martinez-Hackert, E. Determination of half-maximal inhibitory concentrations using biosensor-based protein interaction analysis. *Anal. Biochem.* **2016**, *508*, 97–103. [CrossRef]
43. Bustin, S.A.; Benes, V.; Garson, J.A.; Hellemans, J.; Huggett, J.; Kubista, M.; Mueller, R.; Nolan, T.; Pfaffl, M.W.; Shipley, G.L.; et al. The MIQE guidelines: Minimum information for publication of quantitative real-time PCR experiments. *Clin. Chem.* **2009**, *55*, 611–622. [CrossRef] [PubMed]
44. Livak, K.J.; Schmittgen, T.D. Analysis of relative gene expression data using real-time quantitative PCR and the $2^{-\Delta\Delta CT}$ method. *Methods* **2001**, *25*, 402–408. [CrossRef]
45. Zhang, Q.; Zeng, L.; Chen, Y.; Lian, G.; Qian, C.; Chen, S.; Li, J.; Huang, K. Pancreatic cancer epidemiology, detection, and management. *Gastroenterol. Res. Pract.* **2016**, *2016*, 1–10. [CrossRef] [PubMed]
46. Mistry, S.; Shah, S. Antioxidant activity of methanolic extract of Ficus religiosa linn bark by using DPPH ((1, 1-Diphenyl-2-Picrylhydrazyl). *Int. J. Phytopharm.* **2014**, *4*, 57–58.
47. Williams, A.A. Metabonomics Profile and Corresponding Immune Parameters of HIV Infected Individuals. Ph.D. Thesis, University of Pretoria, Pretoria, South Africa, 2012.
48. Wegert, J.; Bausenwein, S.; Kneitz, S.; Roth, S.; Graf, N.; Geissinger, E.; Gessler, M. Retinoic acid pathway activity in wilms tumors and characterization of biological responses in Vitro. *Mol. Cancer* **2011**, *10*, 136–148. [CrossRef] [PubMed]
49. Watson, J.V.; Chambers, S.H.; Smith, P.J. A pragmatic approach to the analysis of DNA histograms with a definable G1 peak. *Cytometry* **1987**, *8*, 1–8. [CrossRef]
50. Sasaki, N.; Gomi, F.; Hasegawa, F.; Hirano, K.; Fujiwara, M.; Toyoda, M.; Ishiwata, T. Characterization of the metastatic potential of the floating cell component of MIA PaCa-2, a human pancreatic cancer cell line. *Biochem. Biophys. Res. Commun.* **2020**, *522*, 881–888. [CrossRef]
51. Margo, A.; Magro, A.; Shrestha, S.; Brundage, K.; Rankin, G. Metalloproteinase dependent reduction of cell surface cluster determinants upon the induction of apoptosis. *Int. J. Oncol.* **2014**, *44*, 1539–1550.
52. Anaya-Eugenio, G.D.; Eggers, N.A.; Ren, Y.; Rivera-Chavez, J.; Kinghorn, A.D.; De Blanco, E.J.C. Apoptosis induced by (+)-Betulin through NF-kb inhibition in MDA-MB-231 breast cancer cells. *Anticancer Res.* **2020**, *40*, 6637–6647. [CrossRef]
53. Vorobjev, I.; Barteneva, N.S. Temporal heterogeneity metrics in apoptosis induced by anticancer drugs. *J. Histochem. Cytochem.* **2015**, *63*, 494–510. [CrossRef]
54. Coricovac, D.; Dehelean, C.A.; Pinzaru, I.; Mioc, A.; Aburel, O.; Macasoi, I.; Draghici, G.A.; Petean, C.; Soica, C.; Boruga, M.; et al. Assessment of betulinic acid cytotoxicity and mitochondrial metabolism impairment in a human melanoma cell line. *Int. J. Mol. Sci.* **2021**, *22*, 4870. [CrossRef]
55. Xu, T.; Pang, Q.; Zhou, D.; Zhang, A.; Luo, S.; Wang, Y.; Yan, X. Proteomic investigation into betulinic acid-induced apoptosis of human cervical cancer HeLa cells. *PLoS ONE* **2014**, *9*, e105768. [CrossRef] [PubMed]
56. Wang, H.M.; Chiu, C.C.; Wu, P.F.; Chen, C.Y. Subamolide E from Cinnamomum subavenium induces sub-G1 cell-cycle arrest and caspase-dependent apoptosis and reduces the migration ability of human melanoma cells. *J. Agric. Food Chem.* **2011**, *59*, 8187–8192. [CrossRef] [PubMed]
57. Crowley, L.C.; Scott, A.P.; Marfell, B.J.; Boughaba, J.A.; Chojnowski, G.; Waterhouse, N.J. Measuring cell death by propidium iodide uptake and flow cytometry. *Cold Spring Harb. Protoc.* **2016**, *2016*, pdb.prot087163. [CrossRef] [PubMed]
58. Ehrhardt, H.; Fulda, S.; Führer, M.; Debatin, K.M.; Jeremias, I. Betulinic acid-induced apoptosis in leukemia cells. *Leukemia* **2004**, *18*, 1406–1412. [CrossRef]

59. Fulda, S.; Scaffidi, C.; Susin, S.A.; Krammer, P.H.; Kroemer, G.; Peter, M.E.; Debatin, K. Activation of mitochondria and release of mitochondrial apoptogenic factors by betulinic acid. *J. Biol. Chem.* **1998**, *273*, 33942–33948. [CrossRef]
60. Schmidt, M.L.; Kuzmanoff, K.L.; Ling-Indeck, L.; Pezzuto, J.M. Betulinic acid induces apoptosis in human neuroblastoma cell lines. *Eur. J. Cancer* **1997**, *33*, 2007–2010. [CrossRef]
61. Wang, D.; Xu, M.; Li, F.; Gao, Y.; Sun, H. Target identification-based analysis of mechanism of betulinic acid-induced cell apoptosis of cervical cancer SiHa. *Nat. Prod. Commun.* **2022**, *17*, 1934578X2211155. [CrossRef]
62. Dutta, D.; Sarkar, A.; Chakraborty, B.; Chowdhury, C.; Das, P. Induction of apoptosis by a potent betulinic acid derivative in human colon carcinoma HT-29 cells. *Int. J. Sci. Res. Publ.* **2015**, *5*, 7.
63. Shen, M.; Hu, Y.; Yang, Y.; Wang, L.; Yang, X.; Wang, B.; Huang, M. Betulinic acid induces ROS-dependent apoptosis and S-phase arrest by inhibiting the NF- κ B pathway in human multiple myeloma. *Oxid. Med. Cell. Longev.* **2019**, *2019*, 1–14. [CrossRef] [PubMed]
64. Saneja, A.; Kuma, R.; Singh, A.; Dhar Dubey, R.; Mintoo, M.J.; Singh, G.; Mondhe, D.M.; Panda, A.M.; Gupta, P.N. Development and evaluation of long-circulating nanoparticles loaded with betulinic acid for improved anti-tumor efficacy. *Int. J. Pharm.* **2017**, *531*, 153–166. [CrossRef] [PubMed]
65. Zuco, V.; Supino, R.; Righetti, S.C.; Cleris, L.; Marchesi, E.; Gambacorti-Passerini, C.; Formelli, F. Selective cytotoxicity of betulinic acid on tumor cell lines, but not on normal cells. *Cancer Lett.* **2002**, *175*, 17–25. [CrossRef] [PubMed]
66. Zhao, Y.; Krishnan, J. mRNA translation and protein synthesis: An analysis of different modelling methodologies and a new PBN based approach. *BMC Syst. Biol.* **2014**, *8*, 1–24. [CrossRef] [PubMed]
67. Vogel, C.; Marcotte, E.M. Insights into the regulation of protein abundance from proteomic and transcriptomic analyses. *Nat. Rev. Genet.* **2013**, *13*, 227–232. [CrossRef] [PubMed]
68. Nachmias, B.; Ashhab, Y.; Ben-Yehuda, D. The inhibitor of apoptosis protein family (IAPs): An emerging therapeutic target in cancer. *Semin. Cancer Biol.* **2004**, *14*, 231–243. [CrossRef] [PubMed]
69. Liang, J.; Zhao, W.; Tong, P.; Li, P.; Zhao, Y.; Li, H.; Liang, J. Comprehensive molecular characterisation of inhibitors of apoptosis proteins (IAPs) for therapeutic targeting in cancer. *BMC Med. Genom.* **2020**, *13*, 7. [CrossRef]
70. Desagher, S.; Osen-Sand, A.; Nichols, A.; Eskes, R.; Montessuit, S.; Lauper, S.; Maundrell, K.; Antonsson, B.; Martinou, J. Bid-induced conformational change of Bax is responsible for mitochondrial cytochrome c release during apoptosis. *J. Cell Biol.* **1999**, *144*, 891–901. [CrossRef]
71. Gu, Q.; Wang, J.D.; Xia, H.H.X.; Lin, M.C.M.; He, H.; Zou, B.; Tu, S.P.; Yang, Y.; Liu, X.G.; Lam, S.K.; et al. Activation of the caspase-8/Bid and Bax pathways in aspirin-induced apoptosis in gastric cancer. *Carcinogenesis* **2005**, *26*, 541–546. [CrossRef]
72. Korsmeyer, S.J.; Wei, M.C.; Saito, M.; Weiler, S.; Oh, K.J.; Schlesinger, P.H. Proapoptotic cascade activates BID, which oligomerises BAK or BAX into pores that result in the release of cytochrome c. *Cell Death Differ.* **2000**, *7*, 1166–1173. [CrossRef]
73. Chipuk, J.E.; Fisher, J.C.; Dillon, C.P.; Kriwacki, R.W.; Kuwana, T.; Green, D.R. Mechanism of apoptosis induction by inhibition of the antiapoptotic BCL-2 proteins. *Proc. Natl. Acad. Sci. USA* **2008**, *105*, 20327–20332. [CrossRef]
74. Naseri, M.H.; Mahdavi, M.; Davoodi, J.; Tackallou, S.H.; Goudarzvand, M.; Neishabouri, S.H. Upregulation of Bax and downregulation of Bcl2 during 3-NC mediated apoptosis in human cancer cells. *Cancer Cell Int.* **2015**, *15*, 55. [CrossRef] [PubMed]
75. Xia, Y.; Shen, S.; Verma, I.M. NF-κB, an active player in human cancers. *Cancer Immunol. Res.* **2014**, *2*, 823–830. [CrossRef]
76. Xia, L.; Tan, S.; Zhou, Y.; Lin, J.; Wang, H.; Oyang, L.; Tian, Y.; Liu, L.; Su, M.; Wang, H.; et al. Role of the NFκB-signaling pathway in cancer. *OncoTargets Ther.* **2018**, *11*, 2063–2073. [CrossRef] [PubMed]
77. Zinatizadeh, M.R.; Schock, B.; Chalbatani, G.M.; Zarandi, P.K.; Jalali, S.A.; Miri, S.R. The nuclear factor Kappa B (NF-kB) signaling in cancer development and immune diseases. *Genes Dis.* **2021**, *8*, 287–297. [CrossRef]
78. Lin, B.; Williams-Skipp, C.; Tao, Y.; Schleicher, M.S.; Cano, L.L.; Duke, R.C.; Schienman, R.L. NF-kB functions as both a proapoptotic and antiapoptotic regulatory factor within a single cell type. *Cell Death Differ.* **1999**, *6*, 570–582. [CrossRef]
79. Ryan, K.; Ernst, M.; Rice, N.; Vousden, K. Role of NF-kB in p53-mediated programmed cell death. *Nature* **2000**, *404*, 892–896. [CrossRef] [PubMed]
80. Khandelwal, N.; Simpson, J.; Taylor, G.; Rafique, S.; Whitehouse, A.; Hiscox, J.; Stark, L.A. Nucleolar NF-κB/RelA mediates apoptosis by causing cytoplasmic relocalisation of nucleophosmin. *Cell Death Differ.* **2011**, *18*, 1889–1903. [CrossRef]
81. Adesanwo, J.K.; Makinde, O.O.; Obafemi, C.A. Phytochemical analysis and antioxidant activity of methanol extract and betulinic acid isolated from the roots of Tetracera potatoria. *J. Pharm. Res.* **2013**, *6*, 903–907. [CrossRef]
82. Sati, P.; Pandey, A.; Rawat, S.; Rani, A. Phytochemicals and antioxidants in leaf extracts of Ginkgo biloba with reference to location, seasonal variation and solvent system. *J. Pharm. Res.* **2013**, *7*, 804–809. [CrossRef]
83. Anggraini, T.; Wilma, S.; Syukri, D.; Azima, F. Total phenolic, anthocyanin, catechins, DPPH radical scavenging activity, and toxicity of *Lepisanthes alata (Blume) Leenh. Int. J. Food Sci.* **2019**, *2019*, 1–7. [CrossRef] [PubMed]
84. Wakabayashi, T.; Kawashima, T.; Matsuzawa, Y. Evaluation of reactive oxygen metabolites in patients with non-small cell lung cancer after chemotherapy. *MRM* **2014**, *9*, 44. Available online: http://www.mrmjournal.com/content/9/1/44 (accessed on 15 September 2022). [PubMed]

Appendix II: Ethics Clearance Waiver Certificate

UNIVERSITY OF THE WITWATERSRAND, JOHANNESBURG | HUMAN RESEARCH ETHICS COMMITTEE (MEDICAL

Human Research Ethics Committee (Medical)

Research Office Secretariat:
Faculty of Health Sciences, Phillip Tobias Building, 3rd Floor, Office 301/2/4, 29 Princess of Wales Terrace, Parktown, 2193
Tel +27 (0)11-717-1252 /1234/2656/2700
Private Bag 3, Wits 2050
Office email: HREC-Medical.ResearchOffice@wits.ac.za
Website: www.wits.ac.za/research/about-our-research/ethics-and-research-integrity/

Ref: W-CBP-200506-1 06/05/2020

TO WHOM IT MAY CONCERN:

Waiver: This certifies that the following research does not require clearance from the Human Research Ethics Committee (Medical)

Investigator: Miss Karabo Sekopi Mosiane (student no. 1473512) et al

Supervisor: Dr P. Fru

Department: Surgery

Project title: Mechanisms of cell death induced by betulinic acid and dihydroartemisinin polymer drug conjugates in pancreatic cancer cells

Reason: No human participants will be involved in the study.

Dr CB Penny
Chairperson: Human Research Ethics Committee (Medical)

Copy – HREC (Medical) Secretariat: Rhulani Mkansi, Zanele Ndlovu and Mapula Ramaila.

Appendix III: Cytotoxic effect of doxorubicin using an MTT assay

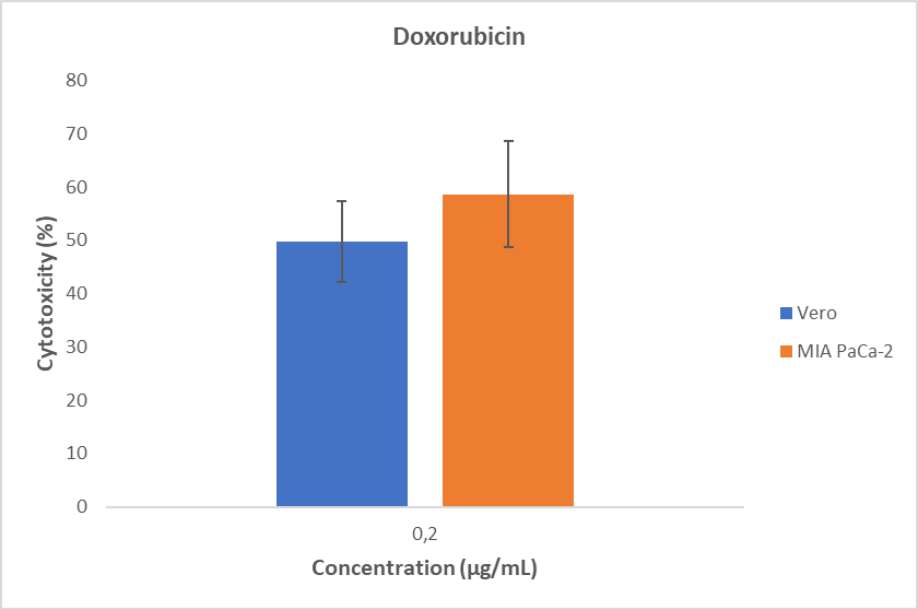

Figure AIII.1: The cytotoxic effect of doxorubicin on MIA PaCa-2 and Vero cells analysed using the MTT assay. The drug induced higher cytotoxicity on the MIA PaCa-2 cells than the Vero cells.

Appendix IV: Cytotoxic effect of BA and PEG-BA using MTT assay

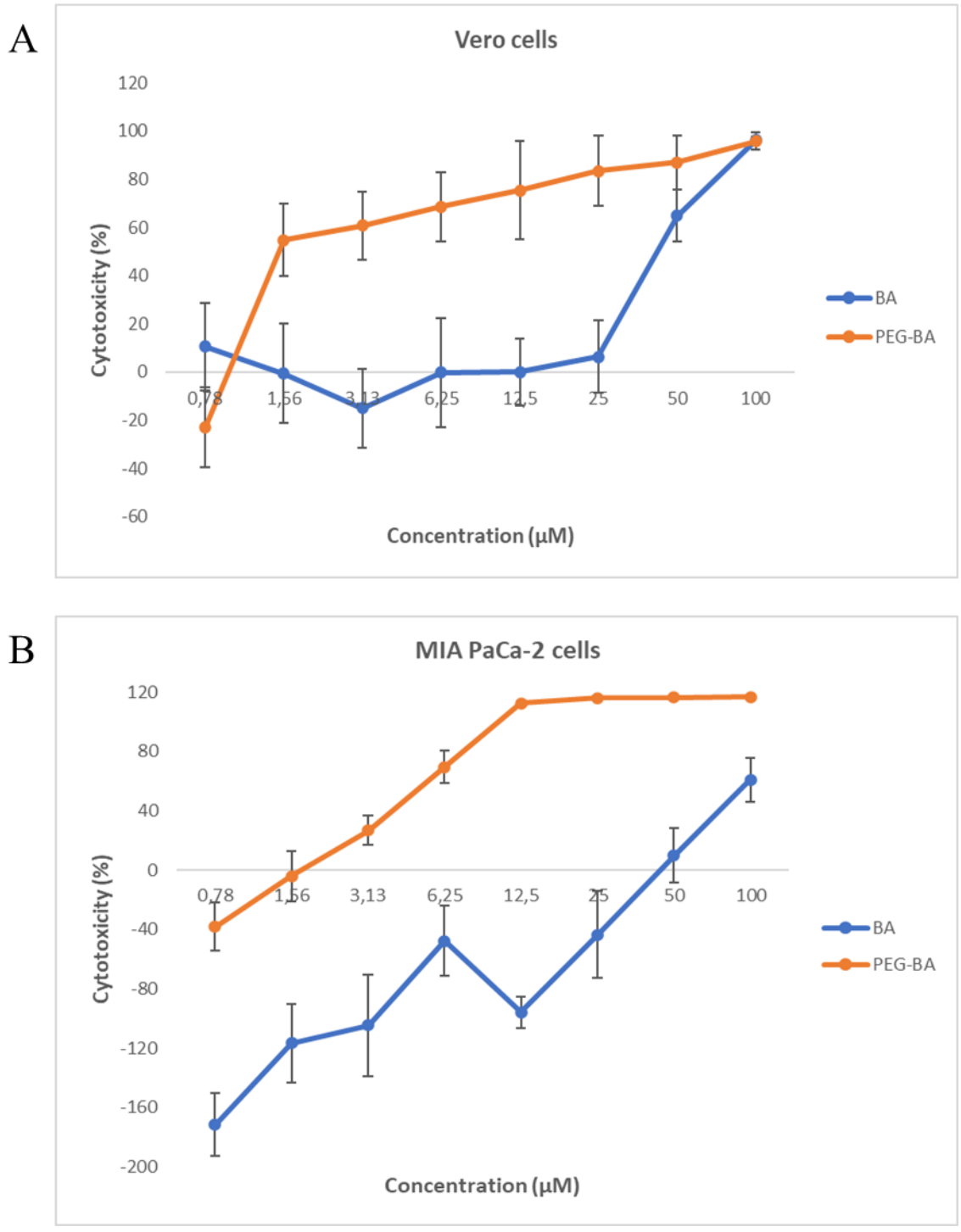

Figure AIV.1: The cytotoxic effect of BA and PEG-BA on Vero (A) and MIA PaCa-2 (B) cells analysed using the MTT assay. In both cell lines, the conjugate produced higher cytotoxicity on the MIA PaCa-2 cells than on the Vero cells. At the same time, BA seemed not to have any effect on the pancreatic cancer cells at concentrations below 50µM.

Appendix V: Cytotoxic effect of polyethylene glycol (PEG)

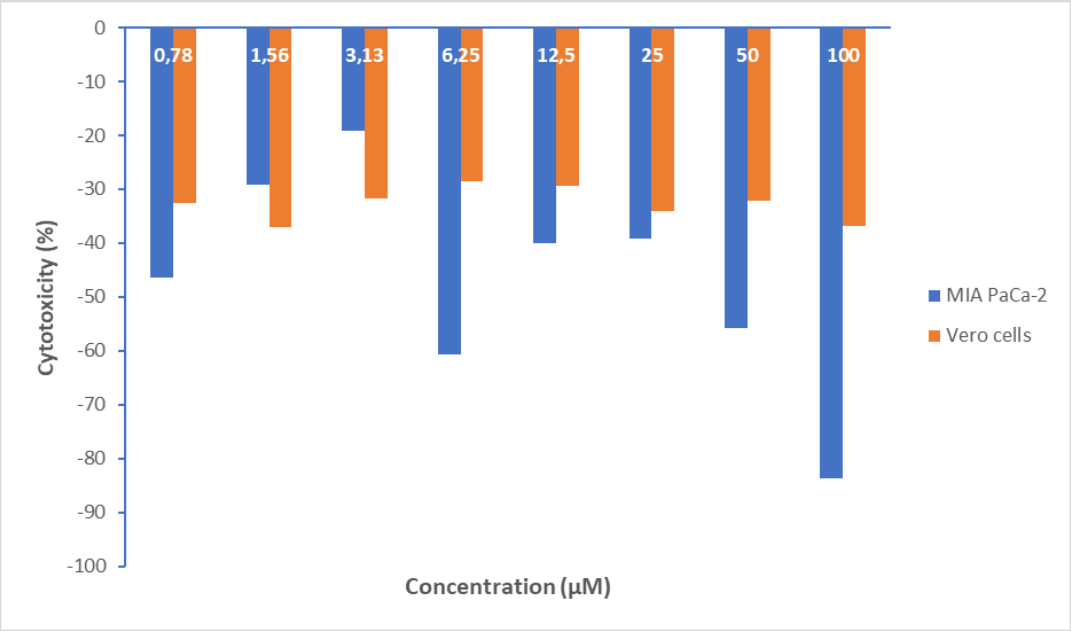

Figure AV.1: The cytotoxic effect of polyethylene glycol (PEG) on MIA PaCa-2 and Vero cells analysed using the MTT assay. The polymer induced minimal to no effect on both cell lines, showing that even the highest tested concentration (100µM) was insufficient to produce a cytotoxic effect.

Appendix VI: Cytotoxic effect of DMSO using MTT and XTT assays

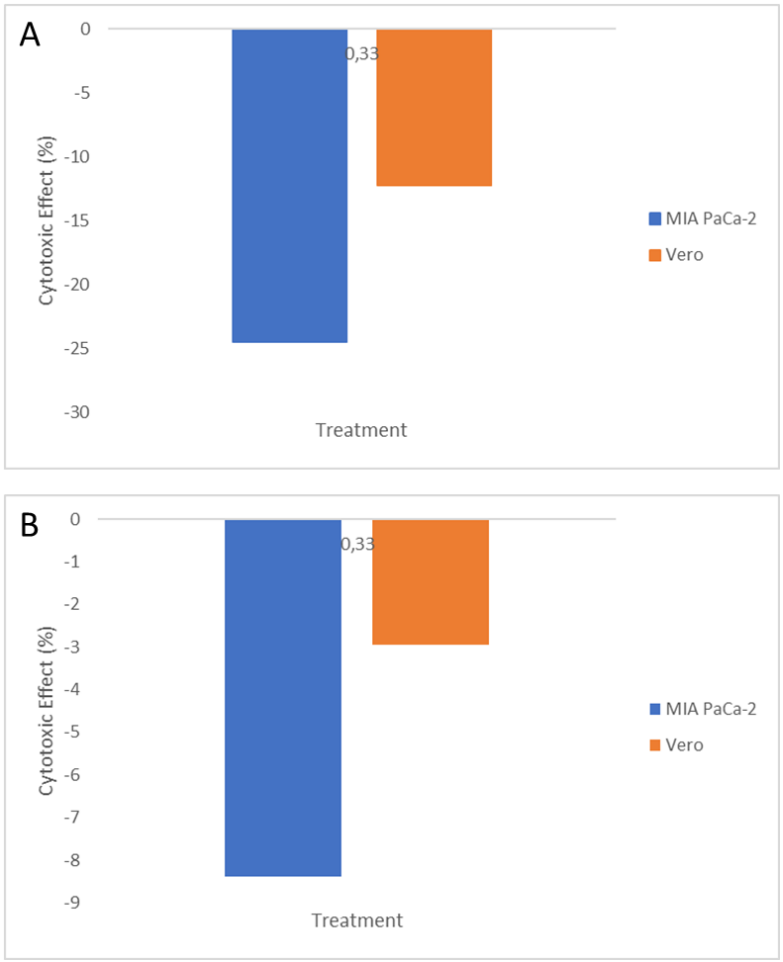

Figure AVI.1: The cytotoxic effect of DMSO on MIA PaCa-2 and Vero cells analysed using the MTT (A) and XTT (B) assays. The results showed minimal to no effect on both cell lines (with both assays) after treatment with 0.33% DMSO.

Appendix VII: MIA PaCa-2 Dose Response Curves

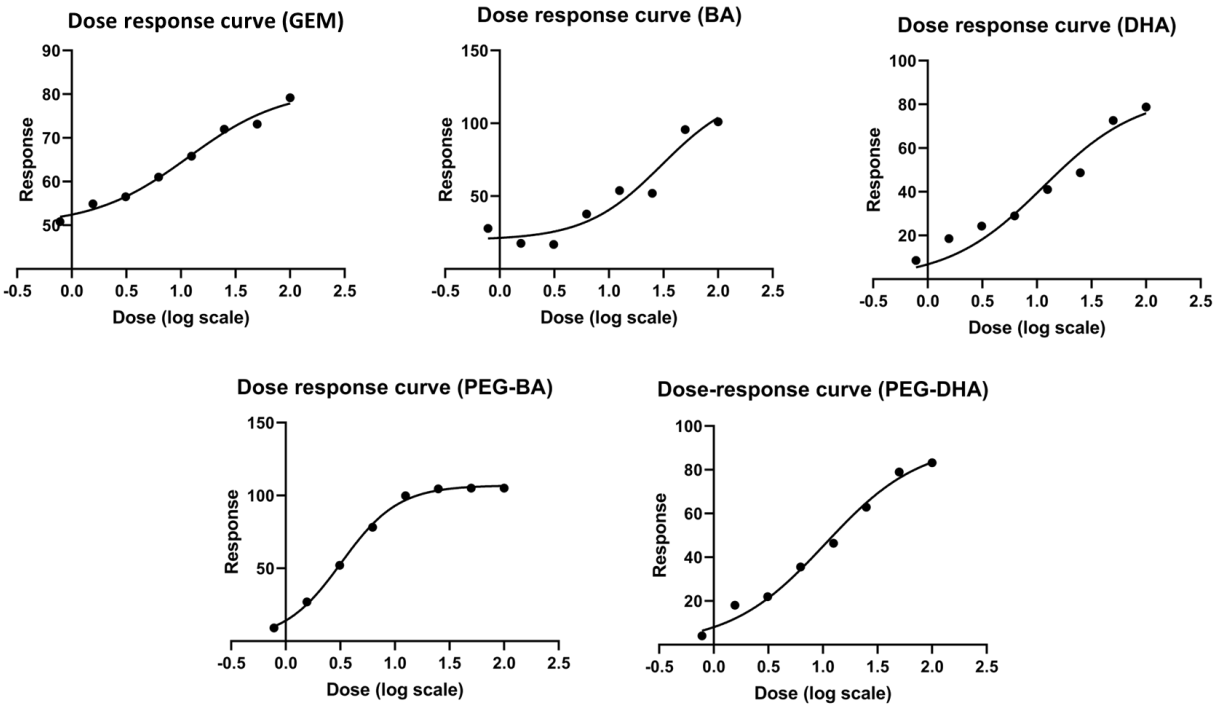

Figure AVI.1: Dose response curves on MIA PaCa-2 cells after 72-hour treatment with gemcitabine, betulinic acid (BA), dihydroartemisinin (DHA), polyethylene glycol (PEG)-BA and PEG-DHA.

Appendix VIII: Vero Dose Response Curves

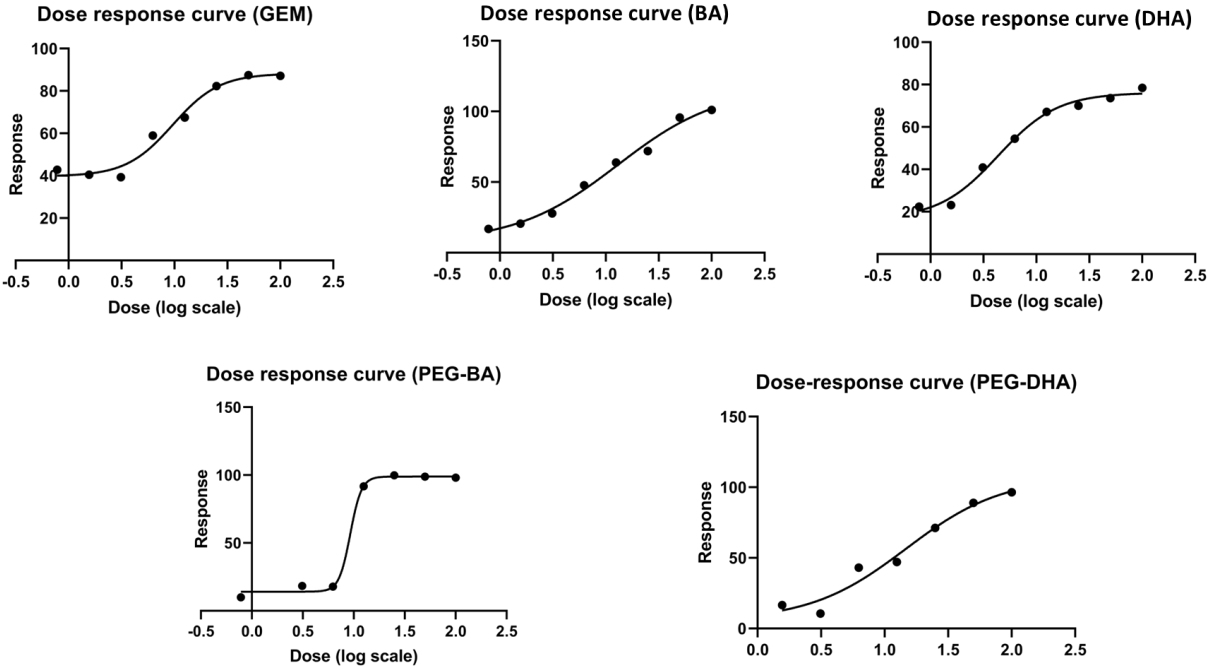

Figure AVII.1: Dose response curves on Vero cells after 72-hour treatment with gemcitabine, betulinic acid (BA), dihydroartemisinin (DHA), polyethylene glycol (PEG)-BA and PEG-DHA.

Appendix IX: Microscopic analysis of MIA PaCa-2 cells after 24 hours

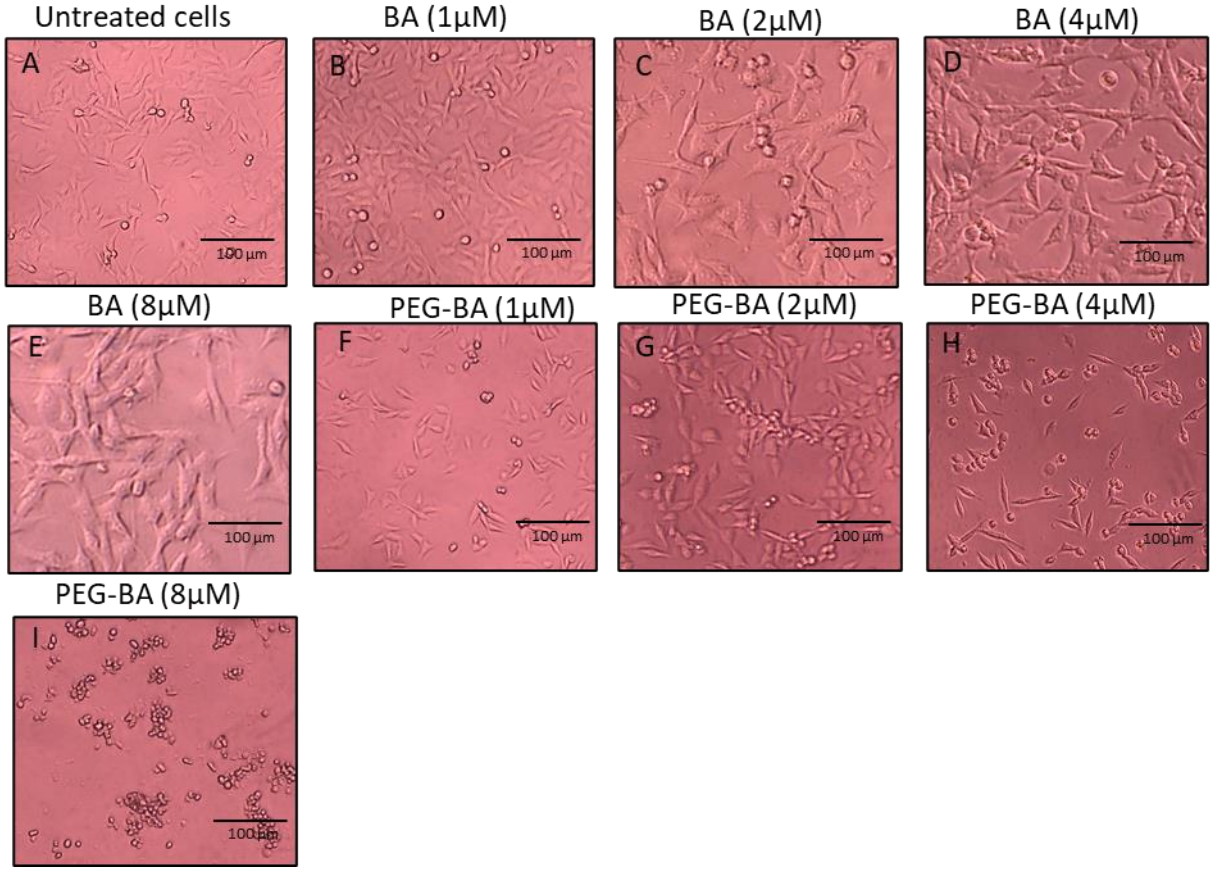

Figure AIX.1: Microscopic analysis of BA and PEG-BA treatment on MIA PaCa-2 cells at 24 h. Untreated cells (A) and cells treated with varying concentrations (1-8 µM) of native BA (B-E) and its conjugate (PEG-BA) (F-I) were analysed for morphological changes using light microscopy. Compared to the untreated and BA-treated cells, PEG-BA treated cells had a higher percentage of cells that formed clumps of rounded cells in a concentration-dependent manner.

Appendix X: Microscopic analysis of MIA PaCa-2 cells after 48 hours

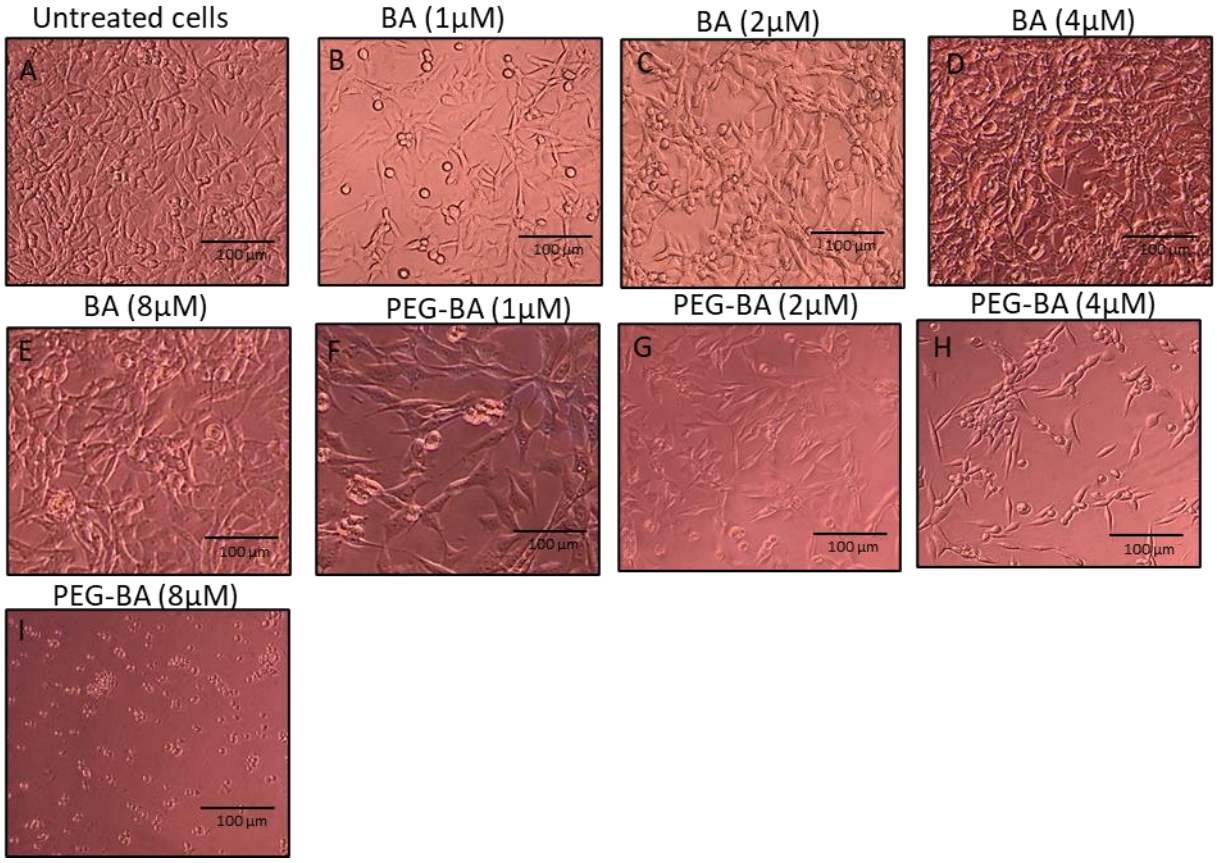

Figure AX.1: Microscopic analysis of BA and PEG-BA treatment on MIA PaCa-2 cells at 48 h. Untreated cells (A) and cells that were treated with varying concentrations (1-8 µM) of native BA (B-E) and its conjugate (PEG-BA) (F-I) were analysed for morphological changes using light microscopy. Like 24 h, at 48 h, PEG-BA resulted in most of the plated cells forming clumps of rounded cells compared to BA-only, in a dose-dependent manner. This also indicated that PEG-BA induces a toxic effect in the MIA PaCa-2 cells in a time-dependent manner since at 48 h, even at 4 µM, most cells start rounding up.

Appendix XI: ROS status after treatment with DMSO

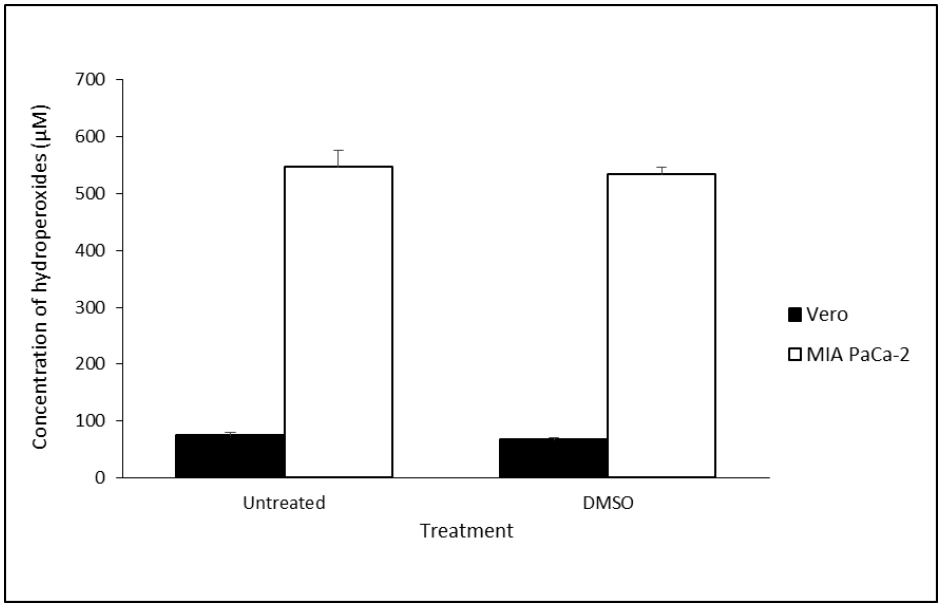

Figure AXI.1: ROS status of the Vero and MIA PaCa-2 cells after treatment with the vehicle control. The results from this assay showed that treating the Vero cells with 0.33% DMSO marginally decreased the concentration of hydroperoxides compared to the untreated sample (74.73 ± 5.70 µM vs 66.94 ± 3,49 µM). Treating the pancreatic cancer cells with the same concentration of DMSO also reduced the hydroperoxide (546.96 ± 29.03 µM vs 533,63 ± 13,50 µM). The results suggest that DMSO had an antioxidant effect against both cell lines.

Appendix XII: Effect of DMSO on apoptosis induction

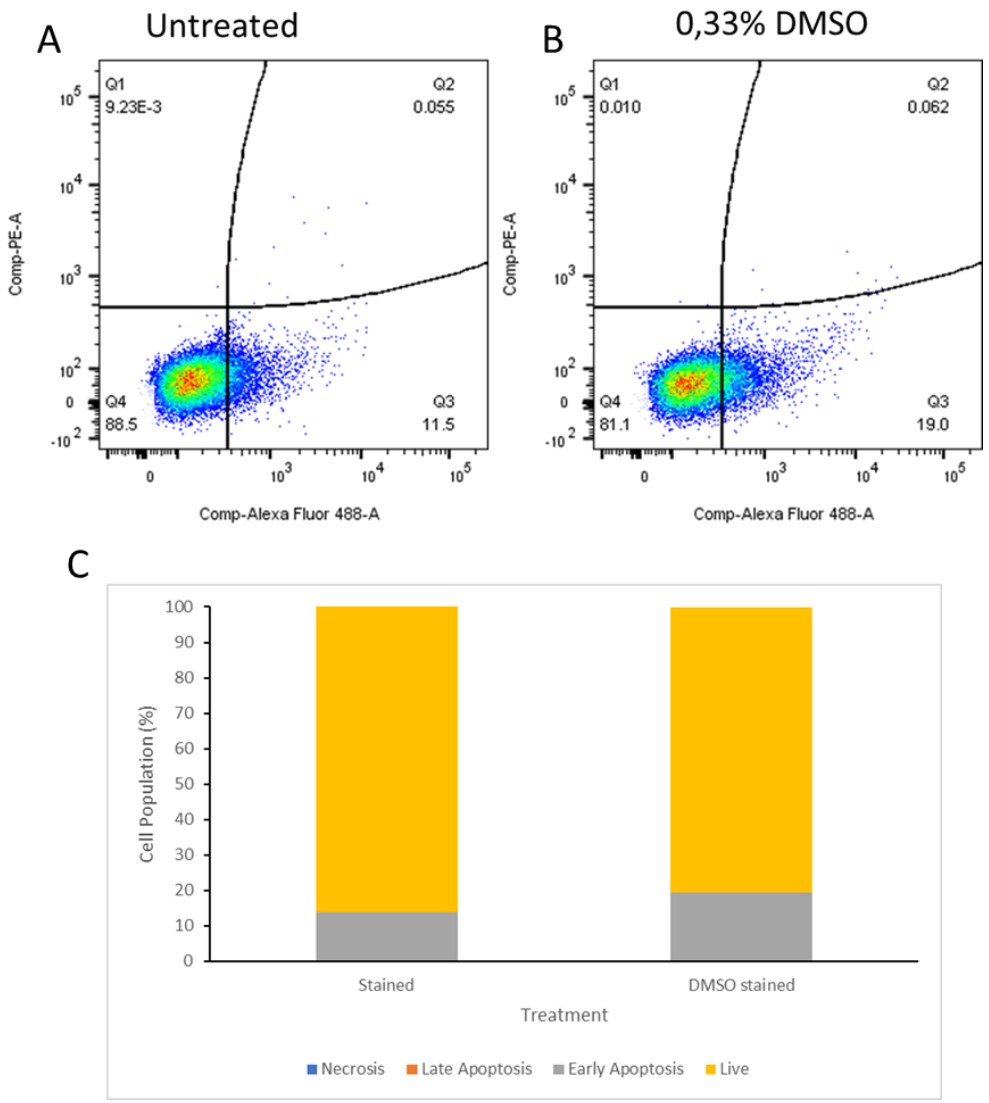

Figure AXII.1: Cell death induction on the Vero cells after 72-hour treatment with 0.33% DMSO using the Annexin V/PI assay. Like the untreated Vero cells, DMSO resulted in a majority of the cells being viable (86.24 ± 8,77% vs 80,47 ± 7,3167%). Furthermore, the level of apoptosis marginally increased after treatment with DMSO (13.81% vs 19.51%). Less than 1% of the cells underwent necrosis (0.0034 ± 0.0017% vs 0.0080 ± 0.0042%). (A-B) Representative dot plots demonstrating (Q1) necrotic cells, (Q2) late apoptotic cells, (Q3) early apoptotic cells and (Q4) live cells. (C) Quantitative bar graphs representing the four modes indicated because of treatment (mean ± SEM), n=3.

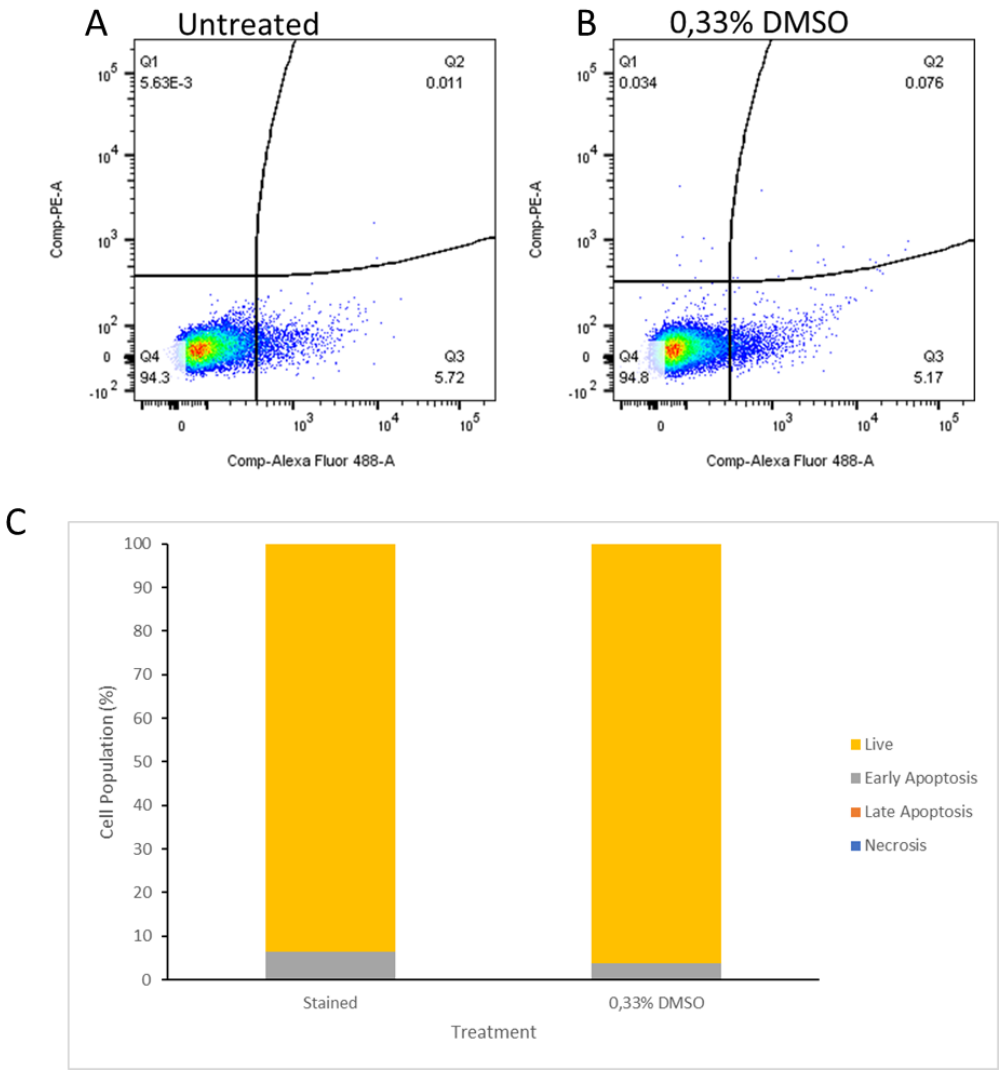

Figure AXII.2: Cell death induction on the MIA PaCa-2 cells after 72-hour treatment with 0.33% DMSO using the Annexin V/PI assay. Similarly, in the MIA PaCa-2 cells, majority of the DMSO treated cells were viable (93.67 ±1.00% vs 96.13 ± 0.67%), induced low levels of apoptosis (6.31% vs 3.83%) and less than 1% of necrosis (0.0105 ± 0.01% vs 0.0187 ± 0.01%). (A-B) Representative dot plots demonstrating (Q1) necrotic cells, (Q2) late apoptotic cells, (Q3) early apoptotic cells and (Q4) live cells. (C) Quantitative bar graphs representing the four modes indicated because of treatment (mean ± SEM), n=3.

Appendix XIII: Effect of DMSO on the cell cycle

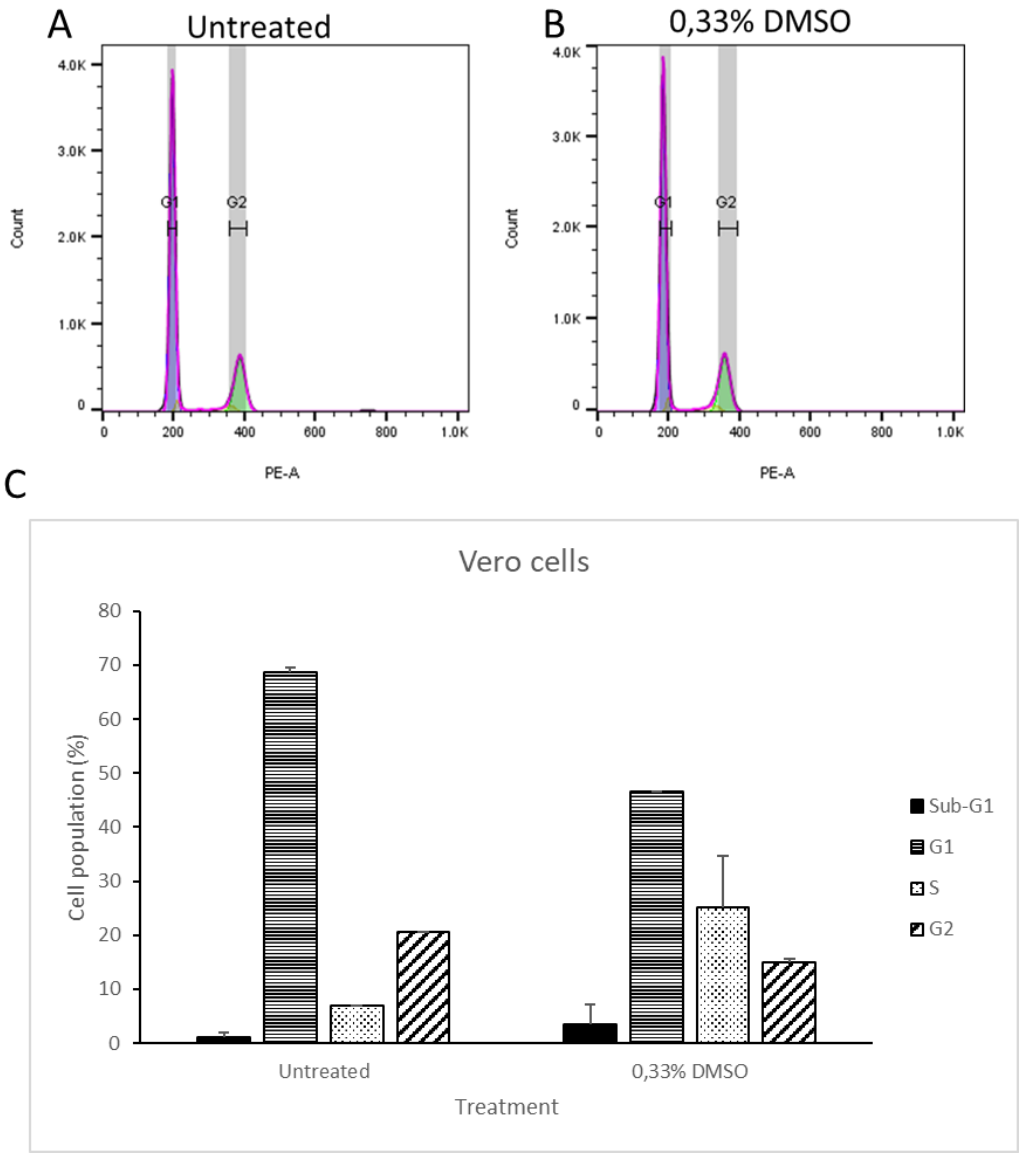

Figure AXIII.1: Cell cycle status of Vero cells after treatment with 0.33% DMSO. Most of the untreated Vero cells were in the G1/G0 (68.67 ± 0.29%) compared to S (6.88 ± 0.02%) and G2/M (20.50 ± 0.14%) phases. It was found that at least 1.12 ± 0.82% of the untreated cells were in the sub-G1 phase. Treating the non-cancerous cells with 0.33% DMSO resulted in a shift of the cells into the S (25.15 ± 9.34%). Furthermore, the population of cells undergoing apoptosis (sub-G1) also increased (3.50 ± 1.47%). These arrests were associate with a decrease of cells in the G1/G0 (46.52 ± 11.41%) and G2/M (14.86 ± 3.04%) phases. (A-B) Representative histograms showing the different phases of the cell cycle indicated by the white (sub-G1), purple (G1/G0), yellow (S) and green (G2/M) peaks. (C) Quantitative bar graphs showing the overall cycling status of the pancreatic cancer cells (mean ± SEM), n=3.

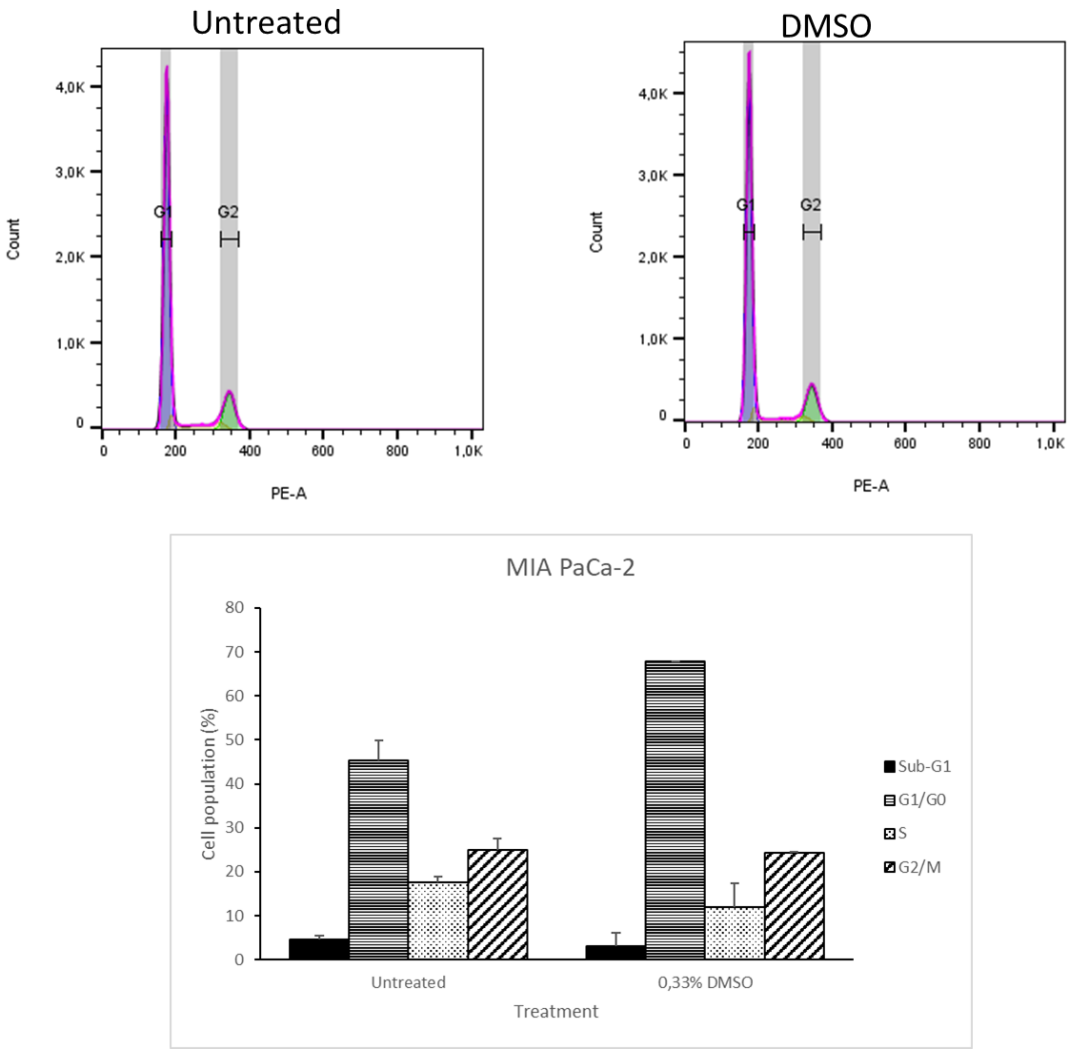

Figure AXIII.2: Cell cycle status of MIA PaCa-2 cells after treatment with 0.33% DMSO. In the untreated MIA PaCa-2 cells, most of the cells were in the G1/G0 (45.27 ± 4.70%) compared to S (17.67 ± 1.22%) and G2/M (25.07 ± 2.44%) phases. The sub-G1 phase was also assessed, and it was found that at least 4.57 ± 0.82% of the untreated cells were in this phase. DMSO treatment led to a G1/G0 phase arrest (67.77 ± 4.21%). This was associated with a decrease of cells in the other phases of the cell cycle (sub-G1: 3.18 ± 2.30%; S: 12.04 ± 1.30% and G2/M: 24.30 ± 5.21%). (A-B) Representative histograms showing the different phases of the cell cycle indicated by the white (sub-G1), purple (G1/G0), yellow (S) and green (G2/M) peaks. (C) Quantitative bar graphs showing the overall cycling status of the pancreatic cancer cells (mean ± SEM), n=3.

Appendix XIV: Standard curve for the NF-κB ELISA

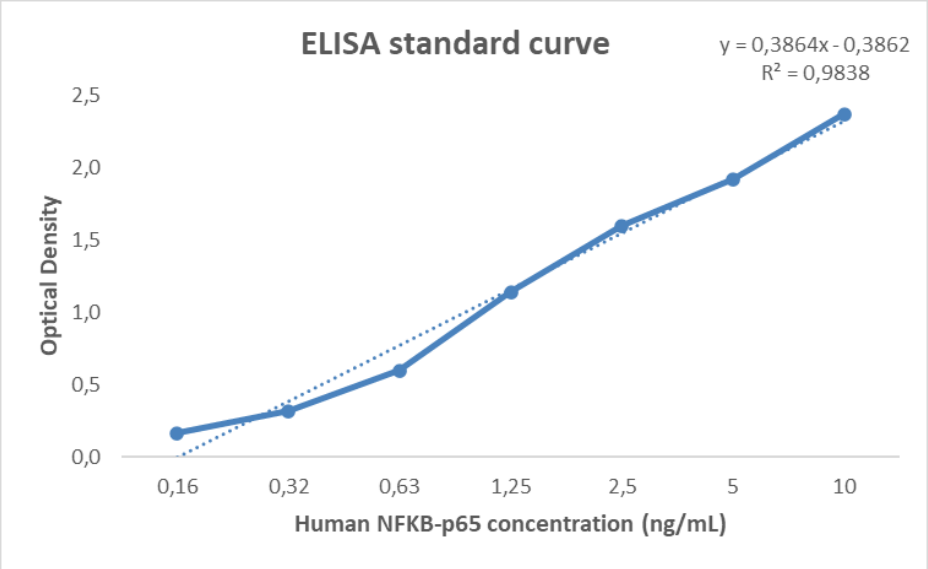

Figure AXIV.1: The NF-κB ELISA standard curve used to quantify the concentration of human NF-κB/p65 protein present in the biological samples. The curve obtained was similar to the manufacturer's anticipated results.

Appendix XV: Relative fold-change of apoptosis-related genes in the Vero cells

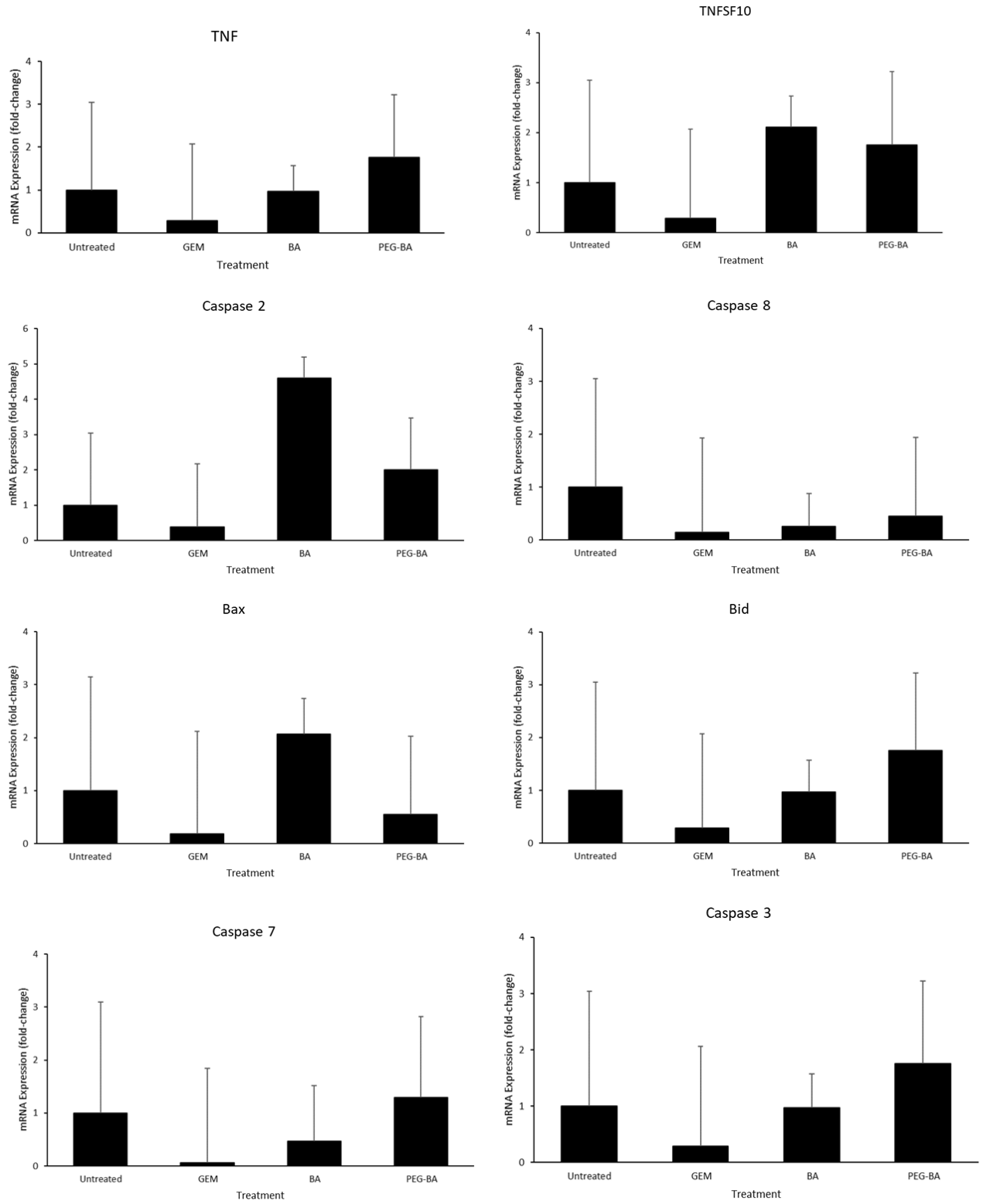

Figure AXV.1: Real-time PCR analysis on Vero cells post-treatment with gemcitabine, BA, and PEG-BA. Gemcitabine treatment resulted in downregulation of all the pro-apoptotic genes. BA upregulated TNFSF10, Caspase 2 and Bax and downregulated TNF, caspases 3, 7, and 8. The conjugate (PEG-BA) upregulated the executioner caspases (3 and 7), proinflammatory cytokines, TNF and TNFSF10, and Bid. All these results showed that BA and PEG-BA induced apoptosis in the non-cancerous cells.

UNIVERSITY OF THE
WITWATERSRAND,
JOHANNESBURG

Department of Surgery

7 York Road, Parktown, 2193 South Africa • Email pascaline.fru@wits.ac.za **• Telephone (011) 717-2476•**

March 29, 2023
The Postgraduate Office,
Faculty of Health Sciences

Turnitin report similarity index for Karabo Mosiane's MSc

This letter serves to indicate that the similarity index 13% of the similarity score for Ms Mosiane's MSc is from her own published MSc work. This means of the 23% similarity reported from her work, only 10 are from other sources. This is acceptable in the department of Surgery as these are all below 1%.

We hope you find this acceptable.

Pascaline N Fonteh, FRU
Associate Professor,
BSc., BScHons, PGDipHE, MSc, Ph.D. (University of Pretoria)

Turnitin Submission-1.pdf

ORIGINALITY REPORT

23%	21%	20%	4%
SIMILARITY INDEX	INTERNET SOURCES	PUBLICATIONS	STUDENT PAPERS

PRIMARY SOURCES

1	www.ncbi.nlm.nih.gov Internet Source	9%
2	www.mdpi.com Internet Source	4%
3	Karabo Sekopi Mosiane, Ekene Emmanuel Nweke, Mohammed Balogun, Pascaline Nanga Fru. "Polyethyleneglycol-Betulinic Acid (PEG-BA) Polymer-Drug Conjugate Induces Apoptosis and Antioxidation in a Biological Model of Pancreatic Cancer", Polymers, 2023 Publication	1%
4	effiloop.com Internet Source	1%
5	www.science.gov Internet Source	<1%
6	www.nature.com Internet Source	<1%
7	www.researchgate.net Internet Source	<1%